NASA Tech Briefs

National
Aeronautics and
Space
Administration

Flat conductor cable, developed for spacecraft use, offers many advantages for building wiring and is being investigated for use in commercial and residential buildings.

The NASA Technology Utilization House, now open to the public, embodies new features such as solar heating and cooling, water recycling, and security systems. Although it incorporates many innovations based on aerospace technology, the house is constructed entirely from materials that are commercially available now.

Vol. 1, No. 4

WINTER 1976

About the NASA Technology Utilization Program

The National Aeronautics and Space Act of 1958, which established NASA and the United States civilian space program, requires that "The Administration shall provide for the widest practicable and appropriate dissemination of information concerning its activities and the results thereof."

To help carry out this objective the NASA Technology Utilization (TU) Program was established in 1962. It offers a variety of valuable services to facilitate the transfer of aerospace technology to nonaerospace applications, thus assuring American taxpayers maximum return on their investment in space research; thousands of spinoffs of NASA research have already occurred in virtually every area of our economy.

The TU Program has worked for engineers, scientists, technicians, and businessmen. And it can work for you.

NASA Tech Briefs

Tech Briefs is published quarterly and is free to any U.S. citizen or organization. It is both a current-awareness medium and a problem-solving tool. Potential products ... industrial processes ... basic and applied research ... shop and lab techniques ... computer software ... new sources of technical data ... concepts ... you will find them all in NASA Tech Briefs. The first section highlights a few of the potential new products contained in Tech Briefs. The remainder of the volume is organized by technical category to help you quickly review new developments in your areas of interest. Finally, a subject index makes each issue a convenient permanent reference file.

Further Information on Innovations

Although many articles are complete in themselves, others are backed up by Technical Support Packages (TSP's). TSP's are available without charge and may be ordered by simply completing the enclosed TSP Request Card. Further information on some innovations is available for a nominal fee from other sources, as indicated at the ends of the articles. In addition, Technology Utilization Officers at NASA Field Centers will assist you directly when necessary. (See page A4.)

Patent Licenses

Many of the inventions described are under consideration for patents or have been patented by NASA. Unless NASA has decided not to apply for a patent, the patent status is described at the end of each article. For further information about the Patent Program see page A8.

Other Technology Utilization Services

To assist engineers, industrial researchers, business executives, city officials, and other potential users in applying space technology to their problems, NASA sponsors six Industrial Applications Centers. Their services are described on page A6. In addition, an extensive library of computer programs is available through COSMIC, the Technology Utilization Program's outlet for NASA-developed software. (See page A5.)

Applications Program

To help solve public-sector problems in such areas as safety, health, transportation, and environmental protection, NASA TU Applications Teams, staffed by professionals from a variety of disciplines, work with Federal agencies, local governments, and health organizations to identify critical problems amenable to technical solutions. Among their many significant contributions are a rechargeable heart pacemaker, a lightweight fireman's breathing apparatus, aids for the handicapped, and safer highways.

Reader Feedback

We hope you find the information in NASA Tech Briefs useful. A reader feedback card has been included because we want your comments and suggestions on how we can further help you apply NASA innovations and technology to your needs. Please use it, or if you need more space, write us a letter.

NASA Tech Briefs

National
Aeronautics and
Space
Administration

WINTER 1976
Volume 1, Number 4

COVERS: The photographs on the front and back covers illustrate recent developments by NASA and its contractors that have resulted in commercial and nonaerospace spinoffs.

About This NASA Publication

NASA Tech Briefs, a quarterly publication, is distributed free to U.S. citizens to encourage commercial application of U.S. space technology. For information on publications and services available through the NASA Technology Utilization Program, write to the Director, Technology Utilization Office, P. O. Box 8756, Baltimore/Washington International Airport, Maryland 21240.

"The Administrator of National Aeronautics and Space Administration has determined that the publication of this periodical is necessary in the transaction of the public business required by law of this Agency. Use of funds for printing this periodical has been approved by the Director of the Office of Management and Budget through August 31, 1977."

Change of Address

Change of Address: If you wish to have NASA Tech Briefs forwarded to your new address, use one of the Subscriptions cards enclosed in the back of this volume of NASA Tech Briefs. Be sure to check the appropriate box indicating change of address.

Communication Concerning Editorial Matter

For editorial comments or general communications about NASA Tech Briefs, you may use the self-addressed Feedback card in the back of NASA Tech Briefs, or write to: The Publications Manager, Technology Utilization Office (Code KT), NASA Headquarters, Washington, DC 20546. Technical questions concening specific articles should be directed to the Technology Utilization Officer of the sponsoring NASA Center (addresses listed on page A4.)

NASA
TU SERVICES

THE NASA TECHNOLOGY UTILIZATION OFFICERS

They will help you apply the innovations described in Tech Briefs.

The Technology Utilization Officer (TUO)

Each NASA Center has a Technology Utilization Officer — An applications engineer whose job is to help you make use of new technology developed at his center. He brings you the NASA Tech Briefs and other special publications, sponsors conferences, and arranges contacts with NASA technical experts.

Technical Assistance

Working together with NASA Scientists and Engineers and the Industrial Applications Centers, the center TUO's can answer specific questions about innovations and related NASA technology.

Technical Support Package (TSP's)

For many of the innovations described in Tech Briefs, the center TUO has prepared additional material that will help you in detailed evaluation and actual use or construction of the new technology. You may get TSP's free of cost by using the TSP Request Card or writing the center TUO.

Who to Contact.

Of course, many technical questions about Tech Briefs are answered in the TSP's, but when no TSP is available, or you have further questions, write the Technology Utilization Officer at the center that sponsored the research at the address listed below.

Charles K. Kubokawa
Ames Research Center
Code AU: 230-2
Moffett Field, CA 94035
(415) 965-5554

Clinton T. Johnson
Hugh L. Dryden Flight Research Center
P. O. Box 273
Edwards, CA 93523
(805) 258-3311, Ext. 568

Donald S. Friedman
Goddard Space Flight Center
Code 704.1
Greenbelt, MD 20771
(301) 982-6242

John T. Wheeler
Johnson Space Center
Code AT3
Houston, TX 77058
(713) 483-3809

Raymond J. Cerrato
John F. Kennedy Space Center
Code SA-RTP
Kennedy Space Center, FL 32899
(305) 867-2780

John Samos
Langley Research Center
Mail Stop 139A
Hampton, VA 23665
(804) 827-3281

Paul Foster
Lewis Research Center
21000 Brookpark Rd.
Cleveland, OH 44135
(216) 433-4000, Ext. 6832

Aubrey D. Smith
Marshall Space Flight Center
Code AT01
Marshall Space Flight Center, AL 35812
(205) 453-2224

John C. Drane
NASA Resident Legal Office-JPL
4800 Oak Grove Drive
Pasadena, CA 91103
(213) 354-6420

Gilmore H. Trafford
Wallops Flight Center
Wallops Island, VA 23337
(804) 824-3411, Ext 201

Louis Mogavero, Director
Technology Utilization Office
Code KT
NASA Headquarters
Washington, DC 20546
(202) 755-3103

COSMIC

(Computer Software Management & Information Center)

AN ECONOMICAL SOURCE OF COMPUTER PROGRAMS DEVELOPED BY THE GOVERNMENT.

COSMIC is sponsored by NASA to give you access to over 1400 computer programs developed by NASA and the Department of Defense, and selected programs from other government agencies. It is one of the Nation's largest software libraries.

COSMIC charges very reasonable fees for programs to help cover part of their expenses—and NASA pays for the remainder. Programs generally cost from $500 to $1000, but a few are more expensive and many are less. Documentation is available separately and very inexpensively.

COSMIC collects and stores software packages, insures that they are complete, prepares special announcements (such as Tech Briefs), publishes an indexed software catalog, and reproduces programs for distribution. COSMIC helps customers to identify their software needs, follows up to determine the successes and problems, and provides updates and error corrections. In some cases, NASA engineers can offer guidance to users in installing or running a program.

COSMIC programs range from management (pert scheduling) to information science (retrieval systems) and computer operations (hardware and software). Hundreds of engineering programs perform such tasks as structural analysis, electronic circuit design, chemical analysis, and design of fluid systems. Others determine building energy requirements, optimize mineral exploration, and draw maps of water-covered areas using NASA satellite data. In fact, the chances are, if you use a computer, you can use COSMIC.

COSMIC is eager to help you get the programs you need. For more information about services or software available from COSMIC, fill out and mail the COSMIC Request Card in this issue.

COSMIC: Computer Software and Management Information Center

Suite 112, Barrow Hall, Athens, Georgia 30602 Phone: (404) 542-3265

WHERE IS THE WORLD'S LARGEST BANK OF TECHNICAL DATA

?

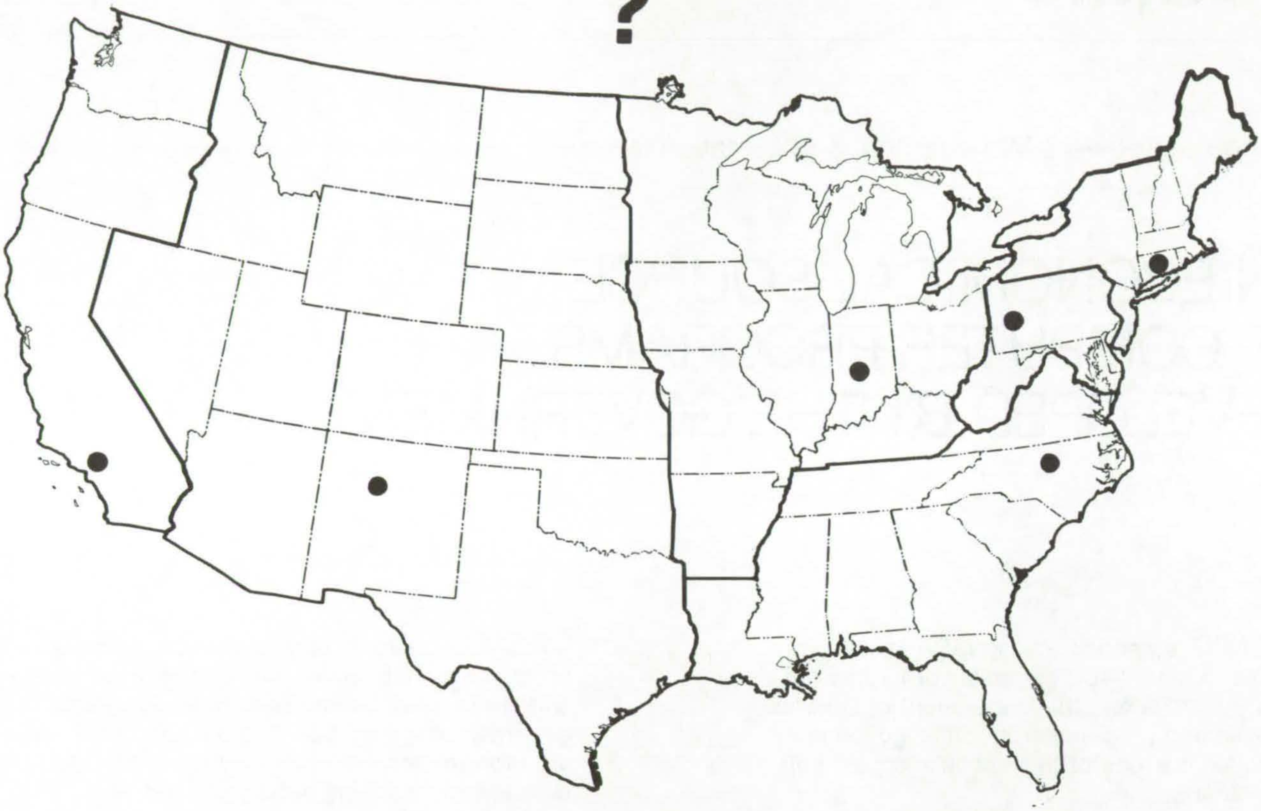

It's in Bloomington and Pittsburgh, it's in Storrs, Connecticut and Research Triangle Park, North Carolina; and it's in Albuquerque and Los Angeles.

NASA IAC's — INDUSTRIAL

You can get more information and more data on more technical subjects through NASA's network of IAC's than anywhere else in the world. About 8,000,000 documents and growing at the rate of 50,000 more each month!

Major sources include:

- 750,000 NASA Technical Reports
- Selected Water Resources Abstracts
- NASA Scientific and Technical Aerospace Reports
- Air Pollution Technical Information Center
- NASA International Aerospace Abstracts
- Chem Abstracts Condensates
- Engineering Index
- Nuclear Science Abstracts
- NASA Tech Briefs
- Government Reports Announcements

and many other specialized files on food technology, textile technology, metallurgy, medicine, business, economics, social sciences, and physical science.

The IAC's are one of the most economical ways of staying competitive in today's world of exploding technology. The help available from the network ranges from literature searches through expert technical assistance.

Literature Searches
Help in designing your search, typically from 30 to 300 abstracts in as narrow or broad an area as you need, and complete reports when you need them. The most complete "search before research" available!

Current Awareness
Consult with our applications engineers to design your personal program — selected monthly or quarterly abstracts on new developments in your speciality. It's like having your own journal!

Technical Assistance
Our applications engineers will help you evaluate and apply your literature-search results. They can help find answers to your technical problems and put you in touch with scientists and engineers at NASA Field Centers.

To obtain more information about how NASA's IAC's can help you —
Check the IAC box on the TSP Request Card in this issue,
Or write or call the IAC nearest you.

APPLICATIONS CENTERS

How to get reports and other documents discussed in this issue of Tech Briefs

Many of the innovations in Tech Briefs are described in detail in reports available at a reasonable cost through one or more of the IAC's. To order a report, call or write the IAC referenced at the end of the Tech Brief article at the address below. Be sure to list the titles and accession numbers (N76-..., N75-..., etc.) of those you wish to purchase.

Aerospace Research Application Center (ARAC)
Indiana University-Purdue University at Indianapolis
1201 E. 38th St.
Indianapolis, IN 46205
E. Guy Buck, Director
(317) 264-4644

Knowledge Availability Systems Center (KASC)
University of Pittsburgh
Pittsburgh, PA 15260
Edmond Howie, Director
(412) 624-5211

New England Research Application Center (NERAC)
Mansfield Professional Park
Storrs, CT 06268
Dr. Daniel U. Wilde, Director
(203) 486-4533

North Carolina Science & Technology
Research Center (NC/STRC)
P. O. Box 12235
Research Triangle Park, NC 27709
Peter J. Chenery, Director
(919) 549-0671

Technology Application Center (TAC)
University of New Mexico
Albuquerque, NM 87131
Stanley A. Morain, Director
(505) 277-4000

Western Research Application Center (WESRAC)
University of Southern California
University Park
Los Angeles, CA 90007
Radford King, Director
(213) 746-6132

NASA INVENTIONS AVAILABLE FOR LICENSING

Over 3,500 NASA inventions are available for licensing in the United States - both exclusive and nonexclusive.

Nonexclusive Licenses

Nonexclusive licenses for commercial use are encouraged to promote competition and to achieve the widest use of inventions. They must be used by a negotiated target date but are usually royalty free.

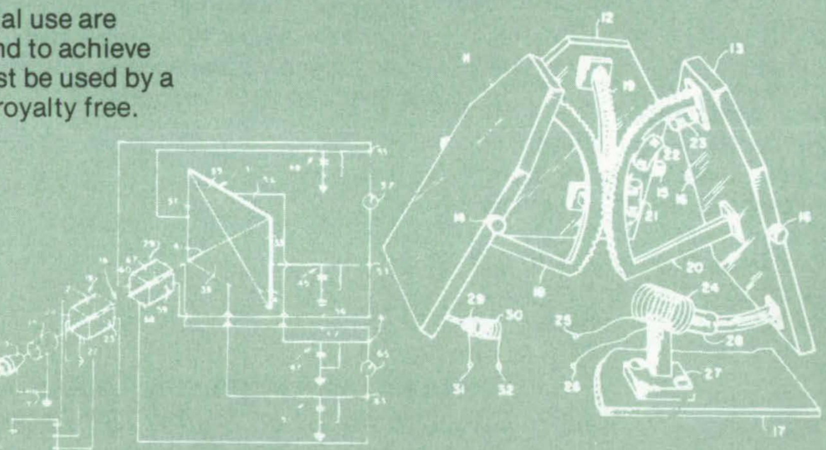

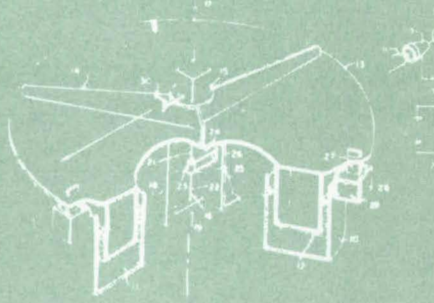

Exclusive Licenses

An exclusive license may be granted to encourage early commercial development of NASA inventions, especially when considerable private investment is required. These are generally for 5 to 10 years and usually require royalties based on sales or use.

The NASA patent licensing program also provides for licensing of NASA-owned foreign patents. In addition to inventions described in Tech Briefs, "NASA Patent Abstract Bibliography," containing abstracts of all NASA inventions, can be purchased from: National Technical Information Service, Springfield, Va., 22151. This document is updated semi-annually.

Patent Licenses and the NASA Tech Brief

Many of the inventions reported in Tech Briefs are patented or are under consideration for a patent at the time they are published. When this is the case, the current patent status is described at the end of the article; otherwise, there is no statement about patents. **If you want to know more about the patent program or are interested in license for a particular invention, write the Patent Counsel at the NASA Field Center** that sponsored the research. Be sure to refer to the NASA reference number at the end of the Tech Brief.

Robert F. Kempf
NASA Headquarters, Code GP
400 Maryland Ave., S.W.
Washington, DC 20546
(202) 755-3932

Darrell G. Brekke
Ames Research Center
Mail Code: 200-11A
Moffett Field, CA 94035
(415) 965-5104

John O. Tresansky
Goddard Space Flight Center
Mail Code: 204
Greenbelt, MD 20771
(301) 982-2351

Marvin F. Matthews
Lyndon B. Johnson Space Center
Mail Code: AM
Houston, TX 77058
(713) 483-4871

James O. Harrell
John F. Kennedy Space Center
Mail Code: SA-PAT
Kennedy Space Center, FL 32899
(305) 867-2544

Howard J. Osborn
Langley Research Center
Mail Code: 313
Hampton, VA 23665
(804) 827-3725

Norman T. Musial
Lewis Research Center
Mail Code: 500-113
21000 Brookpark Road
Cleveland, OH 44135
(216) 433-4000 Ext. 346

Leon D. Wofford, Jr.
Marshall Space Flight Center
Mail Code: CC01
Marshall Space Flight Center, AL 35812
(205) 453-0020

Monte F. Mott
NASA Resident Legal Office-JPL
4800 Oak Grove Drive
Pasadena, CA 91103
(213) 354-2700

NEW PRODUCT IDEAS

NEW PRODUCT IDEAS are just a few of the many innovations described in this issue of NASA Tech Briefs and having promising commercial applications. Each is discussed further on the referenced page in the appropriate section in this issue. If you are interested in developing a product from these or other NASA innovations, you can receive further technical information by requesting the TSP referenced at the end of the full-length article or by writing the Technology Utilization Office of the sponsoring NASA center (see page A4). NASA's patent-licensing program to encourage commercial development is described on page A8.

Portable Solar Radiometer

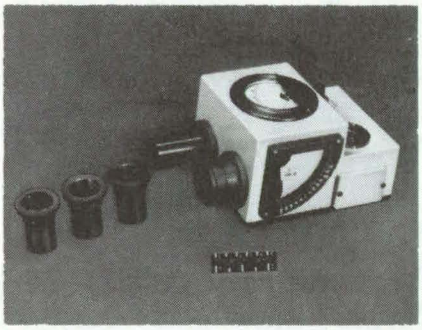

Stack-plume effluents can be measured with a relatively-inexpensive four-channel instrument. It measures the density of particles and aerosols and the concentration of nitrous and sulfurous oxides. The instrument measures the absorption of the Sun's light at four wavelengths: two in the visible region and one each in the IR and UV regions. It is calibrated by measuring "unobstructed" Sunlight in the region near a stack plume. The boresighted instrument is easy to use, and tests of its effectiveness show agreement with measurements made inside of monitored smokestacks.
(See page 548.)

Viscoelastic Foam Cushion

A flexible urethane foam developed for aircraft seats has already had a number of successful applications and has commercial potential in many more areas. The foam equally distributes applied pressure along the interface, will assume the contour of pressing objects, but returns to its own shape when the pressure is removed. It strongly attenuates vibration and impact energy, being firm under impact yet soft to the touch.
(See page 582.)

Ironless-Armature Brushless Motor

A new high-speed torque motor has a low electrical time constant and no frictional torques. Resistance heating is conducted through the housing rather than through the bearings where it could be detrimental. Possible applications include position servos and momentum wheels. The motor utilizes a stator containing the windings and a rotor comprising 12 permanent samarium cobolt magnets that provide a high magnetic flux across the airgap. Hull devices are mounted 120 degrees apart on a sensor ring for commutation.
(See page 530.)

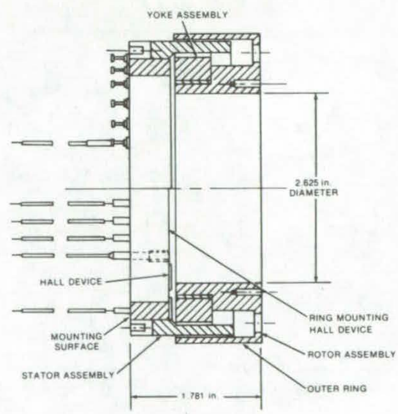

Direct-Reading Inductance Meter

The low-inductance values typical of miniature coils used in breadboarding RF circuits can be measured directly, using a new TTL-implemented meter. Inductances in this range are normally difficult to measure and require complex instrumentation. The meter is of intermediate accuracy, but is as easy to operate as a bench ohmmeter and is relatively inexpensive to manufacture. The circuit consists primarily of a reference and a variable-frequency oscillator. When an unknown inductance is connected in series with larger reference inductance in an L/C tuned circuit, the resonant frequency of the tuned circuit shifts downward. For small inductances, this frequency change is nearly linear function of the unknown inductance.
(See page 527.)

Indicated Mean Effective Pressure Instrument

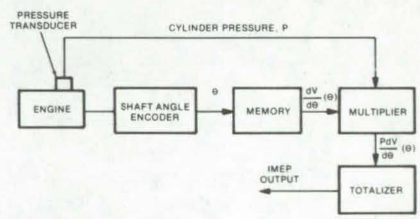

Real-time measurement of the IMEP and mass flow within an internal-combustion engine cylinder is possible with a new analytical instrument. The instrument uses a sensor of the shaft angle to determine the instantaneous volume of the cylinder and a conventional transducer to monitor pressure. Data from these two sources are processed electronically (using read-only memories) to calculate the instantaneous work performed by the engine. Using a digital summation technique, the instantaneous work is integrated to give the work for an entire engine cycle. The needed data are available immediately, and no post-run data reduction is necessary.
(See page 601.)

Forming Hard Aluminum in Complex Shapes

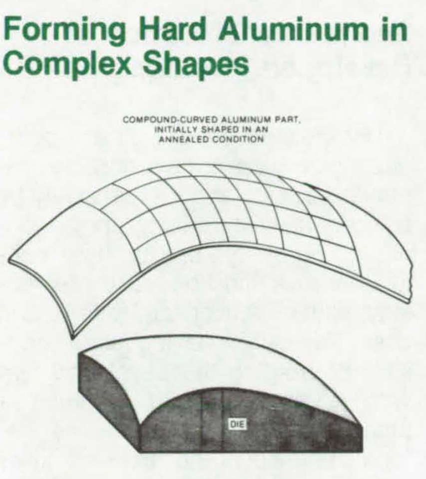

Many of the difficulties normally encountered in forming complex shapes of aluminum in the hard, T8, condition are overcome using a new technique. It could allow the use of hard lightweight aluminum in applications previously limited by formability restrictions. The procedure is a straightforward extension of current forming practices and requires no special training or equipment. Aluminum in a soft (TO) condition is stretched and marked with gridlines. It is then solution treated, refrigerated, and stretched. The controlled stretching induces an intermediate temper that allows the metal part to be brought to the T8 condition, using standard techniques.
(See page 635.)

Aluminum Transfer Method for Plating Plastics

A very hard and smooth film of metal can be bonded to plastics, using a new electroless plating technique. It can be used to plate plastic parts that are formed in molds. When the part is cast, a film of aluminum powder is placed inside the mold; an electroless procedure is used to plate another metal, such as nickel, onto the plastic. No special surface preparation is required; the plate is very smooth and follows the surface detail of the part exactly. The process has been useful with cast epoxy resins and could possibly be adapted to other production methods, such as blow molding and injection molding.
(See page 646.)

Catalysts for Low-Energy Aldehyde Processes

A catalyst for the "oxo" process (hydroformulation), used in industry to produce aldehydes, allows the process to be carried out under conditions much milder than those currently used. If proved effective on a large scale, this new catalyst could contribute substantial savings in both energy and dollars. The catalyst is a transition metal complex, such as dicobalt octacarbonyl, bonded to a polymer such as poly 4-vinyl pyridine via ultraviolet light. With the catalyst, hydroformulation can be carried out at ambient conditions. In addition to producing aldehydes as end products, the process could also be useful in the formation of intermediates for the liquefaction of coal.
(See page 576.)

Multiple-Bubble Detector

A new multiple-bubble detector uses a pair of passive replicators in conjunction with chevron-stretcher detectors. The addition of the passive replicators eliminates problems with stripout that can otherwise occur in the start/stop mode. This device allows outputs to be increased to around 10 mV. The use of two replicators allows two stretchers to be used, thus halving the number of elements needed and similarly reducing the time needed for stretchout. The output can be further increased by adding even more replicator and detector sections.
(See page 493.)

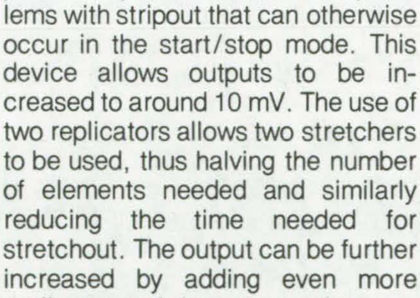

Document Restoration by Computer Techniques

A computerized unit combines optical image enhancement and digital data analysis to restore legibility to old or faded documents. The system not only improves contrasts but also reduces the relative intensity of "noise" (unwanted black dots, stains, and so forth). Broken lines are restored by digital-logic techniques, and the edges of letters are sharpened by using high-pass digital filters. The system includes an electro-optic scanner, a video tape and TV screen, and a microprocessor unit that controls the logic circuitry. The enhanced document can be displayed on the TV screen and reproduced as hard copy or microfilm. The potential applications market in the United States alone is estimated at about 50 million pages of documents in archives, libraries, museums, and law enforcement agencies.
(See page 651.)

Transducer Bonding Kit

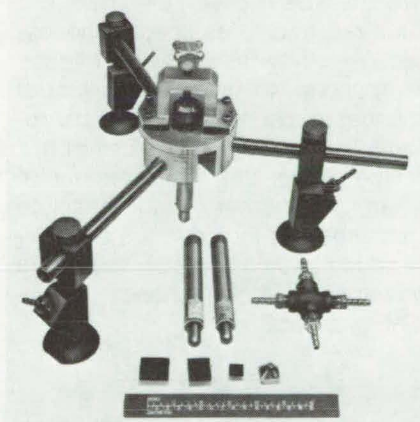

A relatively inexpensive kit can save time in affixing transducers to surfaces too large or convoluted to allow the use of C-clamps or weights. It was developed to bond small rectangular strain gages to aluminum or titanium surfaces, using epoxy resins, but could be used with other parts and surface types. The loading pressure can be set precisely and monitored during curing. Nevertheless, the kit is easy to set up and use. Adapters allow bonding in limited-access areas, and the kit itself can be used on the underside of large planar surfaces. A vacuum-hold system attaches the kit to the surface, and an adjustable-spring clamp is used to set the pressure.
(See page 641.)

Differential-Optoacoustic Absorption Detector

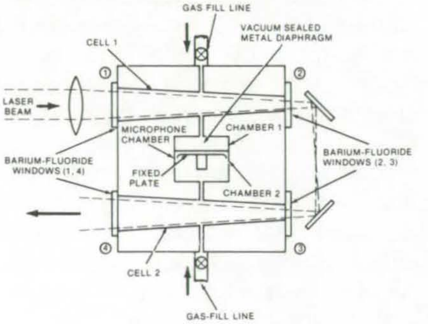

Applications ranging from airborne pollution detection to chemical analysis could make use of a new system for measuring laser-excited components in gaseous mixtures. It consists of a laser, an optical chopper, a novel double-cell gas compartment, and detector circuitry. Devices of this type are often referred to as spectrophones, because they use a capacitance microphone to measure pressure changes caused by optical absorption in a gas. The double cell in this device allows the measurement of differential rather than absolute pressures and thus offers a sensitivity nearly 100 times better than for a conventional spectrophone.
(See page 552.)

Fast Measurement of Bacterial Susceptibility to Antibiotics

A method has been devised for fast measurement of the sensitivity of bacteria in body fluids to a variety of antimicrobial agents. A luciferase/luciferin assay for ATP is the basis for this technique, which reduces the 2- or 3-day delay normally associated with this type of analysis to less than a working day. The technique can be used to determine the presence of infection as well as the susceptibilities to several antibiotics. The method itself could be incorporated into a marketable system that would have technical capabilities and speed superior to currently available technology. A simpler version could be used as an ATP screening version that could, for instance, reduce the culturing requirements in hospital urinalysis by as much as 50 percent. In the process, nonbacterial ATP is removed to determine the presence of infection; if infection is present, the sample is treated with antibodies, incubated, and tested for ATP. The gains in time result from the speed of the luciferase/luciferin technique and the fact that each bacterial strain need not be isolated and cultured separately.
(See page 592.)

Image Intensification of Developed Photographs

Underexposed or other poor-quality developed film can be enhanced quickly and inexpensively by using a new autoradiography technique. Formerly, use of this technique was limited because of problems with effectiveness, safety, and cost. Basically, the technique consists of treating the developed film with a chemical that contains a beta-emitting radioisotope. The isotope attaches to the exposed silver on the film; then the treated beta-emitting film is used to expose a new negative. By replacing the usual radioisotope solution with an organic sulfur compound, (e.g., a thiourea) containing S-35, virtually all the disadvantages previously associated with autoradiography can be eliminated. Processing is simplified and speeded up, radiation hazards are reduced, and the original film is not degraded.
(See page 553.)

PATENT LICENSES RECENTLY GRANTED BY NASA FOR COMMERCIAL USE OF NASA-OWNED INVENTIONS

The patent licenses listed below have been recently awarded by NASA as part of its program to encourage the commercial application of its new technology. For information on how you may obtain nonexclusive or exclusive license for the commercial use of NASA inventions, see page A8 of this issue.

A nonexclusive license to Fibeco, Incorporated, Wickliffe, Ohio, for U.S. Patent Application Serial No. 686,449, covering an invention entitled "Ceramic Thermal Protective Coating Withstands Hostile Environment of Rotating Turbine Blades."

A nonexclusive license to Plasma Technology, Incorporated, Torrance, California, for U.S. Patent Application Serial No. 616,528, covering an invention entitled "Bearing Material."

A nonexclusive license to Fiberite Corporation, Winona, Minnesota, for U.S. Patent No. 3,745,149, covering an invention entitled "Preparation of Polyimides From Mixtures of Monomeric Diamines and Esters of Polycarboxylic Acids."

A nonexclusive license to Avco Corporation, Wilmington, Massachusetts, for U.S. Patent No. 3,916,060, covering an invention entitled "Fiber Modified Polyurethane Foam."

A nonexclusive license to Union Carbide Corporation, Rye, New York, for U.S. Patent No. 3,733,463, covering an invention entitled "Temperature Control System With a Pulse Width Modulated Bridge."

Electronic Components and Circuits

Hardware, Techniques, and Processes

Books and Reports

Computer Programs

Improved Resolution for Sensor Arrays

An interpolation algorithm, simple enough to hard wire by hand, improves resolution by a factor of 5 to 20.

Caltech/JPL, Pasadena, California

A hard-wire interpolation scheme for an array of discrete sensors extends the resolution and accuracy from one element width to one-fifth and, in some cases, to one-tenth of an element width or less. The technique was developed for an optical star tracker that uses charge-coupled devices (CCD's) as sensors, and accuracy was increased from one part in a hundred to the order of one part in a thousand. The same approach could be adapted to other optical sensing requirements (e.g., Sun sensors) or nonoptical sensing when the sensed events are sufficiently numerous to be characterized statistically (e.g., electrons or X-rays).

The scheme is a hard-wired algorithm that is kept relatively simple and easy to implement by controlling the input optics to the array of CCD's. The distribution and input of a point source sensed by the array is characterized by a point-spread function as shown in Figure 1a. The shape of this function depends on the lenses and optics used.

An algorithm circuit compares charge levels in adjacent charge-coupled elements to determine the centroid of the optical input. However, the array, being a discrete-element device, senses the point spread as a discontinuous function, integrated over discrete intervals (Figure 1b).

The centroid of the image point-spread function (and thus the position of the source) is determined from its line-spread function (Figure 1c). The point-spread function is assumed to be symmetrical, and the procedure is analogous to finding the centroid of a solid of revolution: the integral of the moment (i.e., of the line-spread function) is divided by the integral of the density function (i.e., total flux density). For the discrete case, the centroid is determined by the sum of the individual moments divided by the flux for all intervals.

The solution is not straightforward, however, because although the interval sizes are known (the size of the CCD), their position relative to the centroid is not known. This means that in integrating over the intervals in Figure 1c, say along the X axis, the value of X_0 is not known. (The position of the centroid, I, is of course known within an error of Δx, a CCD element dimension, but the point of the algorithm is to achieve better resolution.) This problem is solved without using complex and expensive circuitry by requiring that the actual line-spread function be nearly linear from edge to edge, or in other words, performing a linear interpolation.

In practice, there is considerable tolerance in how close to linear the line-spread function must be. A catadioptric system, in which the center part of the lens is occluded, has been found to work well. (This lens flattens out the intensity peaks in Figure 1.)

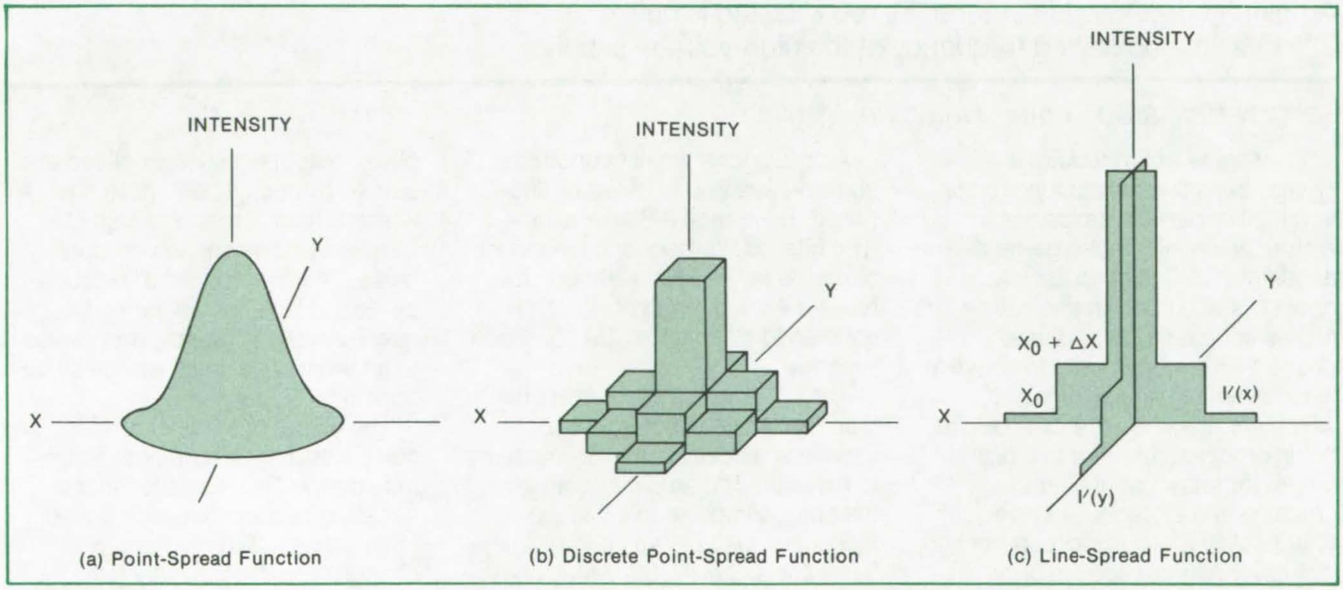

Figure 1. The **Optical Input to an Array** is characterized by a point-spread function as in (a), where the XY plane is the plane in the array and the "vertical" axis is the intensity. Because the CCD's are discrete devices, the function is sensed as in (b). The line-spread function in (c) completely represents the point-spread function because of symmetry.

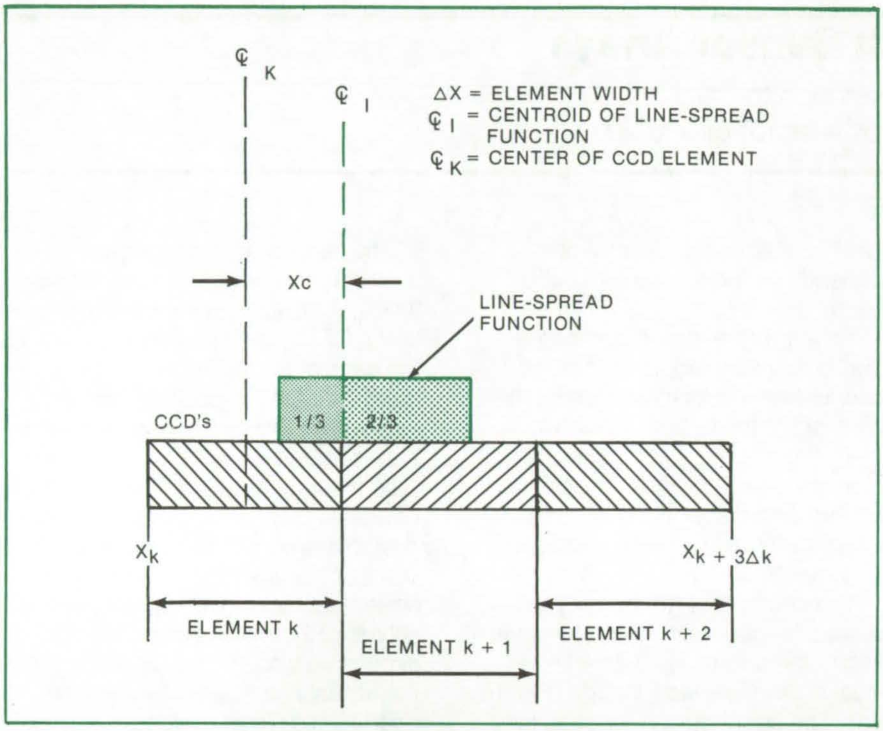

Figure 2. The **Interpolation Geometry** is shown for one axis of the two-element case. For simplicity, the line-spaced function is taken as perfectly flat (the analog to Figure 1c would be a flat rectangular slab); the intensity level is taken equal to one; and the image width is one element wide. The algorithm finds the centroid of the line-spread function relative to the center of the CCD (in the example above, the center is 4/6 of an element width beyond the center of element K).

The interpolation scheme using only two elements is shown in Figure 2. In the simplified case shown, the charge in each CCD is proportional to the percent of the line-spread function that overlaps that CCD; because the function is flat, this relates directly to the centroid of the line-spread function and thus the point-spread function. The accuracy of the algorithm can be increased by using three or more elements for the interpolation, and the line function need not be actually flat to achieve a marked improvement in resolution.

This work was done by Willis C. Goss of **Caltech/JPL.** *For further information, Circle 1 on the TSP Request Card.*
NPO-13745

Charge-Sensitive Amplifier With Notched Frequency Response

Amplifier bandpass is centered at 160 kHz and is nulled at 325 kHz, the operating frequency of the high-voltage supply.

Langley Research Center, Hampton, Virginia

In systems which require a charge-sensitive pickup tube to convert light or particle emissions to electrical signals, a charge-sensitive amplifier (CSA) is often used to boost signal output. In one such pickup scheme a proportional-counter (PC) tube is used to convert X-ray events to analog signals, which are amplified in a CSA before being processed further in a digital circuit for subsequent event counting and storage. However, the effects of noise, pulse pileup, and dc instability (experienced in prior CSA's) tend to deteriorate amplifier output signal quality.

A circuit for a small economical charge-sensitive amplifier is illustrated. It features a Blankenship-type filter with a frequency response centered at 160 kHz. Although four tubes are used, each of which is coupled to a separate CSA, only one is shown.

The PC is series coupled via the tube high-voltage power supply to introduce a positive charge impulse to the CSA. The amplifier converts the charge impulse to a voltage mode step with a 50-μs decay time. Since the signal is sufficiently above noise level, the CSA outputs are multiplexed for economy. The multiplexer output signal is amplified and passed through a band-pass filter which further attenuates high-frequency noise and low-frequency noise. The band-pass null frequency, 325 kHz, is the operating frequency of the PC supply and serves to attenuate this noise source by an additional 30 dB.

The output of the filter is a bipolar pulse with a maximum peak amplitude of 5 V. This is applied to the negative inputs of two high-speed comparators. The comparators change output states only if the pulse applied to the negative inputs exceeds the dc bias voltages refer-

enced to the positive inputs. In one comparator a dc bias is used which is termed the lower level reference; the other comparator is biased 36.32 mV above the first.

If a pulse is applied which has a peak height between the two reference levels, then the anticoincidence gate illustrated enables it to pass. Both comparators and the anticoincidence circuit operate in a window discriminator mode, so termed because the circuit counts only those pulses having amplitudes between the two fixed reference levels during a commanded time period. The discriminator outputs the data to a memory and then counts the next series of data. The output is transferred to the event counter in the digital portion of the CSA.

This work was done by David F. Stout and M. D. Mason of Martin Marietta Corp. for **Langley Research Center.** *For further information, Circle 2 on the TSP Request Card.*
LAR-11317

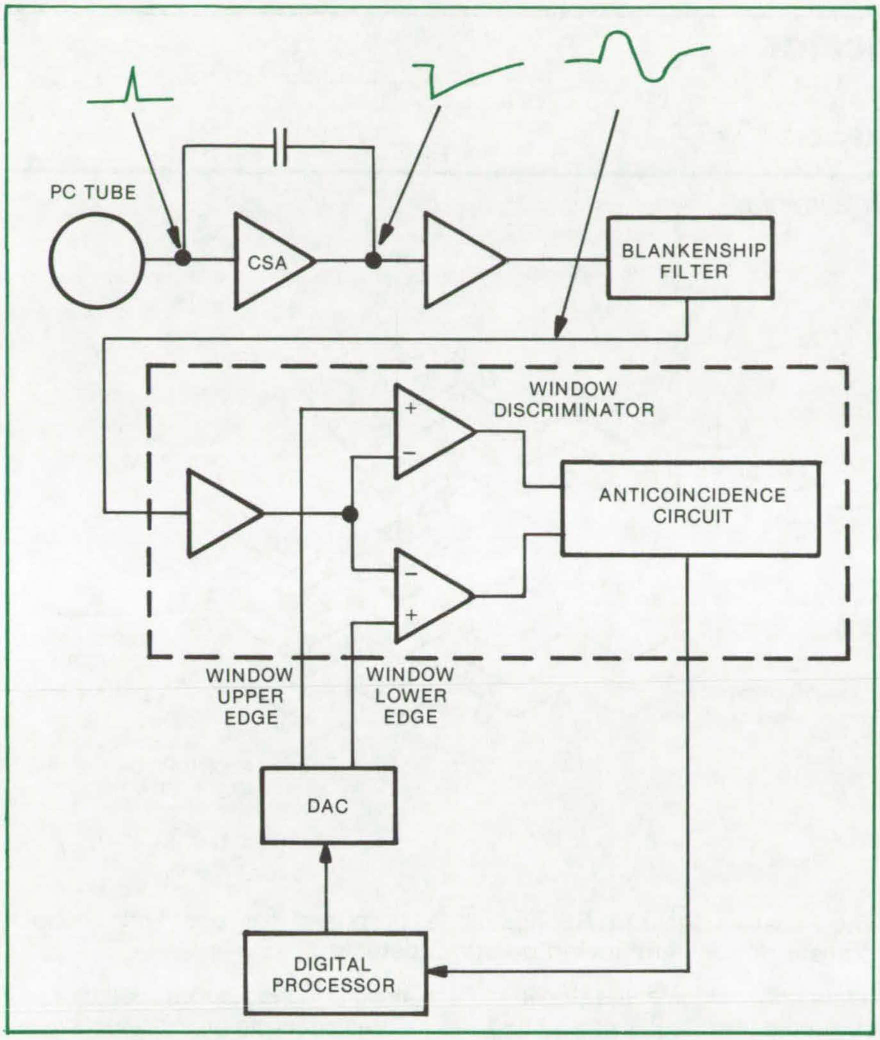

The **Charge-Sensitive Amplifier** outputs a bipolar pulse with a maximum peak of 5 volts. This is applied to the negative inputs of two high-speed comparators. These change output states only if the pulse applied to the negative inputs exceeds the dc bias on their positive inputs. One of the window-discriminator inputs is biased 36.32 mV above the other. The output is transferred to a digital event counter.

Improved Shelf for Electronic Modules

An improved cabinet for electronic equipment is less expensive to manufacture because tolerances can be relaxed. Airflow is improved threefold by a redesigned bottom slide assembly. The elimination of a load-bearing crosspiece reduces installation time yet allows the new assembly to be mounted on existing cabinets.
(See page 632.)

Rigid Cable Support for Blind Installations

A mechanical support structure eliminates the need for line clamps and raceways. It can support electrical cables or hydraulic, pneumatic, and cryogenic lines. The lightweight supports damp vibrations and can be placed on a frame or bulkhead webs for cable penetration and on brackets for additional support.
(See page 639.)

Parylene Coating for Circuit Components

An inexpensive parylene coating is placed over components to be encapsulated in plastic. The coating protects the devices from harmful substances generated during degradation of the plastic-packaging material. It also protects against heat and humidity.
(See page 638.)

A Passive Chevron Replicator

Nondestructive read-out from bubble-domain memories with guardrail detectors

Langley Research Center, Hampton, Virginia

A proposed new passive replicator uses two chevron tracks, one inverted with respect to the other. It should result in increased replicator margins approaching those of other portions of the device.

This replicator design provides a replicate function between the device storage area and the guardrail detector in order that nondestructive read-out of the memory can be achieved. The use of guardrail detectors in magnetic domain (bubble) circuits is a proposed method of increasing detector signal output by increasing detector size without dedicating an excessive amount of device chip area to the detector portion. Bubbles sensed in a guardrail detector are dumped into a safe area outside the device region and do not return to the storage area. While both active (requiring current command pulses for operation) and passive (automatically replicating any bubble which passes through the replicator) replicators will provide this replicate function, passive replicators are desirable when all bubbles passing through are to be detected, since power consumption and number of control leads are both reduced.

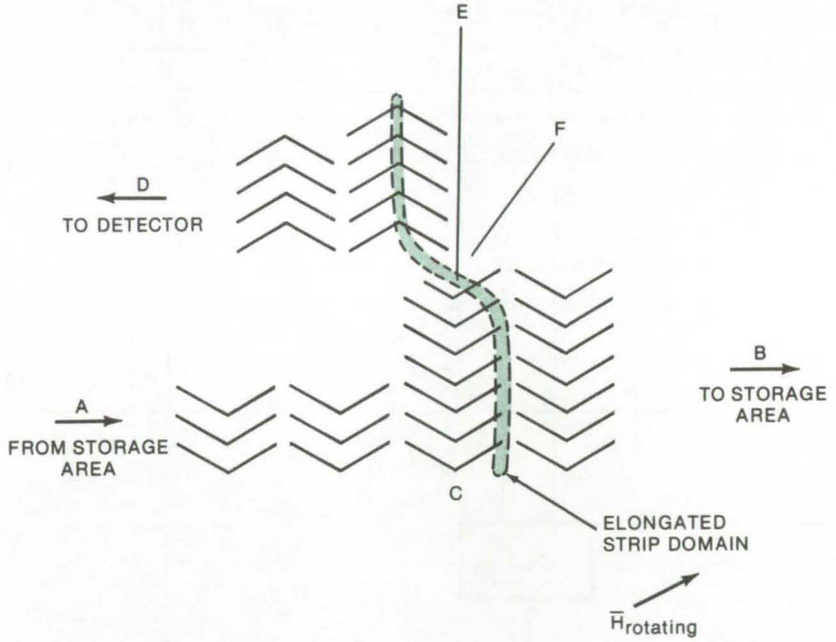

The **Passive Chevron Replicator** is proposed for use with bubble-domain devices employing guardrail detectors.

As seen in the illustration, a bubble from the main storage area of the device is propagated along chevron path A. When it reaches position C, it is elongated into a large strip that simultaneously exists in the lower chevron path A to B and the upper chevron path D. This is accomplished by the presence of like magnetic poles in both Permalloy chevron tracks (for a bubble at position C) due to the interaction of the Permalloy chevron elements with the in-plane rotating magnetic field used for domain propagation. The Permalloy bar (E) aids in bubble strip-out into the top track. As the field continues to rotate, that portion of the strip in chevron track A to B is propagated in B direction (to the right in the illustration) while the portion in track D is propagated to the left.

The presence of Permalloy bars E and F prevent the elongated strip from being pulled off the edge elements of the two tracks as the oppositely directed propagation develops. The magnetic poles generated at the ends of these bars repel the elongated strip, forcing it to assume the position depicted in the illustration. Whenever the elongated domain is in the depicted position, the repelling (collapsing) magnetic poles generated by the rotating field at the bottom ends of bars E and F cause the elongated strip to break in the region between the two tracks. Once broken, the two halves become separate bubble strips. One propagates along B and returns the initial data to the storage area, and the other propagates along D to the guardrail detector.

While replication for detection was used to simplify the operation description, replicators can be employed to provide data for other uses. Also, the exact lengths and placements of Permalloy elements E and F and the top chevron element in A to B in the area where the two tracks overlap are not necessarily those which will be ultimately employed in the finalized device. Optimization for best operation will determine these.

This work was done by Thomas R. Oeffinger and Leonard R. Tocci of Rockwell International Corp. for **Langley Research Center.** *No further documentation is available.*

Title to this invention has been waived under the provisions of the National Aeronautics and Space Act [42 U.S.C. 2457(f)] to the Rockwell International Corp., 3370 Miraloma Ave., Anaheim, California 92803. LAR-11906

New Passive Replicator for Bubble Domain Devices

Bar-spacing tolerances are relaxed in replicator suitable for low-drive field.

Langley Research Center, Hampton, Virginia

A multiple-bar passive replicator that works over a large range of spacings has been designed for low-drive field operation. It is an alternative to existing passive replicators, which have good margins but require that the Permalloy-to-garnet spacing be smaller than desirable for low-drive field operation. The new replicator uses long bars instead of chevrons to do the stretching. The bars are arranged so that at high bias the failure to expand into a strip does not cause hard errors (i.e., the bubble will continue to propagate although it does not replicate).

The arrangement in Figure 1 is particularly attractive as the bars may be made quite long, resulting in a deep potential well at one end which has a considerable stripping effect even at high bias. When the bubble does not elongate, it simply continues propagating in the main chevron track whether the Permalloy spacing is large or small. Measurements on a 16-μm per period device, of the design shown in Figure 1, indicate a bar-to-garnet spacing of 0.58 μm and a margin of 12-to-14 Oe at 50 Oe. The existing replicator design has less than half of this margin. About 2 to 4 Oe are lost at the low-bias end due to stripping of the bubble from the first chevron back to the parallel bars for the field orientation $\mathbf{H}_{stripout}$ as indicated.

Stroboscopic measurements revealed that the situation shown in Figure 2 occurs at low-bias fields and results in a splitoff bubble which eventually runs down the bar to the other end and pops off. There are several alternatives to prevent this, and the simplest is to add one or more additional bars as shown in Figure 3. In this methods, the repulsive poles closest to the chevrons serve to repel the bubble and prevent stripout. Another alternative is to rotate the end bar as in Figure 4 to retard stripout as low bias.

At low bias and small spacings, one other observed failure mode produces stray bubbles. This is caused by cutting, due to the bars adjacent to the cutter element. It is believed to be a result of the large separation between chevron tracks which can be eliminated by moving the tracks closer together. Another alternative is to shorten the bars as indicated in Figure 5.

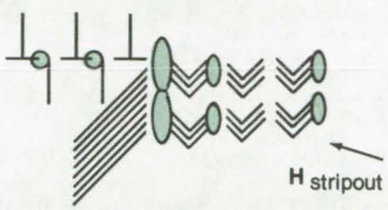

Figure 1. The **Basic Multiple-Bar Replicator** uses long bars to stretch the bubble domain.

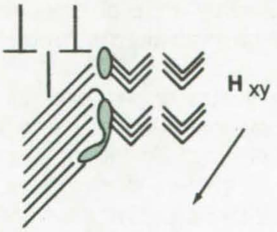

Figure 2. A **Splitoff Bubble** may be formed when the field reaches the orientation above.

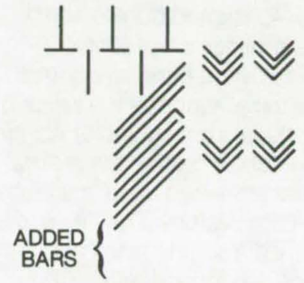

Figure 3. **Additional Bars** retard stripout because the repulsive poles closest to the chevrons repel the bubble.

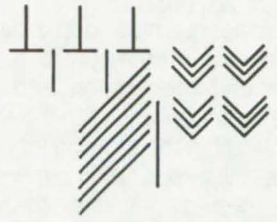

Figure 4. A **Rotated End Bar** will also retard stripout that occurs at low-bias fields.

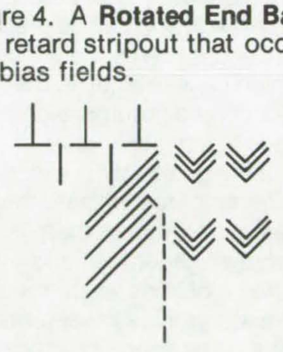

Figure 5. **Shortened Bars** adjacent to the cutter element inhibit the creation of stray bubbles that tend to form by cutting.

This work was done by Peter K. George and Tsutomu Kobayashi of Rockwell International Corp. for **Langley Research Center.** *No further documentation is available.*

Title to this invention has been waived under the provisions of the National Aeronautics and Space Act [42 U.S.C. 2457(f)], to the Rockwell International Corp., 3370 Miraloma Avenue, Anaheim, California 92803.
LAR-11997

Continuous-Data FIFO Bubble Shift Register

Simple loop first-in-first-out bubble-memory shift register has continuous storage capability.

Langley Research Center, Hampton, Virginia

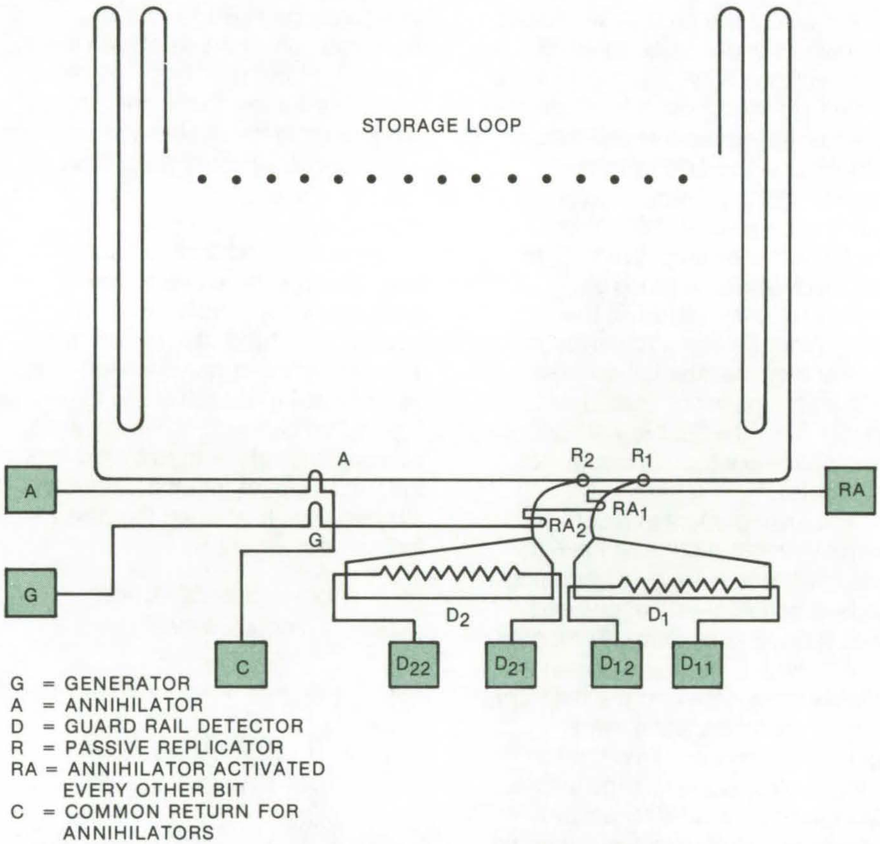

The **FIFO Shift Register** is constructed from passive replicator and annihilator combinations. In the design above, $(R_1 - RA_1) - (R_1 - RA_2) = 2N + 1$, and $(R_1 - A) = (R_1 - G) = (R_1 - D_1) = (R_1 - D_2)$, where (A - B) is the bit difference between components A and B.

A newly-designed bubble shift register simplifies chip-control electronics by enabling all control functions to be alined at the same bit position. It uses only unipolar control pulses, which simplifies the matrixing electronics when used in a large multiple-chip system. The detectors are removed from the track and can be arranged independently without affecting the storage loop. Furthermore, the device can be operated in alternative-bit mode which provides higher detector output and less bubble interaction.

In the present single-loop organization, there are three control functions on a chip (generation, annihilation, and detection). With the detection circuit in the storage loop, there is a finite separation between the detector and annihilator positions. The generator is located in a separate branch and can be placed at the same position as the annihilator, which causes a gap in the memory loop and requires a chip-aline mode in a multiple-chip system. If the generator is alined with the detector to eliminate the gap in the memory loop, there is a delay between generation and annihilation functions which requires additional electronics to keep track of the status and operating mode of the chip.

An ideal situation would be to pull the detector out of the track and aline it with the generator and annihilator simultaneously, eliminating both the data gap in the storage loop and the time delay between the generator and annihilator. This can be achieved by replicating any incoming bubble into two separate bubbles to maintain nondestructive readout. The existing active replicator requires a bipolar control pulse which complicates the driver network. While the passive replicator does not require any control currents, it replicates bubbles continuously and prohibits detector operation in an alternative-bit read mode.

The illustrated design can avoid the above problems by using passive replicator and annihilator combinations. As shown, there are two parallel detector branches connected to the main storage loop. Bubbles are replicated toward each branch by two passive replicators (R_1 and R_2). There are two annihilators (RA_1 and RA_2) connected in series and placed in each branch. They are arranged so that the distance between R_1 and RA_1 differs from the distance between R_1 and RA_2 by an odd number of bits. If RA_1 and RA_2 are energized alternately, all even bits will propagate to one detector when bubbles are replicated toward detectors, and all odd bits will propagate to the other. With these two detectors placed in the same bridge circuit, a full data rate can be reclaimed.

This work was done by Thomas T. Chen of Rockwell International Corp. for **Langley Research Center.** *No further documentation is available.*

Title to this invention has been waived under the provisions of the National Aeronautics and Space Act [42 U.S.C. 2457(f)], to the Rockwell International Corp., 3370 Miraloma Avenue, Anaheim, California 92803.
LAR-11862

Multiple-Bubble Detector

Detector output is improved by using passive replicators.

Langley Research Center, Hampton, Virginia

A new multiple-bubble detector is a large-output chevron stretcher that can read the first and subsequent bits adjacent to the detection element in a start/stop mode. The expansion of a bit in a long chevron stretcher takes several rotating field cycles due to the finite wall mobility of a strip or a bubble. For instance, measured expansion rates for 16-μm devices indicate that (for SmGaYIG) the strip expands about 100 chevrons in one field rotation.

Typical sensitivities for this length of stretch are about 1.0 mV/ma, which limits the outputs to typically 5 mV at room temperature, and the rated output is further limited to from 2.5 to 3 V when the device must operate over the -10° to 70° C temperature range. The associated sense chip is limited to a threshold below 2.5 mV, and the number of possible choices are restricted. About 10 mV is regarded as being more desirable for noise immunity and general system considerations.

Detector output can be improved, without running into the problem of strip-out in the start/stop mode, by using a passive replicator in connection with a multiple-bubble detector, as shown in the figure.

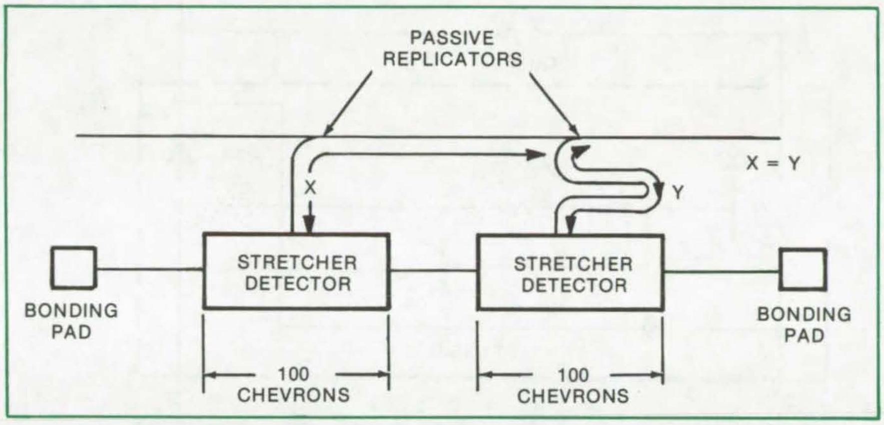

The **Multiple-Bubble Detector** is a segmented multiple-input detector. Bubbles are fed into each section simultaneously.

The distances between each passive replicator and its detector are such that the two replicated versions of the original bubble pass through their detectors simultaneously, thus giving rise to the equivalent of a 200-element stretcher output. Stretch-out can be achieved in each section of the detector, even in the start/stop mode, because each section is only 100 elements. A still higher output can be obtained, if required, by adding an additional replicator-and-detector section. The dummy detector can be incorporated either in front of the active detector or on a separate portion of the chip. With the dummy in front, the dummy and active detectors can be matched exactly.

This work was done by Peter K. George of Rockwell International Corp. for **Langley Research Center.** *No further documentation is available.*

Title to this invention has been waived under the provisions of the National Aeronautics and Space Act [42 U.S.C. 2457(f)], to the Rockwell International Corp., 3370 Miraloma Avenue, Anaheim, California 92803.
LAR-12043

Inductorless Voltage Multiplier/Converter

Cascade-connected stages charge capacitors to the desired output.

Caltech/JPL, Pasadena, California

A new voltage multiplier configuration consists of identical stages connected in cascade to obtain a desired output voltage. It relies on neither single-coil inductors nor transformers to implement the design. In the circuit a number of capacitors are charged, each to the multiplier supply voltage; the capacitors are then discharged in series into an external load. The multiplier supply voltage times the number of capacitor stages plus the original voltage equal the output voltage of the multiplier. One major advantage of this multiplier is that the voltage rating of each capacitor need not appreciably exceed the initial supply voltage rating, an advantage over conventional series-connected voltage multipliers where high-voltage (e.g., more costly) capacitors are charged up to the output voltage.

A schematic of a three-stage version of the multiplier is illustrated. The control voltage (V_{in}) varies

(continued on next page)

the output voltage which can either be taken from both output terminals or from one output terminal to ground. The output voltage is linearly proportional to the resistor R_i input current developed by the control voltage. In the implementation, all like components are similar (the transistors are type 2N3742, or equivalent, and the resistors are 22 megohms each except R_i which is 1 megohm). System gain depends primarily on the ratio between the intrastage and input resistor, and the available output voltage can be arbitrarily increased to any practical value by increasing the number of stages.

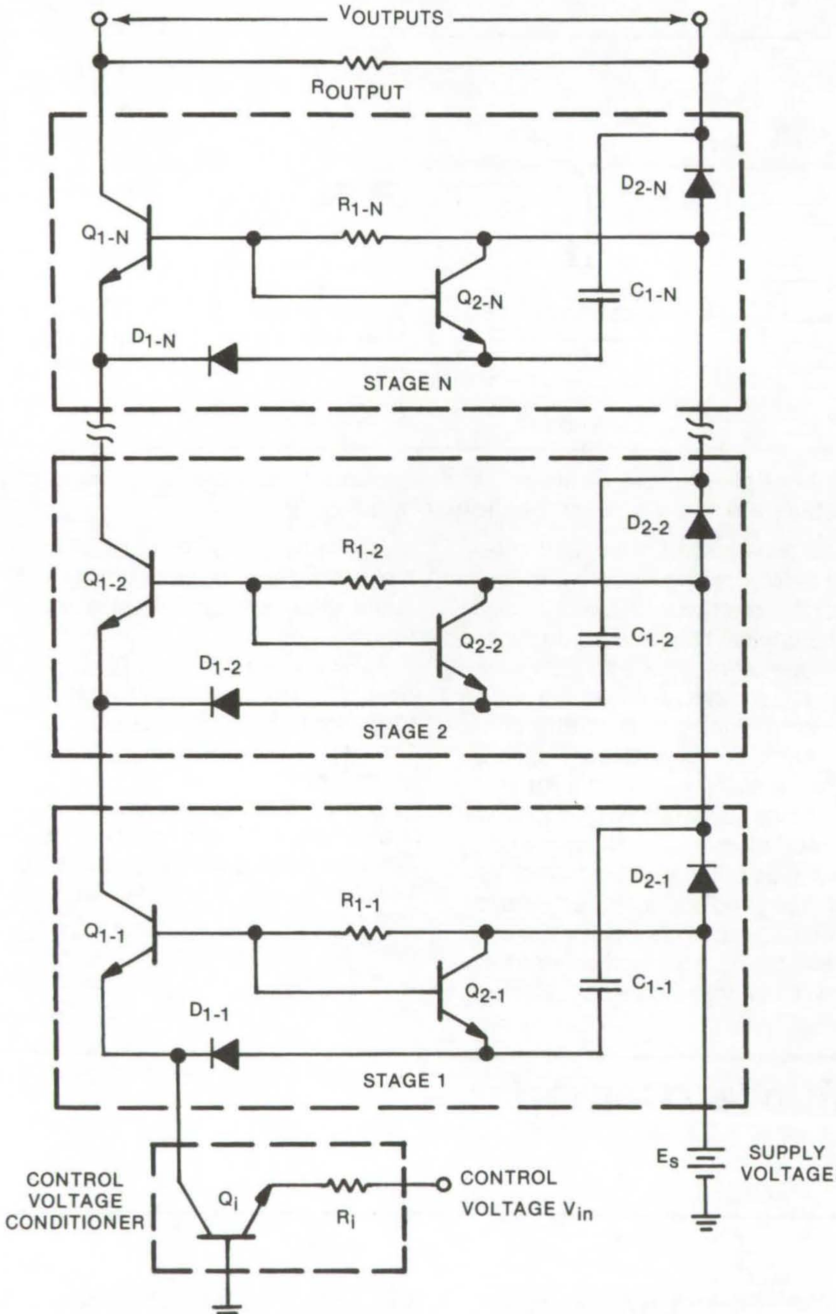

The three-stage version of an N-stage **Voltage Multiplier** is illustrated; each stage is series/cascade connected. An input voltage linearly varies the current flow through each stage, controlling the total gain of all stages and thus the final output voltage across load resistor R_{output}. Solar cells or fuel cells can be substituted for the storage capacitors.

Transistors Q_{2-1}, Q_{2-2}, and Q_{2-n} act as emitter followers. This reduces the output impedance of each stage to a few ohms; system output impedance is equal to battery impedance is equal to battery impedance plus the combined impedances of these transistors. Although total output voltage is reduced by each collector-emitter voltage drop of the follower stages, the loss is negligible.

If the input current (developed across R_i) is increased to a value sufficient to saturate transistors Q_i, Q_{1-1}, Q_{1-2}, and Q_{1-n}, then current also will flow along the path of Q_i, D_{1-1}, C_{1-1}, and D_{2-1}. Capacitor C_{1-1} is charged to a voltage equal to that of the primary power source E_S. Current also will flow through Q_i, Q_{1-1}, D_{1-2}, C_{1-2}, D_{2-2}, and D_{2-1}, so that capacitor C_{1-2} also will be charged to a voltage equal to E_S, and so forth. As soon as the input current is decreased to a level at which the system is no longer saturated, all the diodes will be reverse biased, and the charging cycle stops.

This work was done by Lawrence H. Bannister and Richard H. Baker of Massachusetts Institute of Technology for **Caltech/JPL.** *For further information, Circle 3 on the TSP Request Card.*

Title to this invention has been waived under the provisions of the National Aeronautics and Space Act [42 U.S.C. 2457(f)], to the Massachusetts Institute of Technology, 77 Massachusetts Avenue, Cambridge, Massachusetts 02139. NPO-13757

Digital Varying-Frequency Generator

Accurate linear variation of the frequency of a square-wave output

Lyndon B. Johnson Space Center, Houston, Texas

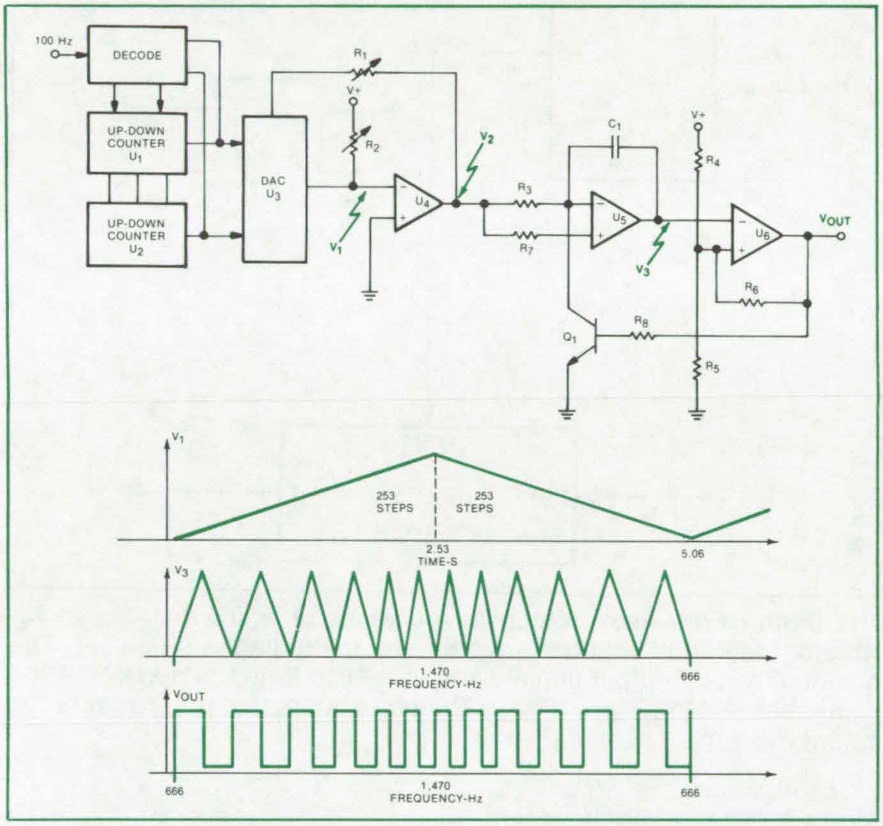

The Varying-Frequency Generator employs up/down counters, a DAC, and an integrator to determine the frequency and the time duration of the output. Signal sequence is shown for various points in the circuit.

Uniform frequency variation in variable-frequency generator output is often controlled by complex, bulky circuits incorporating large, expensive precision capacitors and resistors. Now these circuits can be replaced with simplified, standard low-power TTL components. The results are greater uniformity in frequency variation over a long time period and a significant reduction of the circuit size.

The circuit as shown in the illustration provides a square-wave signal with a frequency that varies linearly from 666 to 1,470 Hz and back to 666 Hz in 5.06 seconds, a simulation of a siren. It includes the up/down counters U_1 and U_2 which are driven by the decode circuit and a 100-Hz square-wave input. The decoder determines whether the up/down counters are counting up or down at the 100-Hz rate. The digital-to-analog converter (DAC) changes the output of the up/down counters into a stairstep triangle waveform. This waveform controls the overall period of the output signal.

The output of the DAC is amplified by U_4. This varying output V_2 is then applied to the integrator circuit of U_5 and U_6. The frequency output is determined by the value of C_1, R_3, the combination of R_4, R_5, R_6, and the voltage V_2.

This type of circuit could be used where a varying signal must be controlled accurately over a long period of time. By changing the frequency of the control signal, the time period can be altered. In addition, the signals controlling the up/down counters could be varied to allow the same generating circuit to produce a variety of output waveshapes.

This work was done by Michael J. Allen of Martin Marietta Corp. for **Johnson Space Center.** *No further documentation is available.*
MSC-16331

Open-Loop Digital Frequency Multiplier

A divide-by-N counter can be used where the multiplier constant is too large for a phase-locked loop IC.

Lyndon B. Johnson Space Center, Houston, Texas

The phase-locked-loop integrated circuit (PLL IC) is often used to implement digital frequency multiplication. However, at high frequencies the PLL IC is limited by its long internal clock period. This limits the effective digital multiplier constant and thus the uppermost multipliable frequency.

A redesigned open-loop multiplier may be used at higher frequencies. It is implemented by using digital IC's where the multiplier constant is too large for a conventional PLL IC. As shown in the block diagram, a 400-Hz clock is generated by a divide-by-N counter from a 1-Hz timing reference. To calculate for frequencies other than indicated, the desired multiplier M is allowed to be greater than unity. If the reference frequency f_{ref} is known, then the output frequency f_{out} is the product of f_{ref} and M. The integer division N is chosen to be as large as is practical. To ensure that f_{out} executes exactly M cycles per period, the oscillator must output a signal falling between the limits

$$\frac{NM - \frac{N}{4}}{\frac{1}{f_{ref(max)}} - \frac{1}{2MNf_{ref(max)}}} < f_{osc} < \frac{NM + \frac{N}{4}}{\frac{1}{f_{ref(min)}} + \frac{1}{2MNf_{ref(min)}}}$$

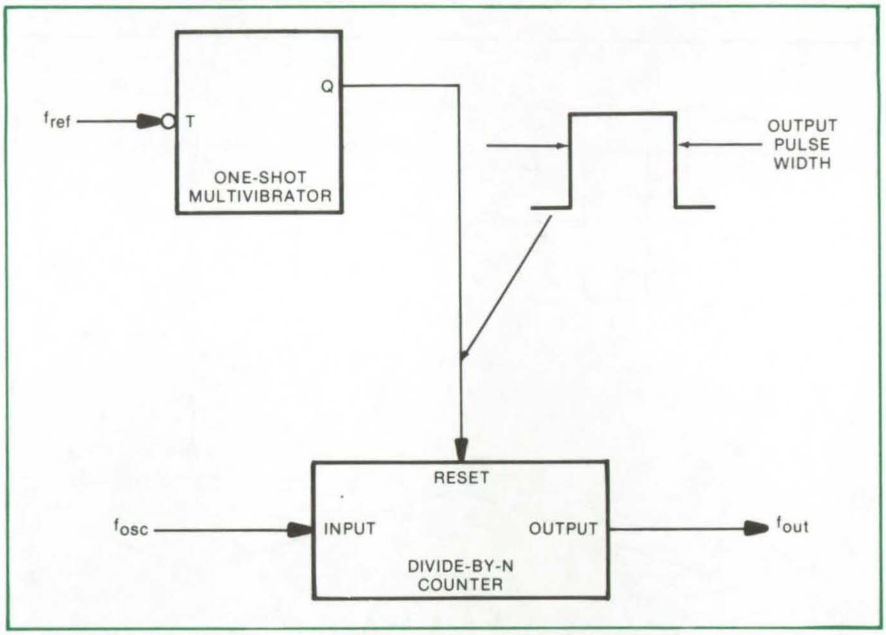

The **Digital Frequency Multiplier** consists of a monostable multivibrator (one shot) which is triggered by the falling edge of f_{ref}. The one-shot has an output pulse width, T, which is the reciprocal of the expression $2MNf_{ref}$ (or $2Nf_{out}$). The one-shot output pulse resets the counter to zero.

This work was done by Robert C. Moore of Johns Hopkins University for **Johnson Space Center.** *For further information, Circle 4 on the TSP Request Card.*

This invention is owned by NASA, and a patent application has been filed. Inquiries concerning nonexclusive or exclusive license for its commercial development should be addressed to the Patent Counsel, Johnson Space Center [see page A8]. Refer to MSC-12709.

Diplexer Switch

Biased GaAs diodes and a resonant coupling structure maintain high isolation and continuous input/output matching.

Langley Research Center, Hampton, Virginia

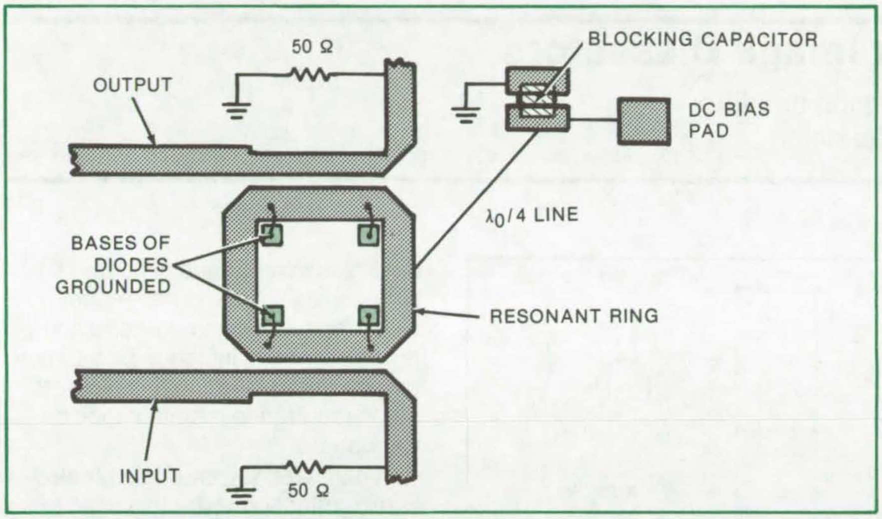

Figure 1. The **Diplexer Ring** has four microwave diodes configured shunt-to-ground at each corner of the resonant ring. When unpowered, the diodes appear to switch elements as high impedances to RF ground. The microwave signal is thus attenuated (58.5 dB at 4.9 GHz). When a positive bias voltage is applied to the diodes, most of the input energy passes from input to the output port. Input-to-output insertion loss is 1.5 dB.

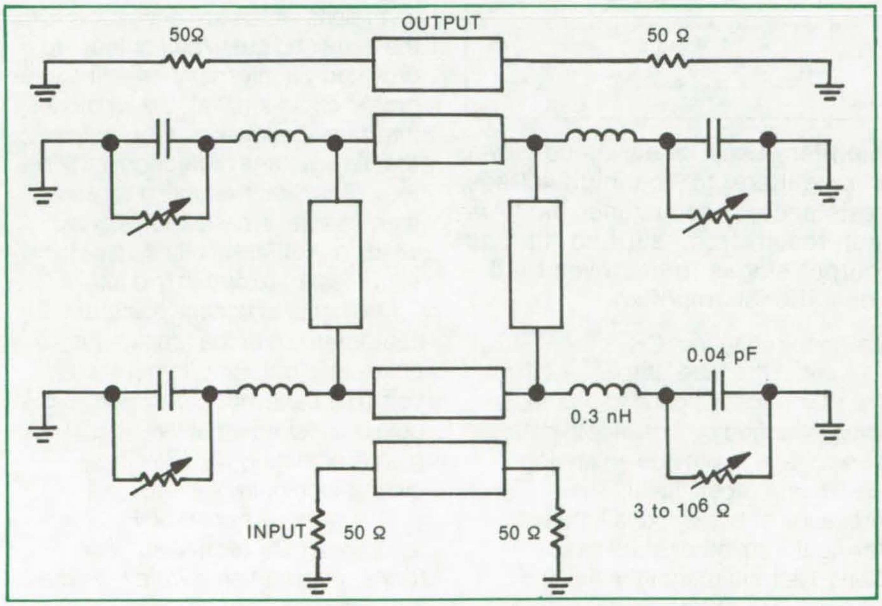

Figure 2. **Computer Analysis of the Switch** gives a theoretical isolation of 100 dB, with diode forward resistance set to 1 ohm. The diode function capacitance and bond-wire inductance is indicated for commercially-available Schottky diodes.

Microstrip switch designs are hobbled by the inability to achieve high isolation and by the inability to maintain a broadband match in all switch positions. High isolation requires the use of several conventional diodes, all electrically matched and mounted in a shunt or series configuration along the transmission line. As the diodes are added to the line, however, input-to-output impedance matching becomes progressively difficult to achieve.

A new ring diplexer switch achieves high isolation and continuous input/output matching by using the resonant coupling structure of the diplexer. Additionally, the dc bias network used to control the switch is decoupled from the RF input and output lines. Voltage transients in external circuits are thus minimized.

The switch uses four microwave diodes (such as gallium arsenide Schottky-barrier types) that are configured shunt-to-ground at the four corners of the diplexer ring as illustrated in Figure 1. The ring diodes are dc biased via a quarter-wavelength line bypassed to RF ground at the ring resonant frequency. When the switch diodes are unpowered, they appear to switch elements as high impedances to RF ground. The switch therefore attenuates the microwave signal at its operating frequency which is centered at 4.9 GHz. At this frequency, insertion loss is approximately 58.5 dB.

When a positive bias voltage is applied to the diodes, the effective diode impedances are lowered, thus shorting both ends of the quarter-wavelength coupling sections of the switch input arms to ground. This decouples the ring from the input and output circuits, passing most of the input energy to the output circuit. Input-to-output insertion loss then is 1.5 dB. The nominal 50-ohm

(continued next page)

impedance matches of the input and output lines are maintained whether the diodes are maximally conducting or minimally conducting or are at any intermediate conduction level.

A computer analysis of the circuit with diode resistance set at 1 ohm gives a theoretical isolation of 100 dB. A model of the switch including diode function capacitance and bond-wire inductance is shown in Figure 2. The values indicated are typical for commercially-available Schottky microwave diodes.

This work was done by C. H. Grauling, Jr., and T. W. Parker of Westinghouse Electric Corp. for **Langley Research Center.** *For further information, Circle 5 on the TSP Request Card.*
LAR-11546

Deflection Amplifier for Image Dissectors

Balanced symmetrical Y-axis deflection amplifier provides precise control of image definition.

Caltech/JPL, Pasadena, California

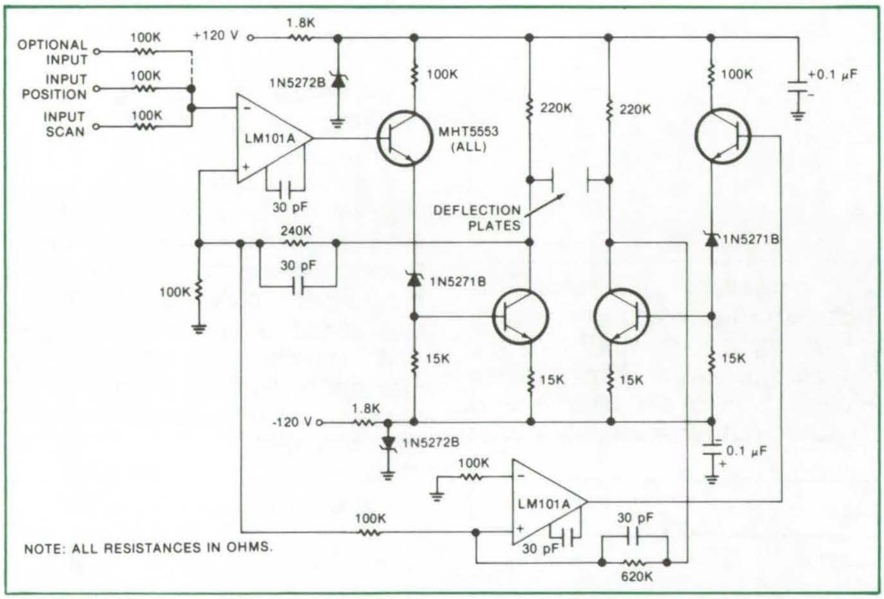

The **Balanced Y-Axis Deflection Amplifier** uses zener-diode level shifting to interface the operational amplifiers to the high-voltage bipolar output stages. The dynamic resistance of each zener diode is very low; signal attenuation does not result from shifting the dc operating level, required to allow the output stages to be driven by the relatively limited output swing of the operational amplifiers.

In celestial navigation systems traditionally the brightest stars in constellations are used as references. In one such scheme, locking in on the second brightest star in the sky (Canopus), the stellar field of view is scanned on an image dissector tube: a scannable photomultiplier with deflection voltage requirements similar to those of conventional cathode-ray tubes (CRT's).

A slit in the tube, through which the star's light is focused, is repetitively scanned by a sawtooth deflection voltage to provide an analog electrical-output signal. The presence of background light and the light from other stars near Canopus require that the field be narrowly restricted. To accommodate relative changes of position between the star and the image tube, the tube scanning-cone angle is varied, in this instance by a binary ring counter providing five discrete steps required to maintain lock on Canopus.

A balanced symmetrical electrostatic deflection voltage is used to sweep the image dissector cone axis. Deflection voltages are provided by the amplifier schematically illustrated. A bipolar 120-Vdc source powers the deflection-plate drive transistors which are driven by a single analog position input. Signal inversions which are necessary for the balanced push/pull output are provided via internally-inverting integrated circuits (IC's). Zener diodes interface the low-power IC stages to the high-voltage deflection transistors. This direct-coupling arrangement results in deflection signals which are differentially symmetrical with respect to circuit ground.

The nominal voltage transfer characteristic of the amplifier is 40 differential output volts per input volt. The bandwidth, between -3-dB points, is approximately 8 kHz. Loop gain is nominally 89 dB with a closed-loop gain of 26 dB.

This work was done by Phil M. Salomon of **Caltech/JPL.** *For further information, Circle 6 on the TSP Request Card.*
NPO-13079

Universal Solar-Cell Terminal

Dissimilar material bonding properties improve terminal reliability

Marshall Space Flight Center, Alabama

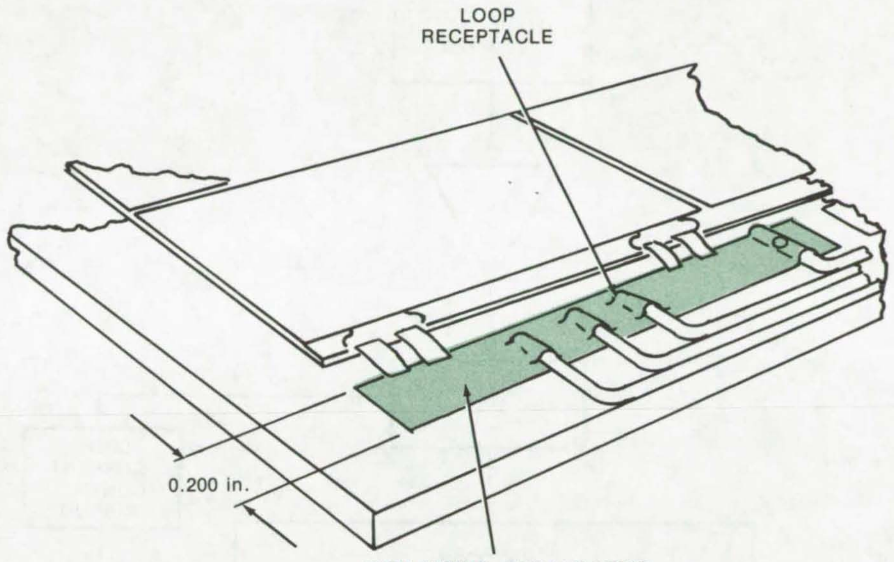

The Universal Solar-Cell Terminals use the dissimilar material bonding properties (metal-to-glass and/or ceramics) of an iron-nickel-cobalt alloy in conjunction with standard termination. Loop receptacles replace the conventional connector posts.

Getting to the "outside world" from miniature integrated circuits is a problem familiar to most designers. Although several orders of magnitude simpler, the problem is relatively as severe for the designers of solar-cell arrays. As the arrays get larger and assume different shapes, connecting the photovoltaic output to power-supply cabling becomes a problem heavily influenced by concern for reliability and assembly techniques.

Conventionally, printed-circuit boards are used to terminate series strings of solar cells that have been mounted by the flat-laydown technique. External connectors are stakelike solder pins that act as terminals for the wires from the cells and cable harness. An insulating disk normally separates the terminal from the metal solar-panel substrate facesheet. It is bonded to the board after installation of the terminal and generally, causes unevenness on the back surface of the PC board. The irregularity in surface finish interferes with the board-to-substrate bond and makes the terminal somewhat unsightly. Furthermore, the protruding lugs on the terminal have a tendency to snag on cleaning materials and on the sleeves of shopcoats worn by the assemblers.

A new universal solar-cell terminal replaces the stakes or lugs in the conventional design with loop receptacles for the wires from the cells and harness. The terminal is made of flat strips of solder-plated iron-nickel-cobalt alloy kinked or looped to accept the wires (see figure).

Aside from the fact that protrusions are eliminated, the overall reliability of the terminal is enhanced because the temperature coefficient of the alloy strip matches that of the silicon solar cells and interconnectors, a matter of vital importance in solar-cell panel design. Also, because the alloy itself forms the connecting loop to which the wires are soldered, the terminal-to-printed-circuit-board connection is eliminated, and reliability is further improved.

The universal terminal is significantly less expensive to produce than the conventional design, it is easier to assemble and integrate harness to array, and the reliability of the connection is improved.

While all of the undesirable aspects of the conventional design are relieved or eliminated by the universal terminal, it has another valuable feature. Whereas several different configurations of conventional terminals might be required on the solar-cell arrays of a single system, the new design can be used for all string terminations. Also, the same part can serve as a "turn-around" at panel edges by overlapping the parts and lap soldering directly rather than by using additional connecting wires.

This work was done by Saul Bashin and Franklin G. Kelley of TRW, Inc., for **Marshall Space Flight Center.** *For further information, Circle 7 on the TSP Request Card.*

Inquiries concerning rights for the commercial use of this invention should be addressed to the Patent Counsel, Marshall Space Flight Center [see page A8]. Refer to MFS-23505.

Solid-State Turn-Coordinator Display

Light-emitting diodes (LED's) are shown feasible for aircraft instrument displays.

Langley Research Center, Hampton, Virginia

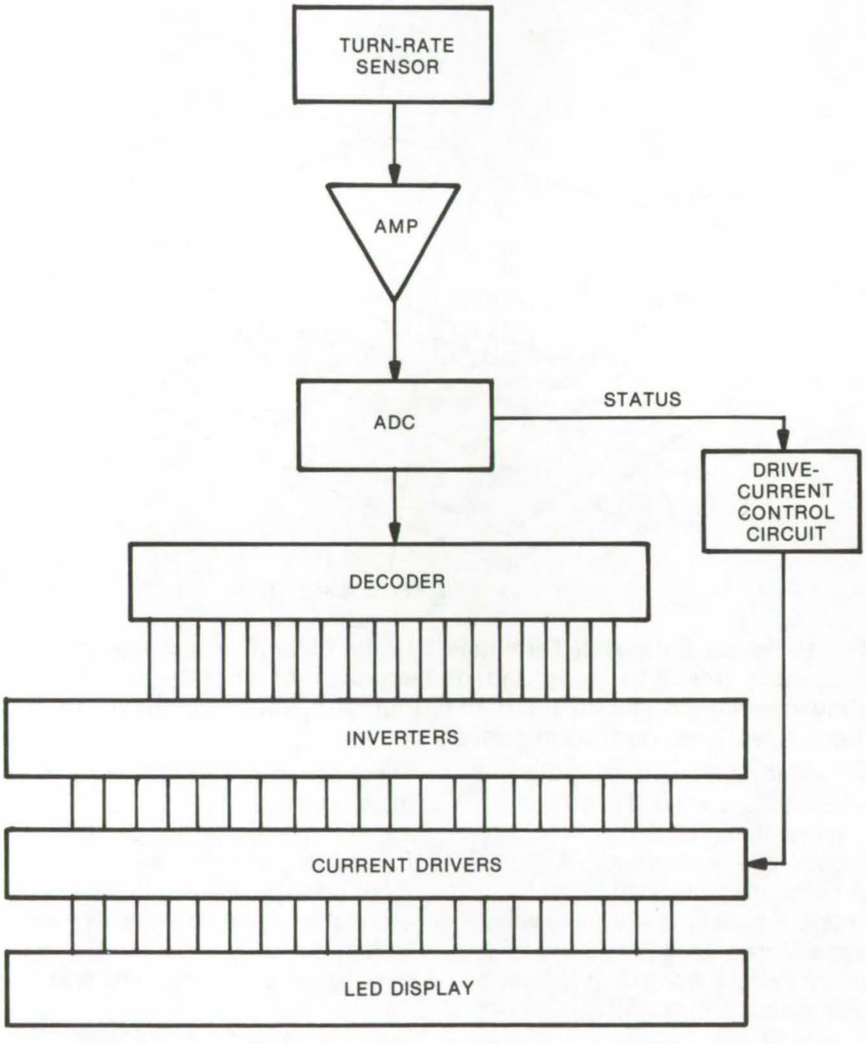

Figure 1. Solid-State Turn-Coordinator Display

A solid-state turn-coordinator display employing light-emitting diodes (LED's) has been developed to demonstrate the feasibility of such displays for aircraft instrument applications.

The sensing device, which responds to angular rotation of the aircraft, is a fluidic inertial-rate sensor adapted for use in a wing-leveler system. The sensor puts out a signal proportional to both the yaw rate and roll rate of the aircraft. The amplified and converted signal is decoded into 1 of 20 mutually exclusive outputs and is inverted for compatibility with the current drivers that control the current to the LED's, as indicated in Figure 1.

For radial display, the LED's were mounted on grooves cut along 20 diameters 5° apart; the LED's in each groove are driven by one of the 20 current drivers (Figure 2).

The actual display, appropriately filtered and mounted in an aircraft instrument case, appears as shown in Figure 3.

This device also offers three levels of brightness to compensate for the varying degrees of ambient light present in the cockpit.

The development of this turn-coordinator display demonstrates the technical feasibility of the design and construction of solid-state aircraft displays employing LED's as

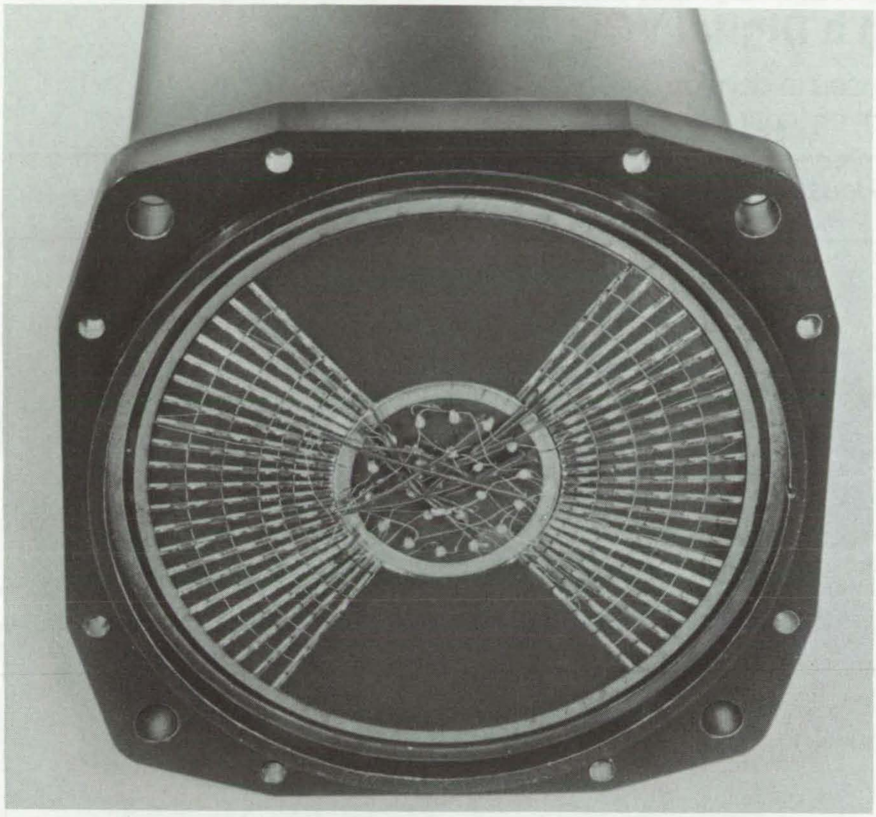

Figure 2. LED Display Without Filter

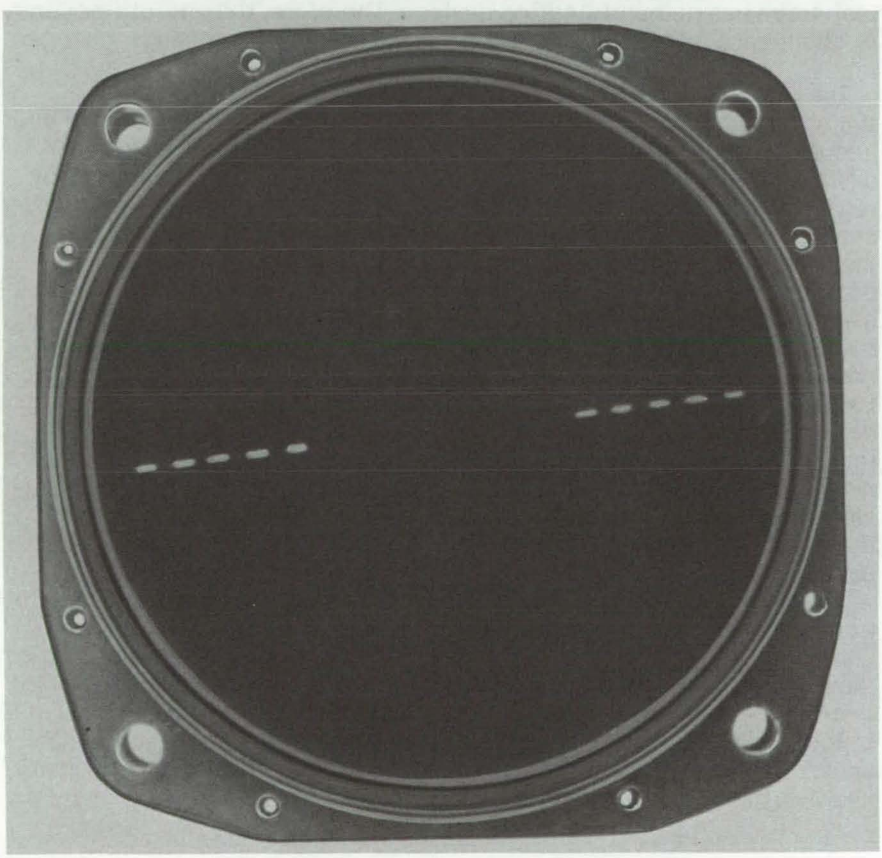

Figue 3. Illuminated Display

the display medium. While mechanical turn-and-bank indicators currently in use are both simple and reliable, this type of display offers significant visual advantages for night flying and can be employed for more sophisticated applications in aircraft instrumentation beyond the capability of mechanical devices.

This work was done by Roger K. Crouch, W. Lane Kelly, and Barry D. Meredith of **Langley Research Center.** *Further information may be found in NASA TM-X-7282 [N76-32186], "Solid-State Turn-Coordinator Display," a copy of which may be obtained at cost from the North Carolina Science & Technology Research Center [see page A7].*
LAR-12090

Doppler Extraction With a Digital VCO

A digital, integrated-circuit VCO is used to develop motion-induced frequency data from an input signal.

Lyndon B. Johnson Space Center, Houston, Texas

A new digital voltage-controlled oscillator (VCO) provides a relatively simple means of extracting Doppler information from modulated RF signals. As designed, it may be useful for data communications systems, or it may be modified to serve as the information extraction component of a microwave or optical system for collision avoidance or automatic braking.

Several methods are known for the extraction of Doppler information from an RF signal, one of the better being the vernier technique; but even with this approach there are constraints. For example, the delay time between a count command and its execution is dependent on the desired resolution and the Doppler frequency. In applications where delay time is of little importance, the vernier technique can provide a resolution which is comparable to the limitations imposed by the best oscillator. However, when a rapid response is sought, the resolution may have to be degraded intentionally.

When the delay time is important and precision is required, a new technique can be used. The basic concept employs a digitally controlled oscillator in a phase-locked loop, which acquires, tracks, and measures the Doppler frequency. The nominal value of the incoming frequency is represented by a digital number, which in turn controls the reference-frequency synthesizer. At phase lock, the incoming frequency and the generated frequency are identical, since only a small phase error will exist. The precision of the frequency measurement is unlimited, since it merely requires a few more bits in the control registers to split one cycle of Doppler to an even smaller fraction. For example, a 20-bit register could provide a resolution of one-millionth of a Doppler cycle.

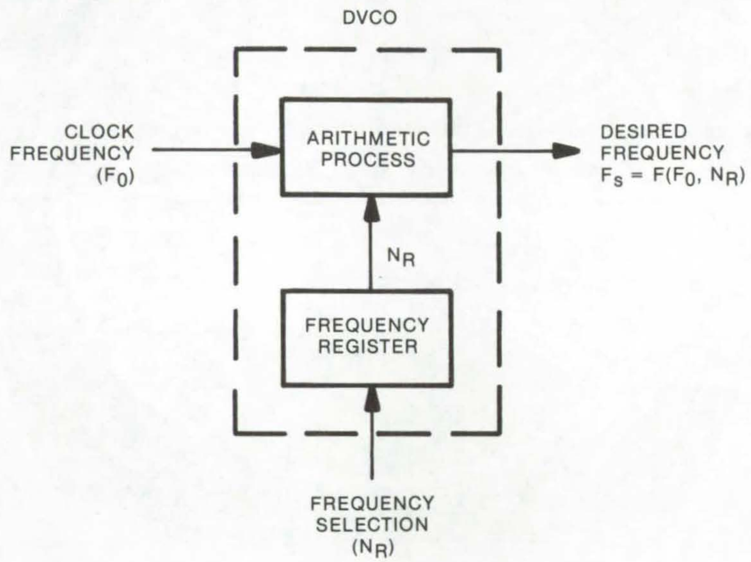

Figure 1. A **Typical Digital VCO** as used in the Doppler extraction technique has no band-limiting devices. Therefore, the output frequency is changed almost immediately after the register number is changed.

The digital VCO is a frequency-synthesizing device with an output frequency specified precisely by a digital number programed into a register (frequency register). By changing the number in the register, the output frequency is changed proportionately. There are several methods of implementing a DVCO, but in general, all of the techniques convert a stable known reference frequency (clock frequency) to the desired output frequency by arithmetic operations on the digital frequency register number and/or the clock frequency. Figure 1 is a functional diagram of a typical digitally controlled oscillator.

To extract Doppler information from a Doppler reference signal, the digital VCO can be phase locked to the Doppler reference in such a way that the feedback error signal controls the frequency register number and maintains phase lock. This is shown in the block diagram of Figure 2. By monitoring the register number, the Doppler reference frequency (and hence the Doppler frequency) can be determined. By continuous monitoring of the register number, the time history of the Doppler frequency can be determined.

The rate at which the frequency register is updated is governed by the bandwidth of the low-pass loop filter. Wide bandwidths allow rapid updates and low phase error between the register number and the Doppler reference frequency. However, they also admit more noise.

Acquisition of the Doppler reference by the DVCO can be accomplished simply by presetting the desired number in the frequency register. If the Doppler reference is known to within the loop bandwidth, acquisition should occur almost immediately. A sweep acquisition can be implemented by periodically increasing (or decreasing) the

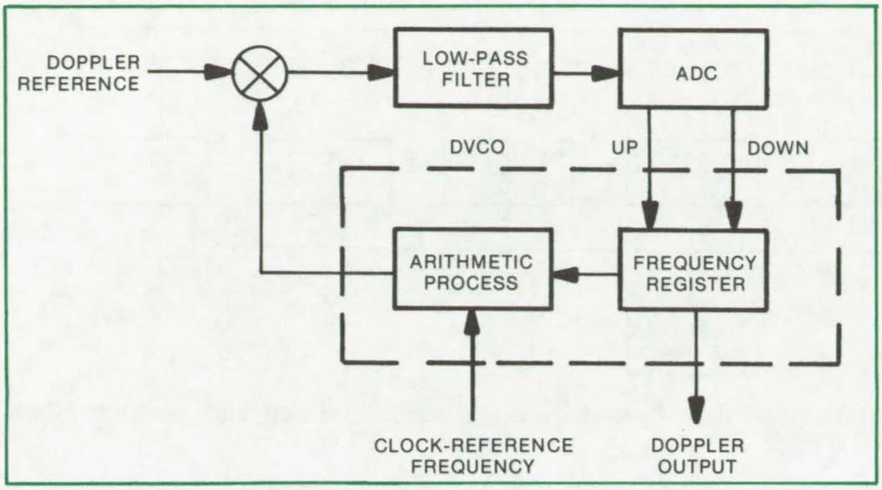

Figure 2. When the **DVCO Is Used as a Doppler Extractor,** the phase-detector output error signal is low-pass filtered and fed to an analog-to-digital converter. The numerical output of the ADC is used to change the frequency register so that the DVCO output frequency remains in phase lock to the Doppler reference signal. At phase lock, the DVCO frequency and the Doppler reference frequency are equal. Thus, the digital number in the frequency register is proportional (or functionally related) to the Doppler reference signal.

register number by a constant increment. The DVCO frequency will then be stepped in precise frequency increments. When acquisition occurs, the register-incrementing device can be removed.

The accuracy of the Doppler measurement depends on the usual external parameters. In a one-way Doppler measurement, the accuracy and stability of the frequency standard is the most serious limitation. In two-way Doppler systems with a common transmit-and-receive oscillator, this is a much less serious problem. The signal-to-noise ratio at the receiver output also affects the Doppler accuracy.

In general, when the receiver is used for voice or data communication, the received power is more than adequate to obtain a high signal-to-noise ratio on the Doppler-shifted carrier component. Residual carrier systems provide this carrier component directly, while the newer suppressed-carrier modulation techniques provide strong reconstructed carrier components to allow error-free data demodulation. A carrier signal-to-noise ratio of 24 dB or better is sufficient to achieve a 0.01-Hz Doppler accuracy in a 1-second period. The signal-to-noise ratio can be controlled by making the loop bandwidth relatively narrow.

This work was done by Eugene R. Starner and Edward J. Nossen of RCA Corp. for **Johnson Space Center.** *No further documentation is available.*
MSC-14814

Signal Enhancement Filters

Digital-data filters smooth out data and data rates.

Lyndon B. Johnson Space Center, Houston, Texas

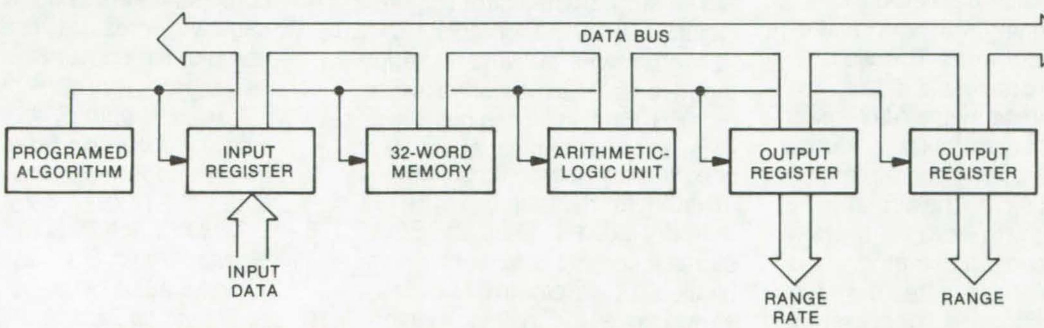

Figure 1. The **Cascaded-Averaging Filter** uses a limited arithmetic-logic unit to smooth the data (range) over intervals of 1, 2, 3, and 4 seconds. Sample rates are 16, 8, 4, and 2 seconds, respectively.

Two filters designed to smooth the digital output of a radar tracking system prevent noise-induced inaccuracies and result in an input/output noise-variance reduction on the order of 10:1. Both filters are implemented as microprocessors; one is a special-purpose device with a limited arithmetic-logic unit, and the other is a true programable microprocessor.

The first filter, a cascaded-averaging device, smooths range data over intervals of 1, 2, 3, and 4 seconds, with sample rates of 16, 8, 4, and 2 samples/second, respectively. The output data-rate (range-rate) word is computed from the

(continued next page)

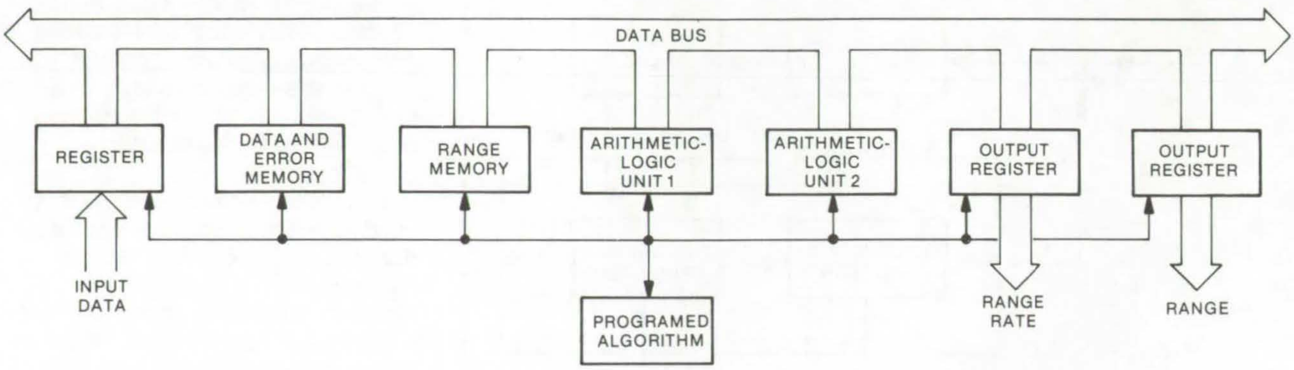

Figure 2. The **Programable Filter** smooths over 2, 4, 8, and 16 range words and can also perform other functions.

most recent range word and the 17 previous range words. The smoothed range word is based on the most recent range word and the 15 previous range words.

The second filter smooths over 2, 4, 8, and 16 range words, with sample-rate options of 2, 4, 8, and 16 samples/second for any of the allowed number of range words. It can be also programed to perform other functions. Both filters update the smoothed range word to correct for the time lag resulting when averaging over N words.

The principal components of the cascaded-averaging filter (Figure 1) are input/output registers, a 32-word memory, and an arithmetic-logic unit (ALU). Read-only memories containing a programed algorithm direct the various data units which are connected by a data bus.

The contents of the memory are scanned beginning with word 1, the most recent data word. This word, along with the previous 5 data words, is summed by the ALU which functions as an accumulator. Words 7 through 12 are read out of memory but are not added by the accumulator. Beginning with word 13, the next 6 words are read out of memory and are sequentially subtracted from the accumulated sum which represents the first 6 words. If subtraction through zero occurs, the algorithmic complement is used.

After the weighting function is entered, the computed range rate is stored in the output range-rate register and in a scratch pad memory for later use in updating the smoothed range word. After word 18 is logged in memory, the memory is automatically reset to word 1. Memory scan begins, and words 1 through 16 are summed by the ALU. After division the average word is present in the accumulator. The smoothed word is delayed by 8 sample times from the incoming data word. A correction factor equal to half the range rate is added or subtracted from the smoothed word to update the computed range word, which is accomplished by retrieving the range-rate word from the scratch pad memory and either adding or subtracting.

The programable filter (Figure 2) includes input/output registers, two 32-word memories, and two arithmetic units. The memories are segmented into two blocks of 16 words each and are identical except that one memory board has pullup resistors for the data bus. The memory labeled "Data and Error" stores incoming data words in one block of 16 words; error words are stored in the second block which, in addition, is used to store computed range words and is the unit which makes it possible to implement the N-parallel filter concept.

Arithmetic-logic unit 1 is utilized for addition, subtraction, and division. When computing error words, the results are stored in the error memory as a 15-bit error word. Bit 16 is the word sign. For negative words the word is automatically complemented so that the magnitude plus sign is stored. When other add or subtract operations are performed, all 16 bits are used as data.

Arithmetic-logic unit 2 operates as an accumulator to compute the error word. The filter scans the error memory twice: On the first scan, ALU 2 sums up all of the positive words; on the second pass the negative words are sequentially subtracted from the accumulated sum. If subtraction through zero occurs, the contents of the accumulator are complemented, and the remaining negative words are added to the complemented word.

This work was done by Harold B. Killen and Walter B. Warren of TRW, Inc., for **Johnson Space Center.** *Further information may be found in NASA CR-147537 [N76-21369], "Radar Range Data Signal Enhancement Tracker," a copy of which may be obtained at cost from the National Technical Information Service, Springfield, Virginia 22151. MSC-14907*

Serial-Data Correlator/Code Translator

New system has improved reliability and reduced complexity and is flexible to code changes.

John F. Kennedy Space Center, Florida

A newly proposed system provides a digital sample of coded serial data at system-required rates. It correlates the sampled data with predetermined acceptance code patterns, translates the acceptable code patterns to a nonreturn to zero (NRZ) code, and identifies data dropouts. A block diagram of the system is shown in the illustration.

The system consists of a sampling flip flop, a memory (either RAM or ROM), and a memory buffer. The memory is addressed by vectored feedback from the buffer and is indexed by the sampled data. Each memory location consists of a vector that points to the next state to be addressed and the output data associated with the vector. The memory vectors are generated from a sequence map.

This system is flexible because changes in the code or code requirements may be made by reprograming the memory element, thus limiting hardware modifications. Another feature is that the printed circuit board complexity is reduced by minimizing the number of chips and the interconnects between chips. The result is increased system reliability and reduced power consumption.

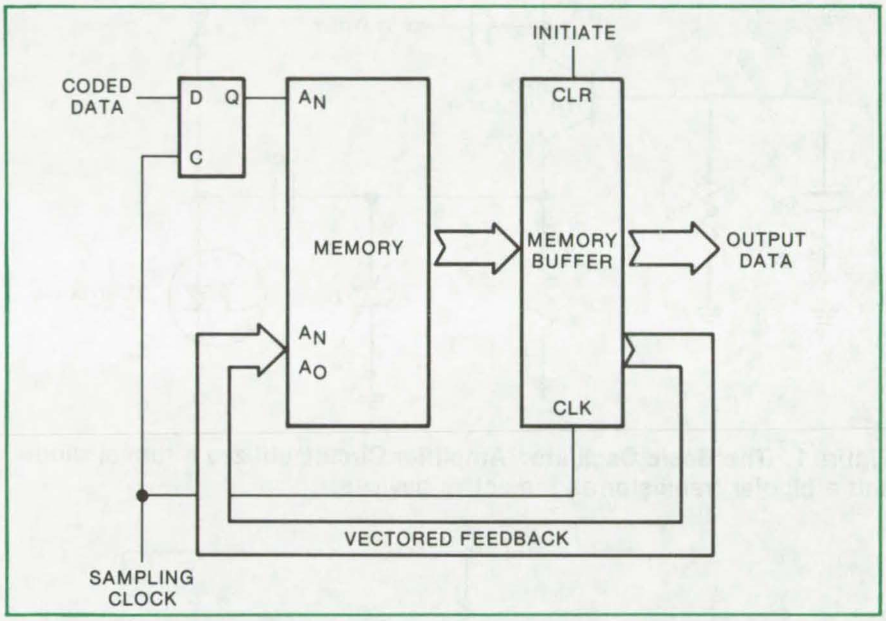

The **Serial-Data Correlator/Code Translator** consists of a sampling flip flop, a memory, and a memory buffer.

This work was done by Larry E. Morgan of **Kennedy Space Center.** *For further information, Circle 8 on the TSP Request Card.*
KSC-11025

UHF/Microwave Oscillator/Amplifier

Lower costs and improved performance at 900 MHz

Goddard Space Flight Center, Greenbelt, Maryland

As the frequency spectrum continually advances upward (to accommodate the growing needs of communications), the design of UHF/microwave oscillators/amplifiers becomes more difficult due to the complex nature of the components used. Inductors are difficult to realize at frequencies near and above 1 GHz, capacitors experience degradation, and active devices acquire complex input/output impedances and gain is reduced. Aside from design difficulties, performance is usually marginal. Attempts to circumvent these limitations have resulted in physically large oscillators/amplifiers with components that are expensive relative to lower frequency design.

An improved, less expensive oscillator/amplifier circuit (see Figures 1 and 2) uses a tunnel diode as a negative resistance and a bipolar transistor as the active devices in conjunction with resistors and capacitors. An inductor is not required in this circuit. The transistor provides the inductance required to produce oscillation and tuning. The quality factor of the capacitors need not be high; hence, costs are lower.

(continued next page)

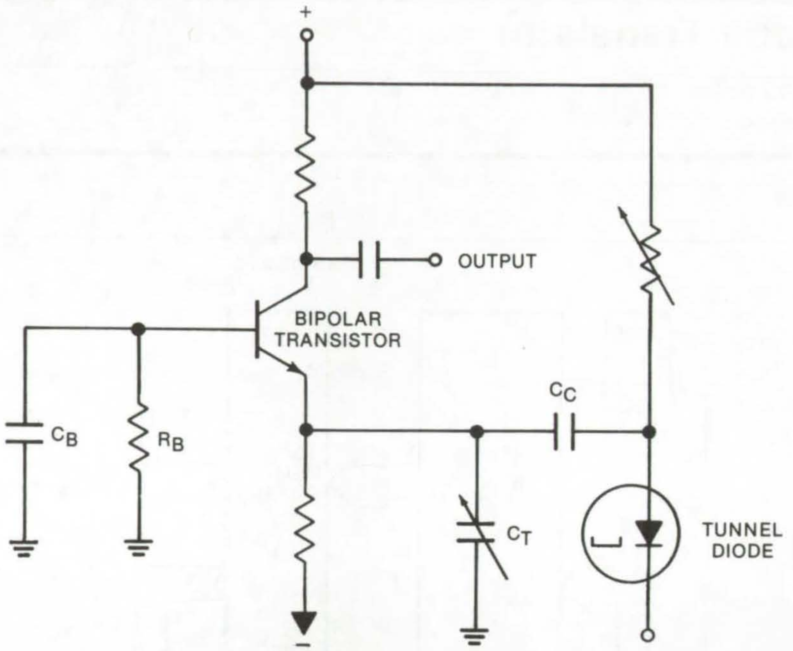

Figure 1. The **Basic Oscillator/Amplifier Circuit** utilizes a tunnel diode and a bipolar transistor as the active devices.

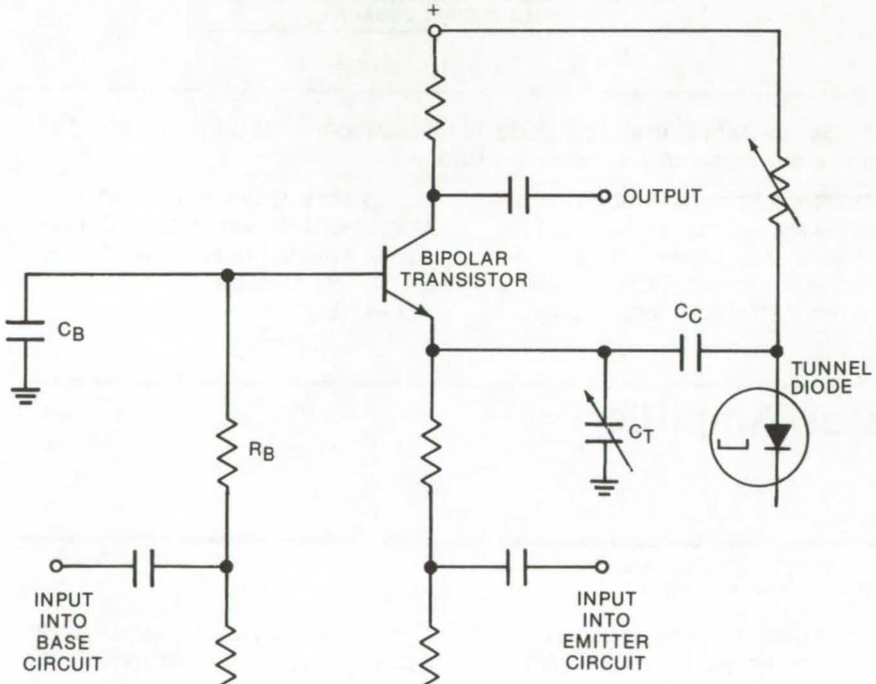

Figure 2. A **UHF/Microwave Oscillator/Amplifier** is shown operable in the amplifier mode by the introduction of a signal either into the base circuit or into the emitter circuit of the transistor. The transistor is adjusted to prevent oscillations.

The output is taken from the collector of the transistor and avoids the unwanted characteristics of a two-terminal oscillator/amplifier. The short-term stability of the device is 1 part in 10^5 to 10^6. The advantages of the design are small size, low cost, and a degree of load isolation via the transistor collector.

This work was done by Leonard L. Kleinberg of **Goddard Space Flight Center.** *For further information, Circle 9 on the TSP Request Card.*
GSC-12113

Capacitively-Coupled Data Receiver Clipper Stage

A circuit technique results in improved data threshold detection.

Lyndon B. Johnson Space Center, Houston, Texas

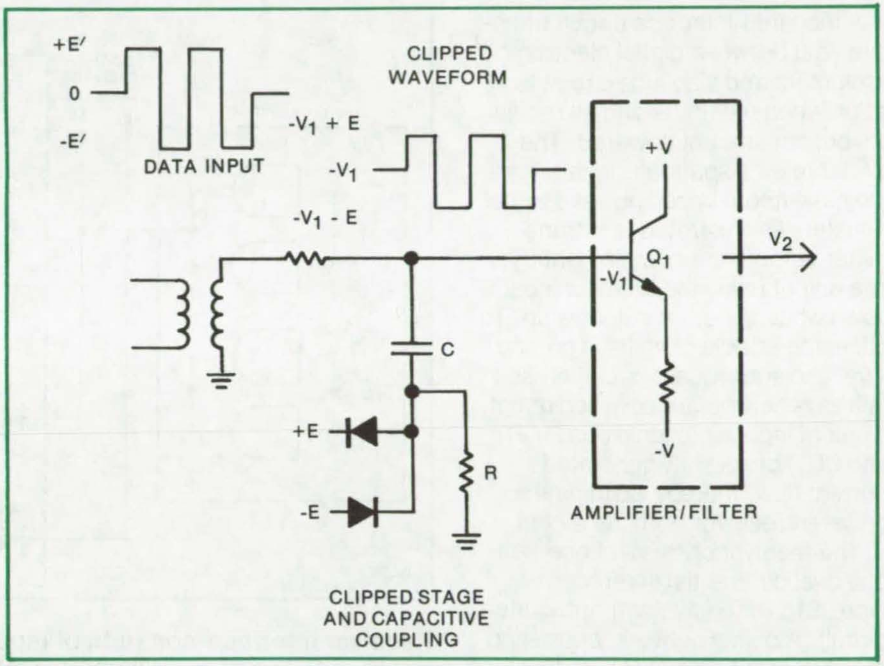

A **Capacitively-Coupled Receiver Clipper Stage** compensates for dc offset and asymmetry in dc clipping levels. For example, if the positive level clips at $E + \Delta E$ and the negative at -E, then the peak-to-peak level applied to the receiver is $2E + \Delta E$. However, the dc component $\Delta E/2$ is blocked, and the input waveform is symmetric about $-V_1$ with values of $E + \Delta E/2$ and $-E - \Delta E/2$. There is no unbalance to cause an offset voltage to appear at the end of a data word.

In data-transmission systems, receivers must accept a wide range of input-signal levels and have error-free threshold detection. Threshold detection levels must be set low enough to recover low-level data. However, high-level data can drive the receiver stages nonlinear (into saturation and cutoff) and cause voltage offsets at the output in excess of established detection levels. To prevent these problems with high-level data, a clipper stage can be added at the system input to keep signal levels within the linear operating range of the receiver.

Although the clipper stage presents high-level signal distortion it can result in asymmetrical positive and negative threshold levels, which degrades signal detection. This is caused by the bias voltage on the receiver input transistor stage and by the asymmetrical operation of the transistors and diodes in the clipper itself.

To deal with these problems a capacitively-coupled clipper stage can be employed (see figure). There is dc isolation from the bias $-V_1$ of the input, and therefore there is no offset of clipping levels. The input is clipped at +E and -E and applied to the receiver input. Due to its symmetry about the bias $-V_1$, there is no unbalance in the input waveform to cause a voltage offset at the end of a data word. Furthermore, any dc component that is generated by asymmetrical operation of the clipper is blocked.

This work was done by Fred W. Saunders of The Singer Co. for **Johnson Space Center.** *No further documentation is available.*
MSC-14989

Elimination of Thermally Generated EMF's on PC Boards

Often, PC boards have contacts made of dissimilar metals that produce unwanted thermally generated signals. These can be eliminated by using a temperature-controlling substrate, such as beryllia, mounted on a metal surface. This keeps the components at the same temperature, eliminating the unwanted EMF's.
(See page 647.)

Prefabricated Strain-Gage Connectors

Prefabricated wire jumpers and main wire leads reduce installation time for strain gages. The terminals eliminate the measurement, soldering, and trimming of individual jumpers. They are made from electrodeposited copper foil with Teflon or epoxy backing.
(See page 648.)

Electrostatic-Discharge Damage to Semiconductors

A study of electrostatic discharge has identified the causes and conditions leading to a difficult-to-detect class of semiconductor damages. Devices examined include a J-FET, an internally-compensated operational amplifier, and a TTL hex inverter. Each exhibits a distinct type of failure mode; however, each had the common characteristic of involving electrostatically induced breakdown of interfaces within the devices.
(See page 640.)

Biased-Circuit Digital Data Line Receiver

Circuit isolation and noise rejection in a data input/output loop

Lyndon B. Johnson Space Center, Houston, Texas

A modified-interface circuit transfers data between digital electronic equipment and also aids circuit isolation when the driver and all receivers but one are not powered. The circuit rejects spurious signals (noise) without impeding valid signal transfer. As illustrated, the transmitter outputs are complementary; one output holds the receiver input down while the other output is up. To offset the effects of shifts in ground level and subsequent circuit cross-talk as receivers are powered or not, a pair of input isolation diodes (CR_2 and CR_3) block shift-generated current flow, thereby isolating the powered receiver from the others.

The receiver consists of one-half of a dual differential line-receiver, type 9615 (or equivalent), integrated circuit. A pullup network, consisting of pnp current sources Q_1 and Q_2, is connected to each input. The transistors feed the input lines, and the receiver inputs via emitter-follower buffers Q_3 and Q_4. Zener diode VR_1, in series with one input of the differential receiver, sources an offset voltage to the receiver; the offset voltage forces the output of the 9615 down when both receiver inputs are open or when the driver is off.

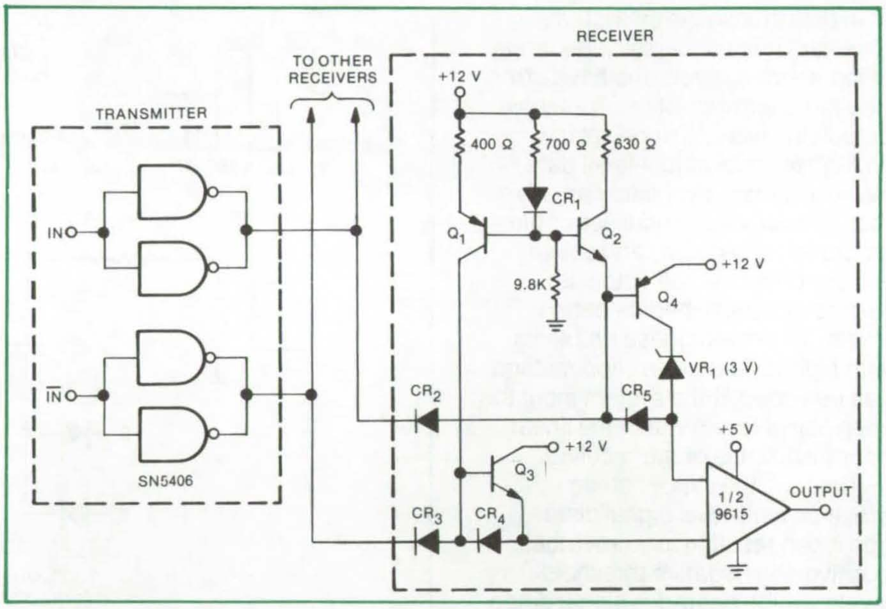

Receiver Interface consists of input diodes CR_2 and CR_3, current sources Q_1 and Q_2, and emitter followers Q_3 and Q_4.

This work was done by Fredric C. Fitzgerald of IBM Corp. for **Johnson Space Center.** *No further documentation is available.*
MSC-14967

Low-Power Programable High-Voltage Supply

The output ranges from 700 to 1,335 volts dc in 127 steps.

Langley Research Center, Hampton, Virginia

A programable high-voltage converter is used to energize a group of proportional-counter event-detection tubes. The supply is programed by using the output signal of a low-voltage digital-to-analog converter (DAC). This programing voltage ranges from 1.53 to 2.91 V in 127 0.0108 mV steps, and it is used to control the converter high-voltage output which ranges from 700 to 1,335 V in a like number of increments. The supply draws about 100 mW from conventional bipolar 5-V and 15-V sources.

The programable supply features low-ripple output voltage over its range and low induced line noise. In the supply a 2-stage 316-kHz oscillator is used to develop a voltage which is transformer coupled to a 28-stage voltage-multiplier circuit. The multiplier converts the oscillator output to the required voltage without expensive or critical high-voltage-rated components. The counter tubes are powered via 100-MΩ isolation resistors, which are labeled R_7 through R_{10} in the schematic.

The output voltage is controlled by pulse-width modulating the base drive of oscillator transistor Q_2. Reverse bias on the emitter-base junction of the 2N2222A is varied via the HA2700; superimposed on this dc control signal is a steady-state voltage obtained through a winding on T1 which is in series with the

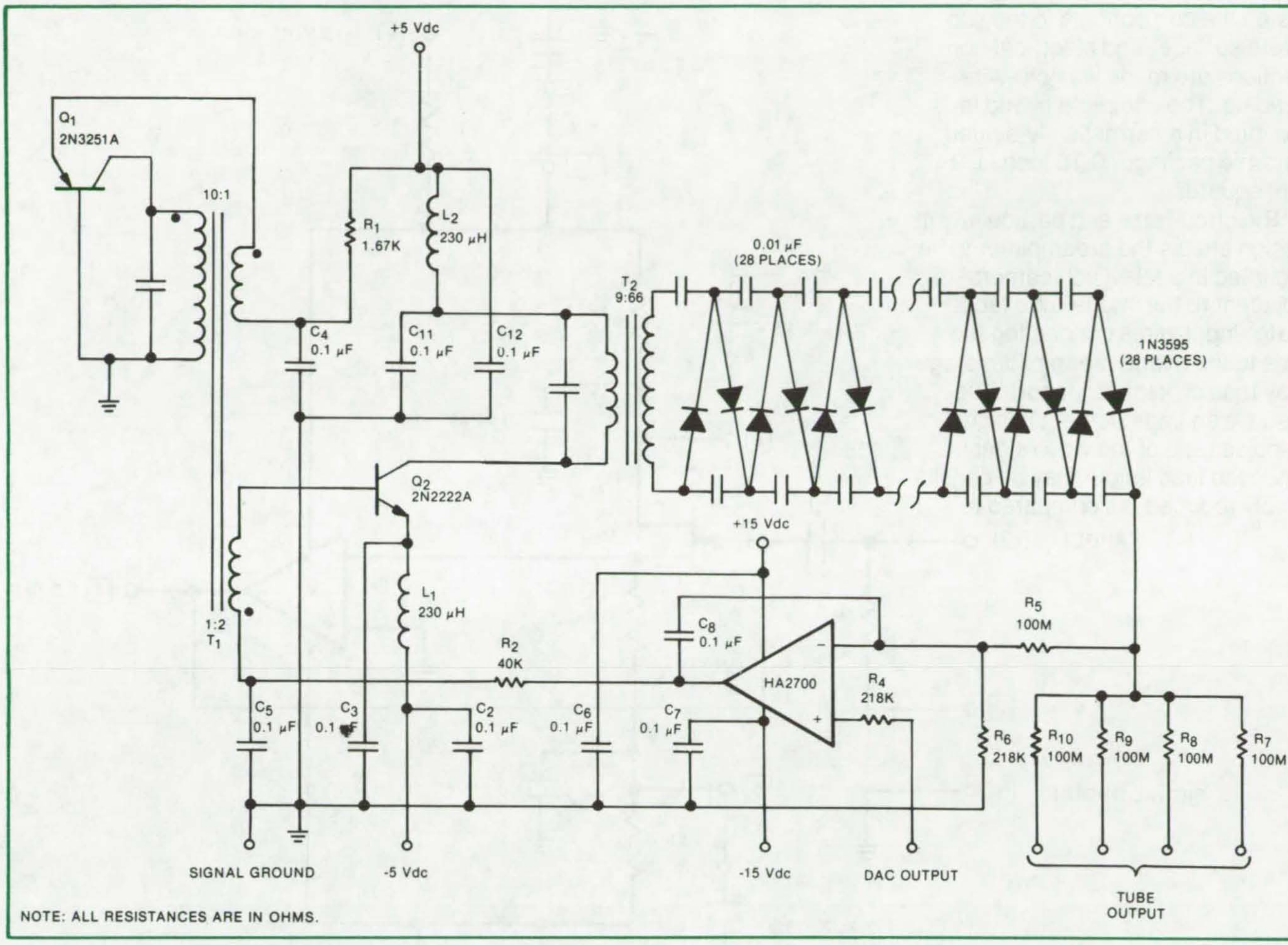

The **Programable High-Voltage Supply** has outputs from 700 to 1,335 volts in 127 steps. The 2-stage oscillator output is up-converted without expensive or critical high-voltage-rated components. The load (proportional counter tubes) is driven via 100-megohm isolation resistors (R_7 through R_{10}).

2N2222A base-drive circuit.

The power transformer, T2, is tuned to the operating frequency for maximum efficiency. The capacitor (C8) between the output and the inverting input of the HA2700 operational amplifier provides loop stability by degrading gain except for very low frequencies and dc. This allows the dc open loop gain to be very high (the operational amplifier gain is 2,000,000). The closed loop gain is therefore set by the resistor divider R5-R6. Output voltage stability then depends only upon R5, R6, and the input parameters of the operational amplifier.

This work was done by David F. Stout and R. A. Perala of Martin Marietta Corp. for **Langley Research Center.** *For further information, Circle 10 on the TSP Request Card.*
LAR-11316

Thick-Film Preamplifier

Circuit for vidicon cameras features low noise and wideband operation.

Caltech/JPL, Pasadena, California

A custom-built thick-film preamplifier with hybrid discrete components and integrated-circuit packaging is designed specifically for use as a television image-tube output signal conditioner. The thick-film circuit is fabricated on an alumina substrate, measuring 0.5 by 0.5 by 0.015 inch (1.27 by 1.27 by 0.038 cm) using a gold-base conductor with conductive gold crossovers and dielectric insulation. It is implemented with chip-style resistors, capacitors, and active components. Adhesive preforms are used to

(continued next page)

fasten the components to the substrate surface, and electrical connections are made via gold-wire bonding. The complete hybrid is mounted in a hermetically-sealed ceramic package, 0.75 inch (1.9 cm) square.

The circuit size and particularly its design enable the preamplifier to be mounted in a television camera adjacent to the image-tube faceplate. Input wires connecting the tube to the hybrid preamplifier stage may thus be kept very short. The result is an improvement in signal-to-noise ratio of the video signal, since the lead length may be considerably reduced, as compared to

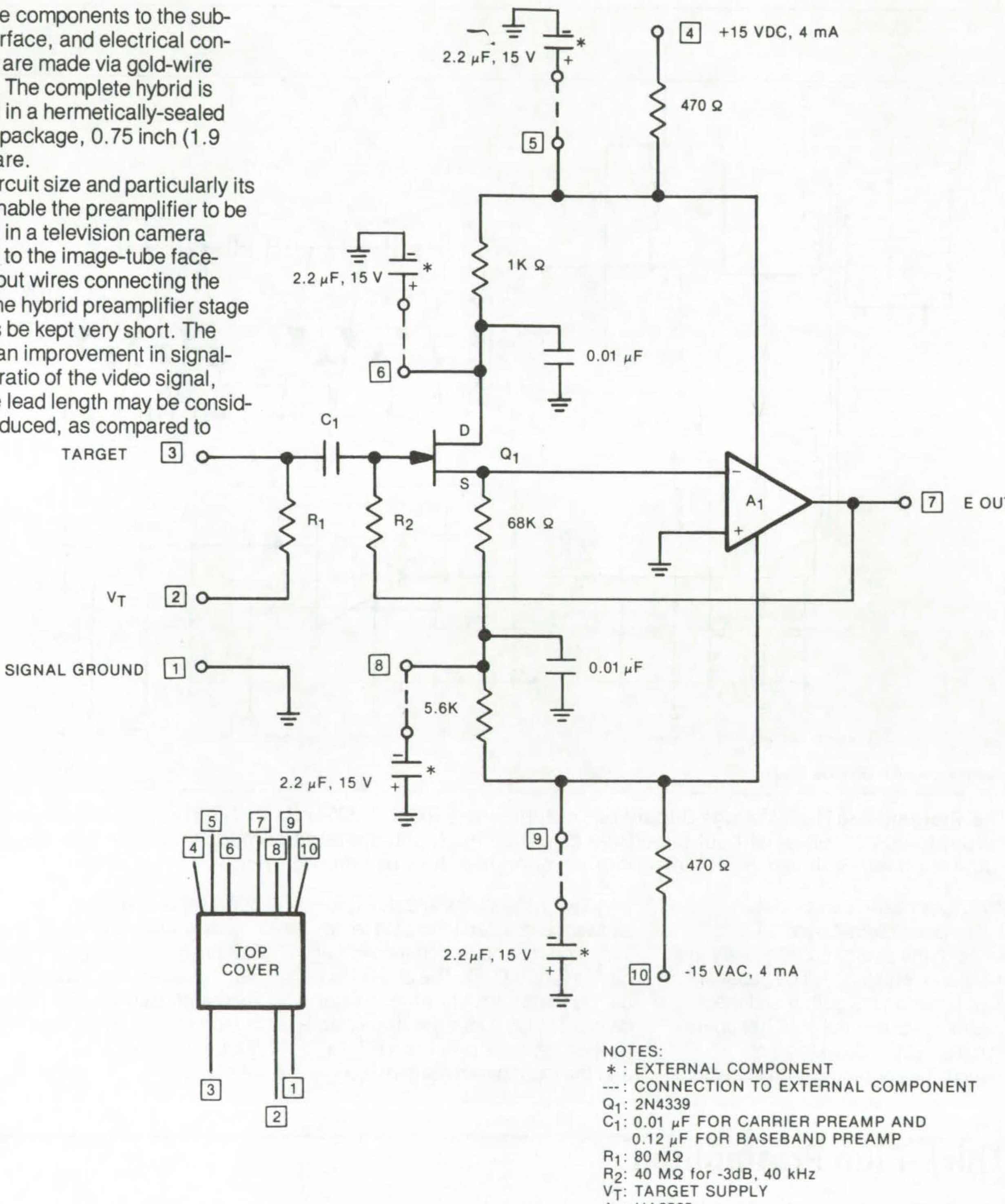

The **Thick-Film Preamplifier** can be designed for a given cut-off frequency, by merely measuring the feedback resistor before installation into the hybrid. From this, the upper 3dB frequency can be calculated knowing the shunt capacity of the resistor. Using this technique, 25 preamps have been fabricated with cut-off frequencies from 8.4 to 500 kHz. In every case, the measured cut-off was within 5 percent of the calculated value.

previous video preamplifier designs. Lead stray capacity, a function of lead length (and also of lead position with respect to circuit ground), is also reduced.

Preamplifier frequency response is determined by trimming only the feedback resistor. No trim capacitors are required across this resistor to achieve the desired amplifier frequency response, since the amplifier rolloff rate to its unity-gain crossover point is well controlled. Amplifier stability and upper frequency response (in this design, variable from 8.4 to 500 kHz) is a direct result of the thick-film fabrication technique.

One unique feature of the thick-film preamplifier is the ability to control bandwidth by grounding the metal cover of the amplifier case. When the case is grounded the bandwidth increases about 1.8 times. A distributed capacity is formed across the feedback resistor, thereby canceling part of the amplifier input shunt capacitance.

This work was done by Gary C. Bailey of **Caltech/JPL.** *For further information, Circle 11 on the TSP Request Card.*
NPO-13416

Microprogramed Telemetry Processor

A PROM controller allows changes to be made to a telemetry processor with a minimum of effort.

Ames Research Center, Moffett Field, California

A minimum-hardware, reliable, microprogramed processor responds rapidly to changing requirements simply by changes in the contents of a programable read-only memory (PROM). The processor was developed for the Pioneer Venus mission, which was expected to require last minute changes in the system package. A random logic system could not be used because time was not available for the incorporation of the additional and expensive hardware that would be necessary to make changes.

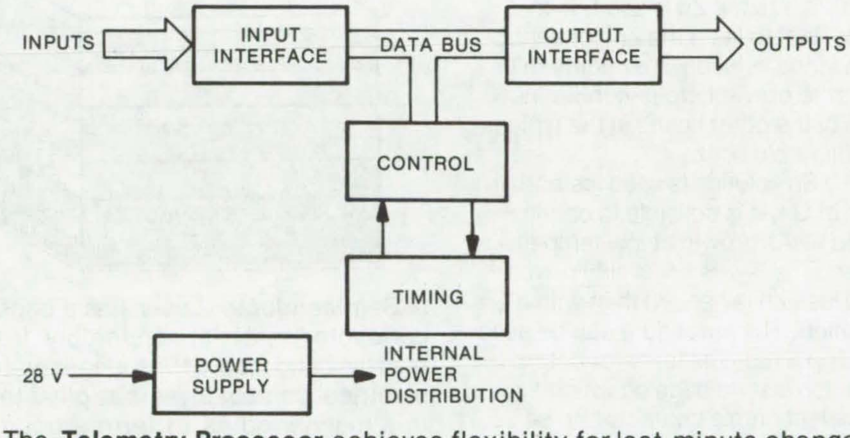

The **Telemetry Processor** achieves flexibility for last-minute changes at a reasonable cost by storing frame formats and control signals in PROM's.

This type of flexibility is also required in many nonaerospace applications, and this particular solution to the problem may be of interest to the designers of other communications systems. The telemetry processor controls the Venus multiprobe bus and the data-handling subsystem for the orbiter spacecraft. It is built around a general-purpose controller and data bus as shown in the simplified block diagram. The controller is the heart of the processor. It can transfer data onto and off a data bus, perform arithmetic and logic manipulations, and store pertinent data in a small internal random-access memory. Frame formats and control signals are stored in programable read-only memories (PROM's) within the controller. Since control of the processor is implemented with PROM's, various control functions can be associated with "routines" within the control PROM.

The processor starts at the beginning of each minor frame word time. When a word is processed, the controller will go to an idle state with the control PROM strobed off to save power. The controller is reactivated by a word-rate start signal.

Processing is limited by the minimum word duration, the speed of the internal controller, and the size of the control PROM. The system was designed conservatively for the Venus mission, and thus the controller clock frequency is limited to 500 kHz; the control PROM, to 256 locations; and the processing, to one-half of a word time or approximately 2 milliseconds. As the bit time decreases, the processing time remains constant, thus reducing the on/off duty cycle. The long processing time allows the implementation of several functions such as data-storage-unit control, so that the external hardware required for interfacing is minimized.

Although sophisticated systems are available and are frequently used to process telemetry signals, this arrangement of relatively inexpensive hardware often can be utilized to provide a modest degree of flexibility for the handling of a number of data inputs.

This work was done by Lee H. Gordon and J. Barry Shackleford of Hughes Aircraft Co. for **Ames Research Center.** *For further information, Circle 12 on the TSP Request Card.*
ARC-11061

Semiconductor Ohmic Contact

A low resistance to GaAs minimizes cross-contamination in the growth process.

A recurrent problem in the growth of GaAs materials, especially lightly doped ones, is that it is difficult to form good ohmic (metal-to-semiconductor) contacts. The best method consists of covering the surface of the material with a highly doped semiconductor. In the case of p-type materials, the usual method is to use a Ga solution doped with Ge or Zn. However, it is difficult to obtain highly doped layers at growth temperatures much below about 750° C. Also, if Zn is used, it is important to keep the Zn concentration in the solution to a minimum in order to prevent cross-contamination of the other layers in the typical multiple-bin boat.

If a Sn solution is used instead of one of Ga, it is possible to obtain good GaAs growth at low temperatures. The layers are highly p-type, and less Zn is needed than with a Ga solution. The procedure can be used to form a topmost layer for heterojunction laser diodes on which excellent ohmic contacts can be formed. A further advantage to using Sn is that the lattice parameter is expanded, resulting in a better lattice parameter match to (AlGa)As. The result is less strain in the structure.

An example of this method is the formation of the ohmic contact on a semiconductor laser, as shown in the figure, with one surface composed of p-type conductivity material. The p material has a wide energy band gap and a large crystal lattice. To the surface of the semiconductor device, a degenerate region of semiconductor material is applied. The material of the degenerate region has a narrower energy band gap and a higher p-type conductivity than the surface of the semiconductor device. The degenerate region is doped with tin to enlarge the crystal lattice of the region to approximate more closely the crystal lattice of the p-type conductivity material at the surface of the semiconductor device. Since tin is an n-type dopant, a p-type conductivity modifier is added to compensate.

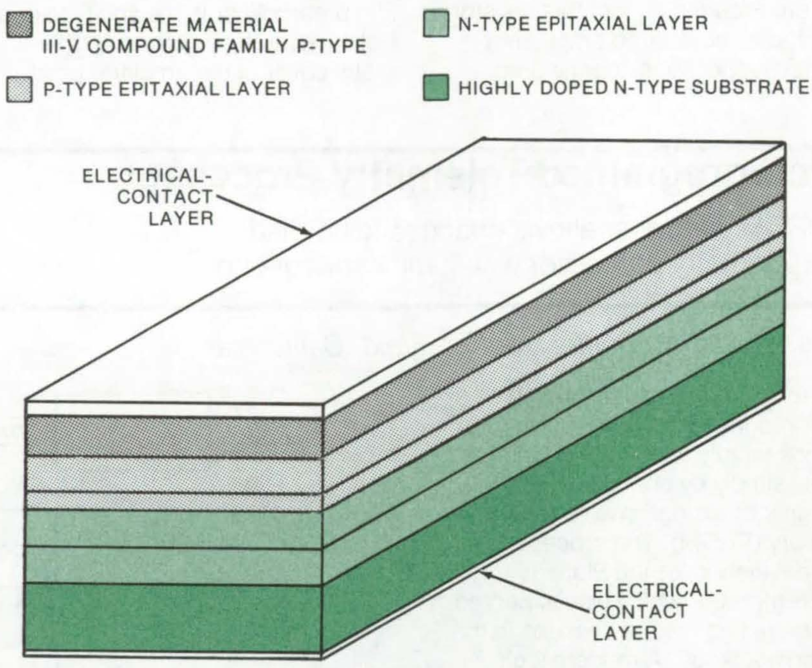

A **Semiconductor Laser** has a degenerate region that consists of semiconductor material, preferably from the III-V compound family. The energy band gap of the degenerate region is less than 1.6 eV. A first electrical contact layer is applied to the surface of the degenerate region in a manner so as to form a good ohmic contact. A second electrical contact layer is applied to the first surface.

The improved ohmic contact that is formed on the p-type surface has several advantages over the previous ohmic contacts. The degenerate region with high conductivity and a narrow band gap provides a surface to which a good metal-to-semiconductor contact can be made. In addition the lattice parameter of gallium arsenide is 5.6533 Å, whereas the lattice parameter of gallium arsenide doped with 1 atomic percent of tin is enlarged to about 5.654 Å. This improved lattice match eases the interface strain which reduces the likelihood of cracking or separation of the semiconductor material at the interface.

This work was done by Frank Z. Hawrylo and Henry Kressel of RCA Corp. for **Langley Research Center.** *For further information, Circle 93 on the TSP Request Card.*

Title to this invention has been waived under the provisions of the National Aeronautics and Space Act [42 U.S.C. 2457(f)], to RCA Corp., Princeton, N. J. 08540.

LAR-11691

Low-Cost Dual-Frequency Microwave Antenna

A single, compact antenna operates on S-band and C-band.

Lyndon B. Johnson Space Center, Houston, Texas

The compact circular-polarization antenna illustrated has been developed for applications where aerodynamic considerations are of prime importance. The antenna, typically matched to a 50-ohm source, can be operated on the S-band and C-band, making the requirement for the radiation window smaller than for two separate antennas operating at these frequencies. The input impedance of the antenna depends on the feedpoint location relative to the disk center.

The antenna is etched on one side of a copper-clad double-sided laminate. The high-frequency radiating element is a disk, and the low-frequency element is a ring. Ring and disk sizes are determined by the operating frequencies and by the dielectric constant of the laminate.

Two metal sections, the phase shifters, are attached to the disk, which can be trimmed to optimize the polarization. The feedpoint is located on the 45° line, intersected to the centerline of these two phase shifters. The input impedance of the antenna at high-band frequency is determined by the location of the feedpoint on the 45° line, the relative dielectric constant (ε_r), and the thickness (t) of the dielectric material. The closer to the disk edge, the higher the high-band impedance. For a 50-ohm system, for instance, the feedpoint is located at middle of radius away from the disk center (for $\varepsilon_r = 2.55$ and t = 1/16 in.). If the line rotates 45° counterclockwise, the high-band antenna has right-circular polarization; a 45° clockwise rotation affords left-circular polarization.

The ring is limited in its width. High-band frequency, f_H, equals or is greater than 2.25 times low-band frequency, f_L. If f_H is less than 2.25 times f_L, the low-band antenna loses its circular polarization. Although a dual-frequency radiating element, the disk or the ring can be operated as a single-frequency radiating element as well.

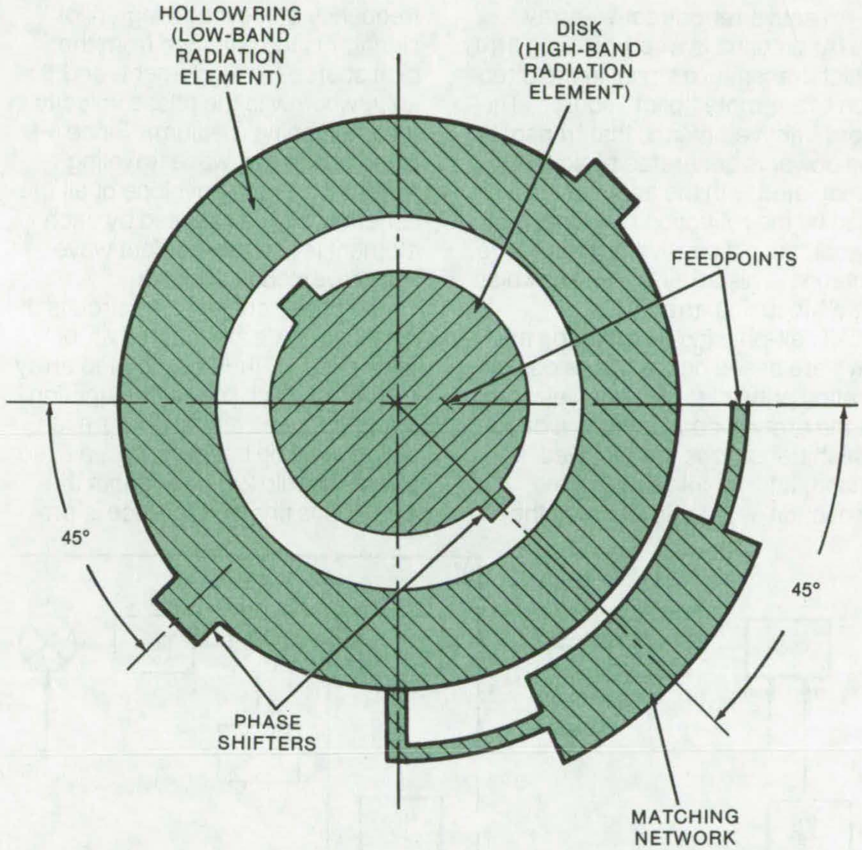

The **Dual-Frequency Antenna** is a circularly-polarized microwave device with high-band frequency and low-band frequency elements. The relatively low impedance of the low-band frequency element can be matched to a desired impedance by adding an etched matching network.

This work was done by I-Ping Yu of Lockheed Electronics Co., Inc., for **Johnson Space Center.** *For further information, Circle 13 on the TSP Request Card.*

This invention is owned by NASA, and a patent application has been filed. Inquiries concerning nonexclusive or exclusive license for its commercial development should be addressed to the Patent Counsel, Johnson Space Center [see page A8]. Refer to MSC-16100.

Active Retrodirective Antenna

Performance is not degraded by the mechanical distortion in large microwave antenna structures.

Caltech/JPL, Pasadena, California

An active retrodirective-array (ARA) antenna is a self-phasing array which transmits a signal in the direction of a remote "pilot" source. The word "active" means that transmitted power is generated by sources associated with the antenna rather than by the reflection of an incident signal, as in a passive retrodirective antenna. This array is also known as a self-focusing array.

All self-phasing transmitting arrays are based on the phase configuration principle; i.e., each element of the array is connected to a circuit which transforms the received phase, $\omega t - \beta r$, into transmitted phase, $\omega t + \beta r$ (ω is 2π times the frequency of the incoming "pilot" signal, r is the distance from the pilot source to the element, and $\beta = \omega / v$, where v is the phase velocity in the intervening medium). Since $+\beta r$ is the phase of a wave traveling toward $r = 0$, the envelope of all the spherical waves radiated by each element is just the incident wave front reversed in direction.

The phase conjugation circuits of existing ARA's are located at, or very close to, their associated array elements. Each phase conjugation circuit requires a phase reference which must be uniform (i.e., a fixed phase modulo 2π) throughout the array. This phase reference is provided by the pilot signal received by one of the elements of the array and is distributed to each of the phase conjugation circuits associated with other elements of the array through transmission lines of fixed electrical length. In order to assure the stability of this phase reference distribution system, the array must be rigid, and therefore (for a given structural material) relatively heavy.

The new ARA overcomes this difficulty by employing a chain topology for the array. In the topology the phase conjugation circuit for the nth element is located at or near the (n-1)th element (the 0-th element is the reference element), and the

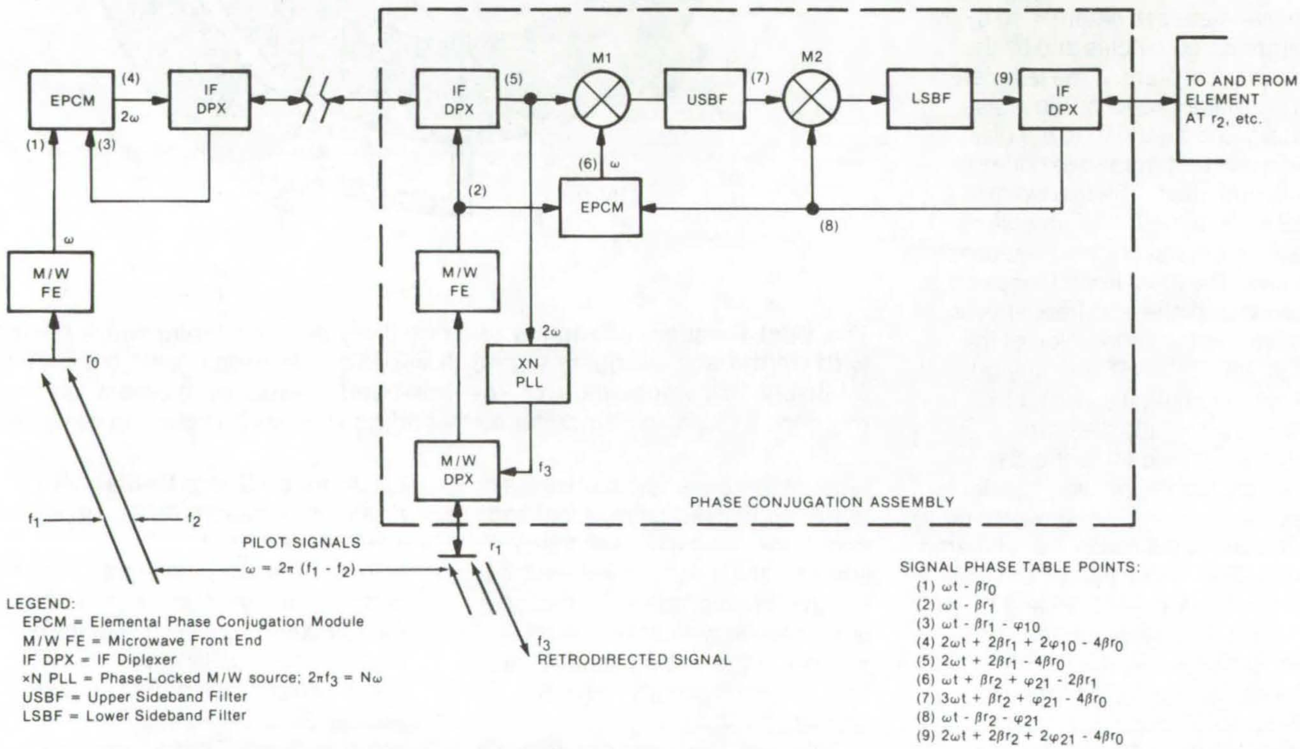

Figure 1. In the **Phase Conjugation Assembly** the elements are connected in a chain with the reference element at the head. Except for the first (reference) the last elements, the phase reference is regenerated at each element in the chain to provide the reference for its right-hand neighbor.

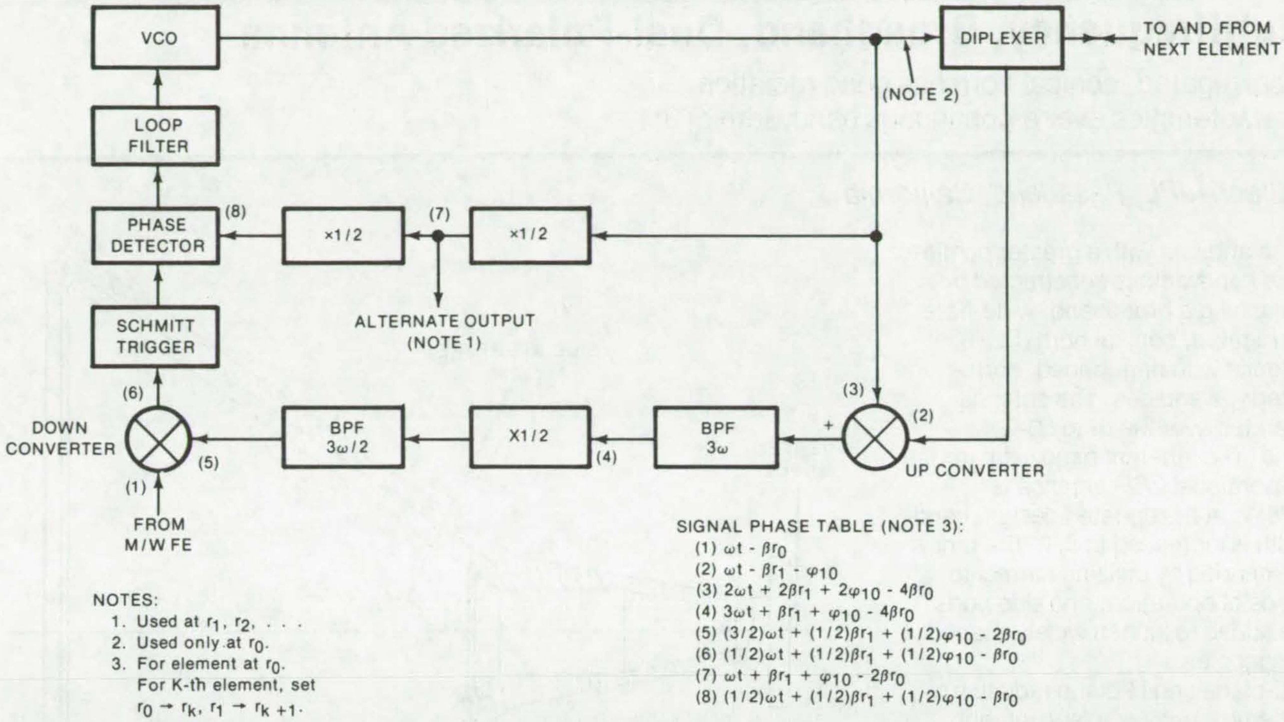

Figure 2. The **Elemental Phase Conjugation Module** (EPCM, in Figure 1) includes, in part, a voltage-controlled oscillator, phase detector, and Schmitt trigger. The phase circuit also functions as a frequency discriminator to aid in acquiring phase lock.

phase circuit in reference (originally supplied by the reference element) is regenerated at each successive phase conjugation circuit in a manner which does not depend on the phase delay of the transmission line connecting successive elements.

The operation of the ARA system is shown in Figure 1. Two pilot signals have frequencies f_1 and f_2 such that $f_1 - f_2 = 50$ MHz. They are mixed in the microwave front end to produce the incoming IF (intermediate frequency) $\omega = 2\pi (f_1 - f_2)$. The phases of the pilot signals received at time t at the element, and at distance r_1 from the pilot source, are $2\pi f_1 t - \beta_1 r_1$ and $2\pi f_2 t - \beta_2 r_2$, respectively. The incoming IF phase is therefore $\omega t - \beta r_1$, where $\beta = \beta_1 - \beta_2$ (point 2 in the illustration). This signal is transmitted to the reference element which is at distance r_0 from the pilot source. At this point (3) the IF phase at time t is retarded by the phase delay, $-\Phi_{10}$, of the transmission line between the elements at r_0 and r_1.

This phase is conjugated and doubled in the elemental phase conjugation module (EPCM) and emerges (point 4) with phase offset $-4\beta r_0$. This signal is then transmitted back through the same transmission line to the element at r_1. By reciprocity this signal is retarded by $-2\Phi_{10}$ which just cancels the $+2\Phi_{10}$ phase advance produced by the EPCM. The transmitted IF phase (point 5) is, therefore, correctly conjugated. This IF then serves as the reference for a phase-locked ×N multiplier which provides an X-band downlink. Having taken care that $2\pi f_3 = N\omega / 2\pi$ is sufficiently far removed from f_1 or f_2, the f_3 signal then is coupled to the element at r_1 and transmitted.

The pilot signal received by the next element, which is at distance r_2 from the pilot source, will be currently conjugated by the phase conjugation assembly at r_2, and so forth, for the elements at r_3, r_4, etc. However, this and successive phase conjugation assemblies differ from that of the first element in that the output of the EPCM is at frequency ω rather than 2ω, and up-converter (M1) and down-converter (M2) mixers are included in the circuit. These modifications are required to incorporate the phase reference regeneration function into the circuit. Figure 1 illustrates how the phase of the signal retransmitted to the r_2 element (point 9) is properly conjugated and has the correct phase offset, $-4\beta r_0$.

The EPCM (Figure 2) includes a voltage-controlled oscillator, a phase detector, a Schmitt trigger, and ×1/2 circuits (flip-flops) which are comprised of emitter-coupled logic integrated circuits. The digital phase detector circuit also functions as a frequency discriminator to aid in acquiring phase lock.

This work was done by Ralph C. Chernoff and Robert C. Tausworthe of **Caltech/JPL.** *For further information, Circle 14 on the TSP Request Card.*

This invention is owned by NASA, and a patent application has been filed. Inquiries concerning nonexclusive or exclusive license for its commercial development should be addressed to the Patent Counsel, NASA Resident Legal Office-JPL [see page A8]. Refer to NPO-13641

Multifrequency, Broadband, Dual-Polarized Antenna

A corrugated, conical horn has good radiation characteristics over a continuous bandwidth of 3:1.

Caltech/JPL, Pasadena, California

An antenna with a greater continuous bandwidth is constructed by combining a broadband, wide-flare, corrugated, conical horn (CCH) antenna with ring-loaded, corrugated waveguides. The antenna operates over the 8- to 50-GHz band. The inherent bandwidth for the conventional CCH antenna is 1.75:1. In the updated design, bandwidth is increased to 3:1. The range is extended by utilizing harmonic bands of operation, and side ports are added to launch widely spaced frequencies.

E-plane and H-plane radiation patterns vary only a few percent over the 8.2- to 26-GHz frequency band. A harmonic band of operation is located around 40 GHz. When the CCH is used with a collimating dielectric lens, efficient focusing of the far-field E-plane and H-plane patterns is obtained for all frequencies in the fundamental band with fixed horn and lens spacing. The phase center of the horn is independent of frequency and polarization.

In one application the CCH antenna is used with a five-channel, dual-polarized radiometer in which the desired channels range over a 5.6:1 frequency band. Radiometer systems require antennas with extremely-low side lobes and insertion loss. This radiometer system feed required 10 ports (both polarizations at 6.6, 10.7, 18, 21, and 37 GHz), with each port sourcing nearly-equal E-plane and H-plane widths for efficient aperture illumination. Feed spillover past the reflector had to be only a few percent of its radiated power, with nearly-coincident, well-defined phase centers for all ports and low insertion loss.

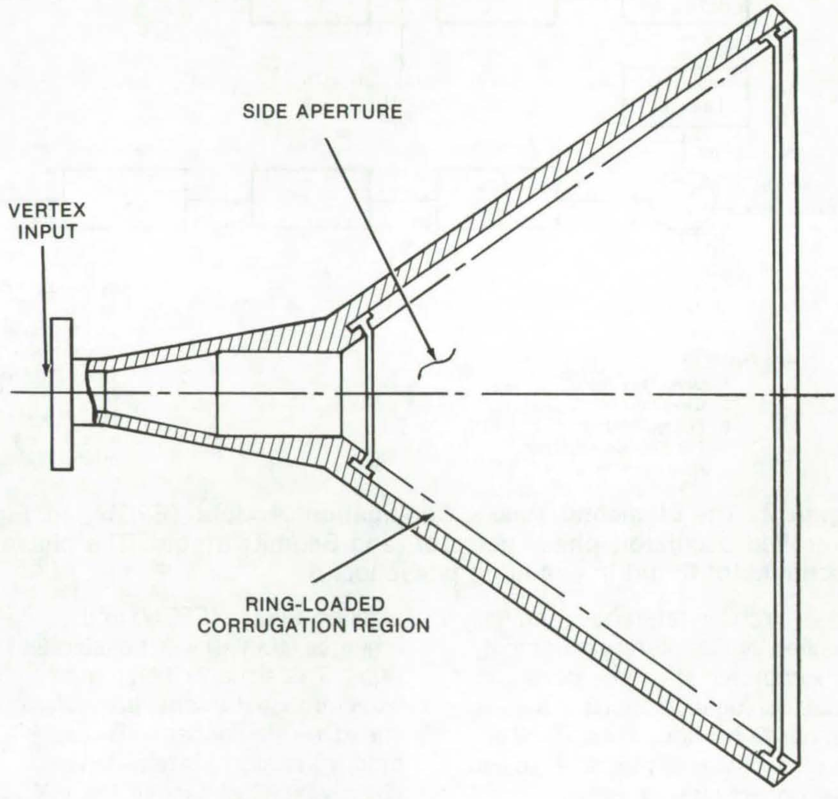

The **Corrugated, Conical Horn [CCH]** antenna is shown above. The ring-loaded CCH can be fed through the vertex of the cone with wideband waveguides, such as double-ridged rectangular or quad-ridged circular, or simply ring-loaded, corrugated waveguides. This is best for extremely wide bands. The antenna is also fed through coupling apertures (or probes) in the side of the cone at appropriate diameters. This is for narrow frequency bands, but multiple elements can be used for frequency bands with wide separations.

In the CCH antenna the frequencies are periodic at which the surface impedance produced by the corrugations is capacitive; harmonic bands of fast-wave performance exist. Actual pattern performance is limited by factors such as: (1) corrugation spacing which should be less than (or at least not equal to) $\lambda/2$, to maintain good impedance match and to avoid higher-order-mode excitation, and (2) the ability to launch only the fundamental hybrid mode with a good impedance match.

This work was done by Kenneth A. Green of Microwave Research Corp. for **Caltech/JPL.** *For further information, Circle 15 on the TSP Request Card.*
NPO-13866

Analog-to-Digital Conversion for Radix [-2]

The analog signal is directly converted, using successive approximation.

Caltech/JPL, Pasadena, California

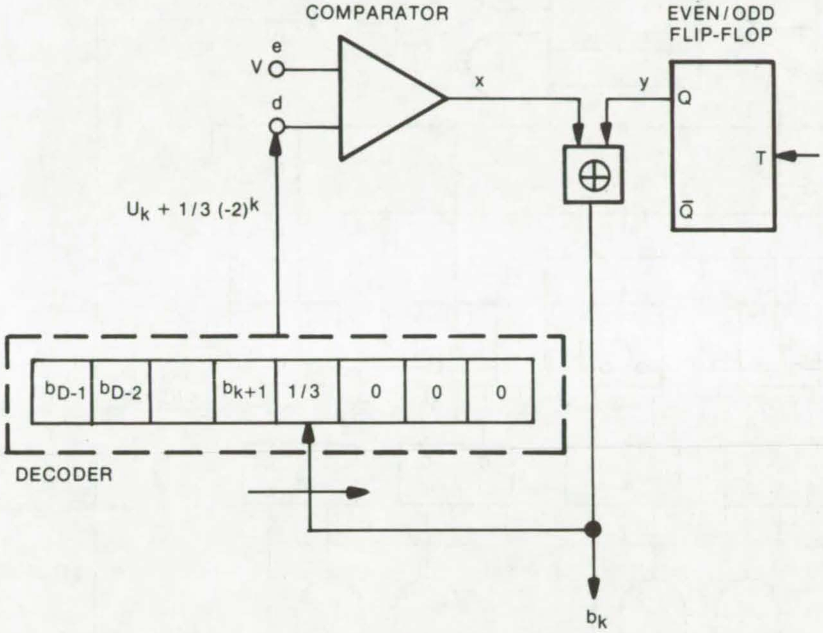

Figure 1. **Basic Conversion Strategy [Determination of b_k]**

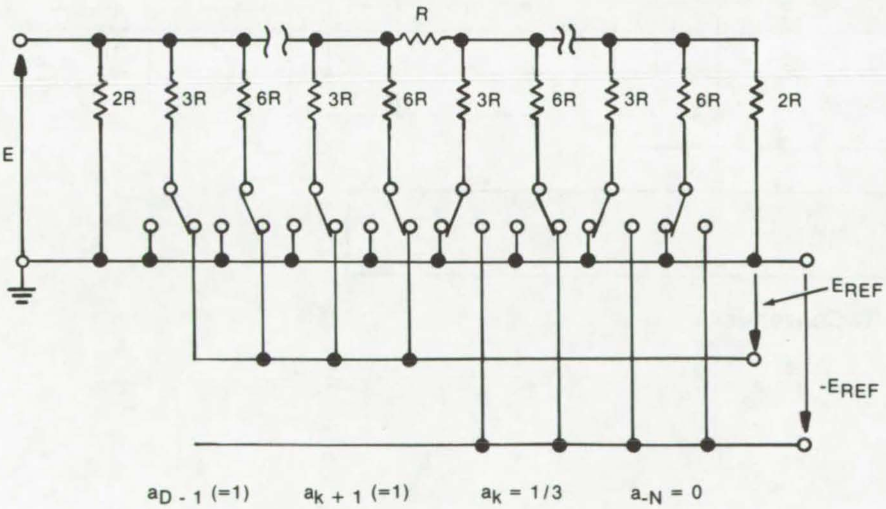

Figure 2. **Implementation of the Decoder of Figure 1**

There has been recent interest in digital devices based on the radix (-2) number representation instead of the standard binary representation. When such a device derives its input from an analog signal, the problem of A/D conversion has to be tackled. One approach is to use a standard A/D converter and to follow it with a purely digital device that converts from radix (+2) to radix (-2). The alternative described here converts directly from the analog signal to its radix (-2) representation.

The device is based on the successive approximation approach and is outlined in Figure 1. The main difference from the standard A/D converter is in the decoder that has to construct the analog of the digital number

$$\sum_i a_i (-2)^i$$

in which all a_i's except one are zero or one. The exceptional a_i has the unusual value 1/3. A possible implementation of such a decoder is shown in Figure 2, while a 3-bit converter using such an encoder is shown in some detail in Figure 3.

(continued on next page)

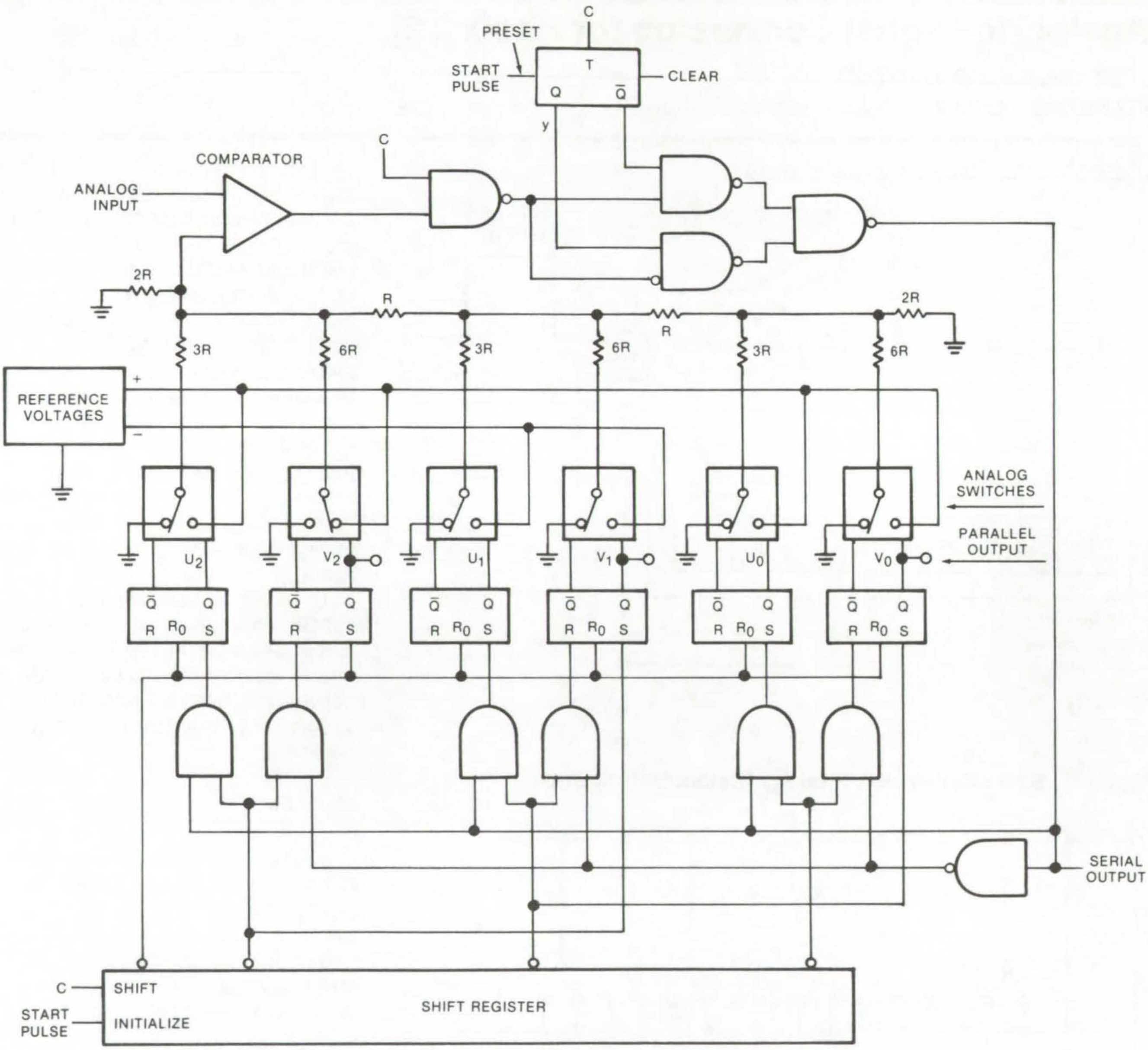

Figure 3. **Three-Bit Negative Radix A/D Converter**

This work was done by Shalhav Zohar of **Caltech/JPL.** *For further information, Circle 16 on the TSP Request Card.*
NPO-13093

Power Supply With Optical-Isolator Control

Cascaded-stages are controlled using optical coupling.

NASA Headquarters, Washington, D.C.

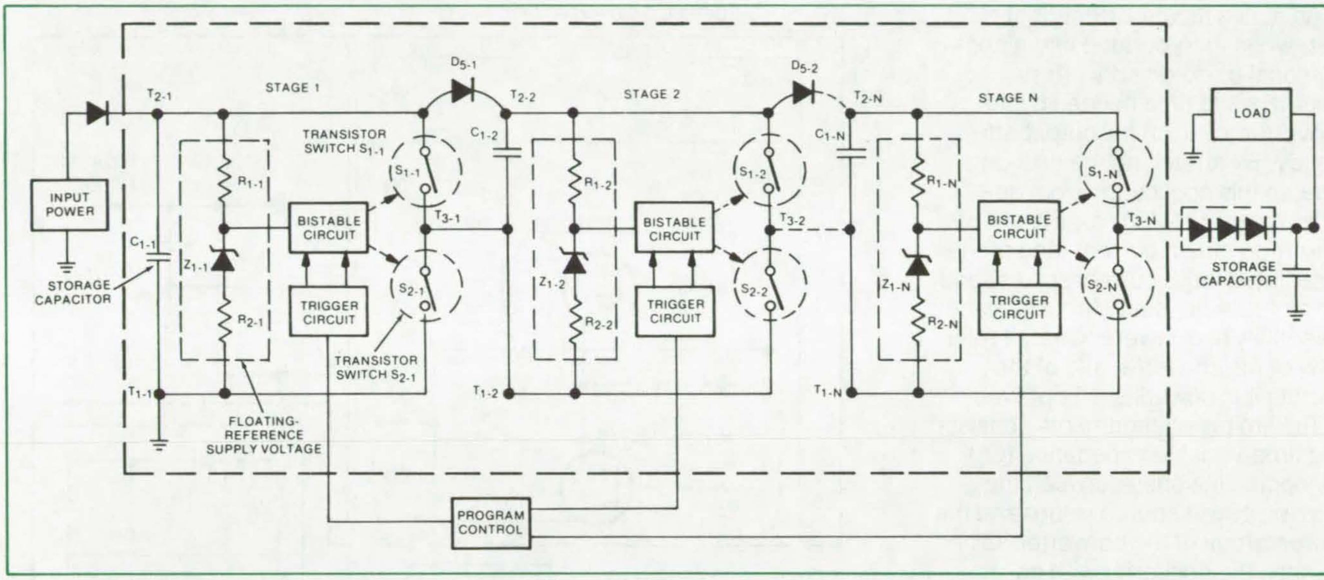

The **Optical-Isolator Controlled Power Supply** may consist of several stages, interconnected and programed for the required output. In the capacitor charging mode, transistor switches S_{2-1} (1st stage) . . . S_{2-N} (Nth stage) are closed. The last stage is in series with a rectifier that prevents current from flowing backward into the circuit. In the capacitor discharge mode, transistor switches S_{1-1} . . . S_{1-N} are closed, and the voltage delivered to the load is the sum of voltages across capacitors C_{1-1} . . . C_{1-N}.

A power supply consisting of cascaded identical stages uses optical coupling to control switching modes. Storage capacitors associated with each stage (C_{1-1} through C_{1-N}, in the figure) are charged from the power source in parallel. Then the capacitors are switched from the parallel-charge configuration to a series or stacked arrangement to produce an output voltage higher than the source voltage. Combinations of series and parallel switching modes for the individual stages can produce various output voltages.

Optical isolators provide coupling from the control input to individual stage switches. This solves the interface problem between the stages and the fixed ground-referenced control as the stages are switched between control ground and higher voltage levels.

Diodes D_{5-1} through D_{5-N} allow charge current to flow to the capacitors but block reverse current back to earlier stages. A storage capacitor, placed across the load, maintains the output voltage during the charge portion of the switching cycle.

This work was done by Richard H. Baker and John T. Wheeler of M.I.T. for **NASA Headquarters.** *For further information, Circle 17 on the TSP Request Card.*

Title to this invention has been waived under the provisions of the National Aeronautics and Space Act [42 U.S.C. 2457(f)], to M.I.T., Cambridge, Massachusetts 02139. HQN-10827

Active Inrush-Current Limiter

Stretching turn-on time in a dc-to-dc converter limits current surges and dI/dt turn-on rate.

Goddard Space Flight Center, Greenbelt, Maryland

An active input-current-limit circuit, when incorporated into a conventional dc-to-dc converter, lengthens the time needed by the converter to reach full output efficiency. By stretching the turn-on time, in this application from approximately 1 to 200 ms, the effects of turn-on inrush current (and of the associated large current spikes) and current rate of rise (dI/dt) are made potentially less severe. Overall reliability of the converter and of the circuits it is powering is improved.

The limiter arrangements consists of a time-variable impedance (Q_3) connected in series between the input dc power source return and the power circuit of the converter. Q_3 sources the converter with an upward-increasing current ramp.

The control circuit (see the figure) initially operates during turn-on in the active region. Having completed the turn-on cycle and during normal converter operation, Q_3 is saturated. Saturation is maintained via a feedback loop from the converter.

The control circuit is comprised of a control transistor, Q_3, and a pair of Darlington-connected driver transistors, Q_4 and Q_5. Q_3 is placed in series with the dc power source return line and the converter.

During the turn-on ramp, the base-emitter junction of Q_6 is reverse biased by the voltage across the base resistor of Q_3 and the voltage across the base-emitter junction of Q_3. The reverse bias continues until the voltage across a second timing capacitor (C4) rises to a value just sufficient to apply a forward bias to Q_6.

The voltage applied to the base resistor of Q_3 rises to a value sufficient to feed a greater saturation drive current to the transistor and also to reverse-bias the base-emitter junctions of the Darlington pair (Q_4, Q_5). Saturation drive current from the power source ceases to flow

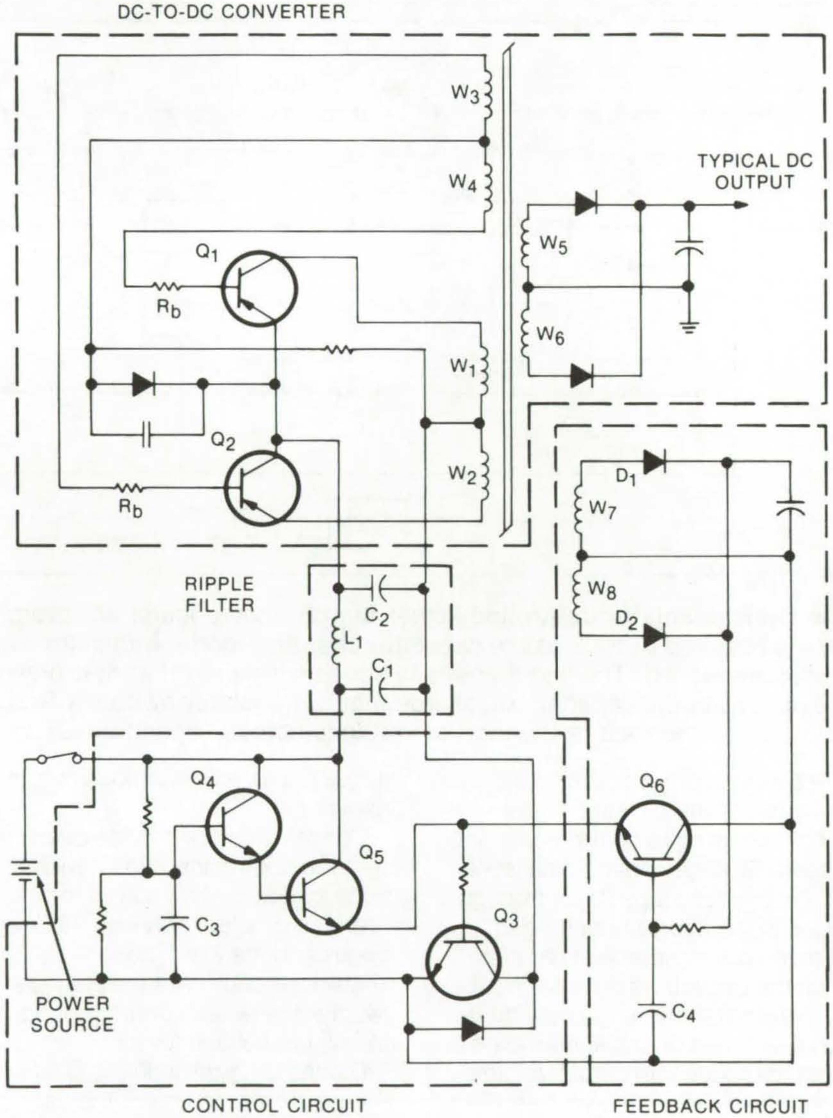

The **Active Inrush-Current Limiter** consists of a control circuit and a feedback circuit. At turn-on (just after the switch connects the power source to the converter) a timing capacitor (C_3) begins to charge to a ratio of the power source level. The base voltages of Q_4, connected to the capacitor, and Q_5 also rise. A ramp current output from Q_5 and its emitter resistor sources the control transistor, Q_3, which, connected in series between the power source and the converter, controls current flow to the converter. Diodes D_1 and D_2 and transistor Q_6 form a feedback circuit which keeps Q_3 saturated once the converter begins operating. The pi filter (C_1, C_2, and L_1) is used to prevent ac ripple currents and current spikes from the converter switching transistors from causing interference elsewhere.

through Q_5 and Q_4, and Q_3 is maintained in saturation by a voltage supplied by the feedback circuit (D_1, D_2, Q_6, and associated components) that is lower than that from the power source.

This work was done by Robert A. Kichak of **Goddard Space Flight Center.** *For further information Circle 18 on the TSP Request Card.*

This invention is owned by NASA, and a patent application has been filed. Inquiries concerning nonexclusive or exclusive license for its commercial development should be addressed to the patent counsel, Goddard Space Flight Center [see page A8]. Refer to GSC-11789.

All-Digital Sequence Correlator

Modular circuit can be expanded to handle pseudonoise codes or other codes of any length.

Caltech/JPL, Pasadena, California

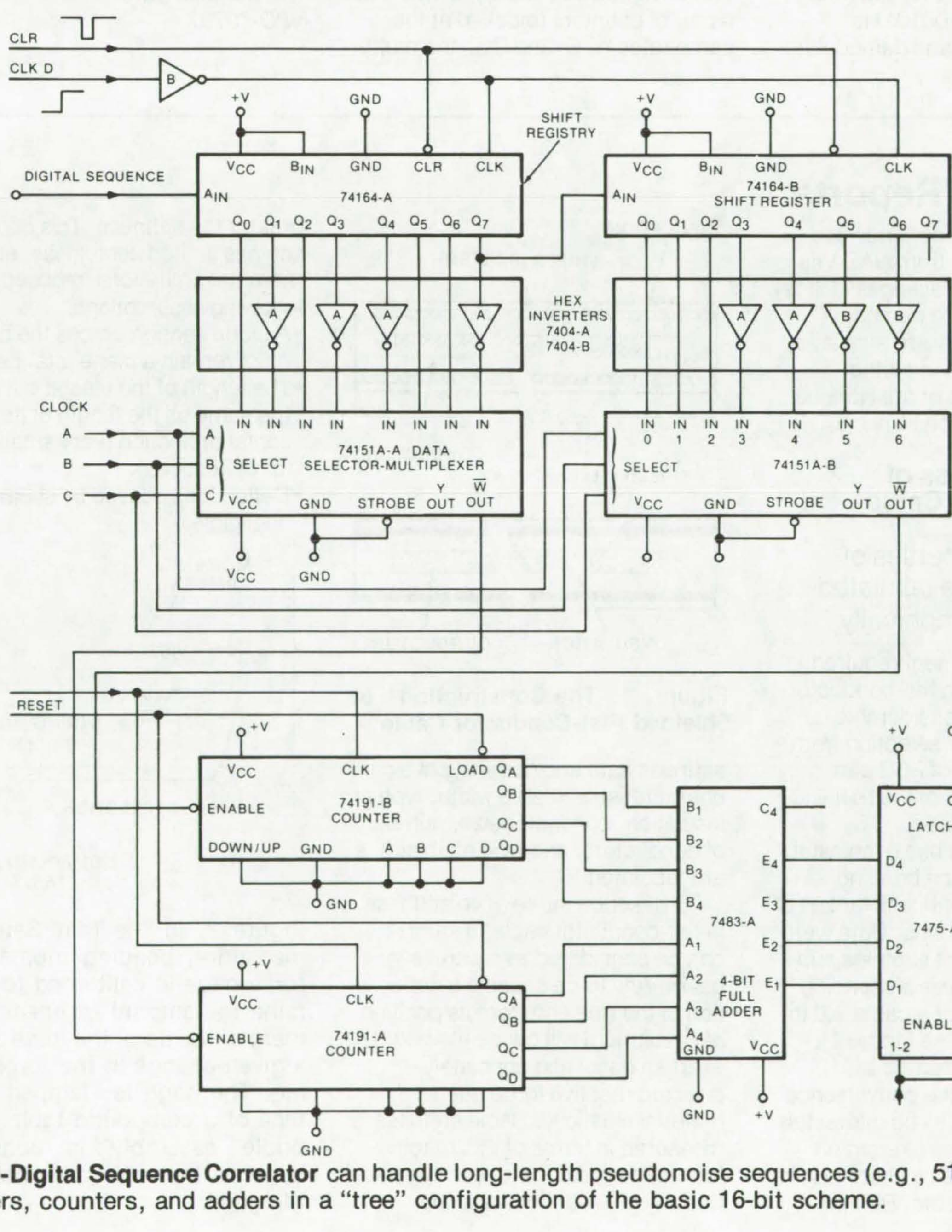

The **All-Digital Sequence Correlator** can handle long-length pseudonoise sequences (e.g., 512) by adding shift registers, counters, and adders in a "tree" configuration of the basic 16-bit scheme.

(continued on next page)

With the use of standard digital logic a correlator has been designed to handle pseudonoise codes or other digital sequences. The circuit is flexible enough to accommodate long sequences by adding shift registers and an additional counter and latch for each shift register. A correlation coefficient of unity or zero is generated when all of the bits of the sequence are received and positioned correctly in the input shift register.

With reference to the schematic diagram of the digital correlator, a 16-bit pseudonoise (PN) sequence (e.g., 1000011101100101) is received at a baseband demodulator and is shifted into a register consisting of two integrated-circuit chips of the same type in cascade. To detect the correct sequence, two hex inverter sets are placed in the output of the shift-register stages (in a "0" state when the pseudonoise word is received correctly) such that all "1"s are input to the two multiplexers when there is a unity correlation coefficient. An address counter (in the data selector-multiplexer), clocked by lines A, B, and C at a frequency higher (X8) than the PN shift clock, multiplexes the $\overline{W}$ output signals to enable the inputs of a pair of counters (clocked at the same rates A, B, and C as the multiplexers). This accumulates counts proportional to the number of "1"s output from the shift registers over a PN clock period. The counters output 4-bit words to an arithmetic logic chip (7483-A). This chip acts as a binary adder to generate a 4-bit word plus a carry. These 4-bit words plus carry are latched (7475-A) over a PN clock period to give the correlation coefficient for each 1-bit shift of the input PN sequence.

This work was done by Allan Laderman of **Caltech/JPL.** *For further information, Circle 19 on the TSP Request Card.*
NPO-13737

Books and Reports

These reports, studies, and handbooks are available from NASA as Technical Support Packages (TSP's) when a Request Card number is cited; otherwise they are available from one of NASA's Industrial Application Centers or the National Technical Information Service.

Relative Stiffness of Flat-Conductor Cable

Mechanical-properties of shielded FCC are tabulated and displayed graphically.

The bending moment required to cause deflections in flat-conductor cable (FCC) is of considerable importance. Proper selection from the available types of FCC can optimize the effects of the bending-moment characteristic.

A simple method has been established to measure the bending moment (relative-stiffness factor) of various FCC specimens. Data were taken on 10 different samples and normalized to express all bending moments in terms of a cable 2.0 in. (5.1 cm) in width (see Figure 1). These data are presented in graphical form for the convenience of designers who may be interested in finding the torques exerted on critical components by short lengths of flat-conductor cable. Relative-stiffness data and nominal physical characteristics (cable width, type of insulation, conductor size, number of conductors, and type of shield) are tabulated.

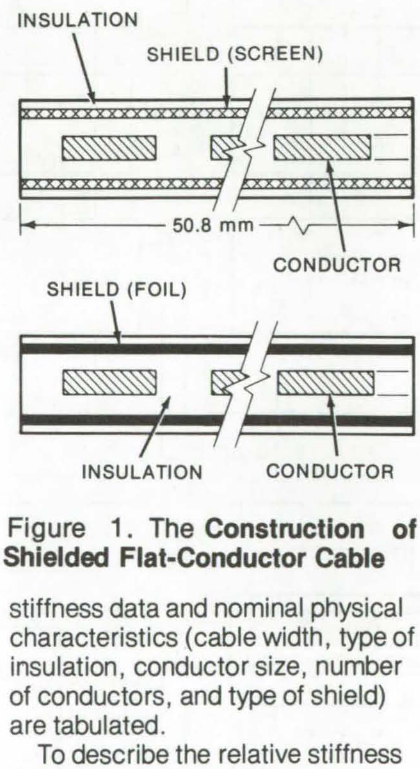

Figure 1. The **Construction of Shielded Flat-Conductor Cable**

To describe the relative stiffness in flat-conductor cable, a sample can be considered as a cantilever beam. Any force causing a deflection of the free end from its position of equilibrium will cause the beam to exert an equal and oppositely-directed reactive force due to material elasticity. Cable stiffness is measured in terms of this reactive force. The greater the reactive force (for any given deflection), the greater the stiffness. This comparison has limited usefulness, and there are limitations imposed by the following assumptions:

- A plane section across the beam must remain a plane after bending.
- The length of the elastic curve is the same as the length of its horizontal projection (very small angular deflections).
- Deflections caused by shear are negligible.

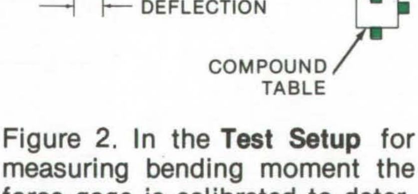

Figure 2. In the **Test Setup** for measuring bending moment the force gage is calibrated to determine the amount of linear movement of the tip of the force arm for a given change in the force reading. The gage is clamped to the face of a compound table, and a bridle assembly is connected between the table and the tip of the gage.

• Stress caused by bending must remain below the proportional limit. (Hooke's law applies.)

The technique used (a version of the cantilever technique) for describing relative stiffness involves measuring deflections produced by forces at various moment arms. The test setup for measuring bending moments in shown in Figure 2.

The micrometer adjustment on the compound table is changed in increments of 0.10 in. (2.54 mm) to move the force gage away from the cable. For each increment that the table is moved, the force gage is read; and the net displacement of the cable is calculated by taking the displacement of the table and subtracting it from the displacement of the tip of the force gage with respect to the table. The deflection of the cable is then measured along a direction perpendicular to the original neutral axis of the cable.

Comparative information can be obtained from the graphical results by defining a relative-stiffness factor as the ratio of the applied force (at a particular moment arm) to a deflection equal to 10 percent of the length of the moment arm. The relative-stiffness factor as defined is a nonlinear function of the moment-arm length: as the moment-arm length decreases, the relative-stiffness factor increases. The curves (of deflection versus force) give an excellent indication of the relative-stiffness factor for moment-arm lengths ranging from 1.5 in. (3.8 cm) to 3.0 in. (7.6 cm).

This work was done by James D. Hankins of **Marshall Space Flight Center.** *For further information, Circle 20 on the TSP Request Card. MFS-23537*

Transformer Design Tradeoffs

Straight-line relationships between parameters aid electrical optimization.

In designing transformers with C-type cores, straight-line relationships may be shown to exist between the area product (A_p) and current density, volume, surface area, and weight of the transformer. By using the relationships to make decisions about parameter-value tradeoffs it is possible to design transformers of improved efficiencies and smaller size and volume. The transformer A_p numbers, which are used to summarize dimensional and electrical properties of C-cores, pot cores, lamination, powder cores, and tape-wound cores, form the basis of "Transformer Design Tradeoffs," an 81-page memorandum.

Core material selection is also treated extensively. To aid in core selection, a comparison of five common core materials is presented to indicate their influence on overall transformer efficiency and weight. Cost differences between core materials of the nickel steel families and those made from low-cost silicon steel are described, the latter being used in tutorial design examples to illustrate the tradeoffs and theories developed in the memorandum.

This work was done by Colonel W. T. McLyman of **Caltech/JPL.** *To obtain a copy of the memorandum, Circle 21 on the TSP Request Card. NPO-13755*

Computer Programs

These programs may be obtained at very reasonable cost from COSMIC, a facility sponsored by NASA to make new programs available to the public. For information on program price, size, and availability, circle the reference letter on the COSMIC Request Card in this issue.

Dielectric Covered Antennas

Evaluation of antenna radiation pattern effects

Traditional solutions for dielectric and radome covered antennas have involved plane-wave transmission theory through multiple dielectric layers. More recent solutions involve Fourier transform techniques and the method of moments for single dielectric cases. Because of simplicity and adaptability, this new program incorporates a modified version of the plane-wave transmission theory including multiple internal reflections and the effects of the ground-plane reflection. Previous methods have not considered ground-plane reflection.

The model assumes an isotropic hemispherical radiator from a point source with individual rays incident upon several dielectric materials. The angles of refraction are determined by Snell's law. Calculations of the critical angle, and therefore the angle above which complete internal reflection exists, are obtained from the dielectric constant. Geometrical and electrical considerations give rise to phase delays in each dielectric material. The transmission coefficient for perpendicular polarization is obtained at each interface. Since there exists the possibility of an infinite number of internal reflections and subsequent retransmissions, the transmission and reflection coefficient magnitude for each interface are determined in order to evaluate only the most significant reflections and retransmissions.

FORTRAN
UNIVAC 1108, EXEC 8
Central Memory Requirement
Approximately 10K 36-Bit Words

This program was written by Jefferson F. Lindsey of McDonnell-Douglas Corp. for **Johnson Space Center.** *For further information, Circle A on the COSMIC Request Card.*
MSC-16186

Electrostatic Analysis of Charge-Coupled Structures

A realistic model for more complete analysis

A package consisting of three computer programs has been developed for the investigation of charge-coupled shift registers, but it should be useful in analyzing any charge-coupled device (CCD) design. The programs perform a two-dimensional electrostatic analysis of the CCD structure to determine whether charge transfer is efficient. Two-channel oxide thicknesses, two levels of metalization, and variable channel doping can be accommodated. One of the programs can be used to analyze three-electrode CCD input/output gates, and the other two programs can be used to analyze two-phase structures containing two or four electrodes with periodic boundary conditions.

In the past, analyses of CCD structures have been conducted for the ideal mode of operation in which the channel is depleted of minority carriers except for those which are gated into the input end of the channel and transferred by the attractive potential produced by the transfer electrodes. In the ideal operating mode no barriers exist in the interelectrode gap, and the necessary condition for transfer, that the attractive potential of the succeeding electrode in the direction of transfer must exceed that of the preceding, is also sufficient for transfer. In practice, potential wells and barriers may exist and preclude complete charge transfer. Their occurrence depends upon CCD structural parameters such as electrode geometry, oxide thickness, and channel doping. Such phenomena must be investigated by two-dimensional analyses.

The complexities which arise in considering a realistic model suggest a numerical approach. In this package an approach based on Gauss' law is chosen because it allows for the treatment of discontinuities in a straight-forward manner. A rectangular cell structure is chosen as convenient for the formulation of a discrete problem from a continuous one. A two-point finite-difference formula is used to define the gradient along each boundary of the cell. The result of the model is typically a large system of nonlinear simultaneous equations. The numerical solution is obtained by application of the Gauss-Seidel method. These programs contain no algorithm for the calculation of the electric field. Data on the electric field is necessary for estimation of transmit time. After a solution has been obtained, a high-order polynomial fit to the potential profile will allow a smooth approximation of the field at grid points.

FORTRAN
UNIVAC 1100
Central Memory Requirement
Approximately 19 K 36-Bit Words

These programs were written by James D. Gassaway of Mississippi State University for **Marshall Space Flight Center.** *For further information, Circle B on the COSMIC Request Card.*
MFS-23507

Electronic Systems

Direct-Reading Inductance Meter

A low-cost instrument
indicates from 30 nH to 3 μH.

Caltech/JPL, Pasadena, California

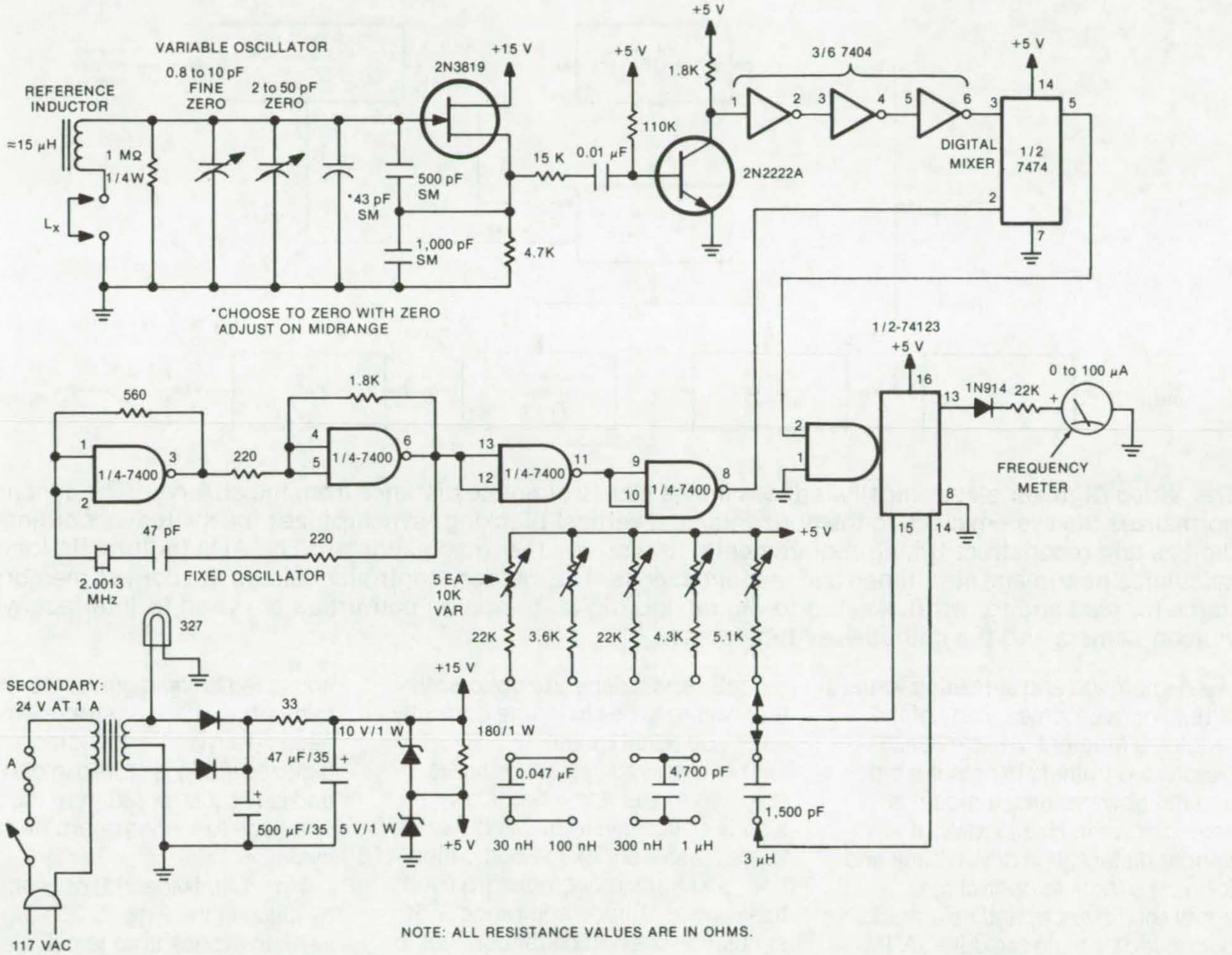

Direct-Reading Inductance Meter indicates from 30 nH to 3 μH. The reference inductor of 15 μH is made by winding 50 turns of No. 26 Formvar wire on a Micrometals type 50-2 (or equivalent) core.

Electrical parameters of low-value inductors, in the range of from 10^{-8} to 3×10^{-6} H, are difficult to measure, considering their often miniscule size and the effect of lead lengths on the measurement of total coil inductance. The inductance of typical miniature coils, mostly used in breadboarding RF circuits, can be measured by using a moderate-accuracy TTL-implemented meter. The circuit eliminates the requirement for complex instrument compensation prior to taking a coil inductance measurement and thus is as easy to operate as a common ohmmeter.

The circuit consists mainly of a reference oscillator (f_r) and a variable-frequency oscillator (f_X). An unknown inductance (L_X) is connected in series with a larger coil (L) in an L/C tuned circuit, causing the tuned-circuit resonant frequency to shift downward. For small values of inductance ($L >> L_X$), this frequency change is approximately a linear function of the unknown inductance value.

The outputs of both f_r and f_X are fed to a dual-D edge-triggered flip-flop (1/2 7474) configured as a digital mixer. The difference frequency ($f_r - f_X$) is sourced to a frequency meter, a one-shot multivibrator used to drive the analog display. Indicated shifts in frequency thus correspond to the inductance of L_X.

This work was done by Richard B. Kolbly of **Caltech/JPL.** *For further information, Circle 22 on the TSP Request Card.*

This invention is owned by NASA, and a patent application has been filed. Inquiries concerning nonexclusive or exclusive license for its commercial development should be addressed to the Patent Counsel, NASA Resident Legal Office-JPL [see page A8]. Refer to NPO-13792.

Video Simulator With Electronic Ranging

An interactive training simulator is made less costly with digital range simulation.

Lyndon B. Johnson Space Center, Houston, Texas

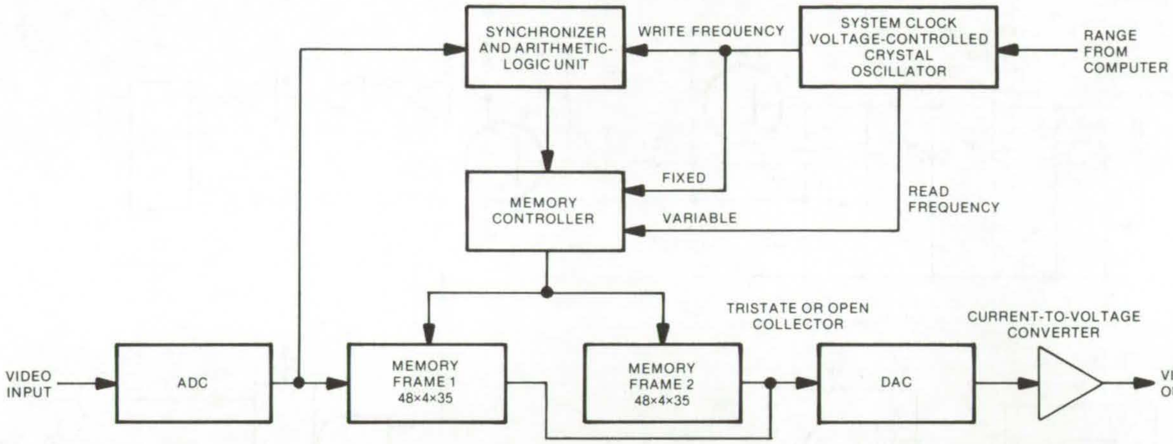

The **Video Digitizer** electronically reduces image size to simulate distance from the observer. The synchronizer normalizes the system clock to the horizontal and vertical blanking, synchronizes the system according to the digitize and reconstruct timing requirements, and stores the image address. The ALU (arithmetic-logic unit) calculates new image start times and readout speeds. The memory controller selects the correct memory-page frame for read and for write. Analog-to-digital and digital-to-analog converters are used to interface with the vidicon camera and the cathode-ray tube screen.

An improved and simplified visual simulator overcomes many of the problems inherent in a previously-used video trainer. In both the old and the new systems a model is scaled down in size to make it appear distant. It is driven back and forth on a track to control the apparent distance, and its attitude is controlled by a gimbal drive. A TV camera that records the motion of the object is also gimbaled, to simulate the observer's attitude. The relative motions of both the observer and the object are displayed on a CRT screen.

In the conventional system, however, limitations in the track length required that two or three models, scaled successively smaller, be used when the apparent maximum object distance had to be much greater than the minimum object distance. One problem with this multiple-model approach was that a separate accurate gimbal had to be constructed for each smaller model. Furthermore, any model changes had to be machined into two or three models, and a separate optical system was required to image correctly each additional model.

The improved system requires only one model and a relatively-simple optical system. Gimbal orientation, raster shrinkage and deflection, and track movement are used to simulate attitude and range. For simulation of short distances, out to 600 ft (183 m), only gimbal orientation and track movement are used. Beyond this range, the gimbal orientation is still used, but electronic raster shrinkage is employed for sizing the image.

Because the same gimbal controls attitude in both cases, the attitude is always mapped onto the vidicon faceplate correctly. There is no need for a dynamic mapping generator.

A key component in the new system is a video digitizer that converts the vidicon camera signal to digital form, processes it to reduce the image size, and reconverts the processed data to an analog signal for display on the CRT. As shown in the block diagram, range information is fed to the digitizer from a computer. There are two memory pages (frames 1 and 2); incoming digitized video is stored in one page and is reconstructed from the other. The page functions alternate each cycle.

Horizontal video is reconstructed by utilizing the long (1,250-μs) vertical flyback time to calculate the image size. To center the reconstructed image about the original, an image offset counter signals the start of a new image. The readout frequency and the offset counter are both dependent upon the range signal. The vertical height of an image is reduced by reading out less than the full number of lines from each six-line raster segment. The entire system has good distortion control with a final resolution of 20 arc minutes.

This work was done by Werner Kraemer of The Singer Co. for **Johnson Space Center.** *For further information, Circle 23 on the TSP Request Card.*
MSC-14965

Infrared Range Sensor

An optical-reflection technique senses range and azimuth of an object 1 to 10 cm away.

Ames Research Center, Moffett Field, California

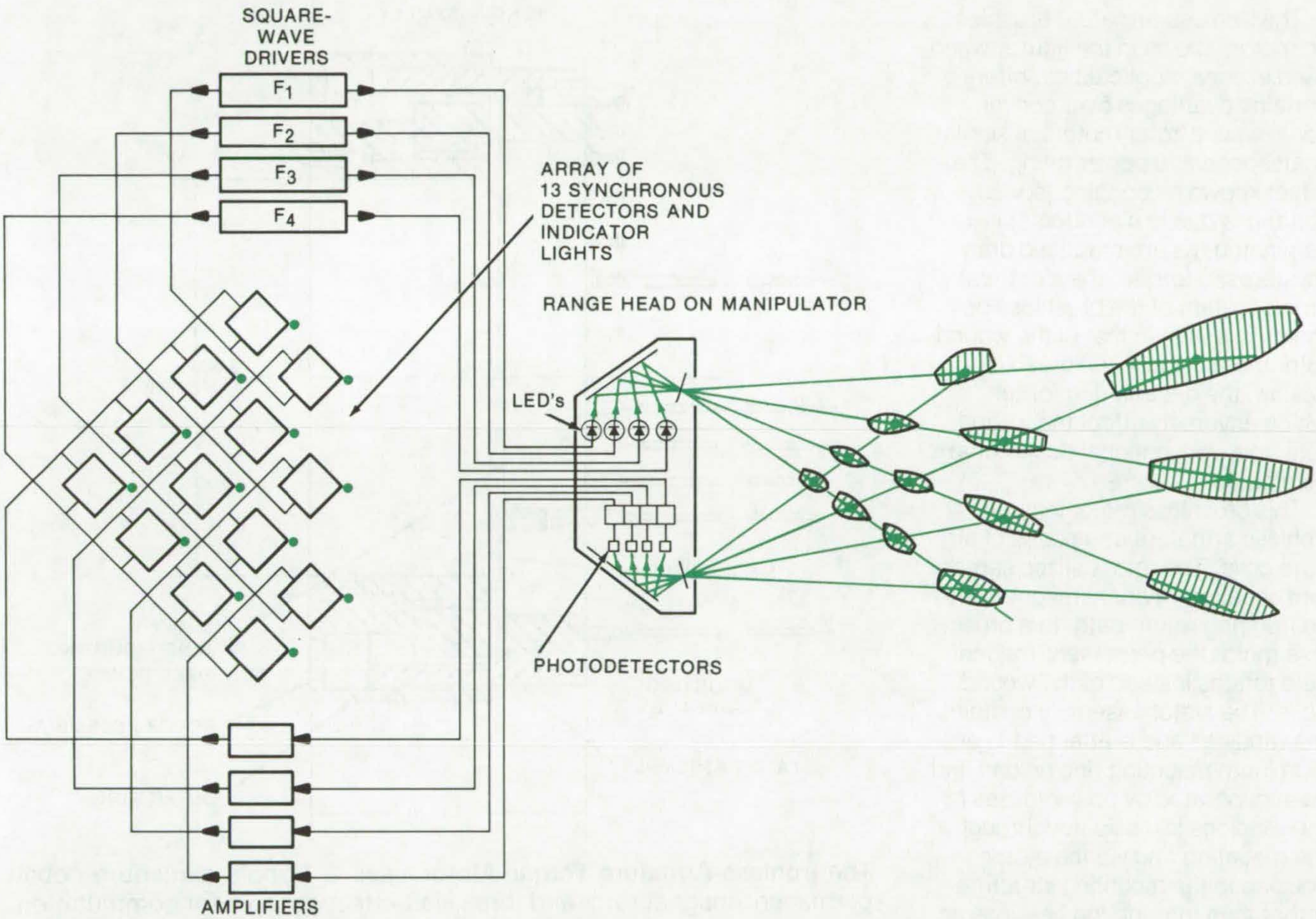

The **Infrared Range Sensor** will detect objects that lie at the intersections of four emitted beams of light and the fields of view of four photodetectors. The shaded areas around the intersections indicate the approximate areas in which an object will be detected. Each area corresponds to a unique detector and indicator light.

An infrared-reflection range sensor, originally developed for the end effector of a remote manipulator, employs a triangulation technique to locate objects. The sensor is based on overlapping fans of light beams and a series of light sensors. Light beams are generated by four LED's that are amplitude modulated (at 2.0, 2.4, 2.8, and 3.2 kHz) so that the beams may be distinguished one from another.

The detectors are four phototransistors. An object located at any intersection point of a beam of light and the line of sight of a given phototransistor will be detected. Signals from individual phototransistors are filtered and identified by individual synchronous detectors, one for each beam-intersection point.

All oscillators, amplifiers, and detectors are contained in a small electronics package that has its own power supplies and an LED display corresponding to the physical layout of the intersecting beams on the front panel. Analog signals proportional to the reflected light at each intersection are applied to a threshold and are converted to on/off (binary) signals that are made available through a back-panel connector.

This work was done by John W. Hill and James R. Woodbury of Stanford Research Institute for **Ames Research Center.** *For further information, Circle 24 on the TSP Request Card.*
ARC-10885

Ironless-Armature Brushless Motor

High-speed motor has a low electrical time constant and no hysteresis or cogging torques.

Goddard Space Flight Center, Greenbelt, Maryland

The ironless-armature brushless dc motor, shown in the figure, when used in servo applications, offers certain advantages over conventional wound-rotor motors of similar shaft speed and power rating. The effect known as cogging (speed variations due to slot effects) is eliminated, as are magnetic drag (hysteresis) torque; the electrical time constant of the brushless dc motor is less than that of the wound-rotor motor, and in the brushless design, the decentering forces which adversely affect the wound rotor in a conventional dc motor are eliminated.

This brushless motor includes an ironless armature composed of air core coils. The rotor utilizes samarium cobalt permanent magnets and an iron ring return path. In a brushless motor the permanent-magnet field rotates instead of the wound coils. The stator assembly contains the windings and is attached to an aluminum mounting ring on one end. Heat generated by power losses in the windings is dissipated through the mounting ring via the motor housing to the mounting structure rather than through the bearings as in the conventional motor.

The stator winding assembly is positioned in a radial gap. It contains no magnetic materials and therefore eliminates magnetic drag torques. The rotor consists of a magnet assembly, an outer magnetic ring, and the aluminum structural elements used to connect the two members. The airgap between the outer ring and the magnet assembly is 0.2 in. (0.51 cm) wide.

The magnet assembly consists of 12 samarium cobalt magnets. These magnets are bonded to the outer diameter of an iron ring. Slots machined on the ring are used to position the magnets. After the magnet assembly is placed on the aluminum support the outer ring is bonded in place. A nonmagnetic shim is placed in the airgap during assembly to prevent the outer ring from being pulled into the magnets.

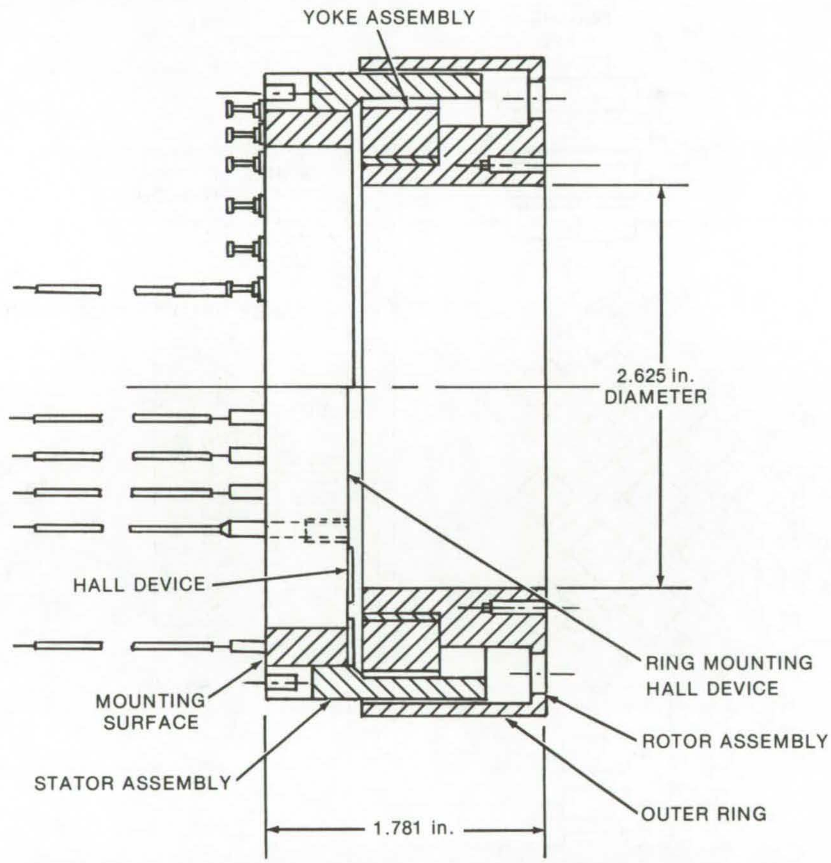

The **Ironless-Armature Torque Motor** uses a 12-pole samarium cobalt permanent-magnet rotor and three Hall-effect sensors for commutation. In a prototype ironless-armature torquer, the torque constant (3-phase delta) is 65 oz-in./amp; electrical time constant (L/R) is 0.2×10^{-3} sec., and armature resistance is 20 ohms.

The motor winding assembly is built with individual coils bonded to an epoxy-glass ring. The coils are connected to terminal posts, and the assembly is finally potted. An aluminum mounting ring with terminals is provided at one end. The coils were wound on a rectangular coil form; the wire is coated with epoxy as it is wound to aid coil shape retention after it is removed from the coil form.

A set of three Hall-effect sensors, each mounted 120 electrical degrees apart, provide motor commutation. These are mounted in an epoxy ring in such a manner that the ring slips into the winding assembly. The sensor ring assembly is adjustable for phasing the sensors with the winding for the most efficient commutation.

This work was done by Robert L. Fisher of Sperry Rand Corp. for **Goddard Space Flight Center.** *For further information, Circle 25 on the TSP Request Card.*
GSC-11880

Full-Color Hybrid Display

A full-color display for landing maneuvers in an aircraft simulator.

Ames Research Center, Moffett Field, California

A new full-color display was developed to present a realistic and properly proportioned image of a runway with its associated lights as it appears at dusk or at night. It was required because ordinary color-television systems do not provide images of sufficient intensity range or resolution. The display employs a high-resolution cathode-ray tube and a color wheel to produce colored lights from computer-generated signals. The lights are then superimposed on a conventional TV display of the runway.

As shown in the diagram, a scene of the runway is produced on a TV monitor by a conventional TV scan system. A computer-generated calligraphic display in black and white is produced on the cathode-ray tube (CRT) as a pattern of dots representing the landing, runway, and other lights associated with the scene. The CRT when combined with the addressable computer locations provides an equivalent scene resolution of 4,000 TV lines and a light intensity range of zero to 1,000 foot-lamberts. The rotation of a color wheel in front of the CRT is synchronized with the time of generation of the dots so that they appear as colored lights. The simulated lights are superimposed on the TV monitor image by means of the beam-splitting mirror which is 50 percent reflective and 50 percent transmissive.

The computer-generated calligraphic signal is synchronized with the TV sweep signal so that the two displays correspond with each other in size, perspective, and relative position, in spite of erratic operation of the controls in the aircraft simulator. In order to preserve signal amplitude and to minimize phase shifts, the synchronizing circuit includes a servocontrol system with a feedback which increases the bandwidth of the servomotors that position the TV camera.

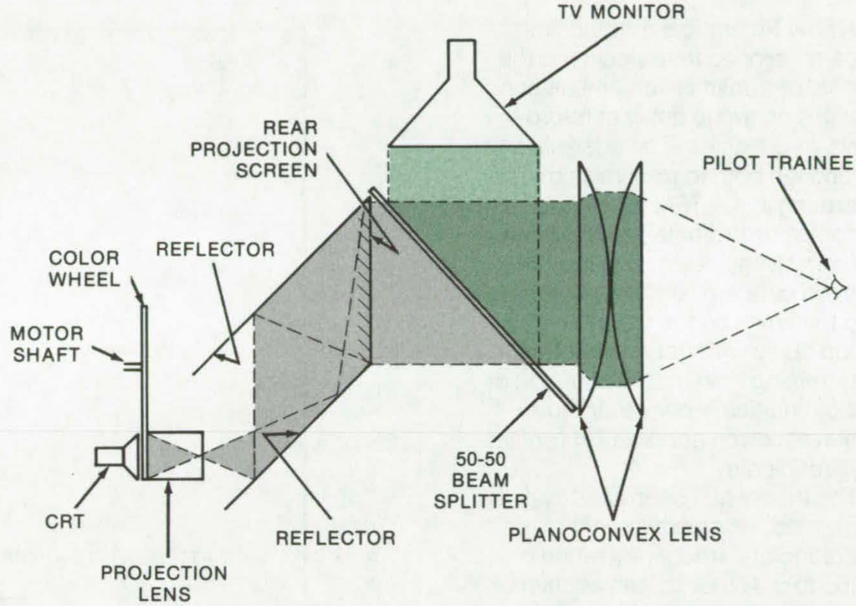

The **Optical-Display System** has an enclosure (not shown) that simulates an aircraft cockpit, with simulated controls for a pilot trainee to manipulate. The enclosure has a windscreen with a collimating lens through which the pilot trainee can view a simulated scene. The topographical features of the scene are produced on a color-TV monitor, and the landing and runway lights of the scene are produced by a calligraphic display. The images from the respective displays are combined via a 50-percent-reflective/50-percent-transmissive beam splitter. A pair of planoconvex lenses produces a realistic image. The cathode-ray tube is monochromatic, and a color wheel (on the shaft of a motor) is placed between the cathode-ray tube and the projection lens. The color wheel has a rigid circular frame to which are secured two diametrically extending, mutually perpendicular ribs. The ribs intersect at the center of the circular frame. There are four equal sectors of the wheel, each one spanned by a transparent tinted membrane or filter (the four-color wheel has red, green, blue, and clear membranes). As the wheel is rotated, the different color membranes sequentially pass between the CRT and the projection lens.

This work was done by Wendell D. Chase of **Ames Research Center.** *For further information, Circle 26 on the TSP Request Card.*

This invention is owned by NASA, and a patent application has been filed. Inquiries concerning nonexclusive or exclusive license for its commercial development should be addressed to the Patent Counsel, Ames Research Center [see page A8]. Refer to ARC-10903.

Effects of Mismatch on Group Delay of Microwave Transmission

An accurate formula determines the effects of discontinuities and helps to reduce errors in range measurements.

Caltech/JPL, Pasadena, California

A new theoretical method has been developed for calculating the effects of transmission-line discontinuities on group delay at microwave frequencies. The analysis can be applied both to transmission lines operating in the TEM mode such as in cables or to single-mode propagation in waveguides in general. The derived data are useful for estimating the limits on the variation of group delay with frequency or in determining how much reduction of discontinuities is necessary to achieve a given accuracy in predicting group delay.

The theory has been successfully confirmed, using equipment operating at a frequency range of 8.365 to 8.465 GHz; and additional supportive data have been taken, using equipment operating at a frequency range of 2.235 to 2.325 GHz.

The analysis is mainly useful for coaxial transmission-line problems, but is sufficiently generalized to include most uniconductor waveguide applications as well. It is not assumed that the discontinuities must be shunt susceptances or that the characteristic impedance of the transmission line is identical to the characteristic impedances of the systems on either side. Furthermore, it is not assumed that the reflections from the discontinuities are small or equal; the discontinuities can be lossy or lossless, and they need not obey the reciprocity condition.

A graph of the limits of $\Delta\tau$ (Figure 1), a function of Θ which varies with frequency, illustrates how the method works. It is assumed for simplicity that the scattering coefficients $|\ell_{22}| = |n_{11}|$ (see Figure 2) and that $\tau_{g0} = 100$ ns. If $|\ell_{22}| \neq |n_{11}|$, one can assume that the line has equivalent identical

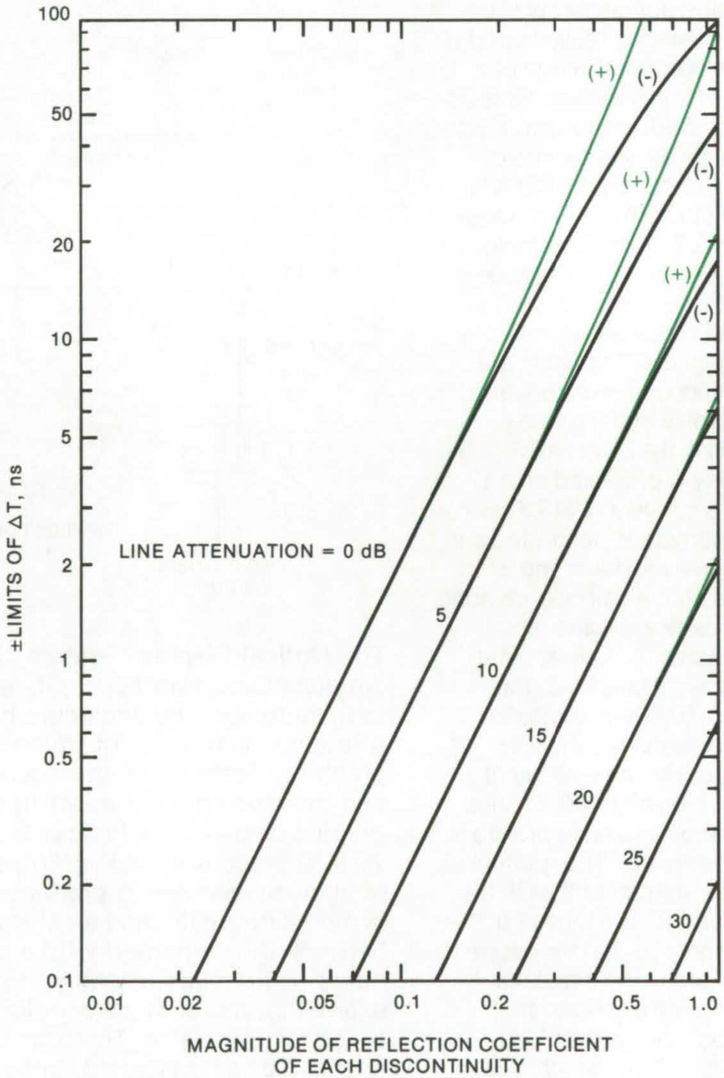

Figure 1. **Calculated Limits of Cyclical Variation of Group Delay** are shown for a 100-ns transmission line with identical discontinuities at each end. As an example of the use of the graph, assume that a transmission line has a delay of 20 ns and a line attenuation of 5 dB prior to adding discontinuities of $|\ell_{22}| = 0.4$ and $|n_{11}| = 0.1$. Then an equivalent discontinuity placed at each end of this line would have a reflection coefficient magnitude of $\sqrt{(0.4)\,(0.1)} = 0.2$. From the graph one finds that if the reflection coefficient magnitude of each discontinuity is 0.2 and the line attenuation is 5 dB for a 100-ns line, the limits of cyclical variation are ± 2.5 ns. The limits of cyclical variation for the 20-ns line thus are $\pm (20/100)\,(2.5)$ ns.

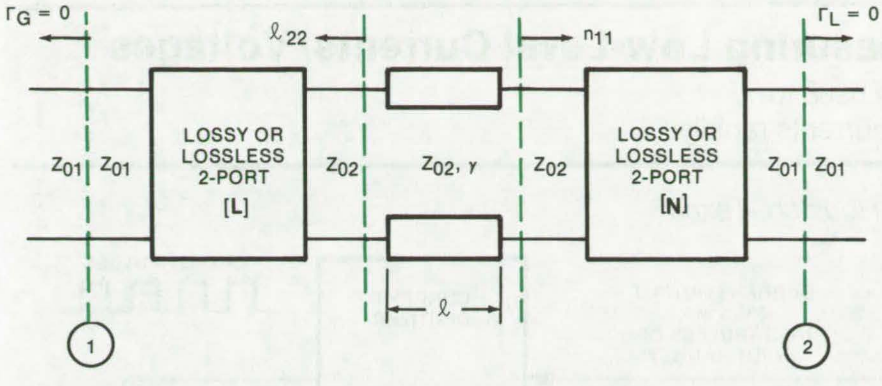

Figure 2. **A Network Model of a Transmission Line:** The line, of length ℓ, has discontinuities at each end which are represented by L and N. Energy is assumed to propagate in the dominant mode from port 1 toward port 2. At point 1, Γ_G is the voltage reflection coefficient of the generator at port 1, and at point 2, Γ_L is the voltage reflection coefficient of the load at port 2.

discontinuities at each end where the equivalent discontinuity has a reflection coefficient magnitude equal to

$$\sqrt{|\ell_{22}||n_{11}|}$$

For a transmission line having the same line attenuation but a τ_{g0} different from 100 ns, the result obtained from the graph is multiplied by the ratio of the actual τ_{g0} in nanoseconds to 100.

This work was done by Robert W. Beatty and Tom Y. Otoshi of **Caltech/JPL.** *For further information, Circle 27 on the TSP Request Card.*
NPO-13863

Reduction of Computer Power Interruptions

A bypass for computer-facility sensing relays can result in dollar and time savings.

Lyndon B. Johnson Space Center, Houston, Texas

Inexpensive latching relays incorporating a one-second time delay proved effective for maintaining system power in place of computer-facility automatic shutdown sensors that are activated by minute power surges or spikes in a 60-Hz input signal.

Many computer facilities use 400-Hz motor-generator units to power computer processors. The 60-Hz power input to these units is continuously monitored for proper voltage and phasing. The 60-Hz line occasionally experiences voltage surges or spikes (possibly from transformer or other equipment malfunctions) resulting in minute interruptions. When these occur, the computer sensing-relay system immediately shuts down the system by disconnecting from the line. This is a standard protection measure to ensure against damage to the computer when steady-state power is interrupted. When auto shutdown occurs, startup is a lengthy process, especially if the system was actively engaged with peripheral inputs at time of shutdown. An alternative involved the installation of an uninterrupted battery-backup system, at considerable cost.

Tests on a working system indicated that the great majority of 60-Hz interruptions were of less than 1 second duration. Furthermore, the 400-Hz motors were able to provide a stable output for at least 1 second subsequent to a 60-Hz input-power anomaly.

A time delay relay was added to the system to delay sensing-system cutoff action for 1 second. During a trial period, starting in 1973, one facility had experienced from 15 to 20 short-duration power interruptions during which the time delay relays prevented normal shutdown. No damage to any of the processors occurred. Costly downtime was markedly curtailed, and requirements for expensive power supplies were avoided. Appropriate relays and time delays can be selected to match the needs of different computer facilities.

This work was done by Clayton C. Oleson of Rockwell International Corp. for **Johnson Space Center.** *No further documentation is available.*
MSC-16136

Instrumentation for Measuring Low-Level Currents/Voltages

A digital measurement technique is used to measure highly-variable low-level currents rapidly.

Lyndon B. Johnson Space Center, Houston, Texas

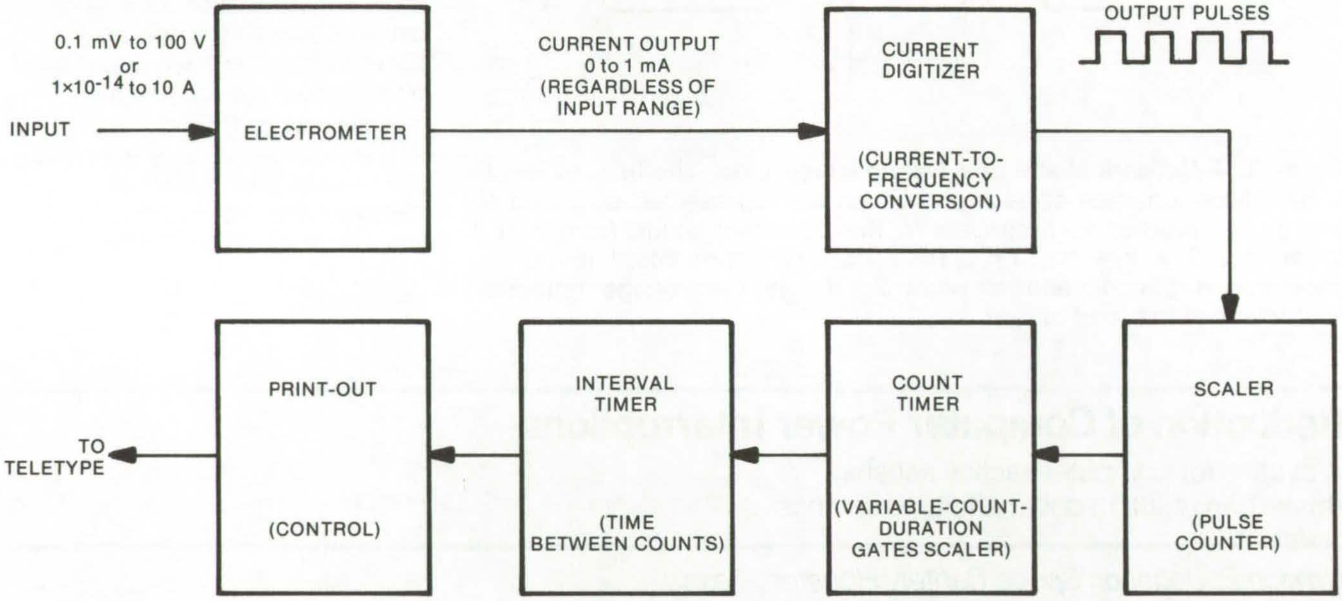

The **Instrumentation for Measuring Low-Level Currents/Voltages** consists of a high-input resistance voltage-measuring amplifier (electrometer) and a current-to-frequency converter (current digitizer) coupled to a set of counters and timers. A digital display of time-averaged signals with amplitudes varying over 11 decades is possible.

For many years experimenters have been plagued with problems in measuring low-current signals in the ampere range of 10^{-10} to 10^{-14} Typical examples include dark currents of ionization detectors, accelerator-beam currents, outputs of Faraday cups, and the like. Measured currents often vary 10 to 50 percent in a few seconds. Previous methods have characteristically used strip-chart recorders and other signal-averaging devices and have been shown to be slow and relatively inaccurate.

A simple method for time averaging and digitizing measurements of low-current signals effectively combines "off-the-shelf" instrumentation. Nuclear counting instrumentation (commonly referred to as nuclear instrumentation modules or NIM) makes up the bulk of the equipment, with the only exception being an electrometer (see figure) to measure current. Outputs from the electrometer are switch selectable, 0 to 1 Vdc or 0 to 1 mA. The current output is used, thereby making the electrometer essentially a high-gain current amplifier.

The amplified signals are routed to a current digitizer (current-to-frequency converter). The most sensitive range of the digitizer is 10^{-9} A, so the electrometer must be used. The output from the current digitizer are simple pulses, counted in the conventional NIM manner with selectable integration count times and selectable intervals between counts. Scaler outputs are easily recorded on a teleprinter.

This work was done by Robert G. Richmond of **Johnson Space Center.** *No further documentation is available.*
MSC-14855

Tracking a Phase-Shift-Keyed Signal

Residual carrier and the converted carrier generated from the demodulated signal and the incoming modulated signal, are summed for a strong tracking signal.

Lyndon B. Johnson Space Center, Houston, Texas

Phase-modulated signals with phase shifts ranging from 0° to 360° may be received and tracked without adjustment, using a new phase-locked detector. The detector, implemented in S-band receivers, tracks residual-carrier signals, suppressed-carrier signals, analog modulated signals, QPSK, and NPSK.

The receiver can track both the carrier component and the series sideband component of the expanded input signal, allowing it to receive signals phase modulated from 0° to 360°. The signal is filtered to pass the carrier component at point D in the illustration. The series sideband components are converted to a carrier signal at point B by multiplying the demodulated signal (point C) and the incoming signal at A. The tracking signal is a weighted sum of the residual carrier and the converted series sideband carrier.

In the detector, a phase shifter is used to generate a negative phase shift opposing the detected phase angle. This produces the converted series sideband and component carrier, with the residual-carrier signal and the converted series sideband and component carrier added together to produce the tracking-carrier signal.

Besides being less susceptible to carrier interference (which may degrade tracking), the detector can track on the converted series sideband carrier if the residual carrier drops to zero or is degraded by interference.

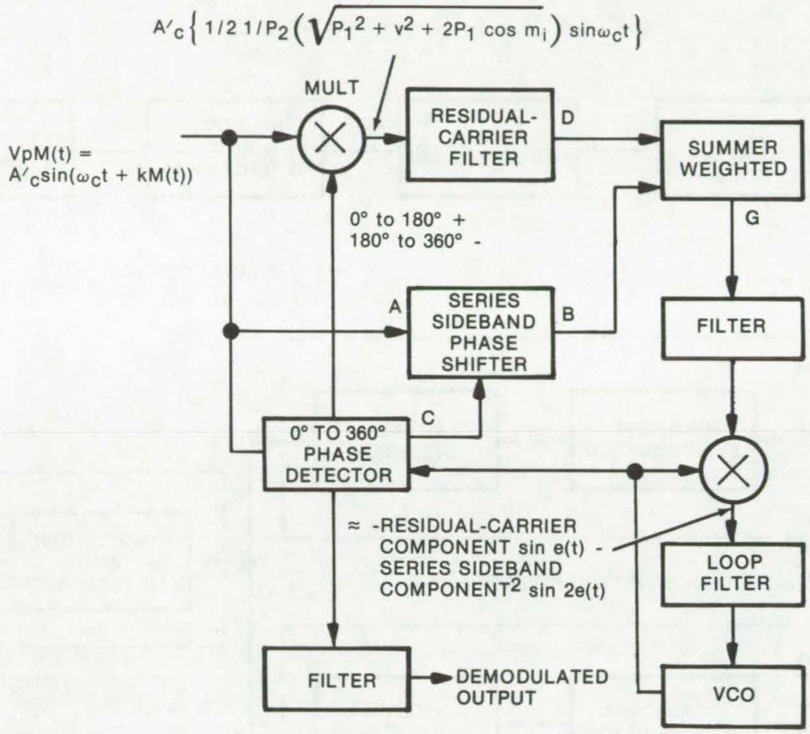

The **Phase Lock Loop Detector** tracks a phase-modulated signal from 0° to 360°. To track a signal with many phases, the detector, at point C, detects the phase modulation from 0° to 360°, and the phase shifter, at point A, generates a negative phase shift opposite in angle to the detected phase angle. The result is a stronger tracking signal for the different phase angles, since the tracking signal consists of both residual carrier and converted series sideband carrier component. It is also less susceptible to carrier interference which may degrade tracking.

This work was done by Salvador Villarreal, Stuart D. Lenett, Herbert S. Kobayashi, and James F. Pawlowski of **Johnson Space Center.** *For further information, Circle 28 on the TSP Request Card.*

This invention is owned by NASA, and a patent application has been filed. Inquiries concerning nonexclusive or exclusive license for its commercial development should be addressed to the Patent Counsel, Johnson Space Center [see page A8]. Refer to MSC-16170.

Advanced Imaging Communication System

Signal-processing methods increase data rate of picture transmission.

Caltech/JPL, Pasadena, California

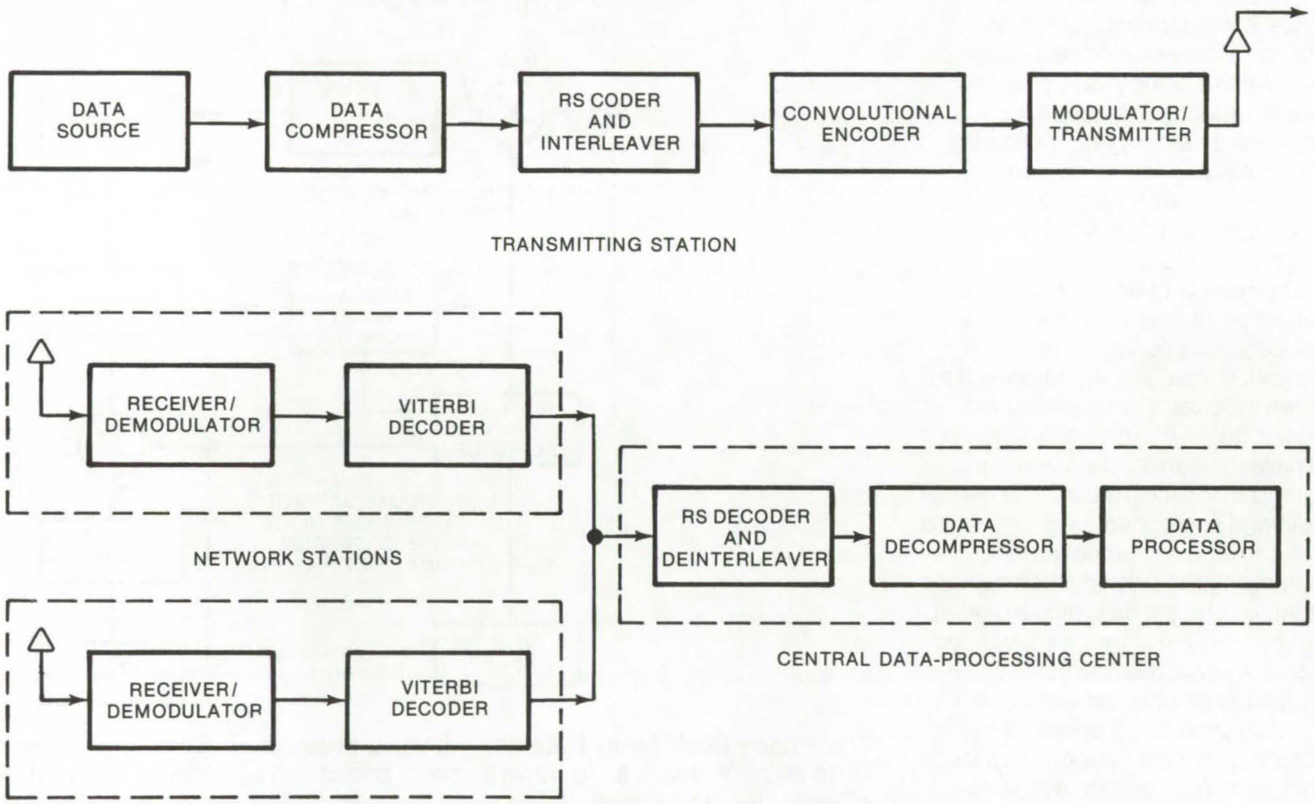

The **Advanced Image Communication System** includes a data compressor which compresses data from a source. The compressed data are first coded by a Reed-Solomon coder and interleaver, followed by a convolutional encoder; its output is modulated and transmitted by a modulator/transmitter, wherein antipodal PSK-PM modulation of a square-wave subcarrier with S-band or X-band carrier takes place. The signals transmitted are assumed to be subjected to wideband Gaussian noise. The system may include several network stations (two shown above). Each station includes a receiver/demodulator that includes a phase-locked-loop coherent demodulator with 3-bit-quantized symbol output, which is decoded by a Viterbi decoder. The output of the latter is decoded by a Reed-Solomon decoder and deinterleaver, located at a central data-processing center. The compressed data are decompressed by a data decompressor; its output is used to produce an approximation of the uncompressed data, originally received by the compressor from the source.

An advanced imaging communication system has improved the efficiency in transmitting visual image information from deep space. The key elements shown in the block diagram are:

- Imaging and nonimaging sensors,
- Data compressor/decompressor,
- An interleaved Reed-Solomon (RS) block coder,
- A convolutional-encoded/Viterbi-decoded telemetry channel, and
- Reed-Solomon decoding.

Data compression provides efficient representation of the sensor data, and channel coding improves the reliability of the data transmission. The interactions of data compression and channel coding are considered jointly in combining elements to increase system performance.

When Reed-Solomon/Viterbi coding is used in conjunction with compressed data, the probability of a block of data being in error reduces rapidly for small increases in channel signal-to-noise ratio. Therefore, a low data-block error rate is achieved for error-sensitive data, at nearly the same data rate as used for error-insensitive data.

Another characteristic of this combination is the tendency of errors to occur as large blocks interspersed between long runs of error-

free data. Compressed data are usually degraded as much by a single error as by large blocks of errors. Therefore, when errors occur in large blocks instead of being randomly distributed, it is not necessary to require an extremely-low average error rate to handle error-sensitive data.

An independent evaluation by scientists demonstrated that use of a specific data compressor as an element of this system results in an "end-to-end" improvement in information return of four to seven times that of present systems.

This work was done by Edward E. Hilbert and Robert F. Rice of **Caltech/JPL.** *For further information, Circle 29 on the TSP Request Card.*

This invention is owned by NASA, and a patent application has been filed. Inquiries concerning nonexclusive or exclusive license for its commercial development should be addressed to the Patent Counsel, NASA Resident Legal Office-JPL [see page A8]. Refer to NPO-13545.

Flexible High-Speed Instrumentation System

A remote multiplexer/demultiplexer for use with an integrated flight-test data system

Dryden Flight Research Center, Edwards, California

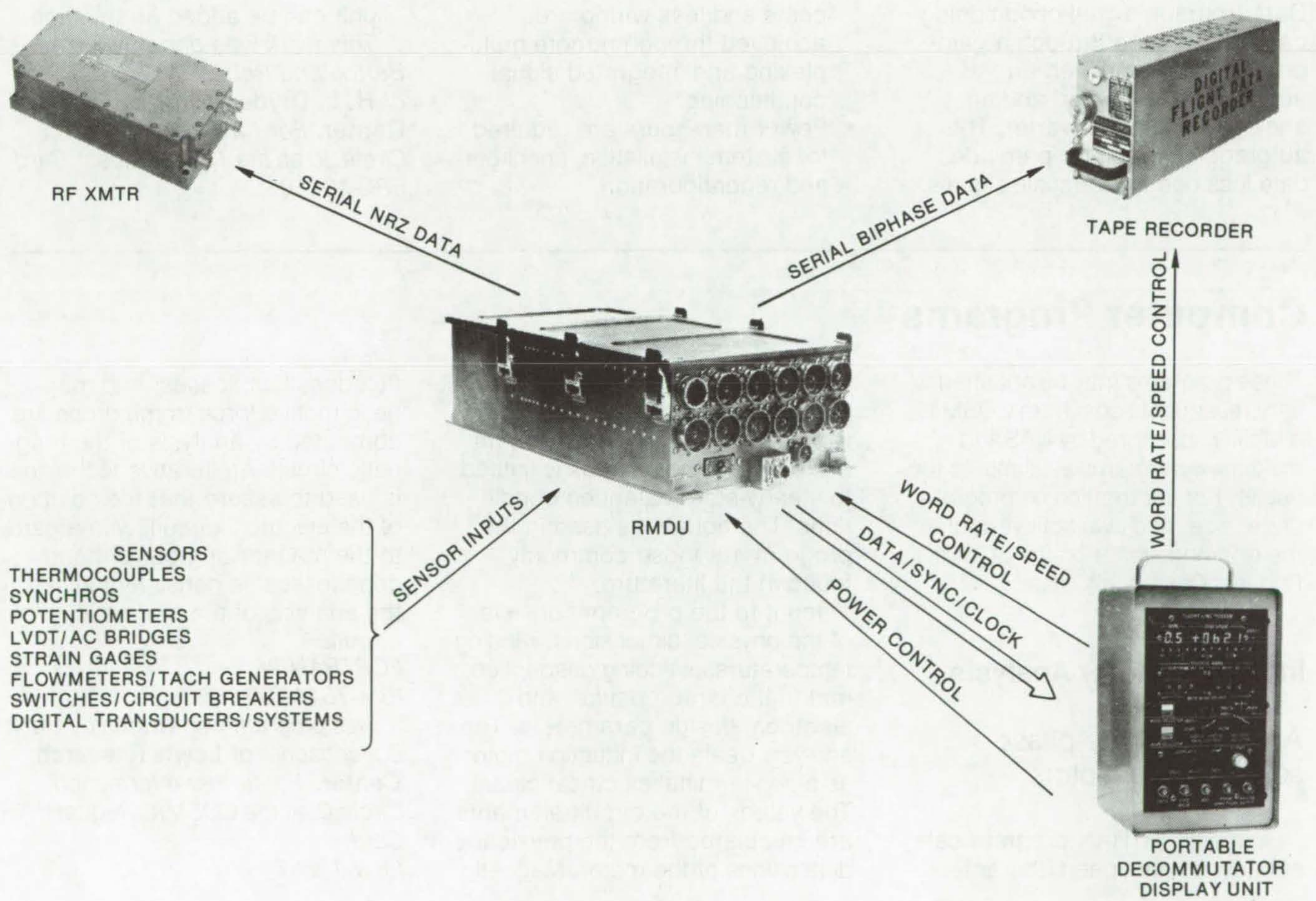

The RMDU and System

A highly-flexible digital instrumentation system which is suitable to both airborne and ground-based data-acquisition/process control applications has been developed. This system has been employed in a variety of research and flight-test applications where great flexibility to accommodate changes in the number of parameters, data-sampling rates,

(continued next page)

and signal conditioning is required.

The Model 4010 remote multiplexer/demultiplexer unit (RMDU) is a data-acquisition system developed for use with the Airborne Integrated Flight Test Data System (AIFTDS — 4000). The Model 4010 RMDU when used as an independent data system is commonly referred to as operating in the "stand-alone" configuration.

In addition to controlling and processing signals in a completely random (programable) sequence, the stand-alone RMDU can, in addition, provide sensor excitation. Twenty-two different types of interchangeable signal-conditioning cards are available, permitting an RMDU to acquire signals from a wide variety of analog or digital signal sources. Data from the signal-conditioning cards are routed through a gain-programable amplifier, an autoranging amplifier, and an analog-to-digital converter. The autoranging amplifier precludes data loss due to overscale signals. Data-channel addressing and data-cycle format are internally programable.

The RMDU power supply is a bolt-on unit which is integrally connected to the RMDU housing. The design of the power supply unit permits the selection of an ac or a dc power source as well as different capacity ratings to meet system power requirements.

The RMDU has several useful characteristics:

- The high speed of the system permits all data to be handled digitally, eliminating voltage-controlled oscillators and FM recording and subsequent conversion of the data to a digital form.
- Lower total-system hardware costs and less wiring are achieved through remote multiplexing and integrated signal conditioning.
- Fewer man-hours are required for system installation, checkout, and reconfiguration.
- Total flexibility of parameter changes is achieved by interchangeable signal-conditioning cards and internal RMDU programing.
- Internal calibration, available during each data cycle, contributes to higher system accuracy.
- Ease of access without tools is made possible by using thumb-release fasteners on the RMDU housing cover.
- The stand-alone concept permits lower weight, volume, and power consumption for the system.
- System growth is provided for without hardware obsolesence or modification. A computing system or data management unit can be added at any time.

This work was done by Febo Bartoli and Robert W. Borek, Sr., of **H. L. Dryden Flight Research Center.** *For further information, Circle 30 on the TSP Request Card.*
FRC-10110

Computer Programs

These programs may be obtained at very reasonable cost from COSMIC, a facility sponsored by NASA to make new programs available to the public. For information on program price, size, and availability, circle the reference letter on the COSMIC Request Card in this issue.

Induction Motor Analysis

Analysis of three-phase squirrel-cage motors

A new FORTRAN program calculates torque-speed characteristics, electrical characteristics, magnetic flux densities, and weight plus other parameters. In this program the analysis is limited to steady-state balanced conditions. The equations used in the program are those commonly found in the literature.

Input to the program consists of the physical dimensions, winding temperatures, winding description, material characteristics, and electrical design parameters. The analysis treats the induction motor as a two-terminal electrical circuit. The values of the circuit elements are calculated from the physical dimensions of the motor. Magnetic flux densities, losses, and magnetic motive force (mmf) drops are computed by analysis of the magnetic circuit. An iterative technique is used to assure that the solution of the electrical circuit, with regard to the magnetizing current and cone losses, is consistent with the analysis of the magnetic circuit.

FORTRAN IV
IBM 7044-7094

This program was written by Gary Bollenbacher of **Lewis Research Center.** *For further information, Circle C on the COSMIC Request Card.*
LEW-12687

Physical Sciences

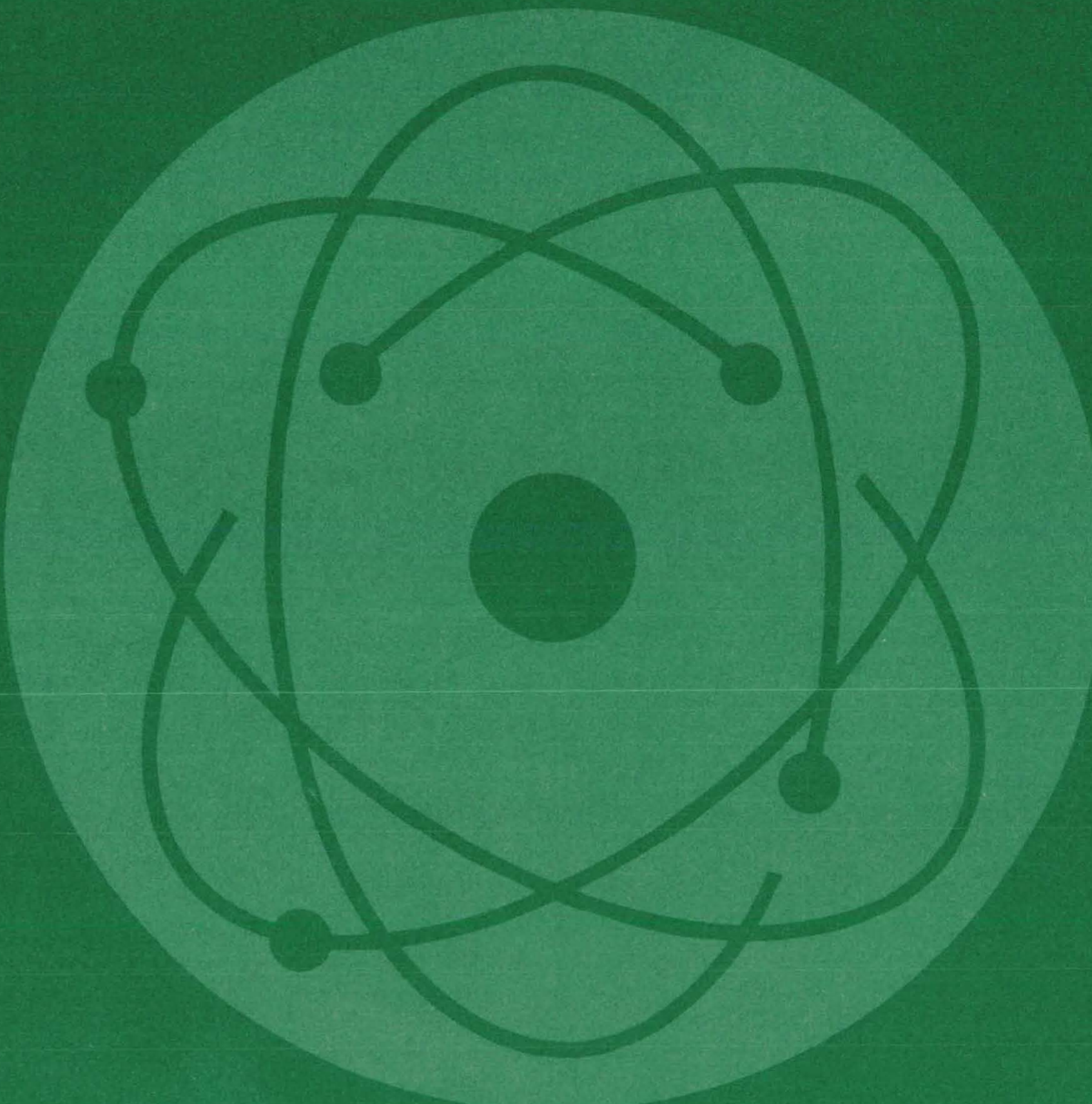

Hardware, Techniques, and Processes

Computer Programs

Energy Conversion System

Chemical decomposition and recombination is suggested for converting "low-temperature" (300° C) energy to "high-temperature" (500° C) energy.

Caltech/JPL, Pasadena, California

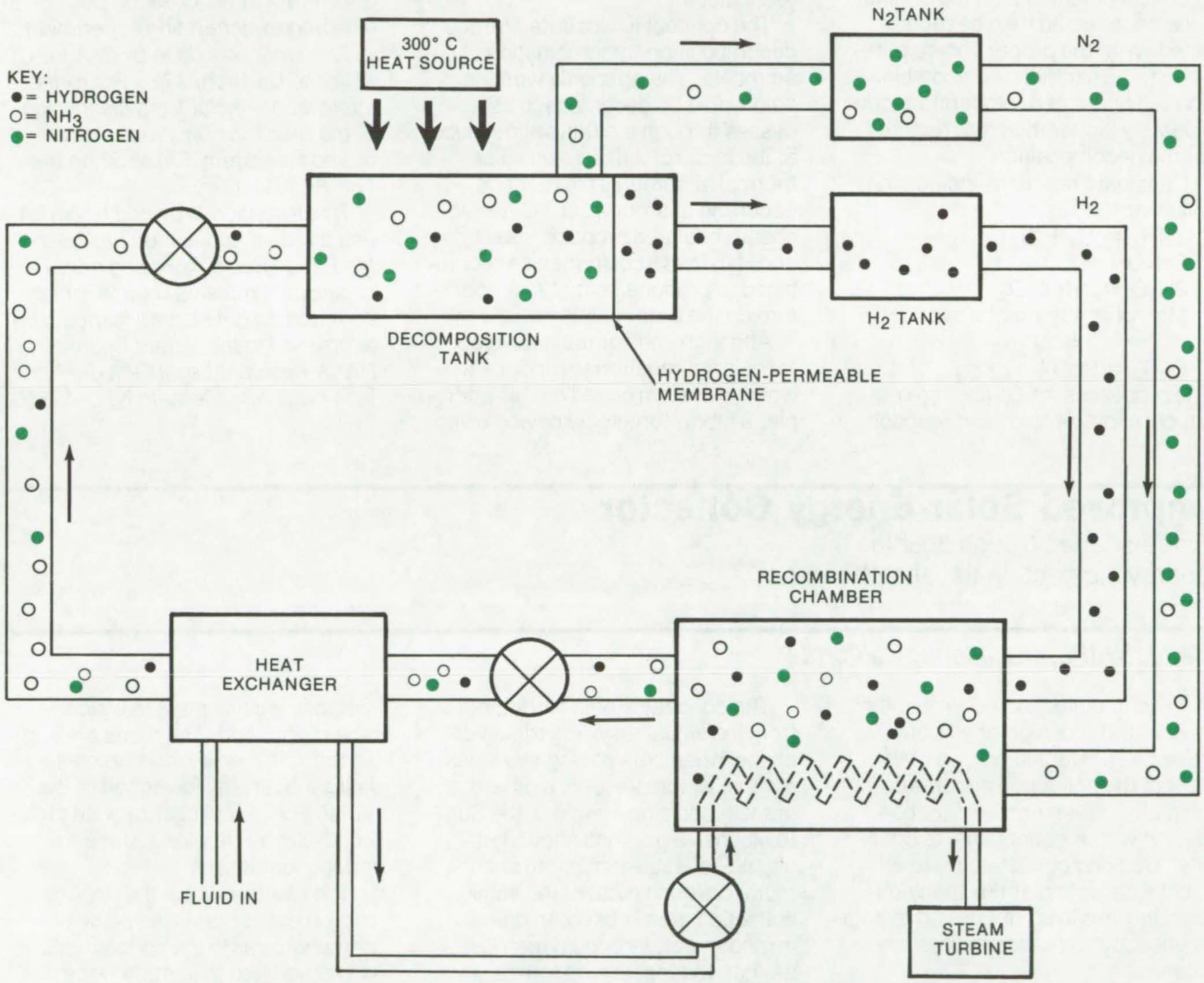

The **Ammonia Energy-Conversion Concept** illustrated above converts thermal energy from a relatively-low temperature device, such as a fixed solar concentrator, to a higher temperature for efficiently driving a steam turbine. In the decomposition tank, NH_3 is in equilibrium with H_2 and N_2. Hydrogen is withdrawn from the chamber through a semipermeable membrane to shift the equilibrium and enhance the decomposition. After the decomposition of ammonia is well advanced, nitrogen and any undecomposed ammonia are routed to a storage tank. The H_2 and N_2 are recombined at a high temperature and pressure to heat a coil carrying the turbine working fluid. The NH_3 and unrecombined N_2 and H_2 are recycled through the decomposition tank.

A number of alternate energy sources now under development collect energy and concentrate it in a fluid or other medium at temperatures ranging from 200° to 300° C. These include geothermal and waste-material sources and solar thermal collectors with a fixed orientation. Vapor-driven turbines for generating electricity can be made to operate at temperatures around 300° C, but the efficiency is much less than modern electric generators driven by superheated steam at 550° C.

A scheme based on chemical decomposition and recombination has been suggested as a technique for converting energy collected at relatively low temperatures (e.g., 300° C) to the higher temperatures required for efficient operation of steam-driven electrical generators.

(continued on next page)

The proposed approach would utilize one or more of a class of cyclical reversible chemical reactions in which a compound is made to decompose and absorb thermal energy at a "low" temperature by shifting the equilibrium. The decomposed substances, having a higher chemical potential than the original substance, could then be recombined. With the proper choice of reactant, the exothermal recombination will occur at a temperature considerably higher than that required for the decomposition.

Candidate reactions include the following:

$2NH_3 \rightleftharpoons N_2 + 3H_2$
$CH_3OH \rightleftharpoons CO + 2H_2$
$2H_2O \rightleftharpoons 2H_2 + O_2$
MgH_2 (or other metal hydride) $\rightleftharpoons Mg + H_2$
$BaO_2 \rightleftharpoons BaO + 1/2\,O_2$

The processes, of course, are not simply implemented, and reaction efficiencies and kinetics must be considered in designing the system. For instance, the decomposition should be carried out at low pressure, and the recombination at high pressure; the efficiency could be augmented by thermal diffusion, molecular skimming, or similar techniques.

The concept is illustrated for the decomposition/recombination of ammonia. The ammonia working fluid would be decomposed as it passes through a catalyst-lined tube at the focus of a fixed-axis solar thermal absorber. This reaction, occurring at around 300° C, would absorb heat and produce free N_2 and H_2. These could then be recombined to produce heat at a temperature on the order of 500° C.

Although considerable development is yet required to produce a working system based on this principle, a laboratory-scale device using the decomposition and recombination of H_2O is described in NASA Tech Brief B75-10314. Although not a closed system as described here, and operating at higher temperatures, it has been shown possible to remove hydrogen by diffusion through selective membranes to accelerate the H_2O decomposition in a hydrogen-generating experiment.

This work was done by Charles G. Miller of **Caltech/JPL.** *For further information, including a discussion of the reaction conditions for an ammonia system, Circle 31 on the TSP Request Card.*

This invention is owned by NASA, and a patent application has been filed. Inquiries concerning nonexclusive or exclusive license for its commercial development should be addressed to the Patent Counsel, NASA Resident Legal Office-JPL [see page A8]. Refer to NPO-13510.

Improved Solar-Energy Collector

A vee-shaped trough doubles the energy incident on the absorber ratio.

Caltech/JPL, Pasadena, California

In solar collection schemes, the concentrator design often determines a substantial portion of the cost of the collection apparatus and ultimately whether the collection device will be economical to operate. Tracking collectors more efficiently collect solar flux than nontracking versions, but this advantage is offset by increased maintenance costs.

A fixed, but reversible, concentrator with a vacuum tube receiver has been developed which combines much of the efficiency of a tracking concentrator with the lower cost of a fixed design. The trough concentrator can maintain a year-round concentration factor of 2 (or better) for the most significant collection period of the day, with the factor improvement most noticeable around the winter and summer solstices. To date, the trough has been used with an evacuated receiver and also with a fixed, flat-plate collector.

The concentrator is fabricated from individual, asymmetrical vee-shaped members having two sides, each of which presents a different preselected slope angle to the Sun. Inexpensive polished sheet metal or plastic-reflector-laminated sheet metal covering most of the solar collection area is used. In one arrangement, individual members are ganged together to form a modular assembly adapted to ease reversing their orientation at appropriate intervals. In another arrangement, the concentrator is made up of hinged flaps which form opposite sides of the vee trough. Corresponding sides of the trough members are ganged together for operation via push rod; orientation is reversed at appropriate intervals by manipulating the rods.

When the vee-trough reflector is used with an evacuated-tube energy receiver (absorber), each absorber includes a black plate to which a tube is attached. The tubes are supported within an evacuated clear-wall cylinder; the lower half of the surface of the cylinder may be provided with a reflector surface to reduce rear losses.

The plane in which the apparent motion of the Sun takes place is perpendicular to the collector plane (which is tilted to latitude twice a year on spring and fall equinoxes). The tilt of this plane during winter and summer seasons is less than 90° or more than 90°, respectively, as shown in the figure, whereas symmetric vee-trough reflectors would require collector periodic tilt changes to maintain efficiency. The asymmetric reflector, however, eliminates the need for a collector tilt change; instead, the mirror assembly is reversed on the equinoxes. Year-round concentration thus is possible.

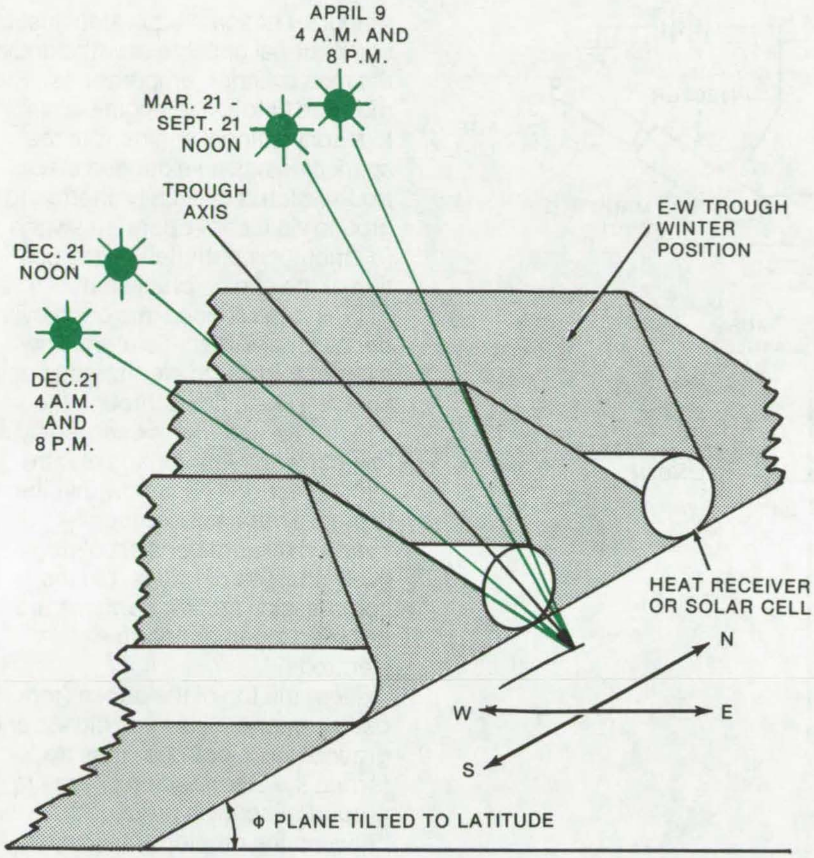

Seasonal Adjustments for the Vee-Trough Reflector are performed twice yearly to optimize collector efficiency. The trough is shown for winter operation. Solar position indicated for late December, March (and September), and for the first week in April is referenced to the trough axis. To maintain year-round efficiency, the collector/vee-trough assembly is rotated 180° along the east-west axis. In the new position, solar energy is collected by the troughs as when in the winter position. At the optimum design point (an average year-round concentration factor of 1.95 and an operating temperature of 177° C) system construction cost is estimated at $1,400 per kilowatt of electric energy (kWe).

This work was done by M. Kudret Selcuk of **Caltech/JPL.** *For further information, Circle 32 on the TSP Request Card.*

This invention is owned by NASA, and a patent application has been filed. Inquiries concerning nonexclusive or exclusive license for its commercial development should be addressed to the Patent Counsel, NASA Resident Legal Office-JPL [see page A8]. Refer to NPO-13813.

Electrostatic-Discharge Ignition

A concept for firing very lean mixtures of hydrocarbon liquid fuels in an Otto-cycle engine

Caltech/JPL, Pasadena, California

Plant safety engineers are well aware of the dangers posed by electrostatic ignition of loose, powdery materials such as are found in coal mines, grain elevators, or warehouses. In each of these instances, a very lean mixture of "fuel" particles is ignited by the discharge of electrostatic charges placed on the particles. The charging action is created as the particles move across the containment surfaces. An increasingly greater charge with respect to a grounded surface is formed until a potential of ignition force is attained. The same principles which result in these uncontrolled discharges may be utilized to ignite ultralean ratios of hydrocarbon fuel to air in an Otto-cycle engine.

The proposed new engine provides electrostatic ignition within each cylinder, with the use of a modified conventional electrical-spark ignition system. The proposed engine design (shown schematically in the figure) includes cylinders lined with an insulating coating. These coatings may be aluminum oxide

(continued on next page)

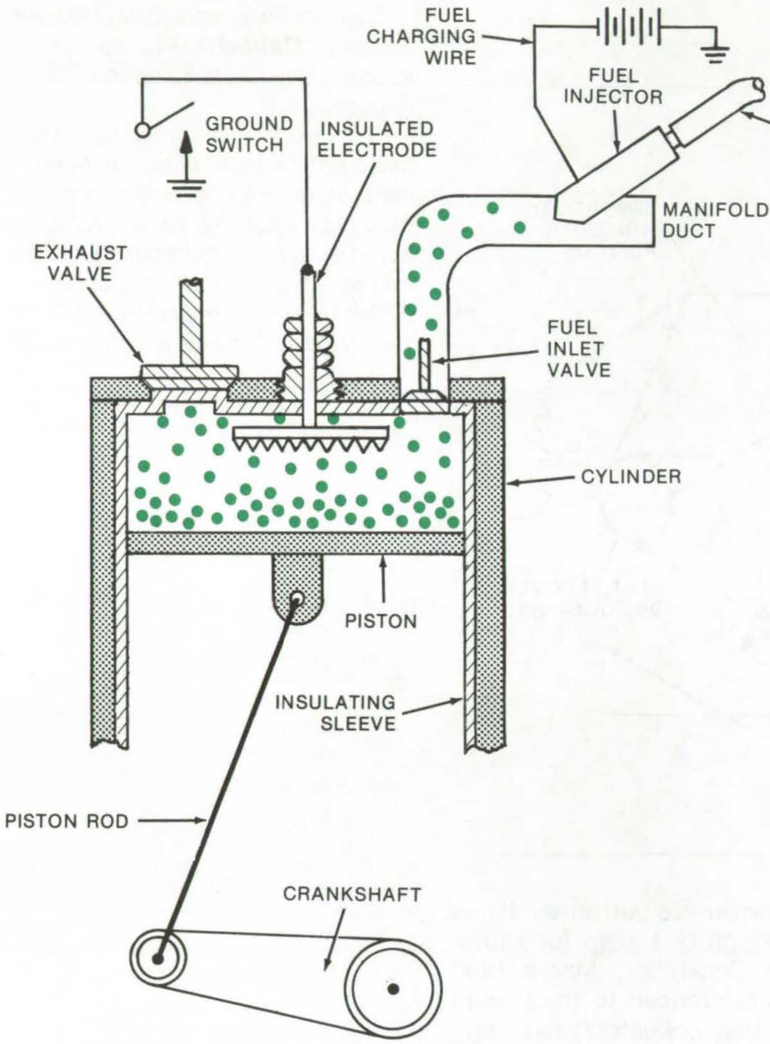

In the **Electrostatic-Discharge Ignition** system, an electrode in the engine cylinder permits the charge to transfer during the compression stroke at top dead center in an internal-combustion engine. The charge transfer produces the spark which causes the ignition of the droplets without resort to other ignition devices which are incapable of igniting ultralean mixtures. The system enables the use of ultralean fuel mixtures, thereby reducing pollutants.

(anodize) or some equivalent insulating material capable of withstanding the high cylinder temperatures. The modified Otto-cycle engine is similar to a conventional engine, but the spark plug has an extended electrode which is cyclically shorted to ground via a cam-operated switch (distributor) controlled by the position of the engine crankshaft.

Fuel is introduced into each cylinder by an electrostatic atomizing injector (similar to electrostatic paint sprayer). As it flows through the injector tip, the fuel is charged by a low-current, high-voltage electrostatic electrode housed within the injector. The electrostatically charged mixture consists of negatively charged particles. On the compression stroke, particles are crowded together near the electrode.

Near the top of the stroke (top dead center), the switch closes and grounds the electrode, thus transferring the electrostatic charge to ground. A spark is produced between the droplets which ignites them.

This work was done by James B. Stephens and Charles G. Miller of **Caltech/JPL.** *For further information, Circle 33 on the TSP Request Card.*

Inquiries concerning rights for the commercial use of this invention should be addressed to the Patent Counsel, NASA Resident Legal Office-JPL [see page A8]. Refer to NPO-13798.

Thermal/Vacuum Testing of Laser Corner-Cube Retroreflectors

Corner-cube reflectors are used to reflect, or retransmit, a laser signal back to its source. A test procedure for such retroreflectors has produced data useful in the design of optical communications systems. The test technique can be used to assay performance under various thermal conditions and laser incidence angles. The test procedure does not degrade or change the performance of the retroreflectors.
(See page 608.)

NASA Technology Utilization House

NASA's Technology Utilization House incorporates numerous energy-saving features and other aerospace spinoffs. However, it can be constructed from materials and techniques available in today's marketplace. It features solar heating and cooling, improved insulation, a water-recycling system, security and fire-alarm systems, and many other innovations. It is now open to the public.
(See page 625.)

Economical Solar Heating for Homes

A do-it-yourself system to supplement existing forced-air heating may be installed by a homeowner. Materials are readily available, no professional skills are required, and costs are low enough to be recovered by savings in fuel. Information on construction and performance is available.
(See page 626.)

Hydrofoil Controls Outfall Effluents in Rivers and Oceans

A hydrofoil system directs or disperses flows in moving water.

Langley Research Center, Hampton, Virginia

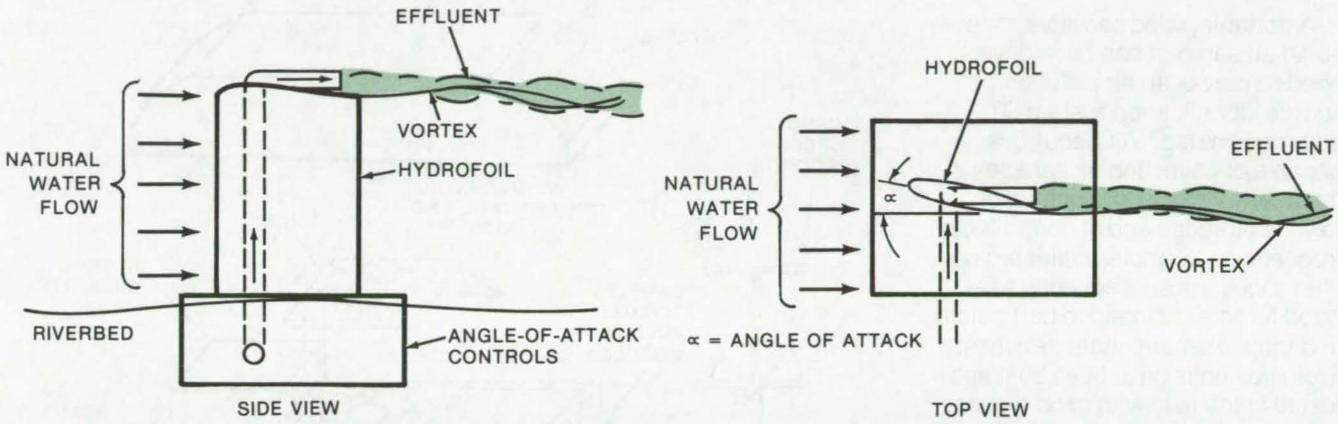

The **Hydrofoil System** can be used to control outfall waste that is piped in below the water bed. The waste travels upward within the hydrofoil and is ejected into the horizontal vortex that forms near the tip of the hydrofoil and trails far downstream.

A specially-designed hydrofoil system can be used at any facility discharging waste into natural-flowing waters, such as rivers, channels, or the oceans, to direct the flow of such pollutants and to control their dispersion. It could be used similarly at offshore oil terminals which are susceptible to oilspills. The hydrofoil works by keeping these pollutants concentrated within a long, trailing vortex generated by the hydrofoil and either deflecting the vortex away from sensitive regions or sweeping it from side to side for rapid dispersion. This hydrofoil system as illustrated consists of a vertical semispan hydrofoil anchored in the water bed and set at an angle of attack with respect to the ambient water flow.

The hydrofoil exerts control, for an extended time, over the direction of flow and dispersion of concentrated pollutants after they have entered natural-flowing waters. The pollutants are confined by the vortex, until it breaks up at some point far downstream, and can be deflected horizontally, at angles up to about 10° from the direction of the free stream, by adjusting the angle of attack and configuration of the hydrofoil. In this manner the effluent flow may be deflected away from oysterbeds, beaches, and other regions where it would be harmful. It can also be swept from side to side by alternating the settings of the hydrofoil, in order to accelerate dispersion of the pollutant.

The point where the effluent is released can be extended further downstream by placing a second hydrofoil at the vortex breakup point to regenerate the vortex. With the addition of successive hydrofoils, the effluent pipeline can be continued almost indefinitely in water where the flow direction does not vary with time. Minor changes in the flow direction may be corrected for by varying the angle of attack of each hydrofoil to keep its vortex alined with the next hydrofoil.

It is also possible to use a horizontal hydrofoil that is mounted on a streamlined strut and is oriented perpendicular to the flow. If set at a negative angle of attack, the hydrofoil generates two trailing vortexes that are deflected upward to the water surface where Sunlight and air would interact with the effluent. Alternatively, setting the hydrofoil at a positive angle of attack would deflect the trailing vortexes and the effluent downward to the water bed.

This work was done by Robert C. Costen of **Langley Research Center.** *For further information, Circle 34 on the TSP Request Card.*

Inquiries concerning rights for the commercial use of this invention should be addressed to the Patent Counsel, Langley Research Center [see page A8]. Refer to LAR-12045.

Portable, Wind Sensitive, Directional Air Sampler

Programable automatic sampling system collects airborne particles for analysis.

Lewis Research Center, Cleveland, Ohio

A portable, wind sensitive, directional air sampler has been developed as part of an air pollution source identification system. The unit, designated "Air Scout," is capable of collecting air samples in the field automatically with respect to wind direction and at controllable frequencies. Samples collected on filter slides are subsequently analyzed for total suspended particulate and trace element characteristics. Prototype units have been built and tested in the field with good results.

The principal components of the Air Scount are shown schematically in the figure. The unit receives wind direction signals from the wind vane. Airborne material is collected on a filter slide using a standard high-volume air sampler drawing air through a porting arrangement which tracks the wind direction and permits collecting discrete samples.

The filter slide contains nine separate filters: a central filter through which air is drawn continuously and eight peripheral filters (corresponding to the eight major compass headings) through which air is drawn selectively depending on the wind direction. Eight individually controlled ports with solenoid-actuated shut-off valves (not shown) control the airflow through the eight peripheral filters. A rotating cam connected to the wind vane shaft sequentially operates eight miniature switches. As the wind vane and cam rotate and close a switch, the corresponding porting valve opens allowing air to flow through one of the eight peripheral filters, thus sampling the air coming from one particular 45° compass arc.

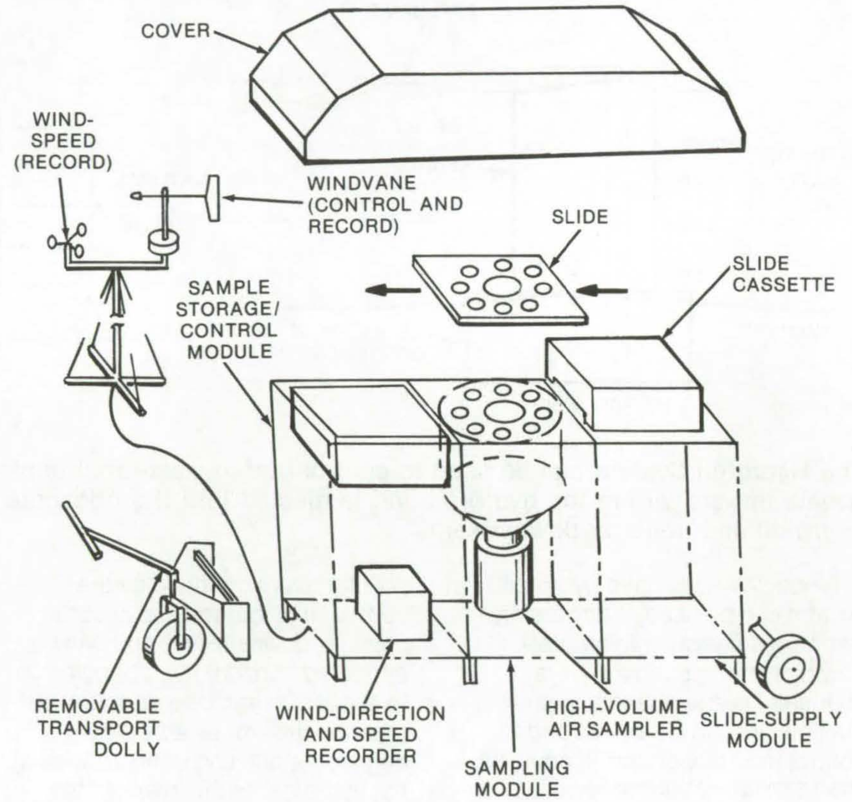

Air Scout is a portable unit with a modular chassis design. Airborne particles are collected on up to eight peripheral filters on a slide along with a record of the wind speed and direction.

The unit is loaded with up to 12 filter slides. A preset timer controls the length of time each slide is in the sampling position. At the end of the selected sampling period, a fresh filter slide is automatically moved into the sampling position, and the exposed filter slide is displaced into the storage compartment. Thus, the Air Scout may be set up at a field location, loaded, programed, and left to acquire samples automatically. The prototype units operate in this mode collecting samples unattended at a preselected interval of from 1 to 30 hours for each filter slide. A wind-speed sensor and a recorder provide a record of both wind speed and direction during the sampling period.

This work was done by James N. Deyo, Robert B. King, and John Toma of **Lewis Research Center.** *Further information may be found in NASA TM-X-71687 [N75-19623], "Development and Testing of a Portable Wind Sensitive Directional Air Sampler," a copy of which may be obtained at cost from the New England Research Application Center [see page A7].*

Inquiries concerning rights for the commercial use of this invention should be addressed to the Patent Counsel, Lewis Research Center [see page A8]. Refer to LEW-12743.

Remote Sensing of Vegetation and Soil

A microwave technique is applicable to crop inventory and natural-resources management.

Goddard Space Flight Center, Greenbelt, Maryland

The intensity and state of elliptical polarization of reflected microwaves can be used to determine the water content and height of vegetation and the moisture content of a soil substrate. Data are taken and analyzed automatically, with a reduction in manpower and cost.

The sensing method used is microwave ellipsometry. A circularly polarized train of microwaves is reflected from vegetation at a predetermined angle of incidence to determine the ratio of intensities of the electric-field components and their phase differences. The refractive index (given by the water content of the vegetation) and the thickness of a layer of vegetation are computed from a formula.

The formula, based on Maxwell's equations, is derived in terms of Fresnel reflection coefficients for the component plane waves. It relates the refractive index of a substrate, the refractive index and thickness of a dielectric film covering the substrate, and the reflection coefficients and absolute phase shifts of the two component plane waves of the electric-field vector of a polarized wave reflected from a film-covered substrate.

Since the theory is valid for all electromagnetic waves, the relationship holds in the microwave region as well as in the optical region. A layer of vegetation on a soil substrate appears to microwaves much as a thin film on a thick substrate is seen by visible light. The height of the vegetation corresponds to film thickness, and the effective refractive index of the vegetation (which at microwave frequencies depends on its moisture content) corresponds to the refractive index of the film. The basic difference is that all dimensions are enlarged by a factor between 10,000 and 2 million.

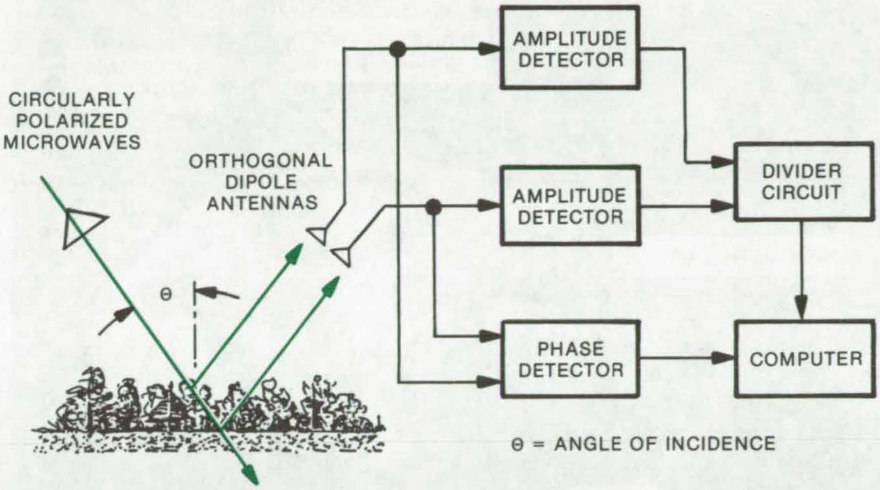

Microwave-Ellipsometry Apparatus is used for remotely detecting soil and vegetation characteristics. There may be as many as five unknown variables. These can include the dielectric constant of the vegetation, the dielectric constant of the soil substrate, and the thickness of the vegetation layer. For a single measurement, three of five variables have to be known to solve for the other two. If only two of the five variables are known, the other three can be determined by taking measurements at two different angles of incidence.

In the system (see figure) a train of circularly polarized microwaves emerges and is directed toward the vegetation. The intensities of the orthogonal field components of the circularly polarized wave (in the plane of incidence and normal to it) are equal and have a phase difference of 90°. The microwaves are reflected from the vegetation and the soil substrate.

After reflection, the components are received by two orthogonal dipole antennas and are detected in amplitude detectors. A phase detector measures phase difference, and a divider circuit determines the ratio of the intensities of the vector components. The information is fed into a computer, and the refractive indices of the vegetation and soil substrate and the thickness of the vegetation are determined.

This work was done by John B. Schutt of **Goddard Space Flight Center** *and Siegfried O. Auer of the National Academy of Sciences. For further information, Circle 35 on the TSP Request Card.*

This invention is owned by NASA, and a patent application has been filed. Inquiries concerning nonexclusive or exclusive license for its commercial development should be addressed to the Patent Counsel, Goddard Space Flight Center [see page A8]. Refer to GSC-11976.

Portable Solar Radiometer Measures Stack-Plume Effluents

Four-channel instrument monitors particulate and aerosol opacity and concentration of NO_2 and SO_2.

Langley Research Center, Hampton, Virginia

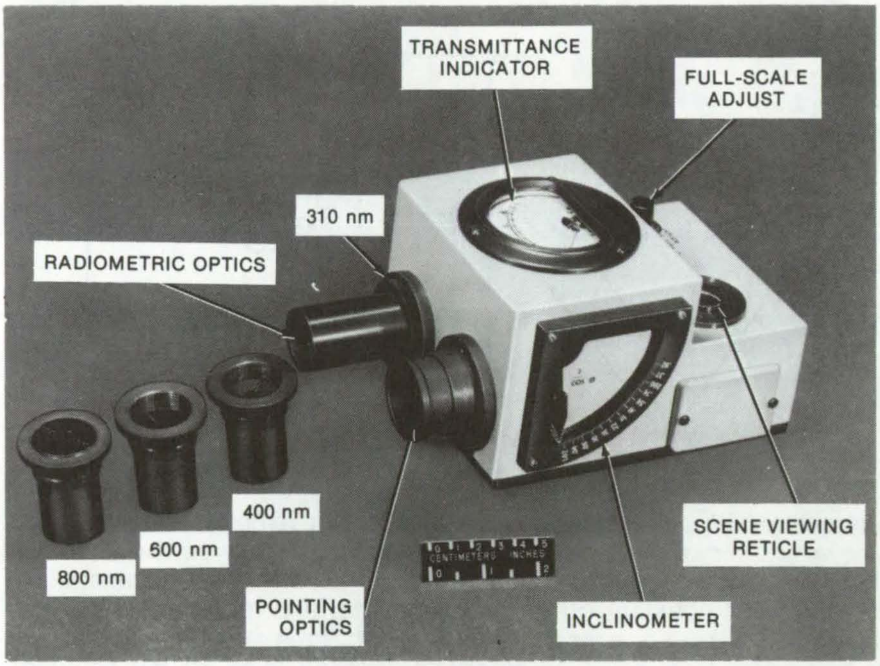

Figure 1. The **Solar Radiometer,** shown above with its filters, is a compact instrument for the determination of particulate density and NO_2 and SO_2 concentration in gaseous suspensions such as smokestack effluents.

A simple and inexpensive portable instrument monitors stack-plume effluents from ground level. This four-channel solar radiometer uses the Sun as a background source and measures the attenuation of solar radiation through the stack plume.

The radiometer (Figure 1) features two optical arrangements: an easy-to-aline pointing optical system that is boresighted to the second radiometric optical system which utilizes four filters to select the wavelengths.

In order to use the radiometer, the Sun must be in an accessible viewing position, and the sky adjacent to the Sun must be free of clouds. The operator selects and inserts the filter system to be used and situates the radiometer as shown in Figure 2.

Attenuation is measured at four selected wavelengths:

Wavelength (nanometers)	Characteristic
310	UV
400	Visible
600	Visible
800	IR

The IR channel measures the effects of particulates and aerosols. The two visible channels superimpose the effects of NO_2 absorption, and the UV channel measures the effects of SO_2. Stack-plume measurements of opacity and of the concentration of NO_2 and SO_2 made with this instrument were found to be in basic agreement with in-stack determinations.

The simple, remote operation eliminates troublesome in-stack measurements, and the radiometer is less expensive than other remote measuring devices such as those utilizing laser backscatter and correlative spectroscopy. The portability and accuracy of this radiometer make it extremely attractive as a low cost, ground level device for monitoring stack pollution at powerplants, factories, and other stationary sources.

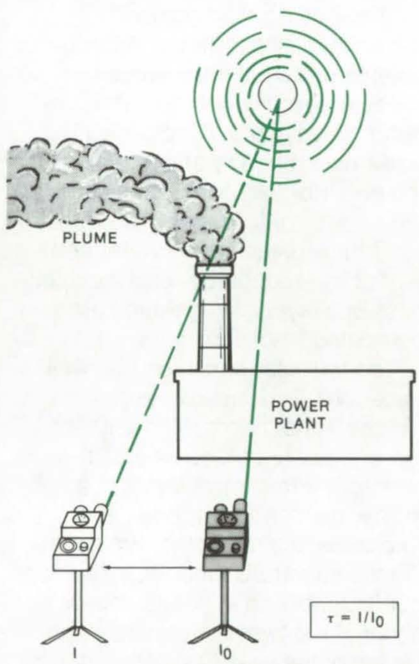

Figure 2. **Effluents Are Monitored** by aiming the radiometer directly at the Sun. A second measurement is taken with the radiometer aimed at the plume. The transmittance (τ) of the plume is the ratio of the measured solar intensities (I_0 and I).

This work was done by Reginald J. Exton and Ray W. Gregory of **Langley Research Center.** *Further information may be found in NASA TN D-8182 [N76-26718], "A Four-Channel Portable Solar Radiometer for Measuring Particulate and/or Aerosol Opacity and Concentration of NO_2 and SO_2 in Stack Plumes", copies of which are available at cost from North Carolina Science and Technology Research Center* *[see page A7].*
LAR-12123

Remote Moisture-Content Balance

An automatic balance monitors the wetness of wood samples to determine forest fire hazards.

Ames Research Center, Moffett Field, California

The probability of a forest fire may be estimated by monitoring the moisture content of a remotely-placed "fuel model." The fuel model, as illustrated, consists of four wooden dowels that will absorb moisture from precipitation and humidity at a rate related to moisture absorption by forest wood. The wetness of the model is determined from weight changes as monitored by an electronic balance. Weight data are transmitted to a central station for analysis.

The model is attached to one end of a balance beam. At the other end, there is a damper to reduce wind disturbance. The damper is a disk attached to the end of the beam and immersed in a jar filled with oil. Between the wind damper and the fulcrum point, a linear voltage-displacement transducer is suspended from the beam. It is sensitive enough to detect weight changes on the order of fractions of a gram.

The transducer has a 100-gram full-scale reading; the balance beam has a lever arm with a mechanical advantage of 4. Thus a 25-gram weight change at the end of the beam will result in a full-scale output of 5 volts. The transducer signal is processed by an electronics package and is converted for telemetry.

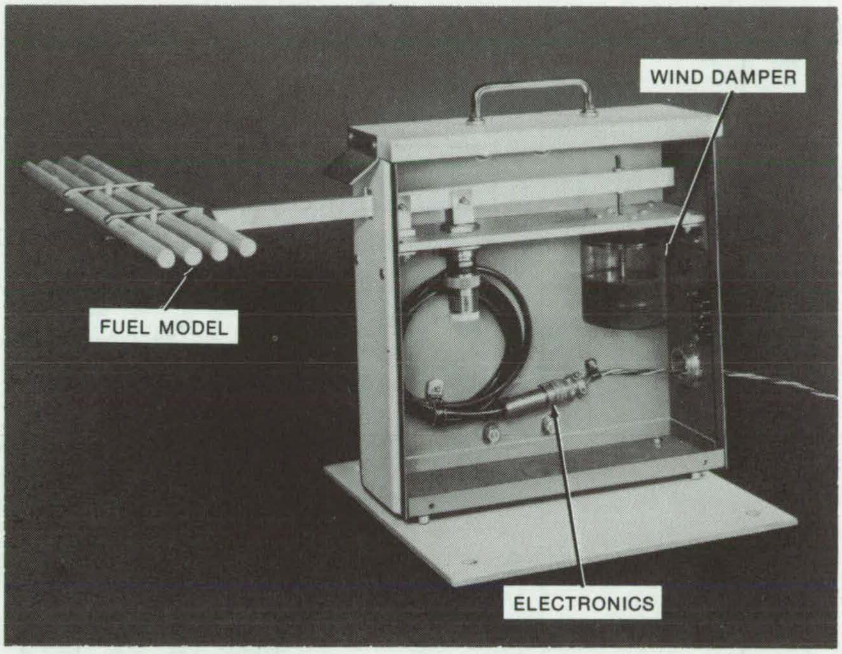

The **Automatic Balance** uses a fuel model of four wood dowels, approximately 45 by 1.25 cm, and weighs 100 grams when dry. The package is approximately 30 by 30 by 10 cm. An increase in weight of from 2 to 12 grams is considered significant and is attributable to the absorption of moisture by the wood.

This work was done by Robert A. Blomseth, Henry Lum, Jr., and Yutaka Matsumoto of **Ames Research Center.** *For further information, Circle 36 on the TSP Request Card.*
ARC-11032

Data System for Multiplexed Water-Current Meters

Flow rates at 32 flood-plain locations are measured simultaneously by a single digital logic unit with high noise immunity.

Marshall Space Flight Center, Alabama

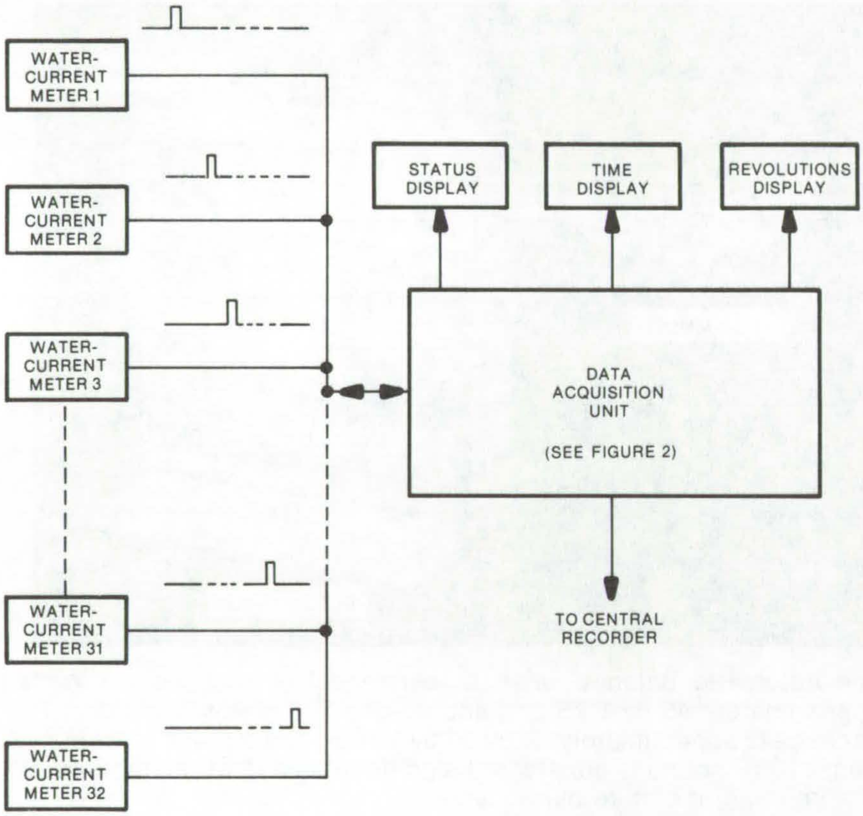

Figure 1. This **Multiplexed Data System** for monitoring water currents at 32 flood-plain locations has a data acquisition unit designed for particular sensors. However, its use of memory is broadly applicable where one processing unit serves many measurement channels.

Waterflow rates sensed by pygmy meters at as many as 32 different locations can be continuously measured and recorded by a single data acquisition unit, as shown in Figure 1. This system, which was developed for flood-plain monitoring, functions reliably even when the electrical contacts of the watermeter are submerged. Moreover, the operating life of the contacts is prolonged by the time-division multiplexing in this system. The data acquisition unit is inexpensive, compact, and portable and operates in open air over wide ranges of temperature and humidity.

The water flowing through the pygmy current meter rotates an element that closes an electrical contact once every revolution, so the rate of flow is measured by counting the number of closures in a time interval. For this purpose the data acquisition unit is connected to the electrical contacts of each of the 32 watermeters by a twisted pair of wires. Using a master clock for timing and control, the unit sequentially pulses these sensor lines for 5 microseconds, 100 times per second. If the contacts are closed at the moment of pulsing, they carry a husky 300-milliampere signal, which is easily distinguished from the electrical leakage and noise signals that can occur when open contacts are pulsed. The low duty cycle at each meter — 5 μs out of every 10 ms — protects the contacts against burnout.

As shown in Figure 2, a sensing multiplexer scans the 32 sensor lines in synchronism with the pulsing multiplexer and connects each line in sequence to a level comparator. The comparator determines whether the electrical conduction at the meter contacts indicates an open or closed state; a density counter then makes a statistical analysis to reject closure indications caused by short-term noise. The state of any selected meter can be displayed on the control panel of the data acquisition unit.

A true closure triggers a one-shot multivibrator that provides pulses for starting and stopping a time counter and a revolution counter. Readings of these counters for a selected channel are also displayed on the control panel of the data unit.

The counters and other logic stages are sequentially connected to a 1-kilobit random-access memory

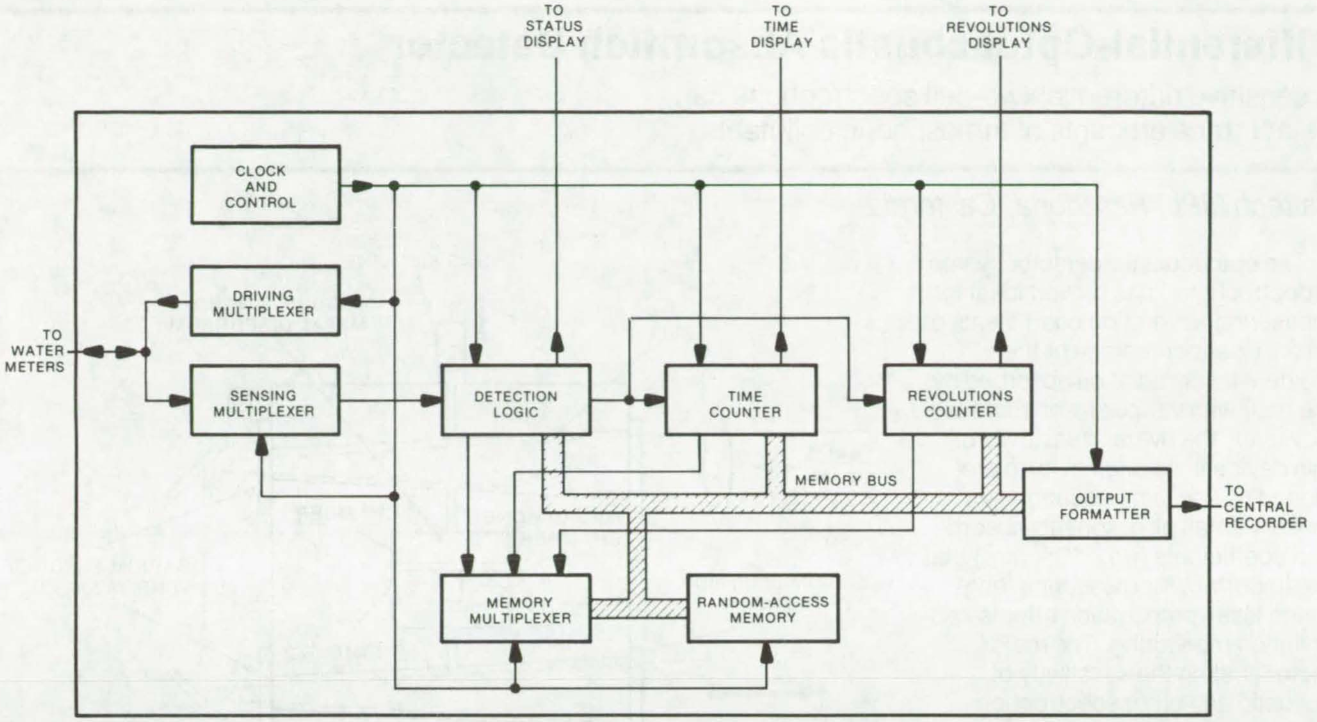

Figure 2. The **Data Acquisition Unit** contains a clock that controls all of the timing, multiplexing, and logic stages. The memory bus carries information to and from storage and to the formatter for serial transmission to the recorder.

(RAM) that stores and outputs data. The output consists of revolution counts, time counts, and status flags for the 32 channels, serialized and transmitted via a single twisted pair to a central recording location. Data from up to four units — a total of 128 channels — are interfaced to a digital recorder and a display.

The circuitry in this data acquisition system is specifically designed for use with waterflow meters. However, other applications can use a RAM for time sharing one set of processing circuits to serve 32 data channels in a similar manner.

This work was done by Charles R. Ramsey of General Electric Co. for **Marshall Space Flight Center.** *For further information, Circle 37 on the TSP Request Card.*

Inquiries concerning rights for the commercial use of this invention should be addressed to the Patent Counsel, Marshall Space Flight Center [see page A8]. Refer to MFS-23343.

Less-Costly Activated Carbon for Sewage Treatment

Activated carbon can be more economically produced for waste treatment plants using lignite coal. The new process was developed for processes that convert sewage sludge to activated carbon for use in the process, but require additional activated carbon to be purchased for the purification process. Rather than adding activated carbon, the much less expensive lignite is pyrolyzed along with the dried sludge to produce the needed amount of material. Tests on activated carbon produced in this way show it to be as efficient as the commercial version.
(See page 573.)

Extracting Lignins From Mill Wastes

Lignins, an industrial waste product of wood-processing mills, can be removed from water economically using a new process. Quaternary ammonium compounds (QAC) and activated charcoal produced during the process, are used to precipitate the lignins. The QAC is recycled, and the lignins are recovered in a form sufficiently pure for resale. The process has been tested on a laboratory scale with the chlorine wash from a Kraft process pulp mill.
(See page 571.)

Surfactant-Assisted Coal Liquefaction

A coal liquefaction process entailing intermediate asphaltene species can be made more efficient by the addition of a surfactant. It is added, after an initial decomposition and hydrogenation step, to asphaltene particles in a nonpolar solvent. The surfactant prevents the particles from forming aggregates, thus exposing a greater reaction surface area for subsequent hydrogenation. The yield is increased and the energy costs (pressure, temperature, and hydrogen) for the final step are much less. The solvent and surfactant can be recycled.
(See page 574.)

Differential-Optoacoustic Absorption Detector

A sensitive differential two-cell spectrophone can detect trace amounts of atmospheric pollutants.

Caltech/JPL, Pasadena, California

The optoacoustic-detector system (spectrophone) has proved ideal for measuring absorption coefficients of gases (that percentage of the incident laser radiation absorbed by the gas) with various laser sources. However, the overall sensitivity of this device in its original form precluded its use in measuring extremely small atmospheric-absorption coefficients (i.e., 10^{-6} m^{-1}) that are important for measuring long-range laser-propagation effects and pollution monitoring. The major factor limiting the sensitivity of acoustic and other spectrophone devices is the spurious signal produced by heating cell windows: the absorption coefficient equivalent to window heating is about 10^{-5} m^{-1}/W or higher.

Now, smaller coefficients can be determined by using for measurements of absorption a differential spectrophone that measures only the difference in pressure between two cells with a differential capacitive manometer. The background signal is reduced by the balanced window heating and balanced carrier-gas absorption in the two cells.

To improve further the differential spectrophone, a "folded" optical path is used (see figure). This allows a differential microphone to be placed between two cells with short connecting ports and, therefore, reduces unexcited-gas volumes. Also, the cell walls have been tapered to conform to the light-wave expansion and thus further reduce the nonexcited volume. The background noise is equivalent to a coefficient of 3.3×10^{-7} m^{-1}/W, about 100 times better than a single-cell spectrophone.

The body of the differential spectrophone is a metal block, approximately 4 in. (10 cm) on a side and 1 in. (2.5 cm) thick. Each cell is vacuum sealed; and transverse bores, for introducing carrier and sample gas, connect both the cells to a microphone chamber. A vacuum-sealed metal diaphragm separates the two gas chambers. A fixed plate allows measurement of the pressure difference between cells 1 and 2 by measuring the capacitance changes as the diaphragm responds to differential pressure changes between the cells.

A laser emitting wavelengths in the 9- to 11-micrometer region (such as a carbon-dioxide laser) enters cell 1 through window 1, exits, and is "folded" by two mirrors through cell 2. The only non-laser-excited gas is in the ports, which are short in this configuration.

The carrier gas is introduced into cells 1 and 2 by opening the valves in the gas-fill lines. The capacitance microphone will indicate a balanced pressure in cells 1 and 2 when only the modulated, excited carrier gas is present. The carrier gas is then removed from one cell, and a sample consisting of the carrier gas plus the trace constituent is introduced. The capacitance microphone then responds to the differential pressure due to the laser absorption of the trace constituent.

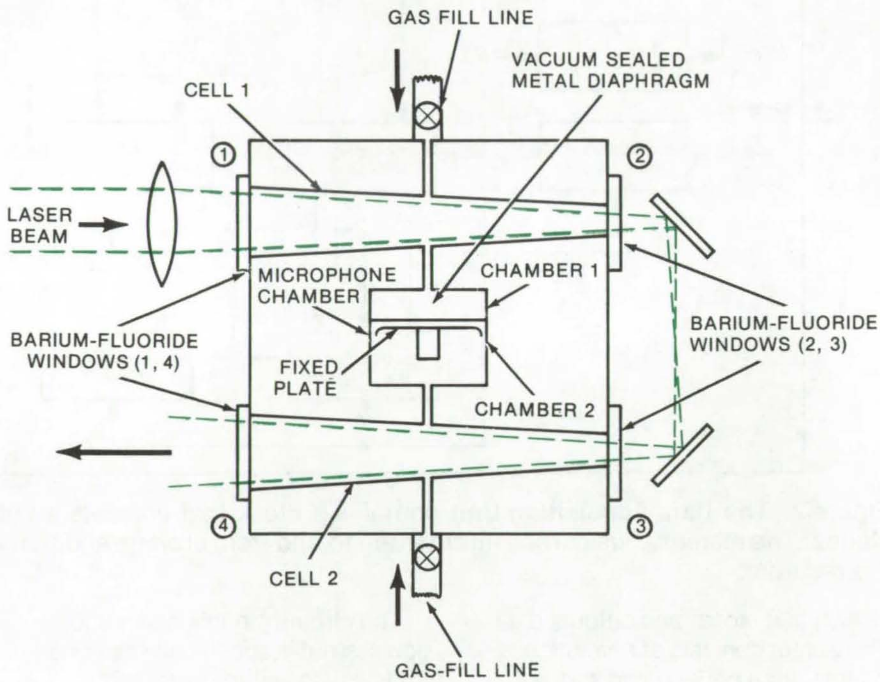

The Improved Differential Spectrophone minimizes non-excited-gas volume and lowers the background signal. A folded laser beam shortens the ports coupling the two cells to the microphone. Special plugs in the ports, and the tapered cells, further reduce the non-excited-gas volume, yielding a higher responsivity and thus a higher signal-to-noise ratio.

This work was done by Michael S. Shumate of **Caltech/JPL.** *For further information, Circle 38 on the TSP Request Card.*

This invention is owned by NASA, and a patent application has been filed. Inquiries concerning nonexclusive or exclusive license for its commercial development should be addressed to the Patent Counsel, NASA Resident Legal Office-JPL [see page A8]. Refer to NPO-13759.

Image Intensification of Developed Photographs

A new autoradiographic technique employing an organic-sulfur solution is simple and effective.

Marshall Space Flight Center, Alabama

A post-processing method for images on films and plates can be used to enhance underexposed films, to retrieve additional information from less dense portions of a developed photograph, and to increase contrast on these films.

The method is an improved autoradiography procedure, used to enhance film images by increasing the contrast or by changing the overall optical-density scale of the exposure. In general, silver in a developed film is converted to a radioactive compound. The level or density of silver in the film controls the optical transmission of the film and forms the image. After converting the silver to a radioactive compound, the image is transferred to a second film which is sensitive to radioactive beta particles.

Conventionally the silver on the film is converted to a radioactive compound by reaction with sulfides or polysulfides consisting primarily of sulfur-35, a β emitter. This process has had several disadvantages that limited its usefulness, such as only moderate effectiveness and the production of toxic and radioactive gases.

The technique of autoradiography has now been made suitable for much broader use by a new method of chemically activating the film or plate with sulfur-35 which bypasses ordinary toning chemistry. This method retains the advantages of using the sulfur isotope and virtually eliminates the disadvantages usually experienced with previous forms of film autoradiography. The activating solution consists of organic sulfur molecules, such as 2-thiourea-S^{35}, dissolved in water. A small amount of alkali is added just before the film is processed. After processing, the film is simply rinsed with water or water-methanol solutions.

Some advantages of this process are:

- There are no colloidal compounds formed in the solution, and there is no problem of colloidal-sulfur settling in the gelatin.
- It is not necessary to convert the image silver to silver halide prior to processing. The extra time, inconvenience, inexactness, and the colloidal precipitation problems caused by this step are avoided.
- The original film is not degraded by this process.
- Sulfur-35 is a pure beta emitter, and there is no accompanying gamma radiation to fog nearby films or cause a health hazard.
- The half-life of sulfur-35 is 88 days. It is long enough for the activating solution to last a reasonable amount of time and for large quantities of autoradiographs to be made from an activated negative. Yet, it is short enough that, if desired, radioactive wastes and negatives can be kept in storage and allowed to become inactive with time. This eliminates most disposal problems.

This work was done by Barbara S. Askins of **Marshall Space Flight Center.** *For further information, Circle 39 on the TSP Request Card.*

Inquiries concerning rights for the commercial use of this invention should be addressed to the Patent Counsel, Marshall Space Flight Center [see page A8]. Refer to MFS-23461.

Solvent for 1-Phenyl-3-Pyrazolidone in Photography

Dimethyl sulfoxide makes an excellent solvent for silver halide developers.

Goddard Space Flight Center, Greenbelt, Maryland

Commercially available preparations of 1-phenyl-3-pyrazolidone and its methyl derivatives are frequently used as photographic developing agents. However, they have limited solubility (about 5 g/l at pH 9) in water, and the dissolution time is considerably longer than for other developer components. Acetic acid, which is known to be an adequate solvent for these agents, is unsuitable for photographic developing because the solutions used must be alkaline.

Dimethyl sulfoxide has been shown capable of dissolving 1-phenyl-3-pyrazolidone at ratios of 2 g/10 ml and higher. The solution is prepared by dissolving 2 grams of the developing agent in 10 ml of dimethyl sulfoxide. A solution of 10 g of sodium sulfite is dissolved in 250 ml of water (pH 9.55). The developer solution is then slowly added to the sulfite solution under constant agitation. The order of mixing is important, since if water is added to the concentrated dimethyl sulfoxide solution, supersaturation will occur.

This work was done by Arnold R. Shulman of **Goddard Space Flight Center** *and Robert Shaffer of Computer Sciences-Technicolor Associates and Edith L. Shulman. No further documentation is available.*
GSC-11992

DC Drive System for Cine/Pulse Cameras

Two brushless dc motors improve camera operation and reliability.

Lyndon B. Johnson Space Center, Houston, Texas

A technique for improving camera reliability without sacrificing performance eliminates mechanical clutches and employs brushless dc motors. Other advantages to be gained are reduced average-power consumption and the simplicity of exposure control.

In the modified system, the camera-drive functions are separated mechanically into two groups which are driven by two separate motors. The first motor, a 90° stepper, drives the rotating shutter. The second, an electronically-commutated dc motor, drives the claw and film transport. The shutter is made of one piece but has two openings: onė 90° segment for slow exposures and a smaller opening for fast exposures (see Figure 1).

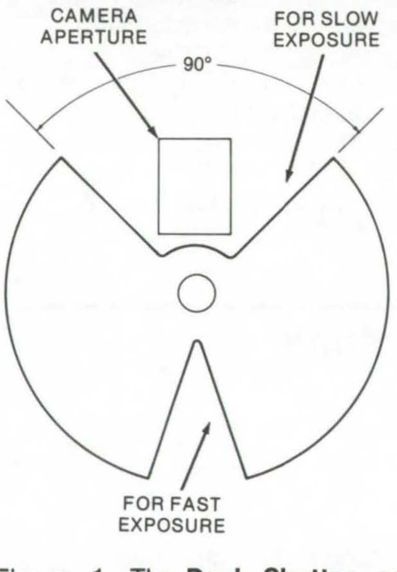

Figure 1. The **Dual Shutter** as viewed from the lens has a 90° opening used for exposure times of 1/125 second. The narrow shutter opening is used for shorter exposure times with the motor rotating continuously through two steps of 180°. Speed is controlled to give the desired exposure time.

There is a 1-to-1 ratio between the stepper motor and the shutter. A single exposure consists of two 90° steps of the motor, the shutter rotates 90° and is held in the open position for a time suitable for correct exposure. It then rotates another 90° to close the shutter. Each succeeding exposure is made by reversing the direction of rotation. For faster exposures, two 180° rotations of the narrow opening are employed.

Optical sensors determine the shutter position (see Figure 2) and are used to time pulses that control the stepper motor. The timing of the input pulses to the motor is controlled to keep the change in shutter angle constant. This provides a uniform exposure. By varying the pulse voltage, the speed of the shutter and thus the exposure time may be changed.

To limit overshoot at the completion of the shutter travel a timed retarding pulse is applied to the stepper motor (see Figure 2). If this were not done, the shutter would be subject to oscillations at the end of each exposure, allowing additional light onto the film plane.

The second motor is operated continuously at high camera speeds (frame rates). For low frame rates and pulse modes the motor is operated in a start/stop fashion. The only requirement on position is that the claw be brought to rest during the portion of the cycle when it is extracted from the film.

A command from the control electronics starts the cycle, and an internal signal triggered from a predetermined position of the claw stops the motor. The master control of frame rate is from the regulated speed of the claw drive for the higher frame rates and from the electronics start command for the lower frame rates. The shutter is synchronized to the claw by a pulse from the claw system which occurs

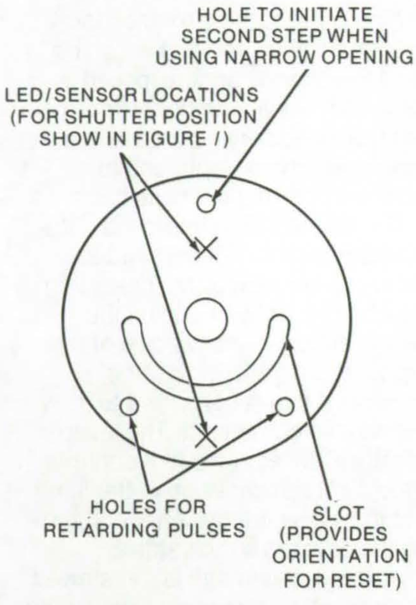

Figure 2. An **Optical Disk** is used to control the stepper motor and the retarding pulse. Input signals are obtained from optical sensors (which detect holes in the optical disk) for uniform shutter speed throughout exposure (stepper-motor control) and to limit shutter overshoot (retarding-pulse control).

at a time after the claw becomes extracted from the film (this is the same pulse that cuts power to the motor in the slow frame rate and pulse modes).

This work was done by Ronald H. Gerlach of **Johnson Space Center** *and James T. Sharpsteen, Curtis D. Solheim, and Louis J. Stoap of The Perkin-Elmer Corp. Further information may be found in:*

NASA CR-147535 N76-22510]
"Development of a Drive System For a Sequential Space Camera" and
NASA CR-147759 [N76-25538]
[Addendum to Above].

Copies of these reports may be obtained at cost from the National Technical Information Service, Springfield, Virginia 22151.
MSC-16085

Elimination of Color Rings on Film Negatives

Inexpensive surface finishing prevents the formation of interference rings during photoprocessing.

Goddard Space Flight Center, Greenbelt, Maryland

An optical-glass surface can be treated to prevent the formation of light-interference fringes (light and dark rings) that form between the glass surface and a contacting surface of a photographic-film negative. There is no need to use and replace antireflection coatings and resins.

In a conventional photographic enlarger, film is positioned on a glass plate, and light passes through the film and glass (see Figure 1). In between the contacting surface of the glass and the film, air wedges are formed. These air wedges act as a thin film causing the formation of interference fringes (alternating dark and light rings known as Newton's rings).

It has been shown to be possible to eliminate this problem by abrasive grinding of the glass surface (see Figure 2). Many small irregularities (peaks and valleys) ground onto the glass surface break up the dark and light fringes.

A grinding-grit size of 22.5 microns is employed. To polish the irregularities for improved light transmission, the contact surface is bathed in an aqueous solution of sulfuric acid and hydrofluoric acid (acid-bath etching). Hydrofluoric acid decomposes the rough texture of the irregularities, and the sulfuric acid provides a medium for holding the hydrofluoric acid close to the contact surface.

This work was done by Charles M. Fleetwood, Jr., Stephen H. Rice, and Rodney S. Spencer of **Goddard Space Flight Center.** *For further information, Circle 40 on the TSP Request Card.*

This invention is owned by NASA, and a patent application has been filed. Inquiries concerning nonexclusive or exclusive license for its commercial development should be addressed to the Patent Counsel, Goddard Space Flight Center [see page A8]. Refer to GSC-12110.

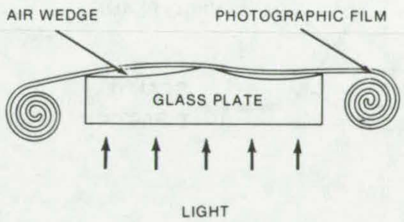

Figure 1. The **Contacting Surfaces** of a conventional glass plate and photographic film are smooth but slightly wavy, causing the formation of color rings. Grinding the glass to produce many smaller irregularities prevents the formation of the rings (interference fringes).

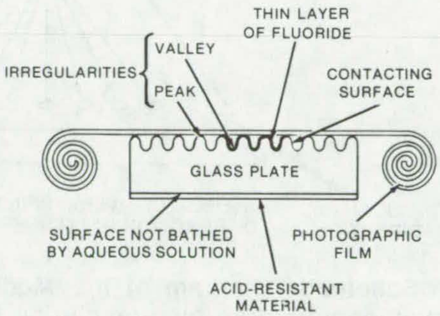

Figure 2. The **Reaction of Hydrofluoric Acid With the Surface** will cause a thin layer of fluoride to be formed on the surface. Therefore even after washing, there may still remain some aqueous solution that will continue to decompose the surface. A soft-bristle brush can be used to loosen and break up the thin fluoride layer.

Biomedical Ultrasonoscope

An ultrasonic system allows real-time noninvasive observation of the heart. The battery-powered instrument uses low-power IC's and is capable of A-mode, C-mode, and M-mode scans. Echoes are presented as a CRT display. Two probes, one containing a single transducer and the other containing an array of ultrasonic elements, are pressed against a subject's chest to pick up signals. Resolution is sufficient to observe the heart's functioning and changes in its shape and size.

(See page 593.)

Heat-Transfer Coefficients of Pin-Finned Cylinders

Heat-transfer data for pin fins on the surface of a single cylinder have been analyzed. Wind-tunnel tests show that the heat-transfer rate can be increased by a factor of 4 when the pins are added to a plain surface. They are shown to be especially advantageous, compared to annular fins, when the flow direction is variable. The transfer coefficient depends, among other things, on pin diameter, spacing, length-to-diameter ratio, and angle from the stagnation point.

(See page 612.)

Determining Eutectic Composition in Metal Alloys

A simplified technique is useful in determining the eutectic composition of new multicomponent alloys in the absence of alloy phase-equilibria data. In the process a section of sample ingot is slowly heated in a special crucible. As the temperature approaches the melting point, the eutectic composition bleeds from the sample surface and is collected. The technique is more effective and economical than zone melting and does not require samples to have a true eutectic composition.

(See page 577.)

High-Resolution Electron Microscope

A synthetic aperture improves the electron microscope and is applicable to biomedical research.

Caltech/JPL, Pasadena, California

In biological research, there is an urgent need to determine the atomic configuration of large molecules such as enzymes that can be made crystalline (or pseudocrystalline in a monolayer). Direct viewing of low-weight atoms (with the electron microscope) is difficult because of the danger of specimen damage, spherical aberration, low contrast, and noisy sensors.

Employing a scanning-transmission electron microscope (STEM) as an interferometer, relative phases of diffraction maximums can be determined by the analysis of dark-field images. A synthetic-aperture (see figure) technique and Fourier-transform computer processing of amplitude and phase information provide high-resolution images at approximately 1 Å. The atomic structures of crystalline and biological materials or specimens are obtained in a single scan (therefore preventing radiation damage). The technique is more efficient than X-ray crystallography, it uses only microquantities of material under investigation, and it can be expanded to noncrystalline material.

In the STEM the two conventional sensors (the bright-field sensor and the dark-field annulus sensor) are replaced by a two-dimensional video camera. High resolution is obtained by using all the signal present in the dark-field images for phase determination. The front focal-plane aperture (2 to 10 microns in diameter) is large enough to allow two diffraction maximums to interact. Relative phases are determined by observing the phase shift of the resultant simple sine-wave interference image.

The electron dose received by the specimen to form a dark-field image is reduced dramatically as compared to a typical scanning use (it is comparable to that received in a conventional microscope). This reduced dose when used with a cold specimen makes it possible to obtain high resolution for crystals containing water.

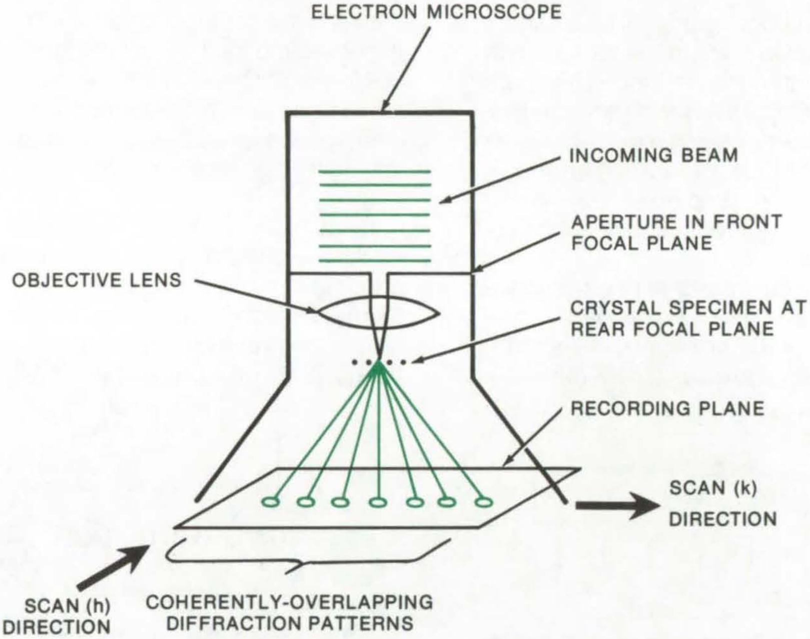

A **Schematic Diagram of the Modified STEM** shows operation for synthetic-aperture high-resolution image synthesis. When a crystal is placed in the rear focal plane of the objective lens, the incoming plane beam (after passing through the lens) converges and passes through the crystal lattice to form a set of coherently-overlapping diffraction patterns in the normal image plane of the microscope. Each of the original diffraction maximums has been convolved with the shape of the aperture. As the input beam is tilted, each point of the recording plane collects a set of dark-field images that represents the Fourier transform of N contiguous diffraction beams.

The modified STEM produces a hard copy of the dark-field image, using a Polaroid camera. The dark-field image contains the relative phase information between two diffraction maximums. Deflection generators are controlled by a television camera and sync generator through a controller, such that the microscope scanning-beam deflection is synchronized with a vidicon scan, creating a 250-line image per TV frame. The diffraction pattern is displayed in real time by a TV receiver. The TV camera output is recorded by a video-tape recorder. Individual lines of the scan raster can be selected for copying by the camera.

Image-processing functions are employed to perform a cross-correlation calculation (to extract phase information) against a reference image (whatever portion of the crystal image appears stable enough for analysis). With the use of a large crystal area, shot noise is overcome by an averaging process inherent in the cross-correlation calculation.

This work was done by Robert Nathan of **Caltech/JPL.** *For further information, Circle 41 on the TSP Request Card.*
NPO-13811

Spatially-Coherent Coupled Semiconductor Lasers

Three GaAs lasers are coupled to produce
an output with triple the power of a single laser.

Marshall Space Flight Center, Alabama

Three homostructural GaAs lasers in a monolithic array have been phase-coherently coupled to produce a spatially coherent output. The mirror faces of the lasers are antireflection coated, and the array is centered within an external optical cavity (see figure) comprising spherical lenses and plane mirrors.

The spherical lenses have a 1-cm focal length. The output mirror has a reflectivity of 0.2. The surface of the other mirror, totally reflecting (reflectivity of 0.97), is subdivided into highly reflecting strips that cause it to function as a spatial filter. The laser array, the planar output mirror, and the spatial filter are located at the focal planes of the internal lenses.

The laser array is mounted on heat sinks that provide common contacts to the lasers. At the second focal plane of the internal lenses, the waves set up by the fields of the lasers in the array occupy the same space. The resultant field distribution at the second focal plane, therefore, is determined by the phase relations between these waves. The spatial filter in the second focal plane is matched to an interference function that results when the fields of the lasers in the array are in the lowest-order transverse mode and when the fields are all in phase. To form the spatial filter, which selects the spatially coherent mode, the surface of the totally-reflecting plane mirror is subdivided into highly reflecting strips subtending the m-order maximums in the interference junction (where m = 0 and 1). Three gold strips (25.4 μm in width and spaced 12.7 μm apart) with a reflectivity of 0.97 are used. Injection current approximates a cosine function with a pulse width of 100 ns and a repetition frequency of 2 kHz.

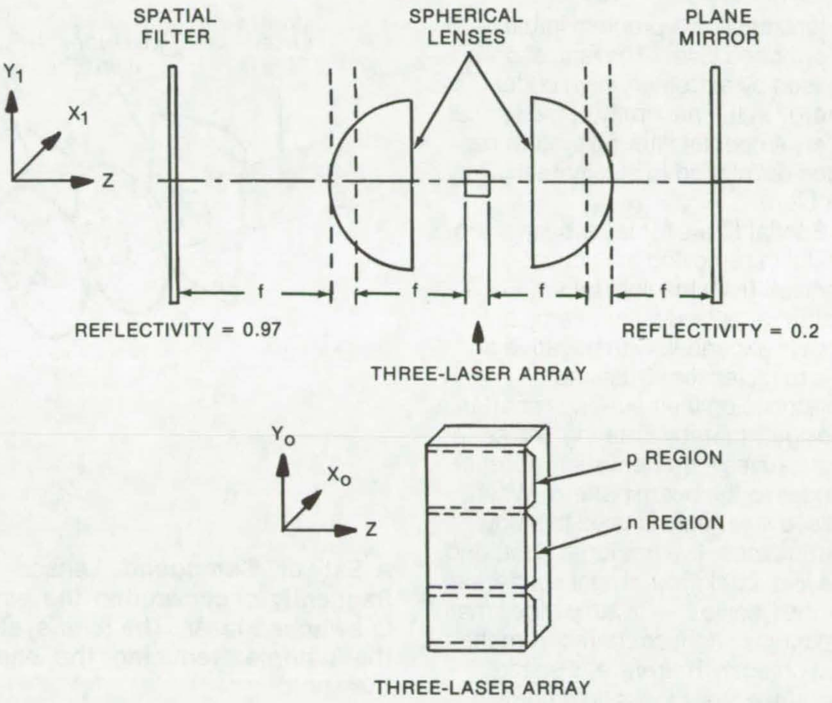

The **External Optical Cavity** for the monolithic array of three GaAs lasers phase-coherently couples the individual outputs to produce a single spatially coherent beam. The Fourier transform properties of the lens and a spatial filter are used to select the coherent mode.

The spatially-coherent beam formation makes use of the Fourier transformation properties of the internal lenses. Transverse modes are controlled by the spatial filter. Optical peak power is 5 W with a peak injection current of about 180 A. The far-field distribution is at the second focal plane of the external spherical lens. Analysis of this synthesized distribution indicates that the laser radiation is spatially coherent. The distribution is evaluated by forming an image on a photographic plate and recording the density distribution of the image, using a microdensitometer.

This work was done by Elisabeth M. Rutz of IBM Corp. for **Marshall Space Flight Center.** *For further information, Circle 42 on the TSP Request Card.*

Inquiries concerning rights for the commercial use of this invention should be addressed to the Patent Counsel, Marshall Space Flight Center [see page A8]. Refer to MFS-23396.

Spatial Filter for Q-Switched Laser

Compound lens system
reduces ionization around the filter.

Lewis Research Center, Cleveland, Ohio

Ionization is a problem in the Q-switched laser. The ionization is caused by extremely-high optical energy in the proximity of the spatial filter. A special filtering system has been developed to eliminate this problem.

Spatial filters for laser beams are useful in removing the optical "noise" from the light beam. For instance, pulsed laser beams are always expanded with negative or diverging lenses. Dust and scratches on their surfaces scatter the light, thereby creating "noise" that causes extraneous interference fringes to the beam pattern. When pulsed laser light is used to study particulates, live bacteria, dust, and the like, background light scattering — the "noise" — swamps the small amounts of light scattered from the test objects. Therefore, a spatial filter (one that blocks light coming from all directions other than the desired direction) is essential to such studies.

Conventionally, laser beams are spatially filtered by focusing the beam through a small pinhole. This approach works with any of the gas lasers such as helium/neon. However, with a Q-switched solid-state laser such as ruby or neodymium (about 1 joule in a tenth of a microsecond), the intense alternating optical-energy fields about the focal region ionize the air and cause a bright spark. A preponderance of the laser energy is absorbed by creation of the spark. Moreover, the proximity of a metal aperture with a pinhole reduces the energy at which breakdown occurs.

A solution other than the obvious one of reducing the power in the laser beam was needed.

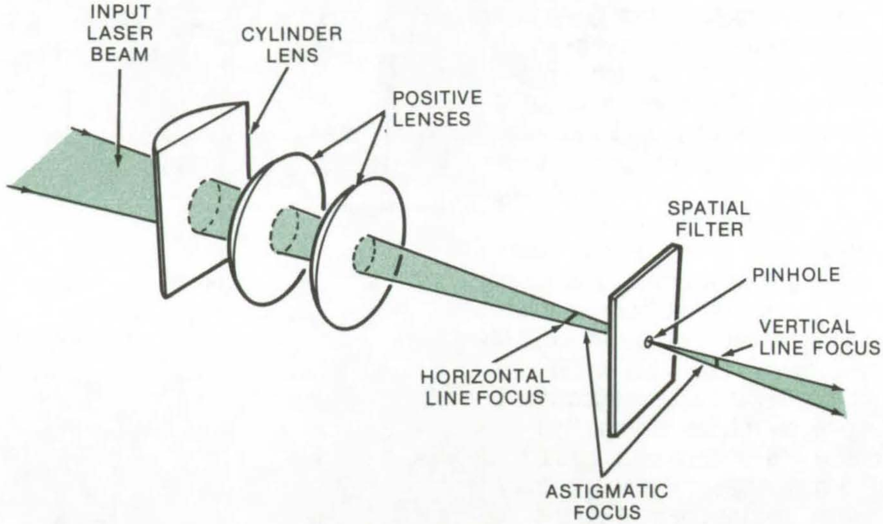

A Set of Compound Lenses reduces ionization and sparks that frequently occur around the pinhole aperture in the spatial filter of a Q-switched laser. The lens system produces an astigmatic focus near the pinhole, reducing the energy level there below the ionization threshold.

This new innovation (shown in the figure) consists of a cylindrical lens which has finite and infinite focal lengths and a pair of lenses having finite focal lengths. This compound lens system produces an astigmatic focus close to the aperture of the spatial filter and thus reduces the high optical energy below the level that produces ionization of air.

The spatial filter is an opaque material (aluminum in this case) having a 1-mm (0.039-in.) pinhole. This filter is positioned between the two astigmatic line focuses. Precise positioning does not appear to be critical.

Tests with the new spatial filter verified that breakdown will not occur with the cylinder lens added. Removal of the lens, however, does result in breakdown and a complete disruption of the incidental laser energy. Other combinations of weak cylinder lenses with short-focus positive lenses were also made to work.

This technique has been proved useful in large-area holography and is probably applicable to all Q-switched pulse laser operations.

This work was done by Lee O. Heflinger and Ralph F. Wuerker of TRW, Inc., for **Lewis Research Center.** *Further information may be found in NASA CR-121264 [N74-18152], "Application of Holography to Flow Visualization Within Rotating Compressor Blade Row," a copy of which may be obtained at cost from the New England Research Application Center [see page A7].*

This invention is owned by NASA, and a patent application has been filed. Inquiries concerning nonexclusive or exclusive license for its commercial development should be addressed to the Patent Counsel, Lewis Research Center [see page A8]. Refer to LEW-12164.

Servo Corrects Interferometer-Mirror Tilt

Error signals in two axes are used to
adjust interferometer mirrors automatically.

Caltech/JPL, Pasadena, California

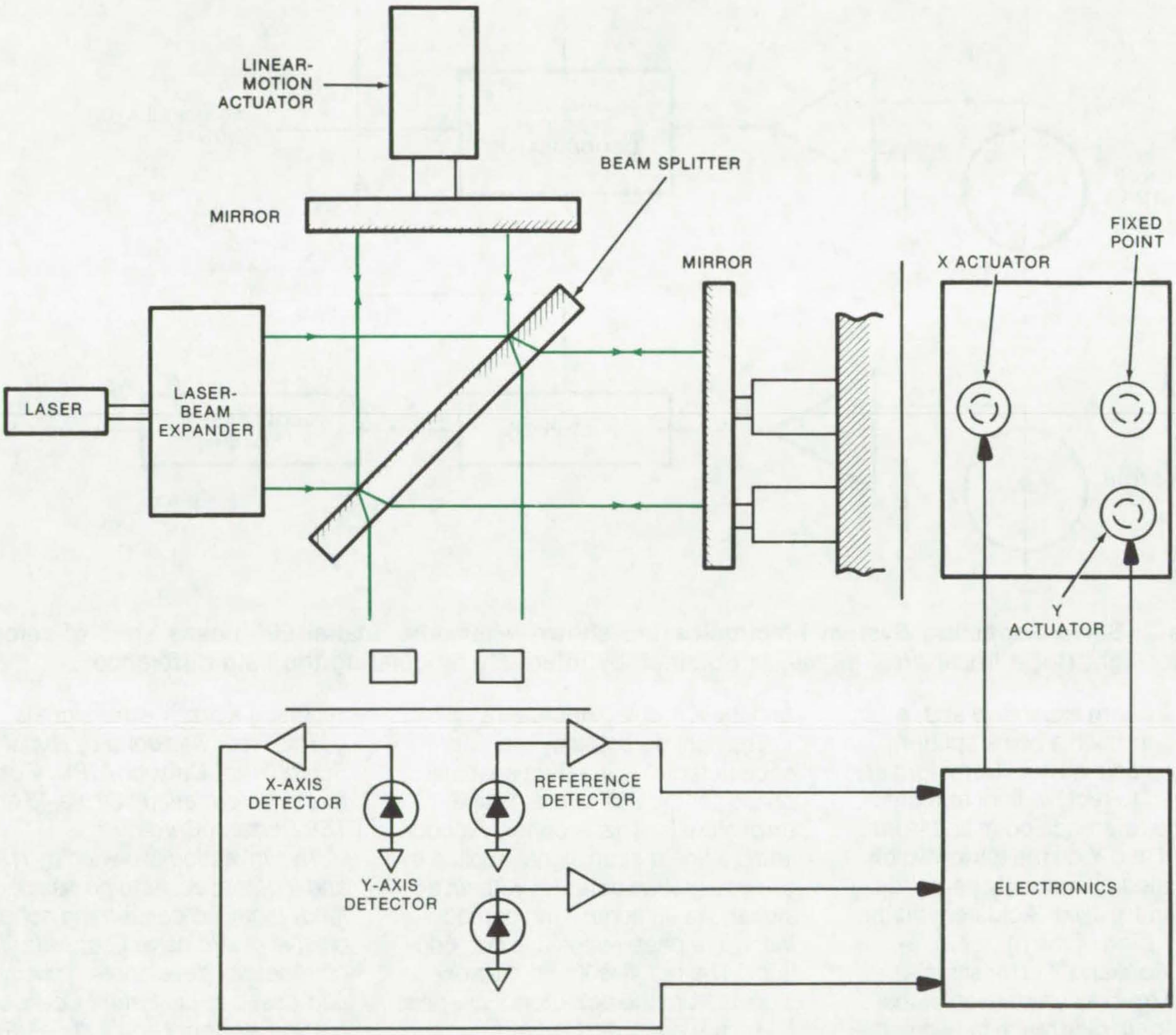

Figure 1. The **Mirror-Tilt Correcting System** is shown as a conventional Michelson interferometer. A He-Ne laser is expanded (larger diameter) into a collimated beam, and error signals are provided in two axes.

The system shown in the illustrations was developed to maintain the position of the two mirrors of an interferometer such that recombining wave fronts are parallel to within 0.5 second of arc. Any tilt in the beam axis of the variable-length path is compensated for in order to maintain the interfering beams parallel at the output.

Three detectors sense a He-Ne laser beam; one senses the reference phase while the others, at right angles to the first, sense the phase offset for each axis. The output of each of the axis detectors is analog multiplied separately by the reference output to give X and Y error signals that are then fed to the respective X and Y actuators. The reference is spatially offset by 90° in order to obtain a linear error signal.

In a setup using a Michelson interferometer, the beam is expand-

(continued on next page)

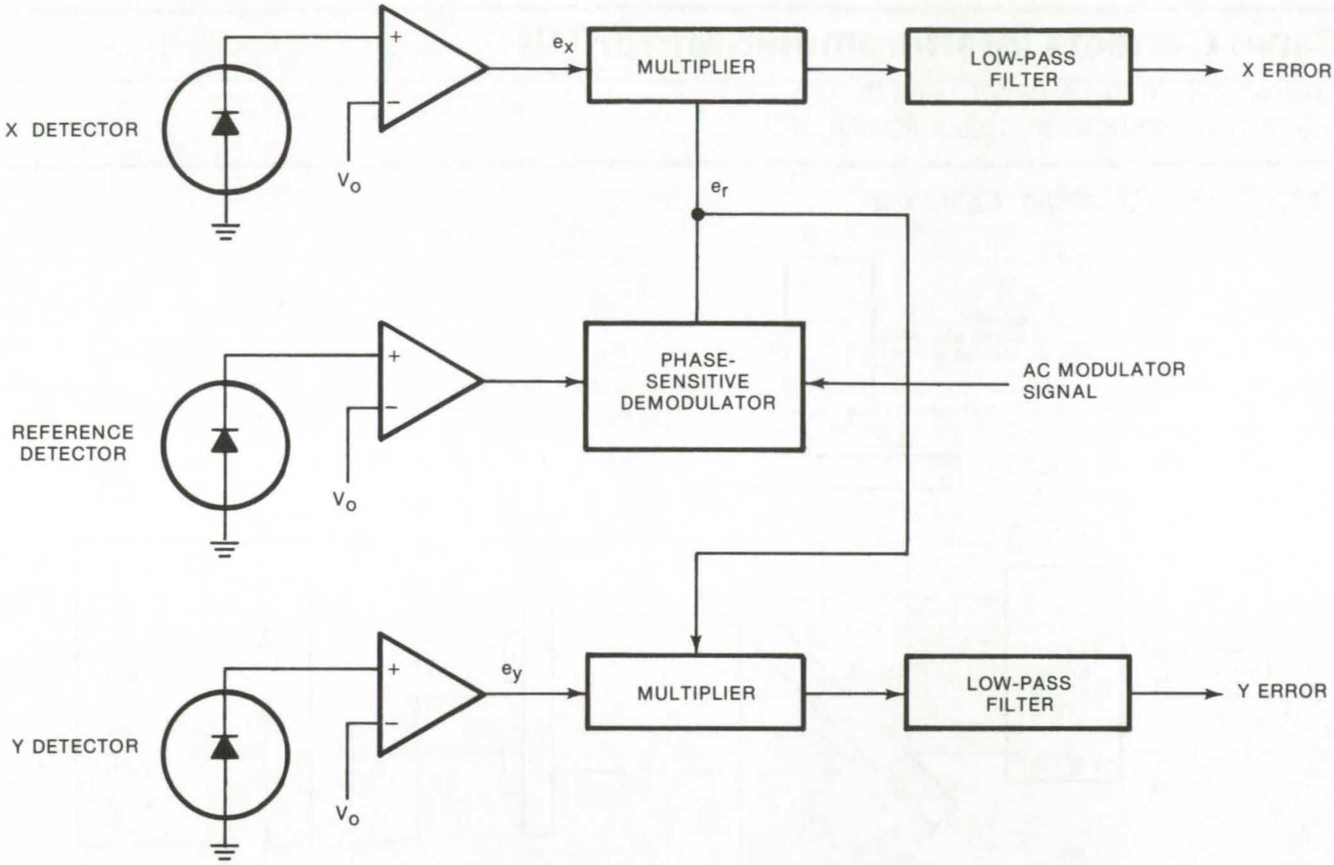

Figure 2. **Servo-Correcting System Electronics** are shown where the spatial 90° phase shift of reference detector light (for a linear error signal) is obtained by internally modulating the path difference.

ed (by a beam expander) and, after passing through a beam splitter, impinges on a mirror. Detectors are arranged to receive light reflected from the reference point and from points X and Y on the mirror which are located on mutually-perpendicular X and Y axes. Actuators tilt the X and Y axes of the mirror in response to X and Y error signals derived from a comparison of the optical-path difference between the light detected by the fixed detector and the X and Y detectors.

The light detected by the reference detector is in effect spatially phase shifted 90° to create linear error signals. This is done by modulating a linear scan signal applied to a linear-motion actuator with an ac signal, via an adder, and demodulating in a phase-sensitive demodulator. The result is X and Y error signals from the detectors. Low-pass filters are employed to filter out unwanted components in the resulting X and Y error signals.

This work was done by Rudolf A. Schindler of **Caltech/JPL.** *For further information, Circle 43 on the TSP Request Card.*

This invention is owned by NASA, and a patent application has been filed. Inquiries concerning nonexclusive or exclusive license for its commercial development should be addressed to the Patent Counsel, NASA Resident Legal Office-JPL [see page A8]. Refer to NPO-13687.

Temperature Reference for Microwave Radiometer Calibration

A precision reference is used to calibrate microwave radiometers at the antenna aperture.

Langley Research Center, Hampton, Virginia

A new temperature reference for a microwave radiometer avoids the need to physically remove the antenna and replace it with a calibrating termination. In this way, a large source of potential error is eliminated. Radiometer calibration is normally achieved by replacing the antenna with a cooled reference termination and then applying corrections for ohmic and reflective losses of the antenna and for the nonideality of the reference termination. However, imprecisions of the correction process for some applications are unacceptably large.

The improved temperature reference is a piece of porous microwave absorber (having a convoluted surface for low reflection coefficient) fitted with a cap of nonporous plastic foam. The foam mating surface is the inverse of that of the absorber. The microwave absorbing material is then soaked with a cryogen such as liquid nitrogen or argon; the nonporous cap forces the liquid to conform to the shape of the absorbing material. This procedure ensures that the temperature at which the microwaves are absorbed (and therefore thermally emitted) is exactly that of the cryogen, and it avoids the reflection that would be produced by the dielectric discontinuity of a plane surface of cryogen.

The microwave reflection from the external surface of the nonporous foam cap is very small due to the low density of the foam. (If necessary, the external surface of the foam could also be convoluted.) The microwave loss within the foam is also very small due to the low density and low intrinsic loss of this plastic material.

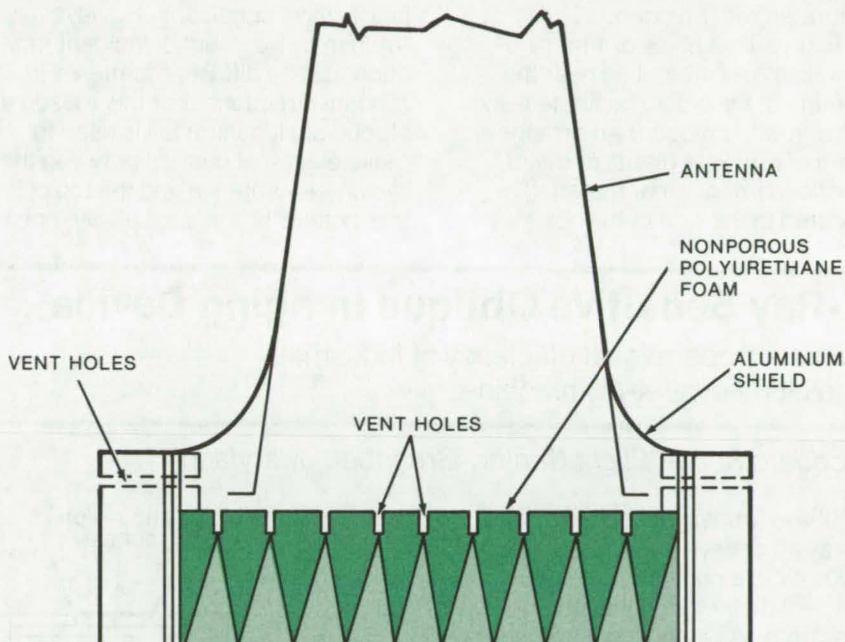

The **Precision Reference Load for an S-Band Radiometer** uses a pyramid-shaped absorber placed at the bottom of a thermally-insulated metal box. A cap of expanded polyurethane is foamed over the absorber. Under far-field plane wave conditions the absorber has a specular reflectivity of -40 dB. When filled with LN_2 to the tips of the absorber, the average VSWR of the reference is 1.020 (2.7 GHz), equivalent to a power reflection coefficient of 1×10^{-4} (emissivity of 0.9999).

A calibration reference load for S-band radiometers is shown. A piece of microwave absorber, 2 feet (0.2 m) square, with convolutions in the shape of close-packed square pyramids is placed in the bottom of a thermally-insulated metal box, and a cap of expanded polyurethane is foamed over it. The foam is then milled flat to a level about 1 in. (2.5

(continued on next page)

cm) above the tips of the absorber. Vertical ventholes 0.5 in. (1.3 cm) in diameter are drilled into the foam at the positions of the peaks of the microwave absorber to allow the escape of the gas produced by the boiling cryogen. The holes also ensure that all of the absorber is saturated with cryogen.

Two vertical holes of 1 in. (2.5 cm) diameter are drilled near the corners of the box to facilitate filling the unit with cryogen. An arrangement of brackets (made of metal, plastic foam, or other material) secured to the side of the box may be necessary to prevent the combined assembly of foam cap and microwave absorber from floating in the cryogen. Strips of expanded polystyrene glued with epoxy to the inner sides of the box are used.

The absorber has a specular reflectivity of -40 dB under far-field plane-wave conditions. However, a fraction of 1 percent of incident radiation may be diffusely scattered in random directions. For this reason a shroud of aluminum foil is used to make electrical contact between the radiometer antenna and the top of the metallic box in such a way that, excluding the small horizontal ventholes, the total assembly could not be penetrated by external microwave sources. This ensures that all energy entering the antenna originates in the cooled absorbing material.

This work was done by Allan W. Love, Marinus J. VanMelle, Albert C. Jones, and Walter N. Hardy of Rockwell International Corp. for **Langley Research Center.** *For further information, Circle 44 on the TSP Request Card.*
LAR-11355

X-Ray Sensitive Oblique Imaging Device

Improved operational efficiency of industrial and biomedical X-ray machines

Goddard Space Flight Center, Greenbelt, Maryland

It is extremely difficult to stop X-rays that have energies of about 100 keV in a photocathode and to convert their energy into photoelectrons. As a consequence, the quantum efficiency (ratio of number of photoelectrons per photon) of an X-ray photocathode is low.

The special photocathode assembly shown in the figure improves the quantum efficiency by a dual process. First, a fraction of the incoming X-rays are converted to photoelectrons at the photocathode. Second, X-rays that pass through the photocathode and a thin X-ray transparent membrane (e.g., glass or mica) enter a phosphor screen.

A light-reflecting surface (an evaporated-aluminum coating or a mirror substrate) backs up the phosphor screen to redirect its rear-emitted light towards the photocathode.

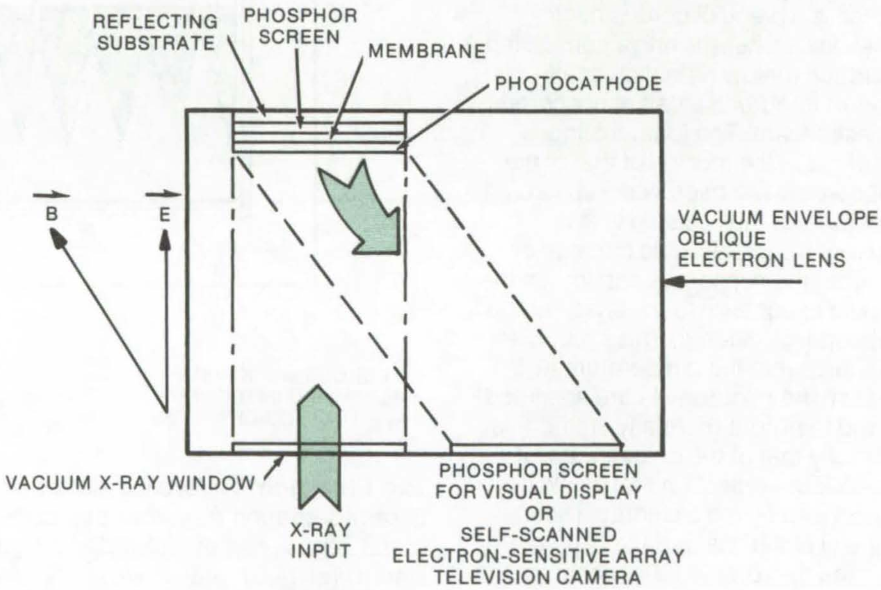

The **X-Ray Sensitive Oblique Imaging Device** employs a light-reflecting surface (an evaporated-aluminum coating or a minor substrate) behind the phosphor screen to improve the effective quantum efficiency.

The X-rays absorbed in the phosphor screen produce light that travels back to the photocathode to produce the bulk of the photoelectrons. The effective quantum efficiency of the photocathode is thereby increased because more photoelectrons are produced in response to each incident X-ray than when the phosphor screen is absent. This phosphor-photocathode sandwich is employed with an oblique electron lens to energize and to transfer the emergent electron image from the photocathode to the target anode. Here the energized electron image may be directly displayed by impacting a phosphor screen.

Another advantage accrues fror use of an oblique electron lens. X-rays are prevented from entering the output phosphor screen, shown in the figure. The contrast in the final image is thereby greater than in other image converter tubes in which semitransparent photocathodes are used and in which the fraction of the X-rays that pass through the semitransparent photocathode can diffusely excite the output phosphor screen.

An alternative to converting the X-ray image to an optical image is to employ an electron input self-scanned array (charge-coupled

device, charge injection device, or photoconductive array) in place of the output phosphor screen shown in the figure. X-rays are deleterious to the proper functioning of a self-scanned array (SSA). However, by using this photocathode assembly design and the oblique electron lens, the X-rays are prevented from entering the SSA. The video signal derived from the SSA can be used to drive a closed-circuit television display, or the video signal can be transmitted to a distant video receiver.

This work was done by Kenneth L. Hallam of **Goddard Space Flight Center** *and Charles B. Johnson of The Bendix Corp. The principle of operation of the oblique electron lens is described in NASA Tech Brief B73-10255. No further documentation is available.*
GSC-11935

Dual-Purpose Holocamera

Bright-field or scattered-light holograms with the same basic camera

Lewis Research Center, Cleveland, Ohio

Improvements in a basic holocamera have resulted in a versatile and unique instrument that can record bright-field holograms (single and double exposure interferograms) or, with minor adjustments, record forward scattered-light holograms. Using the latter arrangement, particles as small as one to three microns have been photographed with acceptable sensitivity and precision.

Versatility is made possible by interchanging beam splitter, prism plates, and reflecting prisms, as shown in the figure. A sliding table has been devised for mounting the various lenses, prisms, and splitters. Moving the plate sideways simply and quickly changes the holocamera from one type to the other. The two types share the same focusing lenses and reference beam.

Optical components are mounted to a frame as rigidly as possible. An aluminum enclosure at one end of the holocamera contains the sliding plate and one front surface mirror (for the focused ground glass configuration); it also serves to anchor the shield between the diffuser and the focusing lens set. The reference-beam prisms are mounted below the aluminum enclosure on a steel plate welded to the tubular framework. The lens for spreading the reference beam is mounted on the same plate.

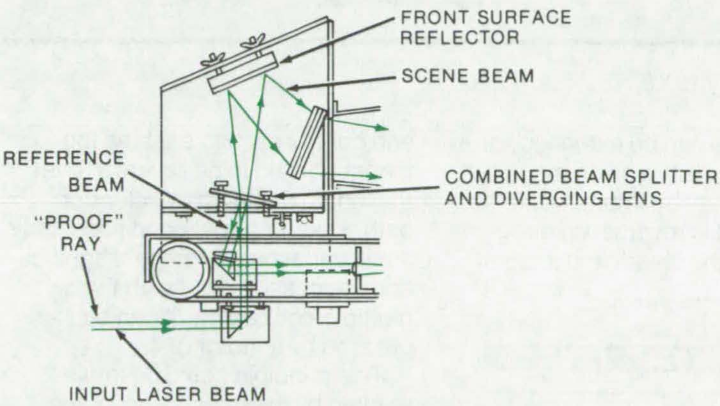

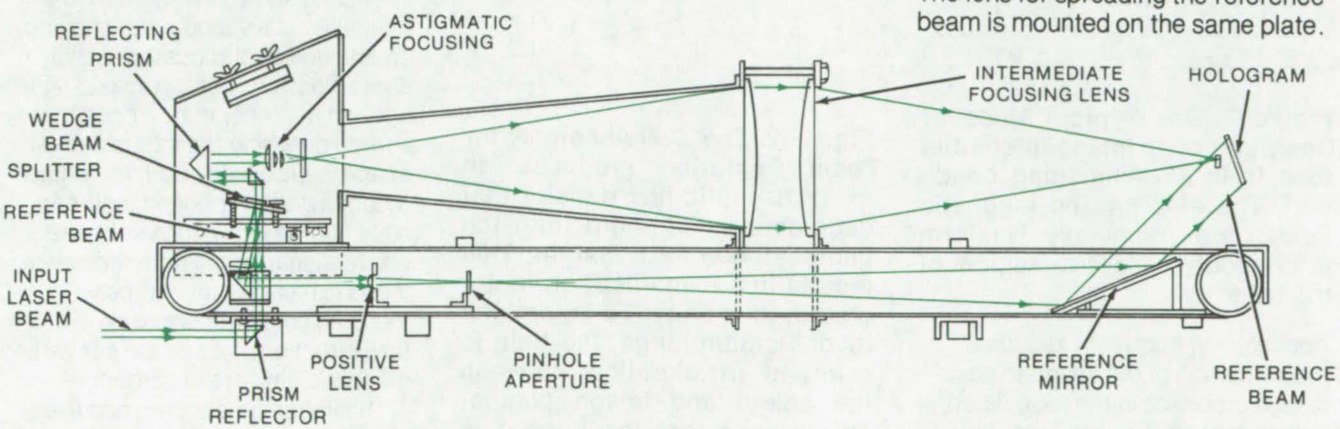

The **Dual-Purpose Holocamera** utilizes the same basic structure for a scattered-light and for a bright-field holography. The components that must be interchanged to convert the camera can be mounted on a sliding plate. This arrangement is an economical way of extending the capabilities and applications of a holography system.

(continued on next page)

The reference beam passes between the two tubular frames and hits the front surface mirror mounted on the far side of the frame. This mirror is mounted on a platform that is tilted to direct the reference beam onto the hologram at an angle of 45 degrees (relative to the axis of the focusing lenses).

The beam from the illuminating laser is deflected into the holocamera by a right-angle reflecting prism. Depending on the position of the sliding plate, the beam either illuminates the bright-field holographic arrangement or the dark-field scattered-light holographic arrangement. The reference path is the same for both the bright-field and scattered-light arrangements.

When configured as a scattered-light holocamera, light from a pulsed ruby laser illuminator is deflected into the holocamera by the prism reflector mounted below the tubular framework. The light is deflected vertically onto a glass-wedge beam splitter which divides it into scene- and reference-beam components. The reference beam is the small portion reflected from the first surface of the wedge. The scene-beam component is the principal amount of light transmitted through the wedge. The intermediate focusing lenses are used to refocus the light just before the hologram.

When in the bright-field arrangement, the portion of the beam passing through the lens hits the front surface mirror mounted at the top of the aluminum enclosure. This reflects the light onto the prism plate, which directs the beam through the focusing lens set onto the hologram photographic plate. This holocamera arrangement is basically a "path-matched" focused ground-glass holocamera.

This work was done by Lee O. Heflinger and Ralph F. Wuerker of TRW, Inc. for **Lewis Research Center.** *Further information may be found in NASA CR-121264 [N74-18152], "Application of Holography to Flow Visualization within Rotating Compressor Blade Row," a copy of which may be obtained at cost from the New England Research Application Center [see page A7].*
LEW-12166

Magnifying Image Intensifier

Multiple-coil design allows variations in image-magnification factor.

Goddard Space Flight Center, Greenbelt, Maryland

A typical mode of operation of magnetically-focused image-intensifier tubes is the nominally 1:1 imaging condition (unit magnification), as illustrated in Figure 1.

Figure 1. The **Typical Mode of Operation** of an image-intensifier tube is in a 1:1 imaging condition. The electric and magnetic fields are nominally uniform throughout the active region of the tube.

Applications frequently require magnification of the image to ease design problems in the associated optical system. For instance, the tube may be required to zoom the image (have the electronic capability of varying the magnification factor).

The magnification range of the intensifier tube can be extended, or the performance at a given magnification value may be improved, if the magnetic field is reversed in direction between the object and image planes (see Figure 2). A multiple-coil design of the field-generation and control section enables the magnetic field to be reversed over the length of the image-electron path. Under normal conditions, only small variations in image magnification are possible; but with the multiple-coil design, it can be increased by a factor of 4.

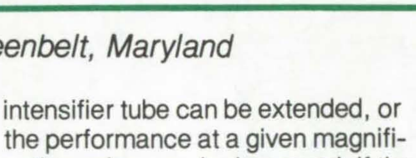

Figure 2. The **Coil Assembly for Zoom Operation** produces an axial magnetic-flux density that decreases in strength from the photocathode to the target. This results in a magnification factor greater than unity. To extend the magnification range, the field is reversed in direction between the object and image planes. This means that the current in coil 3 flows in the opposite direction to the current in coil 1.

This principle could be implemented by the magnifying image intensifier shown in Figure 3. The intensifier is a vacuum tube having, on one end, a photocathode that emits electrons in response to light and, on the other end, a phosphor screen on which the intensified image is produced. Both the photocathode and the phosphor screen have fiber-optic windows. Unlike conventional intensifiers, however, this one has several magnetic-focusing coils with opposing current-flow directions that cause a reversed magnetic field at the screen.

The image tube shown has five focusing coils (forming a multiple-current conducting-coil system) mounted coaxially. The coil current sets up a strong axial magnetic field

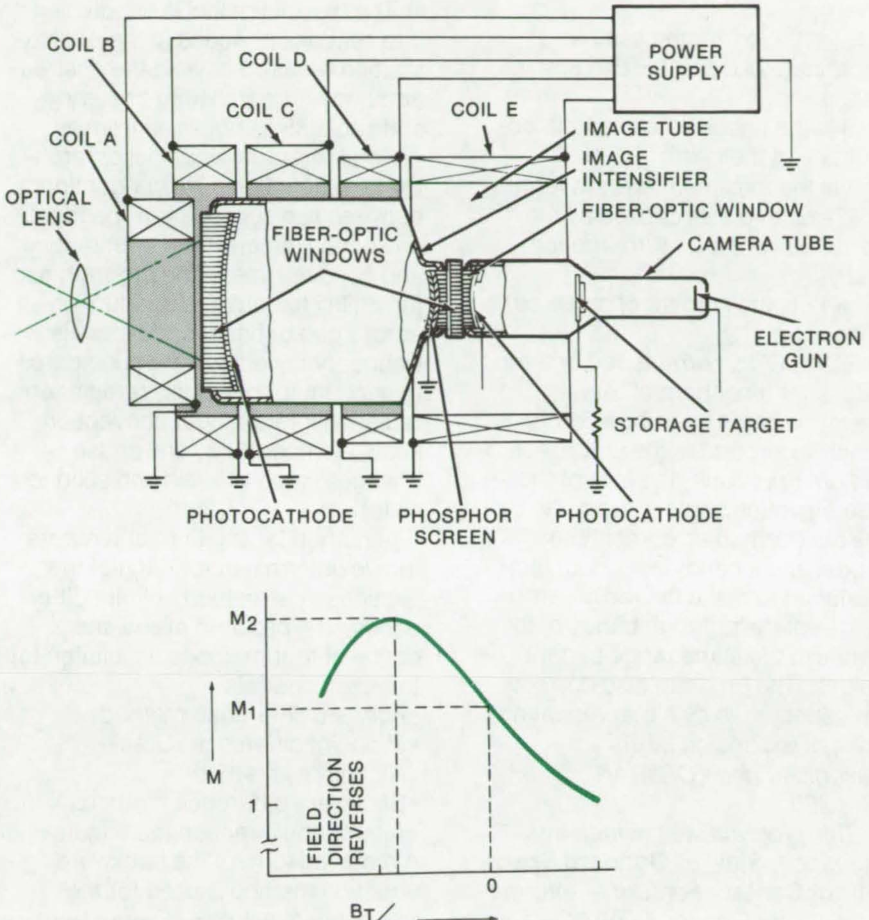

Figure 3. The **Magnifying Image Intensifier** receives light radiation from the scene being viewed, through an optical lens. The light is imaged on a fiber-optic window and is transferred to the photocathode, where photoelectrons are released in direct proportion to the light intensity at each point of the image. The electron beam is then electrostatically accelerated onto the phosphor screen to give an intensified light image. The output of the image intensifier is coupled to a camera tube with an input fiber-optic window.

(a magnetic lens) that focuses the electrons from the photocathode onto the phosphor screen. Current through coils A and B (about the photocathode) is in the direction opposite to that through coils C, D, and E (about the screen). The resulting focusing field has lines of force symmetrical about the longitudinal axis of the electron beam and has an axial magnetic-field component that reverses direction between the photocathode and phosphor screen. The intensifier tube can be used in electron microscopy, ion-field microscopy, for the conversion of infrared and ultraviolet images to visible light, and for X-ray and gamma-ray imaging systems.

In an alternate version of the intensifier (actually implemented) the camera tube has a secondary electron conduction (SEC) target and an intensifier section built into the same envelope. In this tube, no fiber optics are employed; the phosphor-target combination shown is replaced by a SEC target.

This work was done by J. Vine of Westinghouse Electric Corp. for **Goddard Space Flight Center.** *For further information, Circle on the TSP Request Card.*

This invention is owned by NASA, and a patent application has been filed. Inquiries concerning nonexclusive or exclusive license for its commercial development should be addressed to the Patent Counsel, Goddard Space Flight Center [see page A8]. Refer to GSC-12010.

Computer Programs

These programs may be obtained at very reasonable cost from COSMIC, a facility sponsored by NASA to make new programs available to the public. For information on program price, size, and availability, circle the reference letter on the COSMIC Request Card in this issue.

Development Ephemeris Number 96

The fourth official release from the JPL Ephemeris Tape System

Improvements in Development Ephemeris Number 96 include more recent and more accurate observational data, new types of data, better processing of the data, and refined equations of motions that more accurately describe the physics of the solar system.

The JPL Ephemerides are produced through the following steps: Observational data are collected and compared against a base ephemeris; partial derivatives are computed and used in a differential least-squares program to improve the values of the initial conditions of the planets at a given epoch, along with other associated parameters; the differential equations of motion, using the new initial conditions, are numerically integrated, thus producing the new ephemeris; and as a final check, the observational data are compared against the new ephemeris.

The program tape contains two files: File 1 contains all software necessary to create a binary file and perform ephemeris calculations on that file; file 2 of the distributed tape contains the encoded ephemeris data. These data are

(continued on next page)

essentially a blocked listing of a complete dump of the original JPL binary tape, with double-precision data modified to a special form. BCDEPH, the first program on file 1, is the routine that reads file 2 and writes the binary file. This new format is more than four times as compact as the previous "TYPE 50" format. Furthermore, the interpolation error is below 10 cm for all bodies.

This program was written by Michael S. W. Keesey, Xx Newhall, and E. Myles Standish, Jr., of **Caltech/JPL.** *For further information, Circle D on the COSMIC Request Card.*
NPO-14002

Multispectral-Scanner Image Processing

QUIKLOOK provides an approximate but fast enhancement of image data.

The QUIKLOOK program was developed to perform approximate geometric and radiometric corrections of Landsat MSS digital data. The methods of correction used allow fast computation and produce a fairly accurate picture of the Landsat scene.

QUIKLOOK calculates an Earth-rotation (skew) correction from the format center latitude as given by the annotation record of the Landsat bulk computer-compatible tapes. The program then offsets each image line in the output image by an amount given by:

$$O = L \cdot \mathrm{Tan}(a) \cdot A$$

where, O is the amount of offset in 57-meter pixels;
L is the output image line number;
a is the calculated skew angle; and
A is the aspect ratio of the output image.

The mirror velocity profile error is modeled as a trigonometric function and is corrected according to the formula:

$$S_a = S_i - A \sin(2\pi S_i/\mathrm{NPIX})$$

where,
S_a is the corrected sample coordinate of a point within any image line;
S_i is the uncorrected sample coordinate of the point;
A is the maximum error in terms of 57-meter pixels caused by the nonlinearity of the mirror motion; and
NPIX is the number of pixels per image line.

QUIKLOOK corrects radiometric values for a nonnormal Sun-elevation angle by using a formula which incorporates the uncorrected radiometric value, the sine of the Sun-elevation angle value given by the bulk computer-compatible tapes, and a band-dependent factor designed to make the radiometric values of the different bands of the data use the same range of data values. The program also corrects for aspect ratio by either repeating lines or expanding pixels.

Assembler and FORTRAN
IBM 360

This program was written by Maurice I. Stein of **Goddard Space Flight Center.** *For further information, Circle E on the COSMIC Request Card.*
GSC-12135

Multidimensional Heat Conduction

Program developed for design and analysis of Thermal Protective System (TPS) of Space Shuttle

A new program that computes the transient temperature history or the steady-state solution for complex body geometries in three dimensions should be useful for many other types of three-dimensional thermal analysis. The input consists of the geometry of the physical system, its material properties, and the boundary conditions. The program will accommodate a thermal model consisting of a maximum 500 nodes, 4,000 conductors, 3,600 radiation interchange conductors, and 75 each of several types of boundary conditions.

The thermal model is subdivided into sections or nodes to the approximation required to yield the desired accuracy. The transient or steady-state solution is obtained from a general three-dimensional differential heat equation. The conduction between two sections is dependent on section dimensions, orientations, and conductivities. The program has the ability to compute conduction across gap or honeycomb panels. Boundary conditions are considered to account for heat flux, reradiation, radiation interchange, convection, known temperature, and phase changes (solid to liquid and solid to solid).

A numerical solution for temperature is determined for each of the sections by a method of finite differences. The program allows the option of four methods of solution for transient analysis:

- Forward difference method
- Midpoint difference (Crank-Nicholson) method
- Backward difference method
- Alternating direction technique

A modified form of the backward direction method is used for the steady-state solution. Output from the program is a temperature-versus-time history for each section.

IBM FORTRAN, OS Assembler
IBM 370
Central Memory Requirement
Approximately 450K 8-Bit Bytes

This program was written by Theodore C. Connors, Jr., and Lloyd W. Fesler of Rockwell International Corp. for **Johnson Space Center.** *For further information, Circle F on the COSMIC Request Card.*
MSC-16159

Geodetic Control Net

A control net is computed from topographic features.

The Mariner flyby missions required a computer program to compute a control net of the planet Mars from measurements of topographical features identified on the Mariner television pictures. The program developed solved successfully for the areocentric coordinates (lati-

tudes and longitudes) of 115 surface points and the orthogonal camera matrices of 57 far- and near-encounter pictures.

In the program, the conjugate gradient method is employed to solve large sparse matrices. The program computes X and Y coordinates of array elements and their residuals. Then the observation equations are accumulated, and the normal matrix is computed as well as the right-hand-side solution vector. Next the solution to the normal matrix is computed. The method has been used for solving linear systems, where many of the matrix coefficients are zero, arising from a finite difference approximation to Laplace's equation.

There are several variants of the method which arise because of the algebraic relationships among the quantities involved. The program documentation discusses the results of using the conjugate gradient method on a large system of linear equations obtained from a least-squares fit so that the matrix array is positive definite; however, the program is also applicable to semidefinite systems.

This program operates in batch mode, is written in FORTRAN, and has been implemented on the IBM 360/65. Core requirements depend on the number of unknowns, ranging from 120K bytes for 300 unknowns to 1,416K bytes for 6,000 unknowns.

This program was written by Merton E. Davies of the Rand Corp. for **Caltech/JPL** *For further information, Circle G on the COSMIC Request Card.*
NPO-13718

Analysis of Laser Heterodyne Communications

An optical analysis program predicts effects of aberrations.

A new computer program (LACOMA) predicts the effects of optical aberrations on transmitters and receivers used in heterodyne communication systems. LACOMA (Laser Communicator Analysis Program) represents a major advance in the optical analysis of laser heterodyne communication systems and also in general optical-systems analysis, since it includes the effects of gaussian pupil functions. A major difference between LACOMA and other programs in this field is that LACOMA utilizes an algorithm that permits specification of the number and the location of the output points for the computed spread function results. For a given optical system or telescope, the program allows sampling of the Airy disk via grid sizes from 2 by 2 to 101 by 101. The program allows the optional analysis of transmitter or receiver optics. For the transmitter, the program starts with the data for the specified laser beam and propagates the beam through the optical train to determine the far-field intensity function. For the receiver, the program carries the received signal beam through the optical train to the detector. The local oscillator laser beam is also traced to the detector where the two beams are combined, and the various quality criteria are computed. Paraxial analysis, ray trace-optical path difference analysis, amplitude and point spread function analysis, receiver quality criteria analysis, and transmitter quality criteria analysis are performed by the program.

Some optical system parameters and/or configurations which can be accommodated by LACOMA are:

- Catoptric systems
- Catadioptric systems
- Dioptric systems
- Spherical surfaces
- Aspheres
- Cylindrical surfaces
- Toroidal surfaces
- Surfaces with slight cylindrical error or warpage
- Periodic surface errors
- Misalined (tilted, and/or decentered) systems
- Composite vignetting and obscuration
- Afocal systems (via perfect imaging lens)

Any of the analyses can be performed for any of the system parameters or configurations.

LACOMA has been shown to be a useful tool for the analysis of heterodyne communication systems. It has been used for the tolerance analysis of a selected system designed for space communications and for the evaluation of several other systems.

FORTRAN IV
IBM 360/91, IBM 360/95
Requires approximately 350K bytes core storage

This program was written by Steven Cohen of **Goddard Space Flight Center** *and S. H. Brewer and T. A. Nussmeier of Hughes Research Lab. For further information, Circle H on the COSMIC Request Card.*
GSC-12098

Active Optics Simulation System

AOSS: aids design of the mirror control system for large telescopes.

The Active Optics Simulation System (AOSS) is a set of computer programs that simulate the behavior of an entire mirror-surface control system, as well as the behavior of the component subsystems. It can be used to evaluate the merit of a particular active optics control system (or a component subsystem); and once the system configuration is chosen, it can be used as a design aid to optimize the system parameters. AOSS is a valuable tool for determining factors such as the number of required actuators, placement of actuators, and the mirror-surface improvement gained from additional actuators.

AOSS consists of three major computer program packages: the Auxiliary Program, the NASTRAN Structural Analysis Program, and the Active Optics Simulation Program (AOSP). The Auxiliary Program accepts as input an active optics structural model expressed in terms of engineering parameters meaningful to the designer and generates a complete NASTRAN Input Deck which consists of the Executive Control Deck, Case Control Deck, and Bulk Data Deck.

(continued on next page)

NASTRAN performs structural analysis on the following components of the optics system:

- Mirror
- Backing Plate
- Actuators
- Mirror Mounts
- System Reaction Support

In the structural modeling, a lumped element approach is followed. The distributed structural properties of the system are represented by a finite number of idealized elastic elements, which are connected by a finite number of grid points. The boundary conditions are formulated by constraining appropriate degrees of freedom at the boundary grid points. Multipoint constraints are used to describe linear algebraic relations between two or more degrees of freedom where necessary. The main purpose of the structural modeling is to obtain eigenvectors (mode shapes) for use in the control-system equations of the Active Optics Simulator Program by performing a real eigenvalue analysis (normal-mode vibration analysis). In addition, the flexibility matrix of the system is obtained to model the displacement actuators and to calculate static response to thermal, inertial, and mechanical loading.

NASTRAN output in card form is used as input to the AOS Program, which consists of six modules to simulate the entire mirror-surface control system. The Interpolation Module is a curvilinear bicubic spline-fit program compatible with the polar coordinate system as required by the circular geometry of the mirror structure. The Control Law Module simulates the modal control law using the technique of Creedon and Lindgren. The Actuator Module includes the effects of backlash, dead zone, saturation of the electronics, and electronic time constants to simulate the force actuator. The Mirror Module computes the mode amplitude of the mirror surface error. The Disturbance Module simulates the mechanical-force disturbance over the entire region of the mirror or over one portion of the mirror surface. The fourth order Runge-Kutta method is used for the transient analysis of AOSP.

The distribution program package contains the Auxiliary and Active Optics Simulation Programs; it does not include the NASTRAN Structural Analysis Program.

FORTRAN/Interactive Mode
CDC CYBER 70

This program was written by The Perkin-Elmer Corp. for **Langley Research Center.** *For further information, Circle J on the COSMIC Request Card.*
LAR-12104

Digital Image-Rectification System

DIRS removes spatial distortions from remote-sensing data.

DIRS is a digital image-rectification system for the geometric correction of Landsat Multispectral Scanner (MSS) digital image data. DIRS removes spatial distortions from the data and brings it into conformance with the Universal Transverse Mercator (UTM) map projection. DIRS can produce digital-output products suitable for further machine processing and analysis and should fill the need for geometrically corrected Landsat Multispectral Scanner digital data in a number of remote sensing application areas.

Distortions exist in the multispectral scanner digital image data due to the combined effects of sensor operation, orbit and attitude anomalies, Earth rotation, and atmospheric and terrain effects. DIRS attempts to make corrections for all of these distortions except atmospheric- and terrain-induced distortions. Scene data in the form of ground control points (GCP) are used to derive the geometric correction algorithms. Ground control points are features or landmarks which are visible in the image and whose map coordinates can be determined. Manual and automatic techniques for determining ground control points are provided in DIRS. The manual method involves the use of a high-speed line printer in the generation of shade prints of the ground control point area with an image coordinate border. The automatic method of determining ground control points is accomplished by means of an edge correlation technique.

The developed ground control point data is used to define functions which make transformations between map and image spaces. Affine transformation and two-dimensional least-squares techniques for geometric mapping are provided. The affine transformation is one which maps a triangle from one two-dimensional space into a triangle in a second two-dimensional space. In the two-dimensional least-squares method four coordinate dependent functions are computed using a least-squares fit to the ground control points. Entire scenes or selected quadrilaterals may be rectified. Resampling through nearest neighbor or cubic convolution at user designated intervals is available. The output products are in the form of digital tapes in band interleaved, single band, or computer compatible tape (CCT) format in rotated Universal Transverse Mercator projections. These tapes can be used for further machine manipulation and analysis of the image data.

DIRS was designed for implementation on large scale IBM 360 computers with at least 300K to 500K bytes of memory for user application programs and five nine-track tape drives plus direct access storage. DIRS provides adequate flexibility to the user to trade off ground control point location effort for final result accuracy. Thus the user can achieve the level of accuracy required at the lowest cost.

This work was done by Peter H. Van Wie, Maurice Stein, Edward Puccinelli, and Barbara Fields of **Goddard Space Flight Center.** *For further information, Circle K on the COSMIC Request Card.*
GSC-12156

Materials

Extracting Lignins From Mill Wastes

Lignins, byproducts from pulp and paper mills, can be removed from waste water more economically using quaternary ammonium compounds.

Caltech/JPL, Pasadena, California

Lignins are highly colored components of wood, which are released as the wood is converted into pulp. In most processes, the lignins are discharged with the waste water because of the considerable expense of removing them. Although they have no known toxic effects, the lignins and their degradation products add an unesthetic color to the waste water. These highly colored materials prevent light penetration and photosynthesis in bodies of water where they are discharged. The problem is appreciable because over 1.9 trillion gallons of water are discharged into waterways by the pulp and paper industry each year.

A new process that has been studied on the laboratory scale may be able to remove and purify lignins economically enough to encourage adoption throughout the industry. Quaternary ammonium compounds are used to precipitate out the lignins from the waste water. Methanol is used to recover the quaternary ammonium compounds. Compared to a lime-precipitation process currently used, this method may economically recover lignins and clean up an objectional waste water problem (Figure 2).

The process, as described in Figure 1, has been tested with the chlorine wash from a sulfite pulp mill and with the caustic wash from a Kraft process pulp mill. The process was found to be successful with both acid and base washes, and both the methanol and the ammonium compounds can be recycled. In many cases the methanol can be obtained as a byproduct of the primary mill process, and the lignins themselves can be recovered for sale as such or as chemical raw materials.

This work was done by Marshall F. Humphrey of **Caltech/JPL.** *For further information, Circle 46 on the TSP Request Card.*

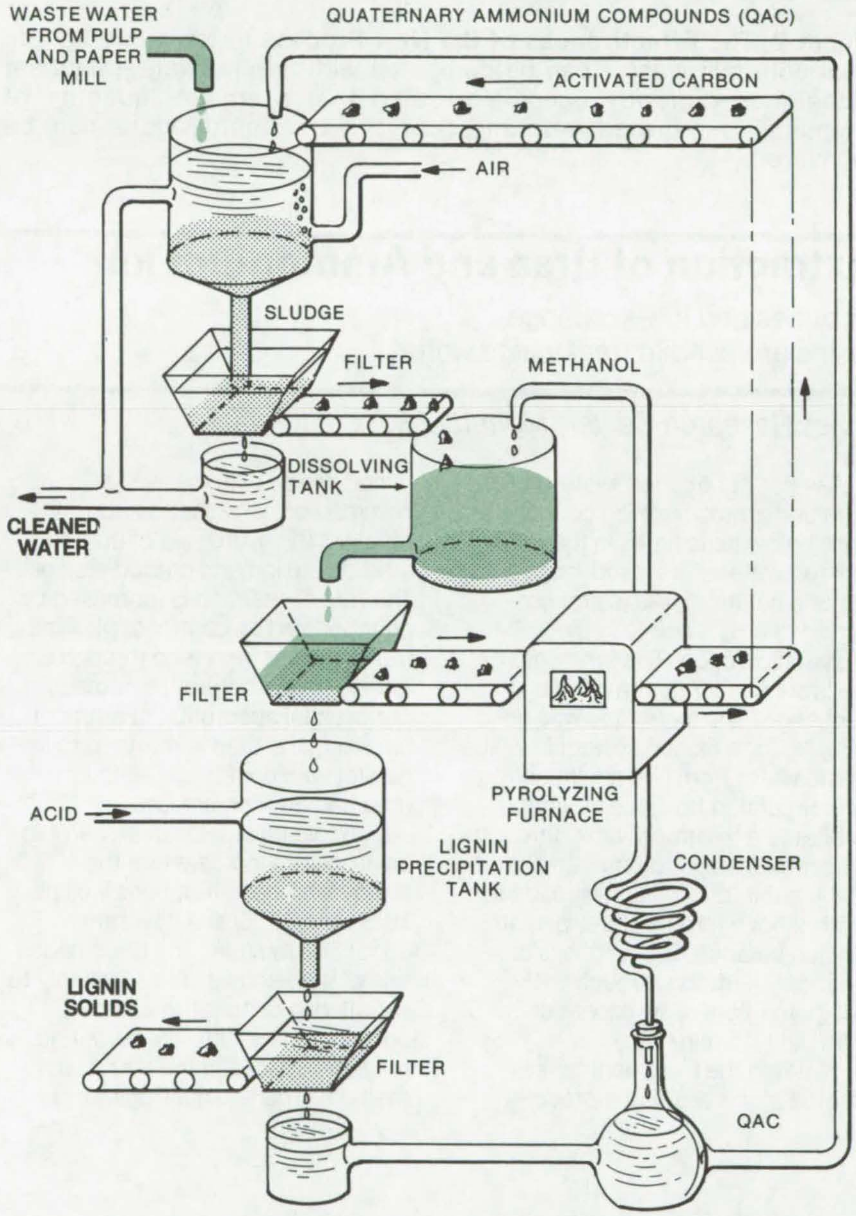

Figure 1. **Lignins Are Removed From Pulp and Paper Mill Wastes** by adding a quaternary ammonium compound (QAC) and activated charcoal, produced from the process, to a settling tank containing mill wastes. A sludge precipitated in the bottom of the tank contains the lignins, and the remaining clean water may be recycled or discharged. The sludge is then dissolved by methanol to form a slurry that is filtered and pyrolyzed to form reusable activated carbon. The liquid from the slurry is treated with a mineral acid that precipitates the lignins out of the methanol. The remaining material is separated into methanol and QAC for reuse.

(continued on next page)

TREATMENT METHOD	APPROXIMATE DOSAGE (pounds/1,000 gallons)	PERCENT LIGNINS AND COLORS REMOVED
Lime Treatment	12.5	70
Lime + Carbon	6.5	90
Bio-oxidation + Carbon	10.5	92
Carbon Alone	42 to 168	95+
Quaternary Ammonium Compounds	3	100

Figure 2. The **Effectiveness of the New Process** in removing lignins from pulp mill wastes can be compared with several water-treatment techniques currently used. Note also that a smaller quantity of chemical is required, and most of the treatment agent can be recovered.

This invention is owned by NASA, and a patent application has been filed. Inquiries concerning nonexclusive or exclusive license for its commercial development should be addressed to the Patent Counsel, NASA Resident Legal Office-JPL [see page A8]. Refer to NPO-13847.

Extraction of Urea and Ammonium Ion

Enzymes and ion-exchange resins are used to treat waste water.

Ames Research Center, Moffett Field, California

A water purification system keeps urea and ammonium ion concentrations below toxic limits in the recirculated water of a closed-loop aquatic habitat. Urea is first converted to NH_4^+ and CO_2 by enzymatic action. The ammonium ion is subsequently removed by ion exchange. The technique was developed for a closed system in which waste water from two adult bullfrogs is recirculated from the aquatic habitat to a treatment tank, through an ion-exchange column, and back to the habitat. Provision is made for control flow, temperature, pH, and oxygen balance. Bioburden is controlled by filtration through 0.45μ Millipore filters or by ozonation for 5 min/gal (1.5 min/liter).

Water in the treatment tank is treated at the onset of a predetermined period with urease, a common enzyme that is known to catalyze the hydrolysis of urea to ammonium ion and carbon dioxide. The rate of reaction is increased by agitation and by control of pH. The treated water is passed through an ion-exchange column, selected for preferential absorption of ammonium ions, and then is returned to the habitat with nontoxic quantities of urea and ammonium ion.

The results of tests in an aerobic environment indicate that the removal process functions well at 16.5° and 25° C at a flow rate of about 360 ml/min. The decomposition of urea shows little sensitivity to variation in concentrations of potassium, sodium, calcium, and magnesium ions in the aqueous medium. The two bullfrogs were maintained for 30 days in recirculated water containing all their dissolved wastes. During this period, the urea and ammonium levels never reached toxic limits, and the presence of urease in the recirculated water had no apparent effect on the physical well-being of the test animals.

This work was done by Robert T. Anselmi, Richard R. Husted, and Jon R. Schulz of Martin Marietta Corp. for **Ames Research Center.** *Further information may be found in NASA CR-137596 [N75-13537], "Urea/Ammonium Ion Removal System for the Orbiting Frog Otolith Experiment," a copy of which may be obtained at cost from the Western Research Application Center, University of Southern California [see page A7]. ARC-11064*

Less-Costly Activated Carbon for Sewage Treatment

Coal and sewage sludge economically converted to activated carbon.

Caltech/JPL, Pasadena, California

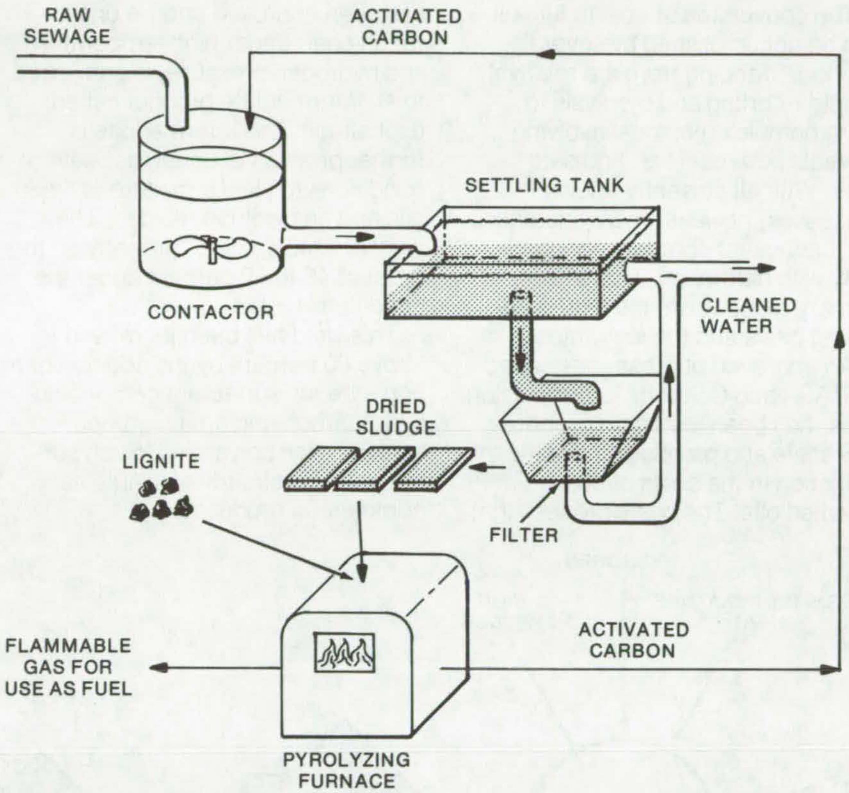

The **Lignite-Aided Sewage Treatment** is based on the adsorption of dissolved pollutants by activated carbon. After settling, the sludge is removed and dried into cakes that are pyrolyzed with lignite to yield activated carbon. The lignite is less expensive than the activated carbon that was previously used to supplement the pyrolysis yield.

One method of treating wastes containing dissolved and suspended organic and inorganic materials, such as sewage, is to mix the waste with activated carbon. The mixture is placed in a settling tank where the dissolved pollutants are adsorbed by the activated carbon, and the carbon and suspended matter, called sludge, collect on the bottom of the tank. A major expense in this process is the activated carbon that must be added continuously.

At some plants costs are reduced by collecting the sludge and converting it to activated carbon. However, it is not possible to produce enough carbon to make the process self-sustaining, and additional activated carbon must be added to make up the deficiency. In a new process, the supplemental carbon is derived from a coal, such as lignite, which costs less than 2 cents a pound delivered, compared to around 25-30 cents a pound for the activated carbon. The coal is pyrolyzed along with the sludge, which acts as a catalyst in the activation process. In addition, pyrolysis of the coal produces flammable gases that can provide part of the energy needed for the process.

Laboratory-scale studies have indicated the feasibility of the method. Coal was pulverized to -40 mesh and mixed with an equal amount of sludge; the pyrolysis and activation conditions were 850° C with steam applied for 20 minutes with about 1 pound of steam per pound of coal/sludge mixture. The resulting activated carbon was 61.7 percent ash and had an iodine adsorption of 684 mg/g of carbon. After a raw sewage sludge sample with a COD (chemical oxygen demand) of 421 was treated with 521 mg/l of the activated carbon, its COD was reduced to 59. (Treatment of the sludge with a commercial activated carbon gave a COD of 60.)

Further tests with bituminous and sub-bituminous coals showed that lignite was the most effective type, although it is also the least expensive. Sodium carbonate can be added to the process to further enhance the activation.

This work was done by John D. Ingham, John J. Kalvinskas, and William A. Mueller of **Caltech/JPL.** *For further information, Circle 47 on the TSP Request Card.*

Title to this invention has been waived under the provisions of the National Aeronautics and Space Act [42 U.S.C. 2457(f)], to the California Institute of Technology, Pasadena, California 91109.
NPO-13877

Surfactant-Assisted Coal Liquefaction

Nonaqueous surfactants increase yields from about 50 to about 80 percent and improve product distribution.

Caltech/JPL, Pasadena, California

The conversion of coal to fuel oil can be accomplished by several methods, ranging from the relatively simple retorting and pyrolysis to more complex methods involving solvents bed reactors, and catalysts. With all currently-known processes, however, coal liquefaction cannot yet compete economically with natural oil. Two of the primary reasons are the high processing costs and the low yields.

An improved process, developed by NASA and Caltech/Jet Propulsion Labs, has been tested on a laboratory scale and promises a significant reduction in the costs of coal-liquefied oils. The basic process that has been improved upon is one in which coal, under high temperature and hydrogen pressure, is converted to an intermediate product called asphaltene. The intermediate is further processed under less severe conditions to yield a mixture of liquid oils and an insolube residue. The yield of usable oils is currently on the order of 40 to 50 percent under the conditions tested.

This yield has been increased to above 80 percent by the addition of a nonaqueous surfactant comprising hydrocarbon and amine groups, such as alkyl polyamine. Such surfactants are already available as commercial products.

The role of the surfactant can be understood from the process descriptions in Figures 1 and 2. Although the exact molecular mechanisms involved have not been proven, it appears that the surfactant prevents the asphaltene molecules from clumping together to form colloidal particles. The separated molecules present more surface area for the addition of hydrogen atoms during the hydrogenation reaction and are also less likely to polymerize to form an insoluble residue.

Economically, this proposed process could lead to reductions in both capital and operating costs by

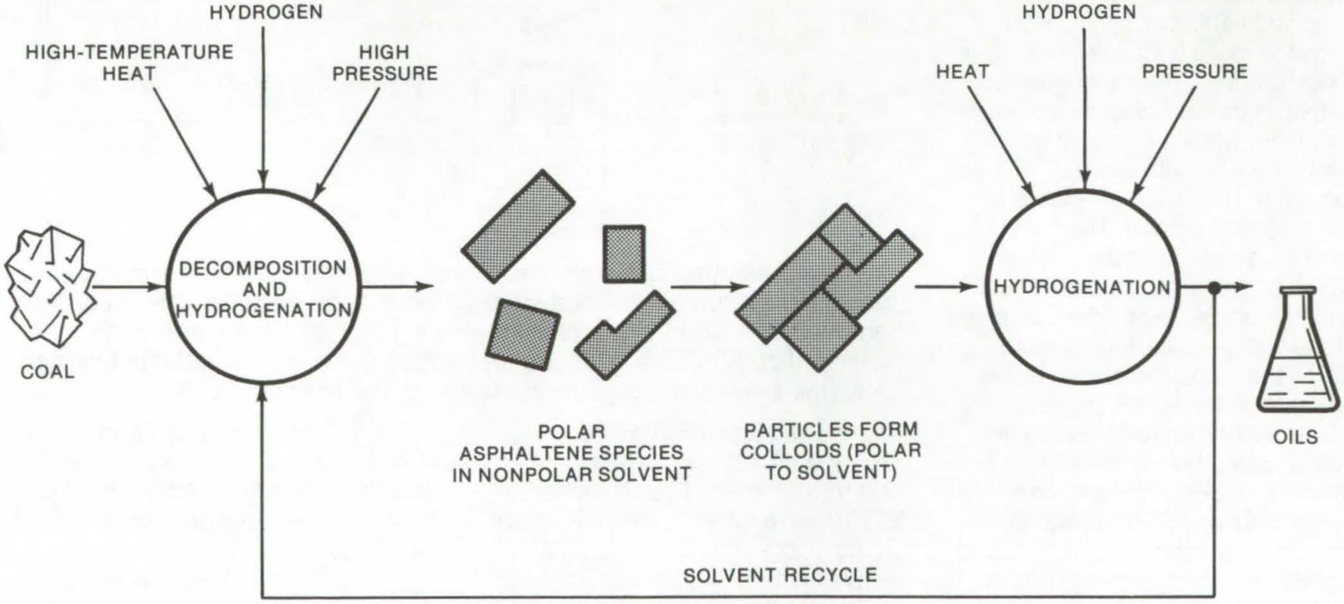

Figure 1. **Coal-to-Oil Conversion** is accomplished by first dissolving the coal in a solvent and decomposing it under high temperature and pressure. Hydrogenation produces an intermediate product, asphaltene, which because of its polar nature tends to aggregate and form colloidal particles. The asphaltene is further hydrogenated to produce a mixture of oils and an insoluble residue.

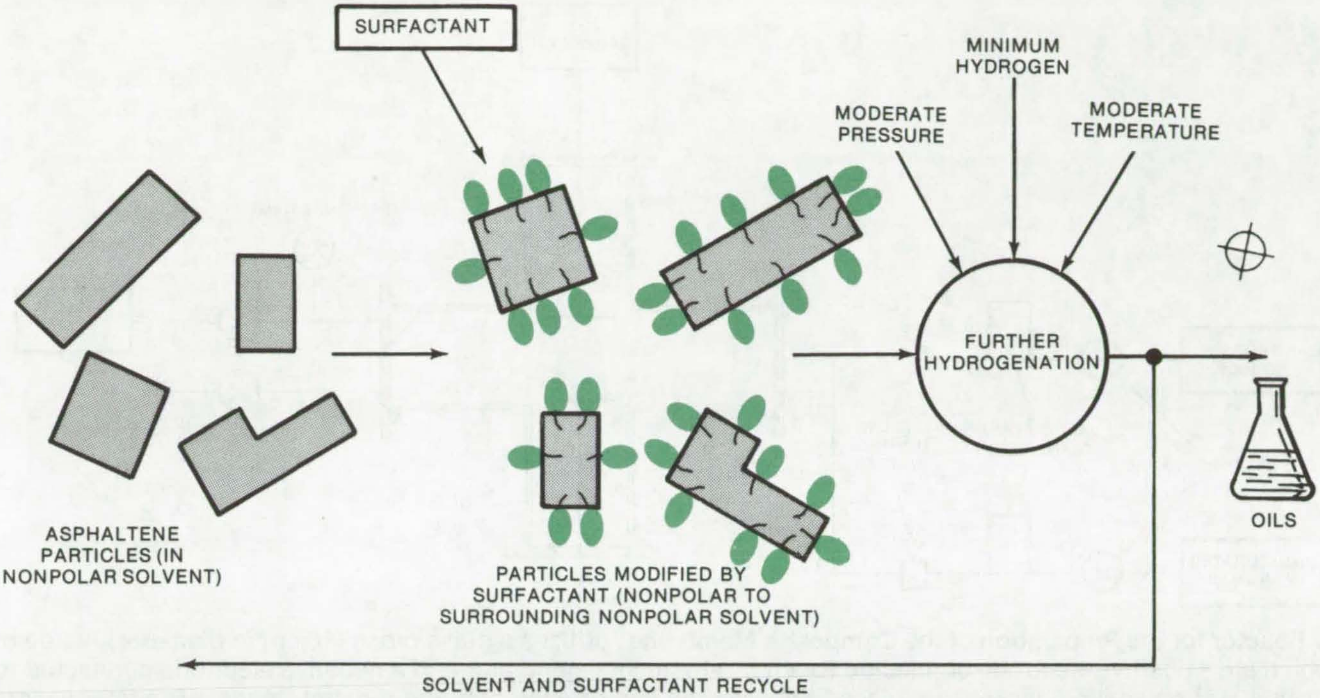

Figure 2. **Conversion Using a Surfactant** appears to prevent the asphaltene molecules from forming colloids. The polar groups on the surfactant probably attach to the polar asphaltene groups, producing a species that appears nonpolar to the solvent. The resulting improved solubility and greater exposed surface area allow less severe processing conditions and result in an improved yield.

increasing throughput, reducing hydrogen consumption, and lowering temperature and pressure requirements. For instance, a rough preliminary analysis indicates that the cost of coal-liquefied oil produced by this method could be reduced from about $20 a barrel to around $13 a barrel. It will, of course, be possible to predict economic benefits more accurately after further study and analysis.

This work was done by George C. Hsu of **Caltech/JPL.** *For further information, Circle 48 on the TSP Request Card.*

Title to this invention has been waived under the provisions of the National Aeronautics and Space Act [42 U.S.C. 2457(f)], to the California Institute of Technology, Pasadena, California 91109.
NPO-13904

Membrane Has High Urea-Rejection Properties

A reverse-osmosis membrane can be used for water purification.

Ames Research Center, Moffett Field, California

A new membrane, made by plasma polymerization of ethylene and nitrogen, is particularly useful in the recovery of potable water from urine without requiring several stages of filtration. Conventional membranes produced in an RF plasma or by casting or dip-coating methods have low urea-rejection properties (less than 25 percent) whereas the new membrane has a urea-rejection ratio better than 80 percent.

The membranes are synthesized from ethylene and nitrogen in an RF plasma (13.56 MHz) at low power (15 W), low gas-flow rates (1 to 2 cm^3 STP/min ethylene and 1 to 2 cm^3 STP/min nitrogen), and low pressure (0.2 torr ethylene and 0.1 or 0.2 torr nitrogen). The membranes are deposited on an asymmetric microporous substrate (250-Å average-pore size). The synthesized membrane is a polymer that contains nitrogen in several oxidation states (as shown by infrared spectroscopy).

Ethylene and nitrogen are used (rather than a liquid monomer containing nitrogen) because the flow rate and partial pressure of each gas can be independently controlled to produce the optimum conditions for synthesizing the membrane. Slow flow rates (1 to 2 cm^3 STP/min) increase the residence time of the gases in the plasma, which in turn produces a tighter, more highly cross-linked membrane. This is a necessary characteristic for a high urea-rejection property.

The most critical parameter in the membrane preparation is the power. When the membranes are deposited

(continued on next page)

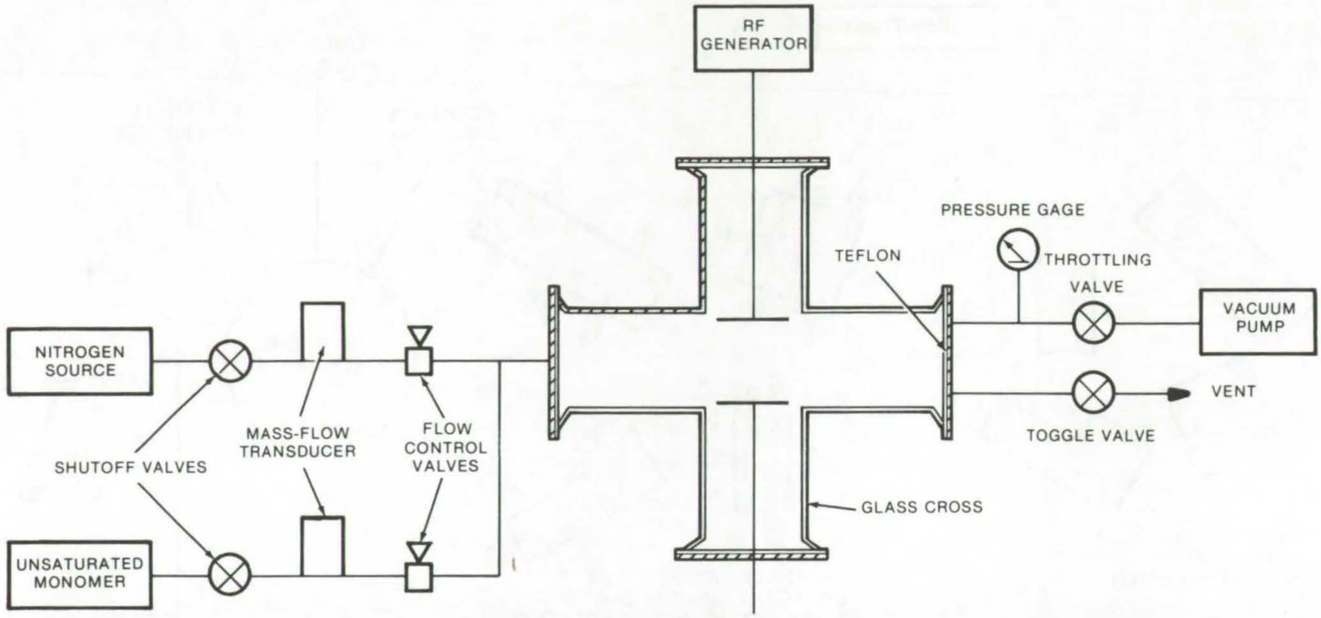

A **Reactor for the Preparation of the Composite Membrane** utilizes a glass cross (10 cm in diameter) inside of which are a positive electrode connected to a radio-frequency generator and a negative electrode connected to ground. Teflon sealing gaskets are placed between the end of each arm and a metal flange. Monomer vapors are admitted into the reactor through shutoff valves and are controlled by mass transducers and flow-control valves. A throttling valve controls the reactor pressure and the residence times of the gases in the plasma. The electrodes are copper disks 9 cm in outer diameter.

for 600 seconds, at 0.2 torr each of ethylene and of nitrogen, a discharge cannot be maintained at less than 15 watts. However, membranes with the highest urea-rejection are formed at 15-watt minimum power level. Various reactor designs can be utilized; one is shown in the illustration.

The membrane can be used for the recycling and purification of water. It is also applicable to rejection of smaller (molecular weight less than 10,000) organic molecules in aqueous solutions when the molecules cannot be removed with commercially-available hyperfiltration membranes. Power used in the technique is relatively low.

This work was done by Catherine C. Johnson and Theodore Wydeven of **Ames Research Center.** *For further information, Circle 49 on the TSP Request Card.*

This invention is owned by NASA and a patent application has been filed. Inquiries concerning nonexclusive or exclusive license for its commercial development should be addressed to the Patent Counsel, Ames Research Center [see page A8]. Refer to ARC-10980.

Catalysts for Low-Energy Aldehyde Processes

Hydroformylation of olefins to yield aldehydes has been carried out at room temperature and pressure.

Caltech/JPL, Pasadena, California

Substantial savings in costs and energy could be realized through the further development of a new catalyst for the hydroformylation (addition of CO and H_2) of olefins to yield aldehydes. The catalyst is photochemically generated in situ by the reaction of a transistion-metal compound with a polymer.

One example of the new category of catalysts is that formed by the photochemical reaction of dicobalt octacarbonyl with polymeric support systems, such as poly 4- or 2-polyvinyl pyridine. The polymer can be used either in bulk form or preferably as particles with a high surface area. Ultraviolet light is required to initiate the reaction of the carbonyl with the polymer. The unreacted dicobalt octacarbonyl is then sublimed, and the polymer-bonded metal catalyst formed is used to convert olefins such as 1-pentene to aldehydes.

This work was done by Amitava Gupta and Alan Rembaum of **Caltech/JPL** *and Claude Frazier and Harry B. Gray of the California Institute of Technology. For further information, Circle 50 on the TSP Request Card.*

Title to this invention has been waived under the provisions of the National Aeronautics and Space Act [42 U.S.C. 2457(f)], to the California Institute of Technology, Pasadena, California 91109.
NPO-13827

Determining Eutectic Composition in Metal Alloys

An economical method of obtaining a eutectic composition from noneutectic ingots

Lewis Research Center, Cleveland, Ohio

In the preparation of an off-eutectic metal alloy, the eutectic constituents form an unknown eutectic composition. This unknown composition must ultimately be separated from the starting materials and analyzed to determine its true composition. A simple technique has been developed for obtaining eutectic material for chemical analysis in order to determine the composition of the eutectic constituent in an off-eutectic alloy. This technique is particularly useful for finding the eutectic composition of a new multicomponent alloy system in the absence of the alloy phase equilibria data. It has been demonstrated successfully on several multicomponent alloys.

A cast ingot of a trial melt, made while seeking the eutectic composition, is placed in a tube crucible. It is then positioned vertically in a furnace as shown in the figure. The bottom end of the crucible is located outside the furnace hot zone.

The sample bar is slowly heated under an inert atmosphere to prevent oxidation. As the temperature approaches the melting point, molten alloy of the eutectic composition characteristically bleeds from the surface of the sample. The bleedout runs to the bottom of the crucible where it accumulates in the space between the bar and the crucible wall. The accumulated melt is solidified at the bottom of the furnace by air or water cooling. When the top portion of the bar completely melts, the furnace power is turned off for solidification of the entire bar. After the specimen has cooled, the bleedout is stripped from the bar and chemically analyzed to determine eutectic composition.

This technique is effective and economical compared with the conventional zone melting technique or computational method. This technique does not require the starting material to be close to real eutectic composition. Indeed, eutectic material for analysis (1) has been obtained from ingots with as much as 60 percent pre-eutectic phase and (2) can be obtained in a single melting step. While the computational method is usually limited to three components, this new technique may be used for multicomponent systems.

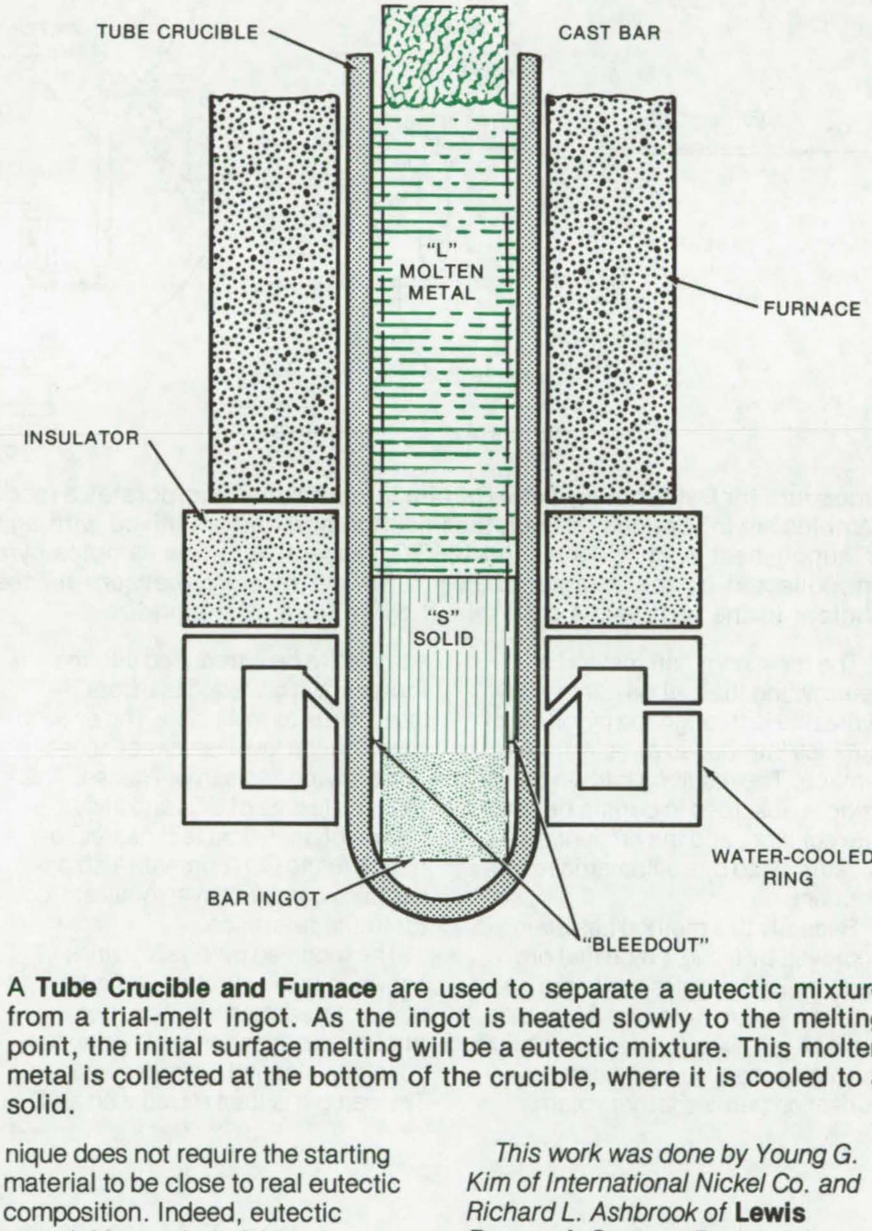

A Tube Crucible and Furnace are used to separate a eutectic mixture from a trial-melt ingot. As the ingot is heated slowly to the melting point, the initial surface melting will be a eutectic mixture. This molten metal is collected at the bottom of the crucible, where it is cooled to a solid.

This work was done by Young G. Kim of International Nickel Co. and Richard L. Ashbrook of **Lewis Research Center.** *Further information may be found in NASA TM-X-71765 [N75-29243], "Directionally Solidified Pseudo-Binary Eutectics of Ni-Cr-[Hf, Zr]," a copy of which may be obtained at cost from the New England Research Application Center [see page A7].*
LEW-12633

Determining Total Carbon in Hydrazine

A safer, more accurate, and
more flexible analytical procedure

John F. Kennedy Space Center, Florida

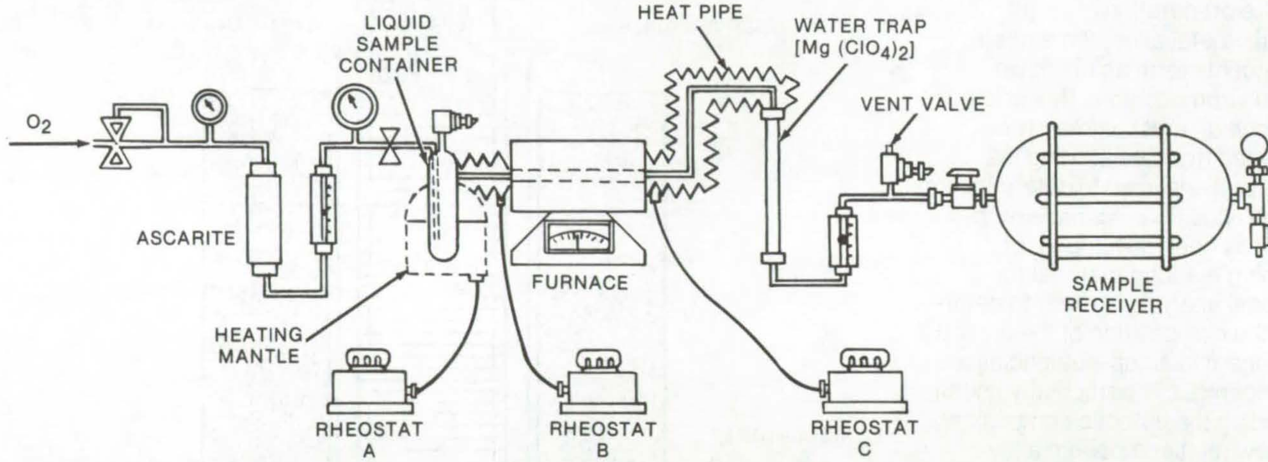

Procedure for Determining Total Carbon in Hydrazine incorporates a modified pyrolysis train. Liquid hydrazine samples are introduced through the injection port and are mixed with an O_2 stream. Three rheostats A, B, and C, supply heat at 210°, 190°, and 105° C, respectively. Gas samples pyrolyzed in the furnace at 850° $\pm$ 25° C are collected by the sample receiver until the receiver pressure reaches 34×10^4 N/m^2 (45 psia). The CO_2 content in the samples is determined by an infrared method.

The most common method of determining the carbon content in hydrazine is through the pyrolysis of samples introduced directly into a furnace. The resulting carbon dioxide is absorbed in barium perchlorate solution, and the amount of CO_2 is determined by coulometric measurement.

Recently this method has been improved by using a modified procedure. The samples are vaporized before they are introduced into the furnace, allowing a safer handling of the highly reactive hydrazine. Vaporization permits larger volume samples to be introduced into the furnace, which reduces errors related to the sample size. The second modification involves direct collection of pyrolyzed sample gases. This reduces losses of CO_2 and allows a choice of analytical techniques to measure the CO_2 content. Also gas samples can be conveniently stored for future reference.

The modified pyrolysis train is shown in the illustration. A liquid hydrazine sample is introduced through the injection port, using a specially-cleaned syringe needle. The sample is then mixed with an O_2 stream, is vaporized, and fed into the furnace. The pyrolyzed gases pass through a water trap to the sample receiver. Infrared spectroscopy can be used to analyze the samples for CO_2 content. The procedure is repeated until two consecutive results agree within 0.1 parts per million of CO_2. The water trap must be changed with every new sample.

This work was done by E. E. Davis of The Bendix Corp. for **Kennedy Space Center.** *For further information, Circle 51 on the TSP Request Card.*
KSC-11022

New Diamine Hardeners for Epoxies

New process yields
improved strength and toughness.

Langley Research Center, Hampton, Virginia

Stronger amine-cured polyepoxides can be obtained by using those diaminobenzophenones and diaminodiphenylmethanes that have amine groups located at ortho or meta positions to the carbonyl or methylene groups joining the two benzene rings.

Epoxy resins are used in a wide variety of applications, including protective coatings, pigmented paints, matrix resins for reinforced composites, molding and casting resins, and adhesives for bonding a wide variety of substrates. They are generally termed thermosetting materials as they do not attain maximum utility until converted into rigid, infusible systems by means of cross-linking or curing agents. The types of curing agents for epoxies include chemical compounds with hydroxyl groups, carboxylic acid groups, acid anhydrides, and various amines and ammonium groups.

The use of diaminodiphenylmethane and diaminobenzophenone compounds containing either one ortho amine group together with a para amine group or both amines meta to the diaryl connecting group (methylene or carbonyl) leads to improved resin strength, as shown by higher lap-shear adhesive specimen tests. For example, the use of m,m′-diaminodiphenylmethane with a commonly used diglycidyl ether precursor gives lap-shear values with aluminum that are at least 33 percent higher than when p,p′-diaminodiphenylmethane is used to cure the epoxy.

The process for producing cured epoxides requires the initial mixing of the diamines with the cured epoxides by one of three methods:

- The diamine is melted and stirred into the fluid or melted epoxide prepolymer.
- The diamine is dissolved in a low-boiling solvent, and this solution is stirred into the epoxide. The solvent is permitted to evaporate as completely as possible within the pot life or working time of the mixed diamine-epoxide system.
- Finely powdered diamine is slurried into a liquid epoxide prepolymer. While good results have been obtained using this procedure, it is the least preferred of the three.

This improvement in strength, in theory, is the result of the greater degree of disorder or nonlinearity of the diaryl diamine molecule when the two amine groups are arranged in the fashion previously described. In addition, the ortho-para and meta-meta diamine arrangements of these curing agents for epoxides provide the advantage of lower melting characteristics than the conventional para-para diamine isomers. This lower melting behavior makes the mixing of the diamine curing agent with the liquid epoxide resin faster and more efficient.

Another important advantage resulting from the more highly discarded diamines is in the lower glass transition (Tg), softening, or heat deflection temperatures resulting from resins cured with these special diamines. The lower the Tg of a thermoplastic resin, the greater the toughness of the cured polymer. Likewise, in thermoset polymers such as amine-cured epoxies, the same effect will be manifest in the lower softening or heat deflection temperature.

This work was done by Vernon L. Bell and Terry L. St. Clair of **Langley Research Center.** *Further information may be found in NASA CR-140522 [N74-34559], "Exploratory Study On the Effects of Novel Diamine Curing Agents and Isocyanate Precursors On the Properties of New Epoxy and Urethane Adhesives," a copy of which may be obtained at cost from the North Carolina Science & Technology Research Center* [see page A7].

Inquiries concerning rights for the commercial use of this invention should be addressed to the Patent Counsel, Langley Research Center [see page A8]. *Refer to LAR-11823.*

Electrolyte Cells Measure Oxygen Fugacities

An inexpensive concentration cell can be used by the chemical and metallurgical industries for gas-mixing systems.

Lyndon B. Johnson Space Center, Houston, Texas

The control and measurement of oxygen fugacity is essential in the study of many geological, chemical, and metallurgical problems.

Gaseous buffering, or gas mixing, has been employed to control oxygen fugacity at 101.31×10^3 N/m^2 (1 atmosphere) pressure in a redox control system. Two gases that undergo reactions to produce oxygen, such as carbon dioxide and carbon monoxide or hydrogen and carbon dioxide, are accurately mixed and flowed over a sample in a furnace. Oxygen fugacities between 10^{-24} and 10^{-3} can easily be produced, depending on the temperature of the gases. This technique assumes equilibrium among the gaseous species involved in order to compute the oxygen fugacity.

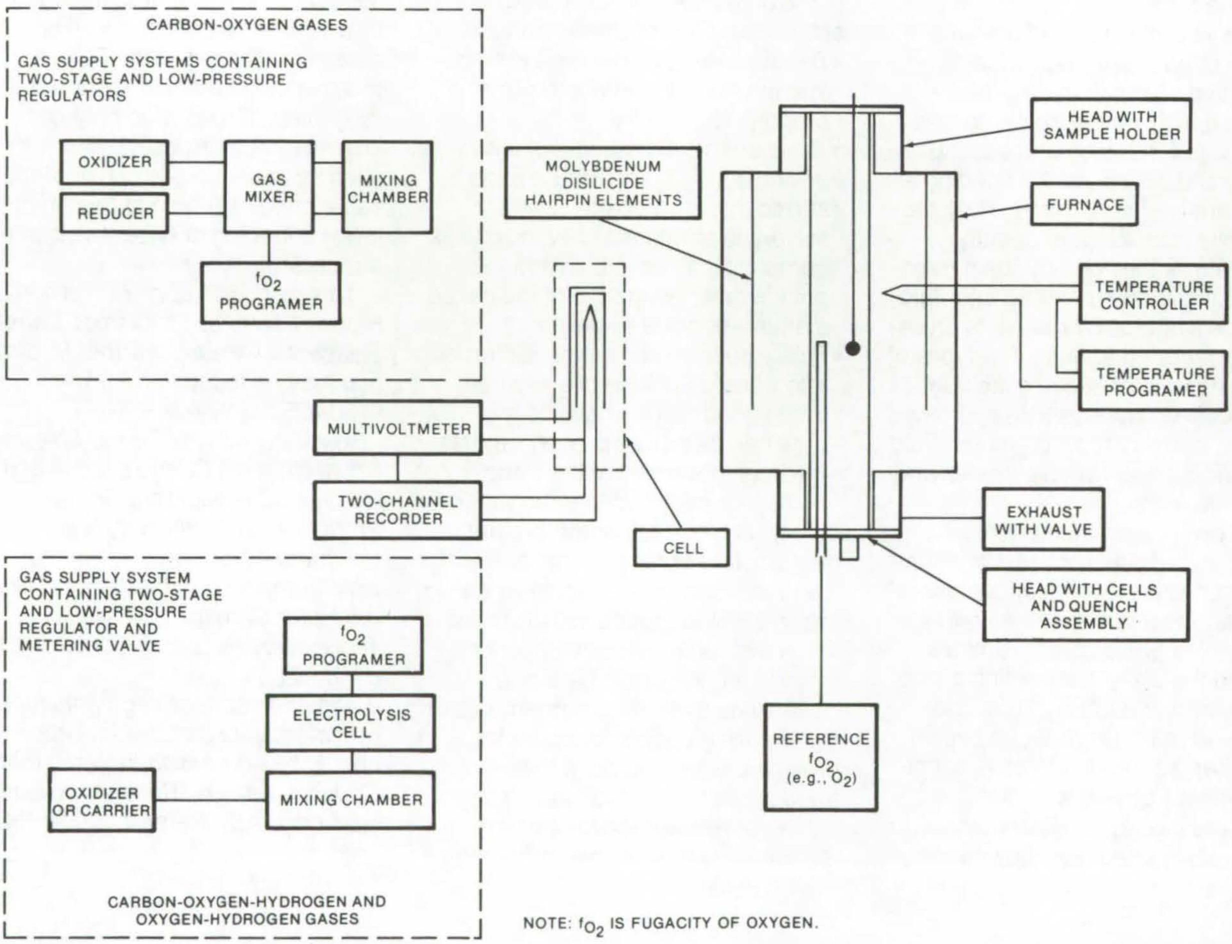

The Gas-Mixing System directly monitors the state of the redox reaction in the furnace by measuring the EMF output from the electrolyte cell. The output signal is used to control electronic or electrochemical currents. An electrolysis cell supplies hydrogen that is carried to the furnace by either a water-saturated carrier gas (e.g., nitrogen or argon) to produce hydrogen-oxygen mixtures, or by carbon dioxide or carbon monoxide for carbon-oxygen-hydrogen mixtures. The output of the cell is used to control the current to the electrolysis cell and therefore the amount of hydrogen. Carbon/oxygen flow is controlled by needle valves. Feedback circuitry drives a reversible variable-speed motor test that turns the needle valves. The oxygen fugacity may be fixed by using the null output of a meter and feedback circuitry to maintain a preset EMF automatically. The furnace may also be programed to execute a sequence of oxygen fugacity/time states by comparing the cell output (from the meter) with a time-varying EMF signal (from multivoltage sources). The actual redox state of the system and the rate at which it can be varied are a complex function of system configuration, composition, and temperature.

However, some investigations have indicated that the gas reactions may not come to equilibrium. Therefore the oxygen fugacities during an experiment may not be the same as those computed for the gaseous mixture.

A system that uses a calcia-stabilized zirconia-ceramic electrolyte in an oxygen concentration cell can directly measure the oxygen fugacity in a vertical-quench furnace, redox-control system (see figure). The system can independently vary temperature and oxygen fugacity during experiments, and it can record these parameters as a function of time.

O-rings are used to produce gas-tight seals against the ceramic, permitting enough slippage to accommodate the differential expansion of the components during heating. The sensing head of the electrode and the sample are symmetrically disposed about the axis of the furnace, but in small-bore systems a coaxial arrangement is necessary.

One leg of a thermocouple is used as the reference lead for the cell because it simplifies wiring and permits the use of heavier lead wire. The heavier wires and contacts extend the cell lifetime. The process-measuring thermocouple is inside the cell and protected from the adverse effects of the furnace gas. Due to the isolation from the furnace atmosphere, the system must be carefully calibrated under actual process conditions to insure that the measured temperature and oxygen fugacity are the same as those experienced by the sample.

The reference for the cell is provided by an oxygen gas purge in the interior of the cell. Oxygen is vented to the laboratory from the base of the cell through the holes carrying the lead wires out of the cell. The electrode is introduced from the bottom of the furnace, and the atmosphere-control gas flow is directed from top to bottom. This procedure provides a stable operation. Any volatiles that condense on the cell (water from hydrogen-containing mixtures) will flow to the bottom of the furnace, and any leaks of reference gas from the cell will be flushed out of the system without affecting the charge.

The furnaces employed have hairpin molybdenum disilicide heating elements that are less expensive than precious-metal wire, are useful to higher process temperatures [1,848 K (1,575° C)] when compared to platinum-wound furnaces, and have a nominal lifetime in excess of 18 months. Zirconia-based insulators are employed to make the high-temperature furnaces lightweight and rugged.

This work was done by Richard J. Williams of **Johnson Space Center** *and Oscar Mullins of Lockheed Electronics Corp. Further information may be found in NASA TM-X-58167 [N76-18246], "A System Using Solid Ceramic Oxygen Electrolyte Cells to Measure Oxygen Fugacities in Gas-Mixing Systems," a copy of which may be obtained at cost from the National Technical Information Service, Springfield, Virginia 22151.*
MSC-16089

Nucleation of Electronic-Crystal Regions

A technique for growing improved ceramic-oxide crystals uses high-viscosity solutions.

Marshall Space Flight Center, Alabama

Crystals for electro-optic and surface-wave acoustic devices generally have defects which are attributable to the Earth's gravitational field. These crystals are usually grown by the Czochralski technique or from seeded low-viscosity fused salts.

An investigation into the growth of crystal by seeding a highly viscous solution (glass or fused solvent) to minimize the convective and temperature variations and to reduce the rythmic feeding of the solute to the seed has been conducted. The technique approximates seeded growth under space conditions, and the resulting crystal has few defects.

The compositions selected on the basis of technical importance, gravity-sensitive properties, high value, and apparent compatibility with the seeded fused-solvent technique were bismuth germanate, $Bi_{12}GeO_{20}$, lithium niobate, $LiNbO_3$, and lead germanate, $Pb_5Ge_3O_{11}$.

The successful nucleation of bismuth germanate on a high-quality seed and the growth of respectable regions of single crystals of the same orientation of the seed have been achieved. The regions were characterized by Laue X-ray techniques, microscopic examination, laser optical-rotation measurements, microprobe analysis, emission spectroscopy, and other techniques to verify single-crystal growth of the same orientation and of similar stoichiometry.

Utilizing a solution of 80 percent by weight of $Bi_{12}GeO_{20}$ dissolved in 20 percent by weight of (0.75) Bi_2O_3, (0.5) Al_2O_3, (1.0) B_2O_3, a cooling rate of 2° C/h in the range of 795° to 767° C produced $Bi_{12}GeO_{20}$ nucleated by the seed crystal.

This work was done by Edward C. Henry, Barry A. Noval, and Donald R. Ulrich of General Electric Co. for **Marshall Space Flight Center.** *For further information, Circle 52 on the TSP Request Card.*

Inquiries concerning rights for the commercial use of this invention should be addressed to the Patent Counsel, Marshall Space Flight Center [see page A8]. Refer to MFS-23409.

(continued on next page)

Viscoelastic Foam Cushion

A durable shock-absorbent foam has many commercial and industrial uses.

Ames Research Center, Moffett Field, California

A flexible urethane foam developed during an Ames Research Center project on aircraft seating (NASA Tech Briefs B72-10692 and B73-10495) is ideal for orthopedic and prosthetic devices, sports equipment, furniture, and crash protection. Its special properties sugest that many more applications will be found in the future.

During development of the foam for aircraft seats, NASA's main goal was to improve impact protection (up to 36 g), while enhancing comfort under varying environmental conditions and passenger weights. The foam developed is viscous and elastic, with unusual and useful temperature, humidity, and compression responses. Acting as a "memory" foam, it equally distributes applied weight/pressure along the entire interface with the foam, thus eliminating any pressure points.

The foam surface flows to meet the contour or shape of the object pressing against it, and it returns to its original shape once the pressure is removed. Vibration and impact energies are strongly attenuated.

Cold hardens the foam, and heat softens it. Its viscoelastic properties are similar to those of a liquid in that the foam becomes firmer under forceful impact but is soft to a light touch. It can be produced in several degrees of firmness, from very soft to hard.

Proved applications to date include mattresses, cushions for wheelchairs and patients recovering from surgery, body-protection equipment for sports including football-helmet interiors, linings for ballet slippers, furniture, crash helmet liners, and motocycle seat cushions. As used for wheelchair cushions and mattresses for bedridden patients, the foam has helped to eliminate decubitus ulcers.

This work was done by Charles C. Kubokawa of **Ames Research Center** *and Charles Yost of Dynamic Systems Inc. For further information, Circle 53 on the TSP Request Card.*
ARC-11089

Books and Reports

These reports, studies, and handbooks are available from NASA as Technical Support Packages (TSP's) when a Request Card number is cited; otherwise they are available from one of NASA's Industrial Application Centers or the National Technical Information Service.

Stress-Corrosion Cracking Due to Hydrazine

The susceptibility of several alloys to hydrazine-based fuels

The stress-corrosion cracking (SCC) susceptibility in the presence of hydrazine has been examined for 6061-T6, Ti-6Al-4V(STA), Inconel 718, 410 stainless steel, and 4130 steel alloys. The relative susceptibilities of these alloys have been shown to increase in the order listed above. The steels 4130 and 410 were examined in detail and were found to be considerably less susceptible to SCC in monomethyl hydrazine and not at all susceptible to SCC in the presence of unsymmetrical dimethylhydrazine over the test period.

The presence and degree of SCC in the two steels depend on the concentration of CO_2 in the hydrazine (a common impurity absorbed from the atmosphere). Stress-corrosion cracking is not found in either steel at any stress intensity for CO_2 concentrations below 15 ppm. Above this level, both incubation times and crack-growth rates depend on CO_2 concentration. Evidence indicates that all proton-forming impurities will probably produce similar effects. The addition of barium oxide to the hydrazine will reduce crack-growth by lowering the active CO_2 content below a critical level.

This work was done by Michael J. Adamson and William P. Gilbreath of **Ames Research Center.** *For further information, Circle 54 on the TSP Request Card.*
ARC-11093

Computer Programs

These programs may be obtained at very reasonable cost from COSMIC, a facility sponsored by NASA to make new programs available to the public. For information on program price, size, and availability, circle the reference letter on the COSMIC Request Card in this issue.

Multispecies Transient Simulator

MTS predicts transient pressure variations in gaseous mixtures.

The Multispecies Transient Simulator (MTS) is a computer program for predicting the transient pressure variation of multispecies gases in large vacuum systems composed of interconnecting compartments. The pumping speeds, gas loads, and conductances are allowed to vary in any prescribed manner. The partial pressure of each gas species and the total pressure is computed for each compartment at preset time intervals. The MTS was developed primarily for the thermal-vacuum environmental chambers at the Johnson Space Center, but it should find applications in many industries involving the use of vacuum technology. In particular, MTS would be very applicable to simulating pumpdown curves, repressurization, sudden changes of pressure, and contaminant propagation in compartments, as well as for finding leaks and computing conductances between chambers and finding chamber outgassing required to reach a specified ultimate pressure.

In an isolated vacuum vessel, the rate of change of pressure is proportional to the difference of pumping speed and pressure and its outgassing rate. For a system of interconnected compartments the rate of change of pressure involves an additional term to account for the flux exchange among compartments. Thus, the system can be modeled by a set of differential equations which, in general, are nonlinear. There are six optional methods of solution in this dynamic model, allowing the user to solve this system of simultaneous equations by any of the following methods:

- Fourth-order Runge-Kutta method
- Modified fourth-order Runge-Kutta method
- Step-doubling method
- Extrapolation method
- Multivalue method
- Method of weighted residuals

There are advantages to each method. The method of solution chosen for a given simulation should consider primarily the stability of the numerical scheme. The mean pressure of each compartment is predicted by the model at preset time intervals. The entire history of the simulation is also plotted by the line printer.

UNIVAC FORTRAN,
Batch/Demand Mode
UNIVAC 1100, EXEC 8
Central Memory Requirement
Approximately 33K 36-Bit Words

This program was written by Alec L. Lee of Lockheed Missiles & Space Co. for **Johnson Space Center.** *For further information, Circle L on the COSMIC Request Card.*
MSC-14862

Multilayer Insulative Systems

One-dimensional numerical analysis of the transient thermal response

A one-dimensional numerical analysis of the transient thermal response of multilayer insulative systems determines the temperature distribution through a system consisting of from one to four layers, one of which can be an air gap. Concentrated heat-sinks at any surface or interface can be included. The computer program based on the analysis will determine the thickness of a specified layer that will satisfy a specified temperature-limit criterion at any point in the insulative system. The program will also automatically calculate the thickness at several points on a system and will determine the total system mass. This program was developed as a tool for designing thermal protection systems for high-speed aerospace vehicles but can be used by any industry involved in thermal insulation systems.

In the documentation, the equations describing the transient thermal response of a system are developed. The governing differential equation for each layer and the boundary condition equations are put in finite-difference form using Taylor's series expansions. These equations yield an essentially tridiagonal matrix of unknown temperatures. A procedure based on Gauss' elimination method is used to solve the matrix.

This program was written by Kay L. Brinkley and Claud M. Pittman of **Langley Research Center.** *For further information, Circle M on the COSMIC Request Card.*
LAR-12057

Rapid Kinetics

Hybrid program rapidly solves flowing or static multispecies problems.

A hybrid program for chemical kinetics provides a rapid solution to problems involving flowing or static, chemically reacting, gas mixtures. The program is designated as hybrid because it combines the problem setup, initialization, and preliminary calculation subroutines of computer program LEW-11467 (M72-10047), previously published as NASA TN D-6586, with the solution of the resulting ordinary differential equations by C.W. Gear's method. [See: Gear, C.W., *Numerical Initial Value Problems in Ordinary Differential Equations* (Prentice-Hall, Inc., c. 1971)]. The Gear numerical solution technique uses a highly efficient strategy in altering step size and order in combination with an extensive history array to achieve a stable rapid solution to a problem involving a number of stiff simultaneous differential equations.

With the consideration of additional chemical species, the stiff condition is aggravated by the inherent addition of a large number of equations. With the Gear method, the incremented step size is restricted in small values, because of accuracy requirements, only where the solution is active. In this region accuracy is achieved by varying both step size and order of the method of solution. The step sizes in regions of stiffness are unrestricted because of small time constants until the terms become active again. This condition requires that the method be implicit, and a system of generally nonlinear equations must be solved at each step. Therefore, the chief advantage of this program is its reduced computational time when the reacting system contains more than 15 different chemical species, although a smaller number of reacting species does not penalize the user with respect to computational time.

The program requires 125K core storage, is designed to run in batch mode on CDC equipment, and will be distributed as a SCOPE INTERNAL tape.

This program was written by Allen G. McLain of **Langley Research Center** *and C. S. R. Rao of Old Dominion University. For further information,* Circle N *on the COSMIC Request Card.*
LAR-12140

Life Sciences

Hardware, Techniques, and Processes

Meal System for the Elderly

A system of packaged meals requires no refrigeration and is nutritionally balanced.

Lyndon B. Johnson Space Center, Houston, Texas

Several recent studies have indicated that many elderly people do not eat well and are often malnourished. This appears to be the result of physiological, psychological, social, and economic factors that occur with aging. The magnitude of the problem can be appreciated when one notes that over 22 million Americans are 65 years of age or older.

In response to this need, the experience and data gained during the development of spacecraft food systems have been used to design a complete meal system for the elderly: nutritious, shelf-stable meals that can be delivered conveniently in multiple units and prepared easily. The system was developed following a series of user surveys, taste tests, and a 15-week field demonstration and evaluation.

The **Meal System for the Elderly** is a shelf-stable nutritious meal package with single-serving portions that can be delivered in multiunit packs and can be conveniently prepared in the home.

An initial preference-and-attitude survey was conducted to determine the food preferences, eating habits, dietary restrictions, cooking habits, disabilities, and nutritional concepts of the elderly. Then candidate foods were identified and tested by a taste panel; further evaluations were made by a group of elderly people representative of those for whom the system was designed.

The program to date is documented in an extensive report (referenced at the end of this article) that includes a description of the development methodology, the results of surveys and tests, nutritional data, manufacturing specifications, processing methods, and labeling and packaging techniques.

The menus described in the report provide at least one-third of the recommended dietary allowances for the male population over 51 years old. Nutritional data on the meals include the amounts of calories, protein, fat, carbohydrates, calcium, phosphorus, iron, vitamin A, vitamin C, thiamin, riboflavin, and niacin in selected foods.

Thermostabilized, freeze-dried, dehydrated, intermediate-moisture, and natural foods were evaluated for weight and stability, Thermostabilized foods met the requirement of a 2-year shelf life when stored at temperatures between 40° and 70° F (4° and 21° C), and rehydratable and wafer foods had a shelf life of 1 year under the same storage conditions.

Manufacturing specifications include information such as applicable U.S. Standards, acceptable ingredients, moisture content, and quality insurance requirements.

Packaging considerations include food protection, multiday meal packaging, shelf life, standardization, ease of transportation, and appeal and esthetics. Packaging systems are rigid cans (tin-plated steel or drawn aluminum) for thermostabilized foods and foil laminate packages for freeze-dried, dehydrated, and intermediate-moisture foods.

Labels for food packages include product name, preparation information, weight, ingredients, and manufacturer. They are color coded (red for hot, blue for cold) and have large bold print and graphic symbols for preparation instructions.

This work was done by Gary R. Primeaux of **Johnson Space Center,** *Ronald G. Ritz of Martin Marietta Corp., and Gene A. Hruzak of Technology Inc. Further information may be found in NASA CR-144516 [N76-10898], "Final Report, Design and Development of a Meal System for the Elderly," a copy of which may be obtained at cost from the National Technical Information Service, Springfield, Virginia 22151.*
MSC-16062

Caution and Warning System

A biomedical-monitoring and display system can be used for intensive-care and patient monitoring.

Lyndon B. Johnson Space Center, Houston, Texas

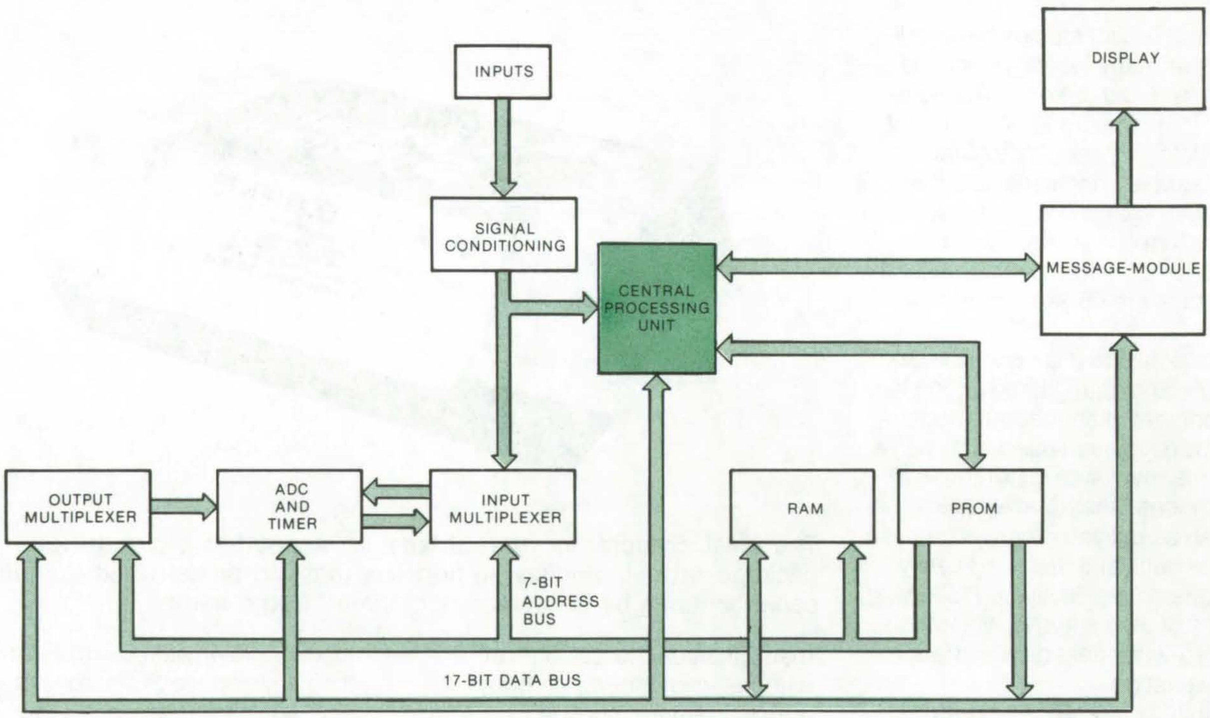

A **Block Diagram of the Caution and Warning System:** The CPU (central-processing unit) is the "brain" of the CWS. It selects the next functional-logic program step (i.e., programable read-only memory information address) based upon data given by sensor inputs, analog-to-digital conversions, time delays, and random-access memory (RAM) status data. The CPU is also constantly on the alert for an interrupt signal generated by one of the five critical-priority parameter inputs. Upon receipt of a priority interrupt, the CPU initiates a branch in the functional-logic software to a priority service subroutine. The RAM is a 64-bit memory that stores information concerning system status, and its contents are changed during the course of CWS operation. For example, if the CWS functional logic determines that a sensor has failed, this bit of information is written into the RAM so that the CWS will take into account the failed-sensor status every time the CWS interrogates that sensor. This memory gives the CWS the ability to "learn" about CWS status during system operation. The RAM can be reinitialized under operator control and will relearn the current CWS status at the time of the reinitialization.

A system consisting of several solid-state logic units linked to auditory and visual display devices and biomedical instruments is employed as a warning and diagnostic system for a life-support system.

The caution and warning system (CWS) represents a substantial improvement in sophistication over earlier systems. Life-support system parameters are continuously monitored. If a malfunction occurs in the life-support system, the CWS will detect and display the out-of-range condition. Proper corrective procedures and present status are automatically presented to an operator.

The system circuit design is based upon a digital, bus-oriented architecture, with its accompanying simplicity, flexibility, and noise immunity advantages. The CWS functional logic is completely contained within a solid-state, electronic PROM (programable read-only memory). This allows the CWS to be 100 percent reprogramable; that is, its operating functional logic can be completely changed by the substitution of the new PROM's for the existing PROM's.

All CWS functional logic is permanently stored on miniature solid-state electronic-memory integrated circuits, which relieves the operator of the responsibility of memorizing life-support system operational details and eliminates extensive checklists. Tests have demonstrated that specific malfunction procedures can be easily and accurately incorporated into a functioning caution

and warning system. By utilizing low-power MOS logic, the power consumption is very low. This is a critical parameter since CWS is designed to operate from batteries.

Eleven different parameters are monitored for 16 different out-of-range conditions. Some of the parameters are input to the CWS as sensor-switch closures, and the others are input as analog voltages from sensor transducers. The parameters are monitored approximately 30 times per second. The first five parameter conditions are assigned a high priority and, if detected, will override lower-order parameter malfunctions. Some of the parameters monitored are O_2 flow, O_2 temperature, vent flow, battery volts, PGA pressure (these are the five priority critical parameters), feed water pressure, log H_2O, O_2 pressure temperature, battery current, and others.

In addition to the continuous parameter monitoring, the operator can, at any time, request a status check on an additional five system parameters. If no status check is requested for a fixed time lapse (10 minutes in the breadboard system), the CWS will remind the operator that a status check is in order by displaying "STATUS CHECK." The operator may then initiate the check procedure at his discretion.

CWS outputs include the message display as well as two different warning tones. Inputs to the CWS are in the form of pushbutton switches for "yes" and "no" responses, a button to request a status check, and a button to shut off the warning tone. A 16-character, alphanumeric, light-emitting diode display allows the CWS to present messages of up to 16 characters in length. Message characters can be selected from the full 64-symbol ASCII-character font. These include the 26 letters of the alphabet, numerals 0 through 9, and 27 special symbols, including the question mark, equal sign, and blank. This display allows great flexibility in the visual presentation.

This work was done by Timothy M. McClung, Joseph T. Parker, and Paul D. Peterson of The Garrett Corp. for **Johnson Space Center.** *Further information may be found in NASA CR-144432 [N75-32760], "Electrical Distribution System [EDS] and Caution and Warning System [CWS]," a copy of which may be obtained at cost from the National Technical Information Service, Springfield, Virginia 22151. MSC-16046*

Interlocking Butterfly "Tourniquet"

A proposed adjustable bandage closes skin lacerations to any desired degree.

Lyndon B. Johnson Space Center, Houston, Texas

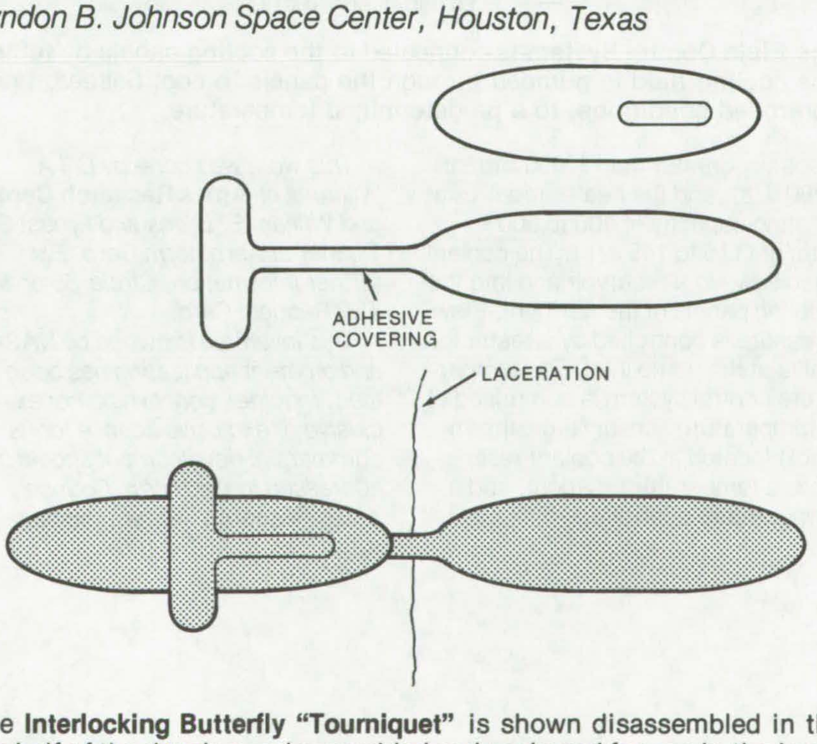

The **Interlocking Butterfly "Tourniquet"** is shown disassembled in the top half of the drawing and assembled and packaged for use in the lower half. The two halves of the bandage are stuck on opposite sides of a laceration. Then the separate covering on the T-shape is removed; the two halves are pulled together to force the laceration to close, and the tourniquet is sealed in place.

Currently-used butterfly bandages are not adjustable and are difficult to position, especially if only one hand can be used. An improved butterfly "tourniquet" was developed for one-handed application. It is better able to close off lacerations and can be adjusted to any desired closure, using one hand.

The bandage as shown in the figure is made from a nonadhering gauze which will not dry into the wound. This prevents the laceration from being inadvertently torn when the bandage is removed.

This work was done by Louis J. Raggio and Billy E. Green of Rockwell International Corp. for **Johnson Space Center.** *No further documentation is available. MSC-19382*

Liquid-Cooled Bra for Cancer Detection

The sensitivity of infrared thermography is improved.

Ames Research Center, Moffett Field, California

The sensitivity of thermographic techniques for detecting breast cancer is improved by cooling the tissue of the entire breast area uniformly with a liquid-cooled brassiere like garment. The warmer temperature of any tumorous areas will be highlighted in the infrared photographs taken during examination. The cooling garment covers the upper torso and breasts. Preshaped cooling panels (see NASA Tech Brief B74-10249, "Liquid-Cooled Liner for Helmets") are made of two superposed sheets of flexible waterproof material, such as rubber, polyurethane, or fabric coated with an elastomeric material. The two sheets are sealed by vulcanizing at the edges and along spaced lines so as to form passageways through which the coolant can flow. Inlet and outlet ports for the coolant are also incorporated. Finally, a panel is fitted into each cup of the garment and is sewn in place.

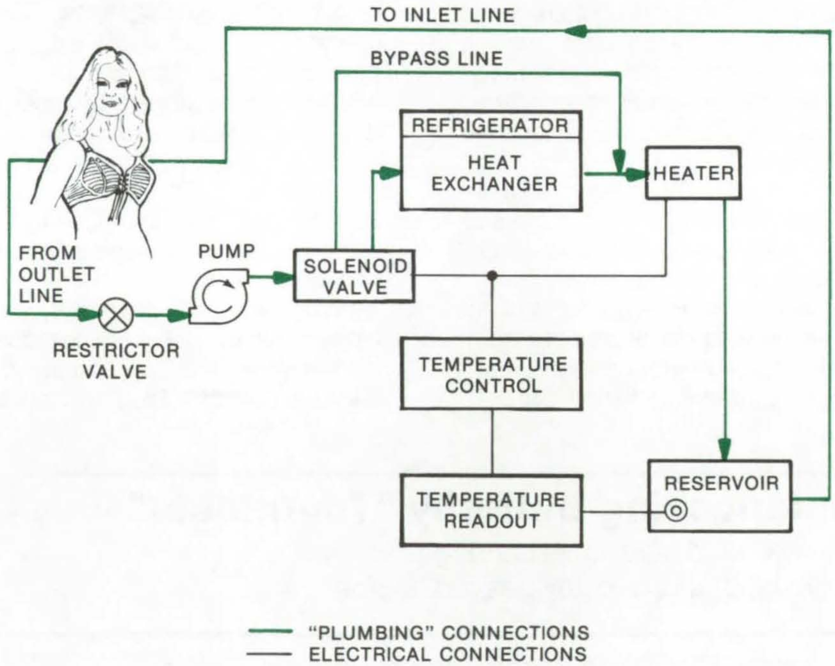

The Fluid Control System is connected to the cooling panels by tubing. The cooling fluid is pumped through the panels to cool tissues, under controlled conditions, to a predetermined temperature.

The flow and temperature of the coolant are controlled by a system which also monitors skin temperature. A coolant pump can move water at 0.5 gal/min (30 ml/s) at a head in excess of 20 psig (140×10^3 N/m^2). The coolant flows at a pressure of 10 to 20 psig (70×10^3 to 140×10^3 N/m^2). A solenoid valve where it is routed either through a bypass line or through a refrigeration unit (depending on desired temperature) to a heating unit. The refrigeration unit should have a cooling capacity greater than 1,000 Btu/hr (290 J/s), and the heater requires a heating capacity of 400 to 500 Btu/hr (115 to 145 J/s). The coolant then flows to a reservoir and into the cooling panels of the garment. Flow pressure is controlled by a restrictor valve at the pump inlet. The temperature control system is comprised of a temperature sensor (e.g., thermistor) located in the coolant reservoir, a temperature readout, and a temperature controller.

This work was done by Bill A. Williams of **Ames Research Center** *and William E. Elkins and Ernest G. Tickner of Aerotherm Corp. For further information, Circle 55 on the TSP Request Card.*

This invention is owned by NASA, and a patent application has been filed. Inquiries concerning nonexclusive or exclusive license for its commercial development should be addressed to the Patent Counsel, Ames Research Center [see page A8]. Refer to ARC-11007.

Inexpensive Portable Drug Detector

Easy-to-use analyzer automatically
graphs fluorescence spectrum of test sample.

Ames Research Center, Moffett Field, California

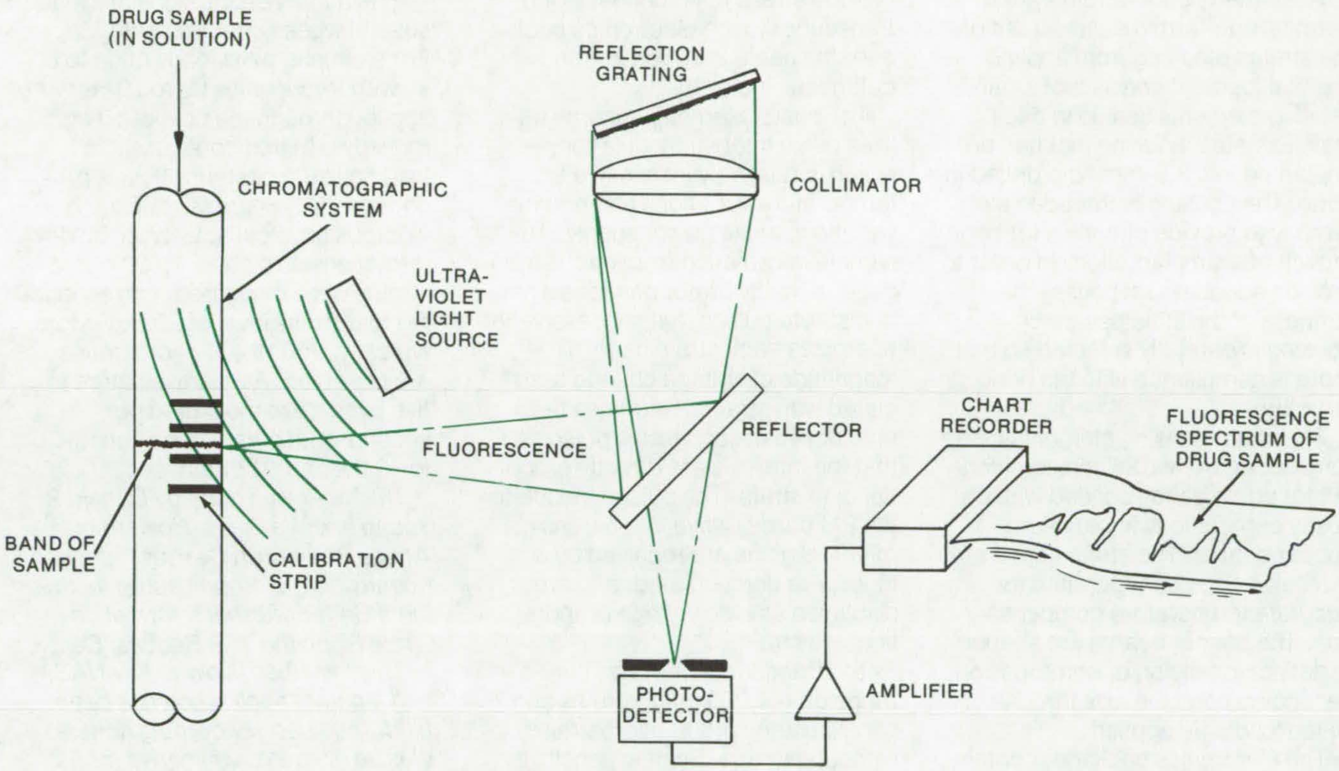

A **Drug Sample is Identified** by its fluorescence spectrum in this inexpensive portable analyzer. Nulls in the spectrogram, caused by the opaque strips on the chromatography column, provide wavelength calibration; by their timing, they also show how fast the sample moves down the column. Direct-reading and without moving parts (except for the chart recorder), this detector is easy to use in forensic and medical field testing.

A portable drug-detection unit can automatically graph the fluorescence spectrum of a drug sample and measure its rate of movement through a chromatographic column for forensic and medical testing. The device has no moving parts except for a chart recorder that plots the calibrated graph of spectral intensity vs. wavelength.

For analysis, a test sample is treated with chemicals that cause various drugs to become highly fluorescent fluorophores. After treatment with these developing reagents, the sample is introduced into a chromatographic column (see figure). The column packing and developing solvents used are similar to those used in thin-layer chromatography for the specific compounds of interest. The drug sample separates into a narrow band as it traverses the column, and ultraviolet radiation striking the band makes it fluoresce with a spectrum that is characteristic of the particular drug. An optical system detects successive portions of this fluorescence characteristic as the band moves down through the chromatographic column, and the optical response is recorded on a moving chart.

Opaque strips on the column produce nulls on the chart to provide a wavelength calibration. Moreover, the time between successive nulls shows how fast the sample descends through the column from one strip to the next.

This detection unit is self-scanning, self-calibrating, easy to operate, and inexpensive. Its portability makes it especially useful for applications in the field.

This work was done by John Dimeff, Alvin H. Heimbuch, and John A. Parker of **Ames Research Center.** *For further information, Circle 56 on the TSP Request Card.*

This invention has been patented by NASA (U.S. Patent No. 3,814,939). Inquiries concerning nonexclusive or exclusive license for its commercial development should be addressed to the Patent Counsel, Ames Research Center [see page A8]. Refer to ARC-10633.

In Vivo Bone-Strain Telemetry

An implantable bone-strain transducer is coupled to an implantable data transmitter.

Ames Research Center, Moffett Field, California

A telemetry bone-strain system permits long-term measurement of the strains resulting from applied skeletal loads. It consists of strain-sensing elements sealed in a stainless-steel housing that can be implanted in a 3.2-mm hole drilled in bone. The housing is threaded externally to provide channels for bone growth after implantation. In order to provide adequate response, the stiffness of the stainless-steel housing is carefully selected so that there is compliance with the bone structure.

The strain-sensing elements in the transducer are two silicon semiconductor strain gages bonded with an epoxy cement to twin beryllium-copper beams. The strain gages are in a half-bridge configuration for accurate temperature compensation. The copper beams are shaped to deflect in tension or compression, depending upon the axis through which loads are applied.

The electronics package, containing a power supply, a radio-frequency switch, and a transmitter, is implanted in the medial thigh about 15 to 50 cm from the transducer. A cable comprised of three stainless-steel stranded wires wound in a helix and potted in a silicone elastomer to provide stress relief connects the transducer to the electronics package; the cable is buried in a subcutaneous incision.

The basic telemetry scheme utilizes pulse interval modulation, which is relatively insensitive to temperature variations and nominal variations in the power supply. To sample information from each strain gage, a multivibrator provides a set of discrete pulses that successively energizes each strain gage. The magnitude of voltage change associated with strain determines the time between successive pulses so that the intervals are directly proportional to strain. The pulses modulate the FM carrier wave in the transmitter. Signals are received by a tuner, are demodulated, and are displayed as a dc voltage proportional to strain.

The transducer operates over a range of $\pm$ 4,000 microstrains and can withstand 6,000 microstrains without damage. System sensitivity is such that 40 microstrains produce 50 mV at the demodulator output. Response is linear, and frequency response is flat from dc to about 90 Hz. Noise level has been measured to be less than 1 percent of full-scale deflection.

Preliminary calibrations are made several weeks after implantation. For example, axial loads of up to 60 kg with frequencies up to 10 Hz were applied through the tibia of 10-kg monkeys. In that configuration, loading in the posterior tibia is predominantly compressive. During vigorous physical activity, tibial deformations as high as 1,000 microstrains were measured, corresponding to a stress level of 200 kg. More typically, 200 to 400 microstrains are observed. As many as three to five events are measured per second, with a rise time of about 30 to 40 ms or 0.01 strain/sec.

This work was done by Donald R. Young and Wayne H. Howard of **Ames Research Center.** *and Eph Koenigsberg of Koenigsberg Instrument Co. For further information, Circle 57 on the TSP Request Card.*

This invention is owned by NASA, and a patent application has been filed. Inquiries concerning nonexclusive or exclusive license for its commercial development should be addressed to the Patent Counsel, Ames Research Center [see page A8].

ARC-11074

Fast Measurement of Bacterial Susceptibility to Antibiotics

Bacterial susceptibilities in infected urines are measured without isolation, using photoanalysis of ATP.

Goddard Space Flight Center, Greenbelt, Maryland

The antibiotic susceptibilities of bacteria in biological fluids, such as urine, blood, and milk, can be determined without the conventional time-consuming isolation and incubation of individual bacterial strains. The method is based on the photoanalysis of adenosine triphosphate, using a light-emitting reaction with a luciferase-luciferin compound proportional to the amount of ATP present ["Quantitative Bioluminescent Detection of Bacteria" (GSC-12003), NASA Tech Briefs, vol. 1 no. 1, Spring 1976]. Besides the inherent speed of the luciferase-luciferin technique, considerable time is saved because it is not necessary to isolate particular strains, using this ATP method. It is sufficient to determine whether a particular antibiotic is generally effective against the dominant strain present in the sample under test.

For analysis, the fluid is first concentrated by centrifuging, and a growth medium is added. One

portion of the test sample is prepared for an immediate ATP assay to determine whether infection is present at all. A detergent and an ATP-ase are added to this sample to rupture nonbacterial cells selectively and to hydrolyze any free ATP. In addition, membrane-bound ATP must be released into solution where it can be hydrolyzed. This can be accomplished by the addition of malic acid.

The treated solution is concentrated, and the interfering compounds (especially the ATP-ase) are removed. An extracting agent is then added to rupture the bacterial cells and free ATP. This solution, after preparation, is reacted with a luciferase-luciferin mixture; the emitted light is measured and correlated with a bacteria count to determine whether sufficient infection exists to merit further investigation.

Susceptibility of the dominant strains to various antibiotics is determined by separating three portions of the test solution for each antibiotic to be examined. A broth is added to the fluid, and it is preincubated to get the organisms into a log growth phase. To one of the three samples the antibiotic is added. This sample and one of the other two are placed in an incubator for about 2.5 hours. The third sample is immediately assayed for the presence of ATP, following the general procedures for the initial infection determination. Upon completion of incubation, the other two samples are similarly assayed.

The results from all three samples can be used to determine an ATP index, using the relationship

$$\text{ATP index} = \frac{B_t - A_0}{A_t - A_0}$$

where B_t is the light reading for the sample treated with antibiotic (incubation time t), A_t is the light reading for the sample not treated with antibiotic (incubation time t), and A_0 is the light reading for the sample neither treated nor incubated. If the ATP index is greater than 0.05, the dominant bacterial strains can be considered resistant to the antibiotic.

This work was done by Emmett W. Chappelle and Grace L. Picciolo of **Goddard Space Flight Center** *and Christian G. Schrock of the New England Medical Center. For further information, Circle 58 on the TSP Request Card.*

This invention is owned by NASA, and a patent application has been filed. Inquiries concerning nonexclusive or exclusive license for its commercial development should be addressed to the Patent Counsel, Goddard Space Flight Center [see page A8]. Refer to GSC-12046.

Biomedical Ultrasonoscope

Real-time noninvasive "observation" of the heart, using a portable battery-operated instrument

Ames Research Center, Moffett Field, California

An improved biomedical ultrasonoscope permits noninvasive examination of the interior of a patient's body and is particularly well suited to real-time examination of the heart. The portable battery-powered scope, which uses low-power integrated circuits (IC's), is capable of C-mode scan display as well as the more common A-mode and M-mode scans. Resolution of the ultrasonoscope enables the operator to observe the functioning of the heart, video-produced metric markers spaced at linear intervals on the scope cathode-ray tube (CRT) display permit measurement of the heart and its changes.

During A-mode, the echoes are presented as vertical deflections of the trace (marker pips) on the CRT screen. Since the time delay between a transmitted pulse and the received echo depends on the distance between the transducer and

(continued on next page)

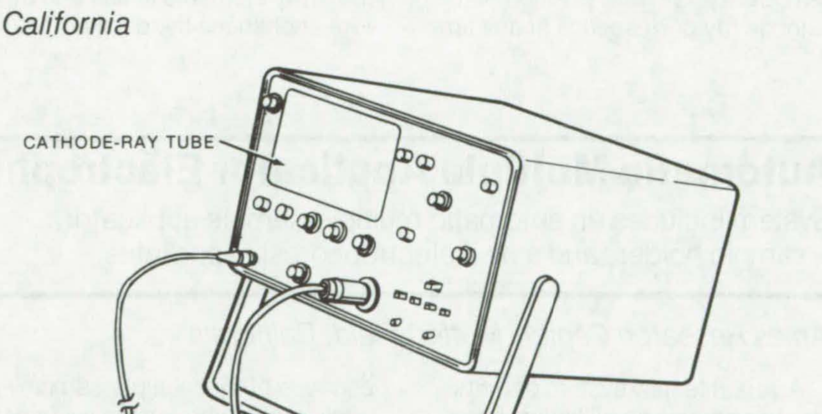

Figure 1. The **Portable Battery-Powered Ultrasonoscope** enables an operator to view organs, particularly the heart structure, in real time. A choice of three scan modes (A-scan, C-scan, and M-scan) affords quick visual observation on the instrument CRT. The single-transducer probe enables A-scan and M-scan viewing; the multiple-transducer probe is for C-scan observation.

the reflecting organ surfaces, the depth of reflection from the end of the transducer is represented along the X-axis. During M-mode, echoes are presented as a brightening of the time-base trace (intensity modulation). The time base is swept at right angles to its direction to plot the position of the heart surface, which appears to move. Elapsed time is indicated along the Y-axis. The depth of the reflecting interface from the end of the transducer is represented along the X-axis.

In the C-mode scan, twenty transducer elements are positioned across the patient's body. A pulsed electrical signal is converted to a pulsed ultrasonic signal via the transducer element. The radiated ultrasonic signal is radiated into the body. Echoes reflected from internal organs are picked up and reconverted to electrical signals. A sequencer connected between the generator and ultrasonic transducers is used to clock the transducer element in cyclic order. A voltage source connected between the clock and the CRT Y-axis input generates a staircase waveform having steps synchronized by the clock pulses.

Echoes are represented as a brightening of the CRT trace in C-mode. The vertical position of the cathode ray corresponds at any time

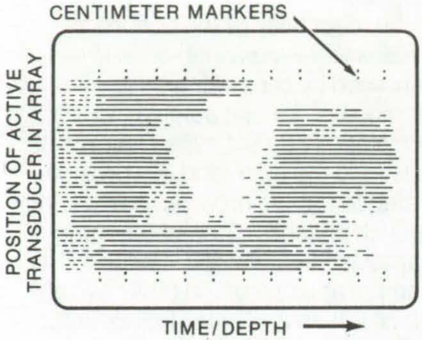

Figure 2. The patient's Chest Wall is viewed on the left side of the CRT. The central white area represents the heart. Video markers spaced along the X-axis permit instantaneous measurement of the heart dimensions. A bias voltage generator is used to offset alternate raster frames to enhance the visual display.

with the position of the active element in the transducer. The depth of the reflecting interface from the transducer to the organ being observed is represented along the X-axis. The number of horizontal lines per frame is selected as twice the number of transducer elements, plus two extra lines at top and bottom for depth markers.

A bias voltage applied to the CRT Y-axis input visually simulates twice the array elements in use and therefore enchances the display. The representation obtained on the CRT graticule is thus a two-dimensional or cross-sectional image of anatomical organs, enabling displacements from a reference surface (the chest wall, for example) to be made.

The instrument, shown in Figure 1, utilizes two probes: The smaller one contains a single ultrasonic transducer element, while the larger transducer houses a linear array of ultrasonic elements. When either probe is pressed against a patient's chest opposite the heart, information is presented on the CRT, as determined by the scan mode. The small single-element transducer probe is used in the M-scan or A-scan mode, while the multiple-element transducer probe is for C-scan mode transmission. When in C-mode scan, a two-dimensional cross-section image of the organ is viewed, as in Figure 2.

This work was done by Robert D. Lee of **Ames Research Center.** *For further information, Circle 59 on the TSP Request Card.*

This invention is owned by NASA, and a patent application has been filed. Inquiries concerning nonexclusive or exclusive license for its commercial development should be addressed to the Patent Counsel, Ames Research Center [see page A8]. Refer to ARC-10994.

Automatic Multiple Applicator Electrophoresis

System includes an automatic multiple-sample applicator, a sample holder, and a new electrophoresis apparatus.

Ames Research Center, Moffett Field, California

A versatile new system permits electrophoresis on all known supporting media, and it can be employed for more complicated procedures requiring electrophoresis as a first step, such as crossover electrophoresis and electroimmunodiffusion. The apparatus can also be used for electrofocusing.

Several new features make this system easy to use and economical. Resolution and accuracy are increased; and time required for electrophoretic analysis of a number of samples is greatly decreased because of the multiple-sample applicator. Although the system will primarily be useful in forensic and clinical laboratories, it will have many applications in other biological studies, including taxonomy, immunology, and genetics.

The electrophoretic unit (Figure 1) consists of a square tank, permanently divided in the center and having four removable baffles. The platinum wires that carry the current are set into grooves in two plastic frames. The frames may be removed to facilitate cleaning or to make room for electrodes with a different geometry for use in electrofocusing.

The electrophoresis apparatus is designed to use either a cellulose acetate membrane or any one of a variety of gels as a supporting medium. When a membrane is used, it is held at controlled tension by a one-piece bridge assembly. When gel is used, it is contained in a flat, square tray that is held in place by special retainers on a temperature-control plate. Greater resolution is achieved by performing two-

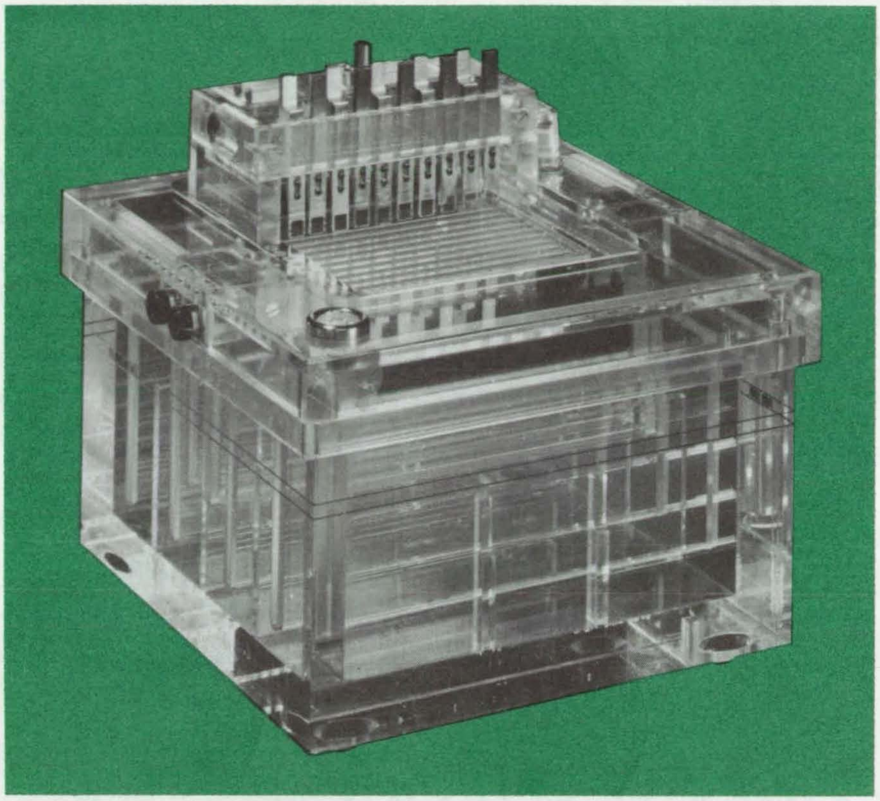

Figure 1. An **Improved Electrophoresis Apparatus** incorporates a multiple-sample applicator and several other new features that both speed up analysis and improve accuracy.

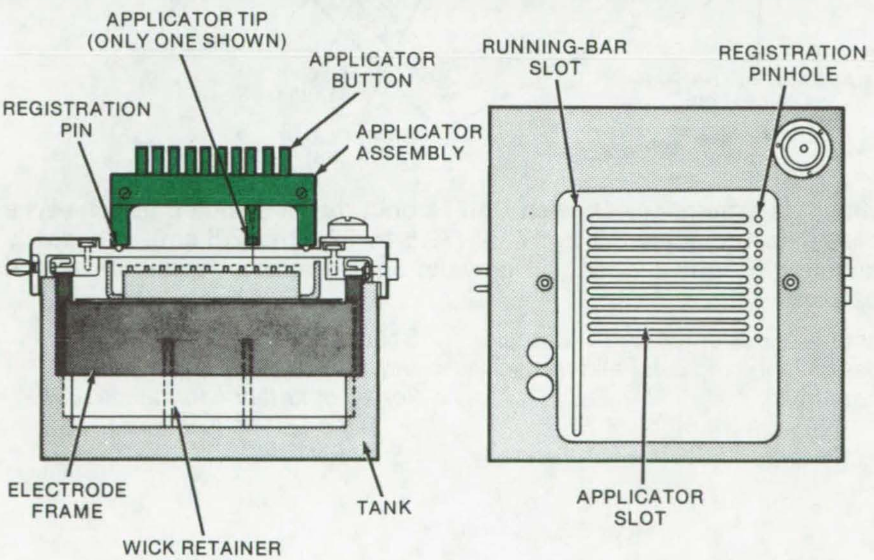

Figure 2. The **Automatic Multiple-Sample Applicator** is shown as used with a specially-designed membrane-medium electrophoresis device. The registration pin is inserted into 1 of 11 pinholes in the cover, and when the middle applicator button is pushed, all 10 applicator tips pass through the slots and release their samples simultaneously.

dimensional migrations. First, the sample is pulled apart in a linear path by the electric current, and then the square gel tray is turned 90° so that the first migration is pulled apart from an orthogonal direction. A retaining slot on the inside ends of the tank holds and alines filter-paper wicks that make contact between the gel and the electrolyte.

The unit is designed for use with an applicator capable of picking up and applying either a single sample or from 2 to 10 simultaneous samples. The samples are drawn from a sample holder adapted to receive the multiple applicator tips.

The cell cover (Figure 2) has 11 slots to receive the multiple-sample applicator tips. The applicator may be placed in any 1 of 11 positions relative to the cathode and anode. It is locked in the selected position automatically and cannot shift accidently. Therefore, all 10 samples can be placed in an absolutely parallel line relative to the cathode and anode. The cover also includes a male and a female plug on opposite sides, thus making it possible to join a number of cells in a row and to use a single power source for all of them simultaneously. Between operations, all the applicator tips may be quickly and simultaneously cleaned in a built-in rinse trough, then dried simultaneously in a built-in blotter trough.

This work was done by Benjamin W. Grunbaum of the University of California at Berkeley for **Ames Research Center.** *For further information, Circle 60 on the TSP Request Card.*

This invention is owned by NASA, and a patent application has been filed. Inquiries concerning nonexclusive or exclusive license for its commercial development should be addressed to the Patent Counsel, Ames Research Center [see page A8]. Refer to ARC-10991.

Miniature Emergency Oxygen Unit

Portable oxygen unit combines resuscitation, inhalation, and aspiration in one compact package.

John F. Kennedy Space Center, Florida

A portable emergency oxygen unit has been designed to include resuscitation, inhalation, and aspiration modes all in one 16-lb (7.3-kg) package. The compact unit can be easily handled by one nurse to treat emergency patients. This reduces the extra time required to carry and operate large-capacity units. A large unit may be brought later if prolonged treatment is necessary.

The unit (see figure) includes: two high-pressure cylinders, each rated at 4.1 ft^3 (1.2 m^3) 2,200 psig (15.2×10^6 N/m^2); a stainless-steel manifold containing an on/off valve, a pressure gage, a burst disk, and a fill/check valve; a first-stage regulator to reduce the varying cylinder pressure down to a constant 50±5 psig ($31.3 \times 10^4 \pm 3 \times 10^4$ N/m^2); a resuscitator head which allows resuscitation (positive-negative-positive) or inhalation (only positive) modes of operation; and the hoses and mask assemblies.

The design of the unit and the selection of components including soft goods offer safe operation in a 100-percent gaseous oxygen service. The valves, regulator, and resuscitator head were selected for their compatible design and materials. Soft goods exposed to the oxygen flow path are Teflon or KEL-F, or equivalent, and masks and hoses are made of silicone rubber. Operation and maintenance are made easier through the simple design of the regulator and resuscitator head.

This work was done by R. S. Gubin and H. H. Franks of **Kennedy Space Center** *and R. G. Baynes and J. A. Johnson of the Bendix Corp. For further information, Circle on the TSP Request Card.*
KSC-11011

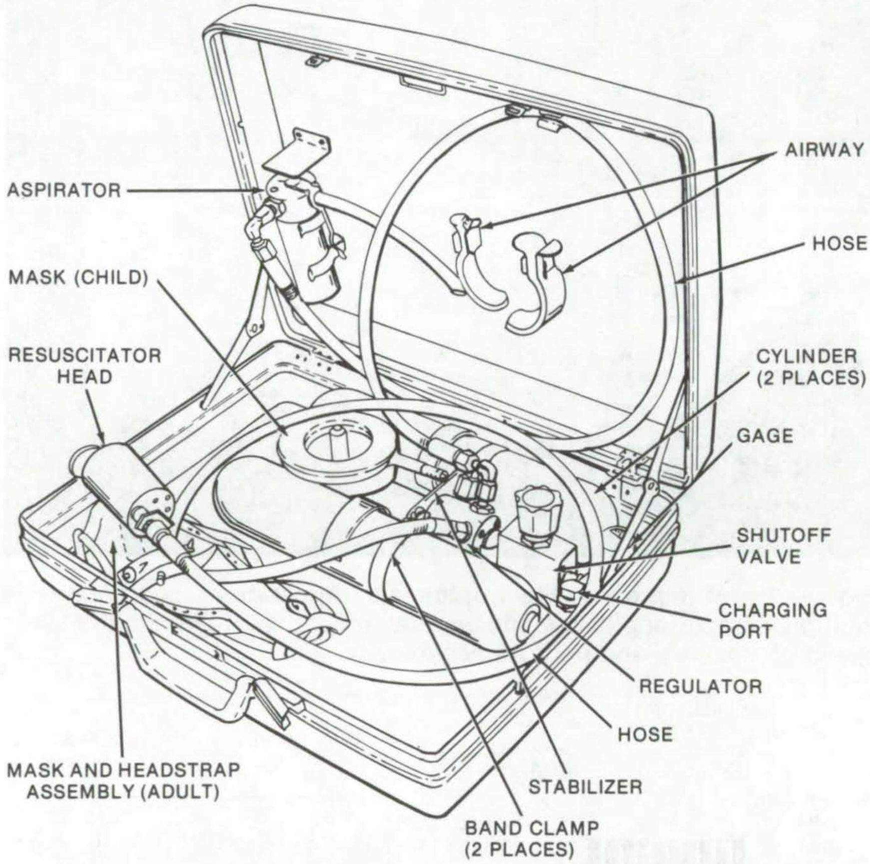

Miniature Emergency Oxygen Unit is built into a standard attache-type case measuring 5 by 13 by 17 in. (12.5 by 32.5 by 42.5 cm). It is easily handled in tight quarters, in crowds, and in remote locations by one person.

Multispectral Imaging for Medical Diagnosis

Visible and near-infrared photography aid in diagnosis of burns.

Caltech/JPL, Pasadena, California

The burn injury is being studied with a new multispectral photography technique to determine the amount of morbidity present in the tissue. This information may enable a diagnostician to evaluate the depth of the burn, thereby providing the physician with an early understanding of its character and leading to accelerated treatment.

The motivation for photography as a diagnostic tool is based upon the ability of various wavelengths of light to penetrate different depths into the skin and upon the different absorptances of each tissue type at different wavelengths. For instance, blood absorbs near-infrared light more strongly than does the surrounding tissue, and infrared photography has had some success in delineating the superficial vascular patterns for the diagnosis of diseases that result in morphological changes in the superficial venous system. Photographs in the visible spectrum are capable of delineating colorimetric patterns of the skin. For some diseases these patterns can be useful diagnostic aids throughout treatment.

A particularly important application of diagnostic photography motivated the development of a new multispectral imaging apparatus incorporating numerical filtering. In the treatment of burns it should be possible to monitor the coagulation of the deep dermal plexus to indicate full-thickness burn and thereby accelerate the diagnostic process and treatment by weeks. The information will allow the physician to remove the proper amount of tissue from the needed areas early in the treatment to accelerate healing without the danger of removing viable tissue that should remain to aid the healing process.

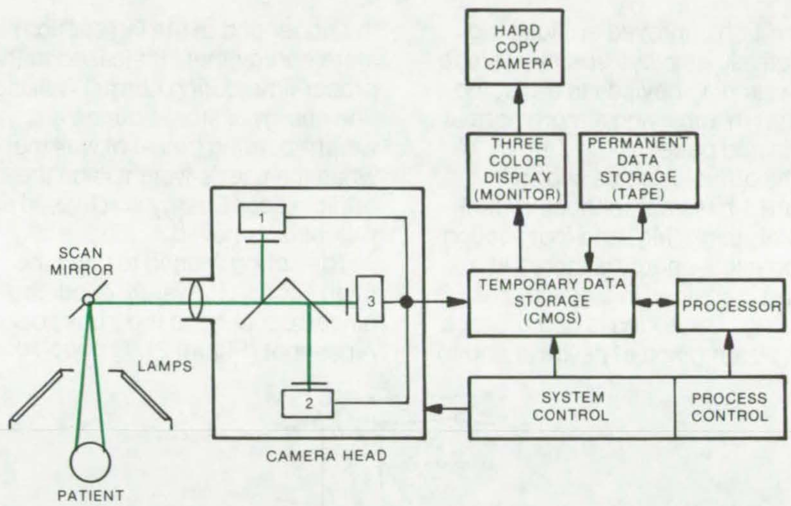

The **Multispectral Imaging System** has three separate imaging detectors with different filters covering the spectral range of interest for a particular diagnosis. These detectors, which are linear arrays of silicon photodiodes, produce an image by measuring spectral reflectance as the detector is scanned over the target area. The three separate images are digitized, and stored by a digital processor. The processor is controlled by a microcomputer and performs all required data storage, processing, and display. Brightness histograms are calculated for each image, and these are used to select the appropriate contrast enhancements. Finally, the processor calculates ratios of the various spectral images and displays the ratios as false-color images from which the diagnosis can be made.

The overall system as shown in the illustration uses three separate imaging systems and operates in near real time. Three single-color images are produced and then combined to give a profile of the damaged area. In the case of burn studies the system shows full-thickness injury as various degrees of white and yellow; deep partial-thickness injury appears red and shallow partial-thickness injury appears blue.

This work was done by Victor J. Anselmo of **Caltech/JPL.** *For further information, Circle 62 on the TSP Request Card.*

Inquiries concerning rights for the commercial use of this invention should be addressed to the Patent Counsel, NASA Resident Legal Office-JPL [see page A8]. Refer to NPO-13922.

An Artificial Leg for Hip Disarticulation

A mechanical leg that uses an energy-storage device can simulate normal-walking movements.

Ames Research Center, Moffett Field, California

A much improved artificial leg effectively employs energy-storage and damping devices to assist the wearer in achieving a more normal stride and pace.

The artificial leg as shown in Figure 1 has interconnected trunk-socket, thigh, leg, and foot sections. Mechanical energy is stored in a spring contained in a cylindrical housing. The spring is compressed by a piston (fixed at its lower end to the upper end of the leg section) to store energy that is released at the proper time during normal walking. The energy is stored during a weight-bearing phase of walking, when the user's weight is on the artificial leg. Energy is released as weight is removed.

The spring is used to pivot the thigh section forwardly about the hinged coupling to the trunk socket. A dashpot (Figure 2), is coupled between the lower end of the thigh and the heel sections to damp the bending movement of the knee joint. The damping action, which occurs after a predetermined amount of ankle movement, is activated by a foot stop. This coordinated release of stored energy and damping result in a more normal step and rate of walking.

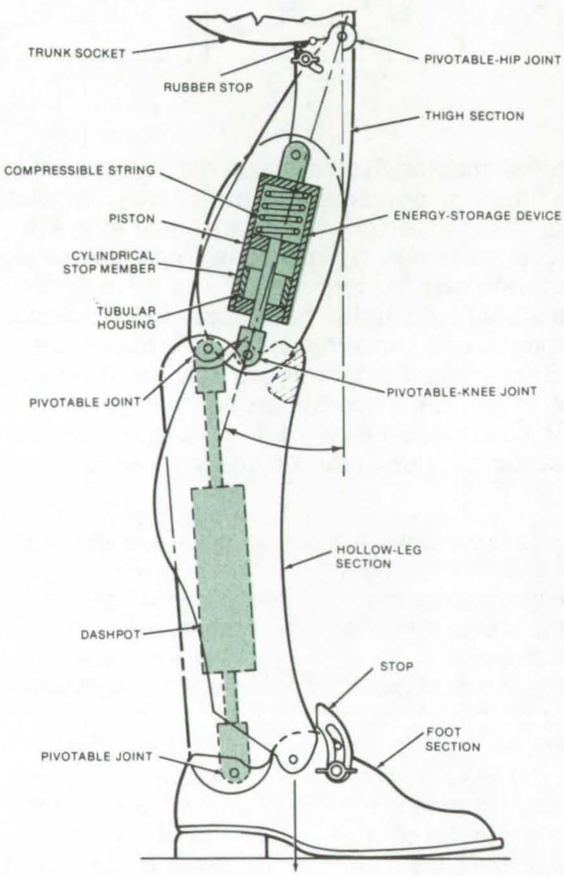

Figure 1. The **Artificial Leg** uses an energy-storage device that is adjusted to produce a moment about the hip joint. When the angle θ between a line connecting the hip joint to the knee joint falls approximately 20° rearward of a vertical line passing through the hip joint, the forward moment exerted by the energy-storage device on the thigh section about the hip joint is near zero. However, as the thigh section pivots forward relative to the hip joint, the moment about the hip joint increases, reaching a peak at an angle θ of approximately -4°. The moment then falls off until the stop engages the piston. This prevents further transfer of energy from the energy-storage device to the thigh section. This occurs at an angle θ of approximately +5°.

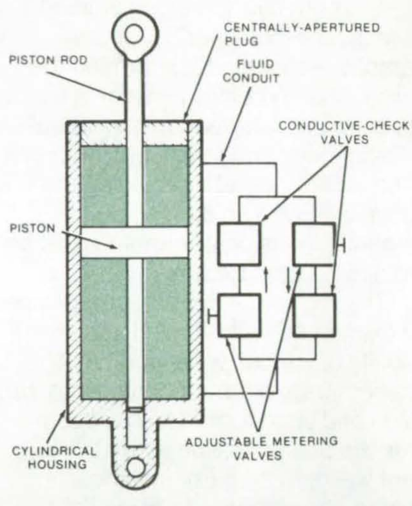

Figure 2. The **Dashpot** is a cylindrical housing with oil-filled compartments on opposite sides of the piston. Metering valves adjust resistance to the fluid flow between compartments in response to piston movements.

This work was done by Wilbur C. Vallotton of **Ames Research Center.** *For further information, Circle 63 on the TSP Request Card.*

This invention is owned by NASA, and a patent application has been filed. Inquiries concerning nonexclusive or exclusive license for its commercial development should be addressed to the Patent Counsel, Ames Research Center [see page A8]. Refer to ARC-10916.

Mechanics

Indicated Mean-Effective Pressure Instrument

Real-time measurement of IMEP
and mass flow in an engine cylinder

Lewis Research Center, Cleveland, Ohio

A new instrument capable of measuring and calculating in real time the indicated mean-effective pressure of internal combustion engines has been designed and tested. In comparison tests, the values of indicated mean-effective pressure (IMEP) obtained by the new instrument were found to be in excellent agreement with values obtained by previously existing post-run data-reduction techniques.

The instantaneous work performed by the engine is the product PdV, where P is the cylinder pressure, and V is the swept-cylinder volume. The integral of PdV for one complete engine cycle divided by the total swept-cylinder volume is called the indicated mean-effective pressure (IMEP). The IMEP has not previously been available as a real-time measurement, severely limiting its potential as an analysis tool and precluding its use as a control parameter for optimizing engine performance.

One early method of measuring IMEP was by directly recording on paper a pressure-volume (P-V) diagram by using various mechanical linkages which connected the recording pen to the piston and pressure measuring devices. The resulting P-V diagram was then cut out and weighed to measure the enclosed area. Later developments included the use of mechanical planimeters for measuring this area, the development of electronic volume transducers, the use of oscilloscopes to display the P-V diagram in real time, and the use of cameras to record the P-V diagram for analysis. More recent efforts have been the use of high-speed digital recorders and computerized analysis.

Despite the relative sophistication of recent techniques, all of these methods involve post-run data reduction. Present research at the Lewis Research Center in the areas of engine efficiency, fuel economy, pollutant reduction, and overall performance analysis has necessitated the development of an instrument for the measurement of IMEP in real time.

The new instrument calculates IMEP according to the following equation:

$$\oint PdV = \int_{\theta=0}^{4\pi} P\left(\frac{dV}{d\theta}\right) d\theta$$

where θ = engine crank angle.

In this form the function $dV/d\theta$ can be determined empirically from the engine geometry and does not need to be calculated in real time.

The instrument approximates the continuous integral by the summation

$$\sum_{n=0}^{1023} \left| P\left(\frac{dV}{d\theta}\right) \right|_{\theta=n\Delta\theta} \Delta\theta$$

where $\Delta\theta = \dfrac{4\pi}{1024}$ rad

Since $dV/d\theta$ can be determined empirically as a function of θ, it can be stored in the instrument. The calculation is then made by measuring θ, obtaining the correct value of $dV/d\theta$ from the stored information, multiplying this value of $dV/d\theta$ by the instantaneous cylinder pressure, and computing the summation. The crank angle is measured with an optical shaft encoder which is connected to the engine crankshaft. The cylinder pressure is measured with a conventional pressure transducer.

The functional block diagram is shown in Figure 1. A more detailed block diagram of the instrument with components as built is shown in Figure 2. The shaft angle encoder generates a 10-bit binary code representing shaft angle in (720/1024) degree increments. The $dV/d\theta$ function is stored in a preprogramed read-only memory. The binary encoder crank angle is used as the address to the memory. The output of the memory is a binary digital value of $dV/d\theta$ for that value of θ. The memory output is multiplied by

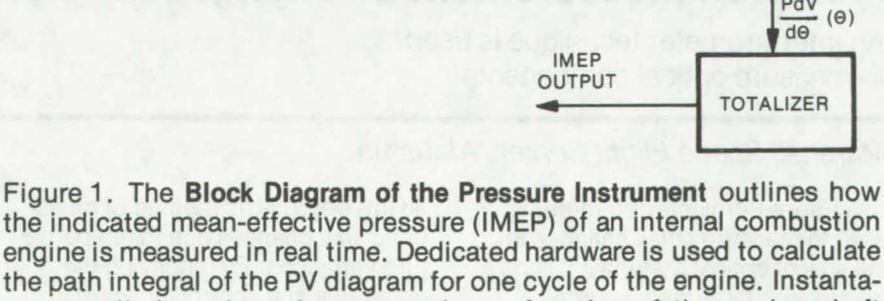

Figure 1. The **Block Diagram of the Pressure Instrument** outlines how the indicated mean-effective pressure (IMEP) of an internal combustion engine is measured in real time. Dedicated hardware is used to calculate the path integral of the PV diagram for one cycle of the engine. Instantaneous cylinder volume is measured as a function of the engine shaft angle, and instantaneous pressure is determined from a transducer on the engine.

(continued on next page)

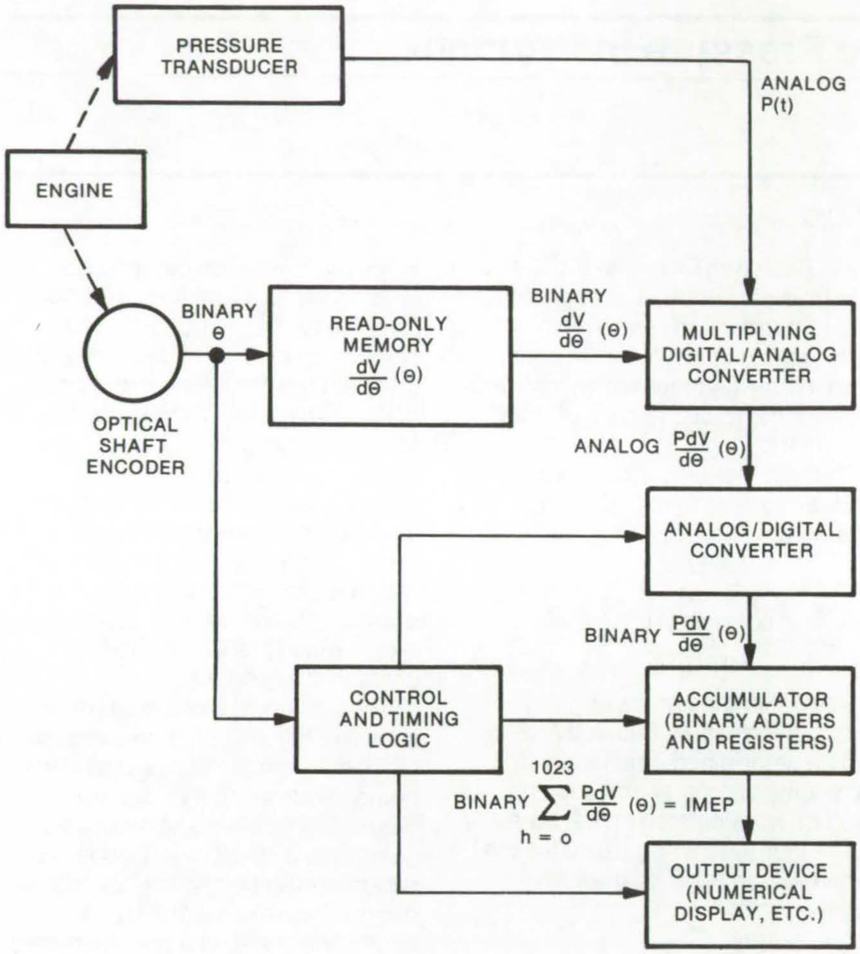

Figure 2. The **IMEP Calculation** is based on an analog signal from the pressure transducer and a digital shaft-angle signal from an optical encoder. The shaft-angle signal is converted to a volume differential by a read-only memory in which angle/volume relationships are stored. The pressure and volume data are multiplied in a combination D/A converter and multiplier. After conversion to a digital signal, the product is integrated by a summation approximation. The summation variable, n, (and thus timing) is based on the shaft-angle position.

the pressure signal, P, using a multiplying digital-to-analog converter resulting in an analog output signal proportional to PdV/dθ. This signal is then converted to a digital binary value with an analog-to-digital converter and added to the accumulator. This process is repeated 1,024 times during a single engle cycle.

The components shown in Figure 2 represent a hybrid digital/analog approach. Many variations are possible, ranging from total analog to total digital implementations. For example, analog function generators could be used to generate dV/dθ, or a digital multiplier could be used if the pressure signal was digitized.

Although the instrument was designed specifically to approximate the integral:

$$\int_{\theta=0}^{\theta} P\left(\frac{dV}{d\theta}\right)d\theta$$

it can generally compute the integral:

$$\int_{x=x_0}^{x} Y(t)F\,[x(t)]dx$$

where F is any single-valued function of X. Specifically, this instrument could be used to provide measurements of mass flow in an engine cylinder. Another application is the measurement of the release energy of a nonlinear spring.

This work was done by William J. Rice of **Lewis Research Center.** *For further information, Circle 64 on the TSP Request Card.*

Inquiries concerning rights for the commercial use of this invention should be addressed to the Patent Counsel, Lewis Research Center [see page A8]. Refer to LEW-12661.

Precision Measurement of Changes in Physical Dimensions

An interferometer technique is used to measure optical components.

Marshall Space Flight Center, Alabama

A Fabry-Perot interferometer is used to measure small changes in the size of optical materials. Using a frequency-stable laser source, precision is one part in 10^9.

The technique is an extension of an interferometric method of measuring size changes due to temperature variations. By modifying the apparatus and controlling for or calculating the effects of temperature, very small size changes due to other causes may be measured. [Shrinkage in 1-in. (2.5-cm) fused-silica and glass-ceramic blocks has been found to be about one part in 10^6 over a 3-year period.] Successful measurements have been

(continued on next page)

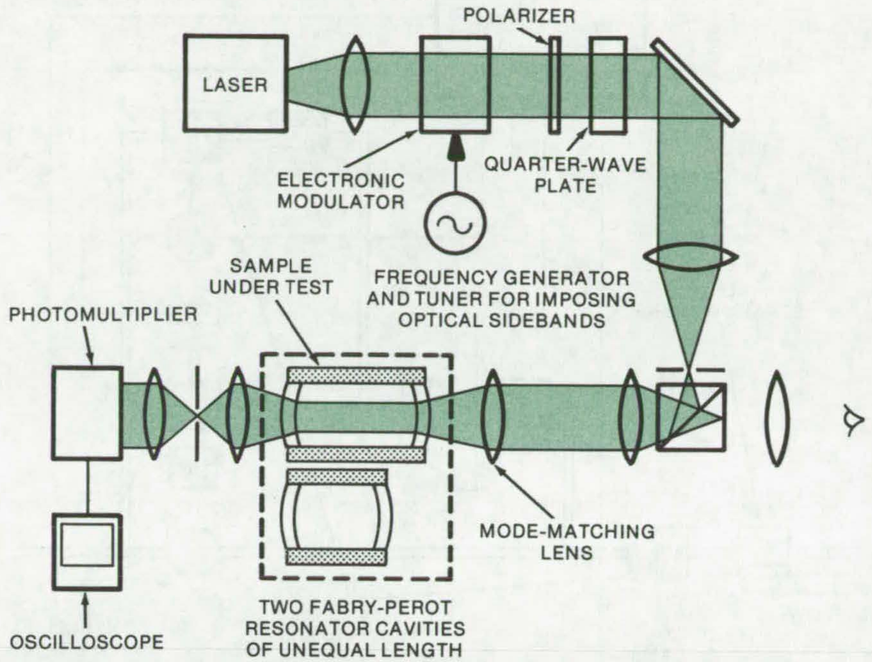

Apparatus for Monitoring Cavity Resonances of eight pairs of confocal resonators: The difference in cavity resonance frequencies $\Delta\nu 2 - \Delta\nu 1$ measures only nonvolume changes (the temporal changes in optical phase shift on reflection plus dimensional changes in the optical contacts that attach the mirrors to the sample spacer).

made on vitreous silica and glass-ceramic materials.

The basic technique is to shine a frequency-stable laser through an optical resonator with the resonator mirrors spaced by the sample material. Using the experimental arrangement shown in the illustration, tunable optical sidebands are impressed on the laser beam. These are used to track, in the electrical frequency domain, drifts in the optical sideband caused by changes in the spacing between the resonator mirrors (thus, changes in the dimension of the mirror spacers under test).

When the technique is used to determine thermal expansion, the sample is heated. Changes in the electrical sideband modulation frequency required to maintain peak transmittance through the resonator are directly related to the expansion coefficient. However, when the technique is adapted to longer-duration experiments to determine dimensional stability over time, complications arise. Specifically, any optical phase shifts that occur with time introduce significant error, as they do not cancel out but rather add up.

This problem is overcome by using parts of Fabry-Perot resonators with unequal lengths as shown in the illustration. It is then possible to evaluate and correct for these phase shifts. A valuable byproduct of this new technique is a method of measuring both the stability of optical phase shifts upon reflection from multilayer stacks and the dimensional stability of optical contacts.

The use of two resonator cavities allows optical-phase-shift data to be separated because, in this experiment, the resonator frequency shifts due to volume changes are identical, irrespective of cavity length. Thus, the difference in the two cavity resonance frequencies is related only to nonvolume changes. These can be identified as temporal changes in the optical phase shift occurring upon reflection plus the dimensional change in the optical contacts that attach the mirrors to the sample spacer under test.

In performing the experiment, it is necessary to measure or control thermal expansion to within 0.002° C. The optical alinement of the apparatus must be precise and reproducible. With these controls and a suitably stable laser, size changes on the order of one part in 10^9 are measurable.

This work was done by J. W. Berthold III, S. F. Jacobs, and M. Norton of the University of Arizona for **Marshall Space Flight Center.** *For further information, Circle 65 on the TSP Request Card.*
MFS-23527

Automated Secondary Standard for Liquid Flowmeters

Calibration time is reduced from 1 hour to 15 minutes.

Lewis Research Center, Cleveland, Ohio

An automated secondary standard for calibrating liquid flowmeters greatly reduces manpower requirements for routine weight/time standard calibrations. Accuracies of flowmeter calibrations using this secondary standard are approximately 99.75 percent. Calibration requires about 15 minutes, compared to about an hour using a conventional primary standard.

This secondary standard utilizes an array of calibrated master turbine-type flowmeters covering the flow range of 0.0004 to 19 l/s (0.007

(continued on next page)

to 300 gal/min). The master flowmeters are built into two manifolds, each consisting of three flowmeters and two electrically operated valves connected in a series-parallel arrangement. One manifold calibrates flowmeters from 0.0004 to 0.6 l/s (0.007 to 9 gal/min); the other manifold calibrates flowmeters from 0.02 to 19 l/s (0.25 to 300 gal/min). A schematic drawing of one of the manifold systems is shown in the figure.

The flow controller and readout accommodate the output of the three flowmeters. Depending on the flow rate, internal logic circuitry adjusts the electrically operated valves to select the proper master flowmeter and also to display the output of the selected meter. Additional features include the choice of automatic or manual control and the availability of thumb switches on each channel to adjust the time base for displaying the output in engineering units.

The meter to be calibrated is installed between any system capable of producing a steady and even temperature flow, such as a primary standard system, and this secondary standard. The temperature of the fluid is brought to the standard temperature [297 K (75.2° F)], and the output of the test meter is examined on an oscilloscope to verify that the meter is functioning properly. The flow rate is adjusted to the full scale of the test meter and is held long enough to record the frequency of the test meter, the frequency of the master meter, and to identify which master is in use. Between 12 and 15 flow settings equally spaced on a logarithmic scale cover the range of the test meter. The data are printed out both in a table and on a plot. Since the final calibration curve is presented on a rectilinear plot, the data are more closely spaced at the low end of the range, and thus the "knee" or dropoff of the curve is better defined. The data reduction and plotting of the results are done by computer.

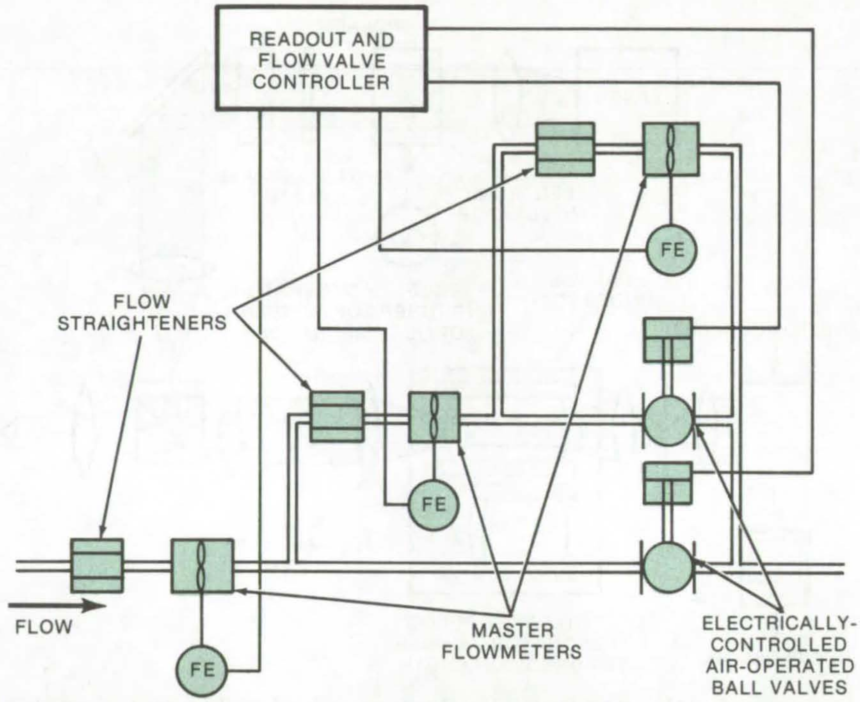

The **Manifold System** incorporating the master flowmeter consists of three flowmeters and two electrically operated valves connected in a series-parallel arrangement. Each flowmeter comprises two manifold systems like the one shown above.

The secondary standard can also be used for testing or setting flow switches and determining the C_V of valves.

This work was done by Howard F. Hobart of **Lewis Research Center.** *Further information may be found in NASA TM-X-71876 [N76-18404], "An Automated Secondary Standard for Calibrating Liquid Flowmeters," a copy of which may be obtained at cost from the New England Research Application Center [see page A7].*
LEW-12695

Nondestructive Interior Examination of Moving Parts

A proposed X-ray audio system could reveal particles not detectable by X-ray alone.

Marshall Space Flight Center, Alabama

A highly sensitive microphone and an amplified audio system have been suggested for use in conjunction with X-ray nondestructive testing to detect foreign particles inside moving hardware when the particles cannot be located by X-ray alone. The application can be made at the same time the X-ray operation is being performed by placing a highly sensitive microphone adjacent to the hardware. As the hardware is rotated through X-radiation, the movement will dislodge loose particles (e.g., weld spatter, chips, etc.). These could be detected by the microphone and the corresponding signal transmitted through an amplified audio system.

This work was done by F. A. Baker of Rockwell International Corp. for **Marshall Space Flight Center.** *For further information, Circle 66 on the TSP Request Card.*
MFS-23378

Flange Weld Pressure Testing

Device proof tests a pipe flange weld without disturbing the rest of the piping system.

Marshall Space Flight Center, Alabama

The integrity of a flange weld on the end of a pipe is easily checked with a tool that allows a localized high-pressure proof test. The accompanying drawing shows the tool in use; it plugs the pipe behind the weld and at the face of the flange and provides access for applying high gas pressure in between. This tool has been used to proof test a weld on a 2-inch (5-cm) pipe to 18,000 psi (1.2×10^8 N/m^2).

The use of this tool eliminates the need to block off the far end of the pipe. Only a small area needs to be cleared of personnel for the proof test, and only a small quantity of pressurizing gas is needed.

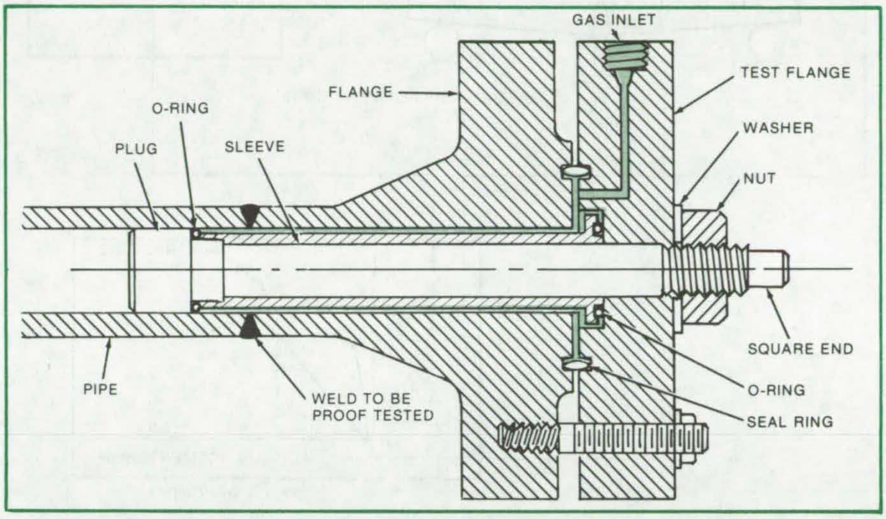

The **Weld Is Pressure Tested** conveniently by use of the tool, which seals off the volume of pipe containing the weld and admits high-pressure gas into that volume.

To perform a test, the seal ring is mounted in the flange, and then the plug, O-rings, sleeve, test flange, washer, and nut of the tool are loosely assembled and inserted into the pipe. The flange studs and nuts are installed and tightened so that the seal-ring joint is pressure-proof. Then the plug is held by its square end while the nut is tightened to compress the O-rings; the ring between the sleeve and the plug is forced against the inner wall of the pipe to provide a pressure seal, and the other ring seals the sleeve-to-test-flange interface. The sealed-off volume between the two O-rings and the seal ring is then pressurized through the gas inlet.

This work was done by C. F. Holden of Rockwell International Corp. for **Marshall Space Flight Center.** *For further information, Circle 67 on the TSP Request Card. MFS-19292*

Ultrasonic Monitoring of Crack Extension

New method does not interfere with fracture toughness tests.

Lewis Research Center, Cleveland, Ohio

It is difficult to detect the onset of crack extension and to monitor crack growth in materials undergoing fracture toughness tests without interfering with the progress of the test. During such testing, the usual test record of load versus load-displacement does not distinguish between the processes of plastic deformation and crack extension, particularly for the tougher, more ductile materials. Consequently, a system consisting of a commercial ultrasonic flaw detector with a transducer clamped to the specimen and an x-yy′ recorder has been developed to provide a permanent record of crack extension which results in a clear indication of the onset of cracking that is relatively insensitive to plastic deformation.

Acoustic energy in the form of high frequency waves is transmitted from the ultrasonic transducer into the test specimen in a direction normal to the plane of the starter notch (fatigue crack). The acoustic mismatch at the metal/air interface of the fatigue crack causes partial reflection of the ultrasonic energy impinging on it. The amount of energy reflected from the crack back to the transducer is directly related to the crack surface area, the intensity of the incident ultrasonic wave, and the tightness of the crack.

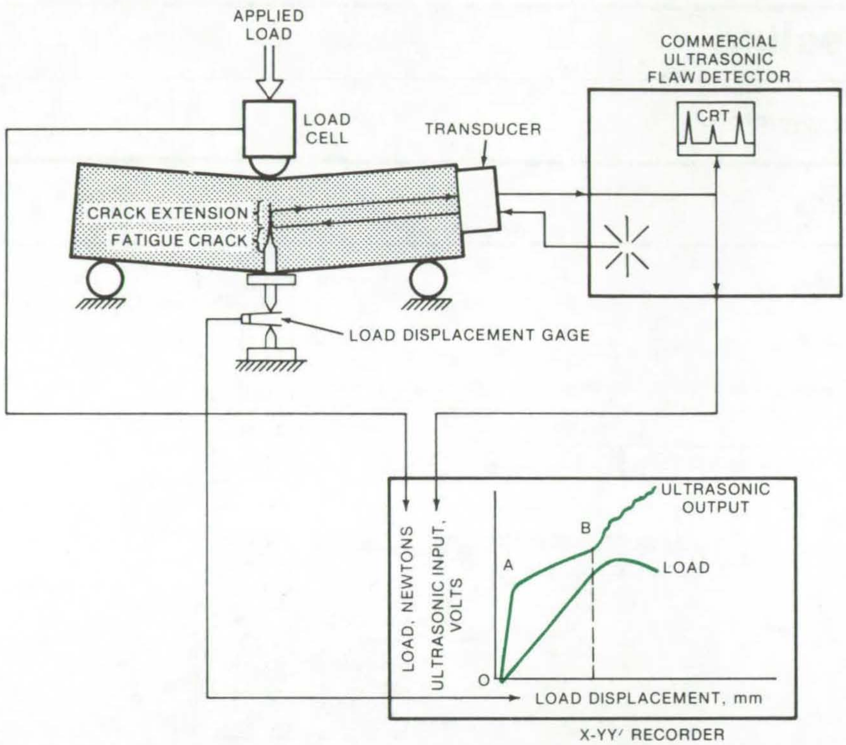

Schematic of System for Monitoring Crack Extension

A typical transducer/specimen arrangement is shown in the sketch. The transducer is used both as a sender and receiver. A coupling agent such as glycerin, silicone, or petroleum lubricant is used to transmit energy across the transducer/specimen interface. The signals received from the crack are amplified and displayed as a voltage spike on the cathode-ray tube in the commercial flaw detector. The amplitude of the voltage spike, after passing through a time gate, is recorded on the y-axis of the recorder. Specimen displacement in the loading direction is measured by means of a piston and cylinder device which incorporates a standard double-cantilever beam-displacement gage as the transducer. The output is recorded on the x-axis. The applied load is simultaneously recorded on the y′ scale by utilizing the output from a load cell in the testing machine.

The ultrasonic output voltage versus load-displacement curve is generally composed of three parts. The portion of the curve from O to A represents a rapid increase in ultrasonic voltage level due to the opening of the fatigue starter crack. The second stage, from A to B, shows a less rapid voltage rise, possibly due to plastic deformation. At point B, the curve typically exhibits an abrupt increase in slope indicative of onset of crack extension. Further application of load to the specimen causes increased crack extension with a proportional increase in ultrasonic voltage output due to the increasing crack area. Onset of crack extension at point B was confirmed metallographically by sectioning selected specimens. Note that crack extension is signaled by the ultrasonic voltage output curve long before any indication can be observed on the load versus load-displacement curve (see dashed line).

This system can be potentially applied to any material part that contains a starter flaw that might be expected to propagate and form a larger crack.

This work was done by Stanley J. Kliman, Douglas M. Fisher, and Robert J. Buzzard of **Lewis Research Center.** *Further information may be found in NASA TM-X-71754 [N75-30606], "Monitoring Crack Extension in Fracture Toughness Tests by Ultrasonics," a copy of which may be obtained at cost from the New England Research Application Center [see page A7].*
LEW-12632

Mechanical Loader for Testing Composites

Fixture applies constant preload
to environmentally cycled specimens.

Lewis Research Center, Cleveland, Ohio

To evaluate the performance of composite structures under varying temperature and humidity environments, it is necessary to test coupons of the basic laminate under the anticipated mechanical and environmental loading conditions. The application of mechanical loading to large numbers of coupons subjected to environmental cycling requires the design of a compact, rugged, and reliable fixture.

Since mechanical loading with dead weights is cumbersome and impractical in view of the high loads required and since hydraulic loading is feasible but is not very versatile and requires expensive fixturing, the concept of simple and reliable spring loading in individual fixtures was adopted.

The figure shows the construction and dimensions of a typical fixture. Each fixture is used to load a single specimen and consists basically of a reaction frame,

(continued on next page)

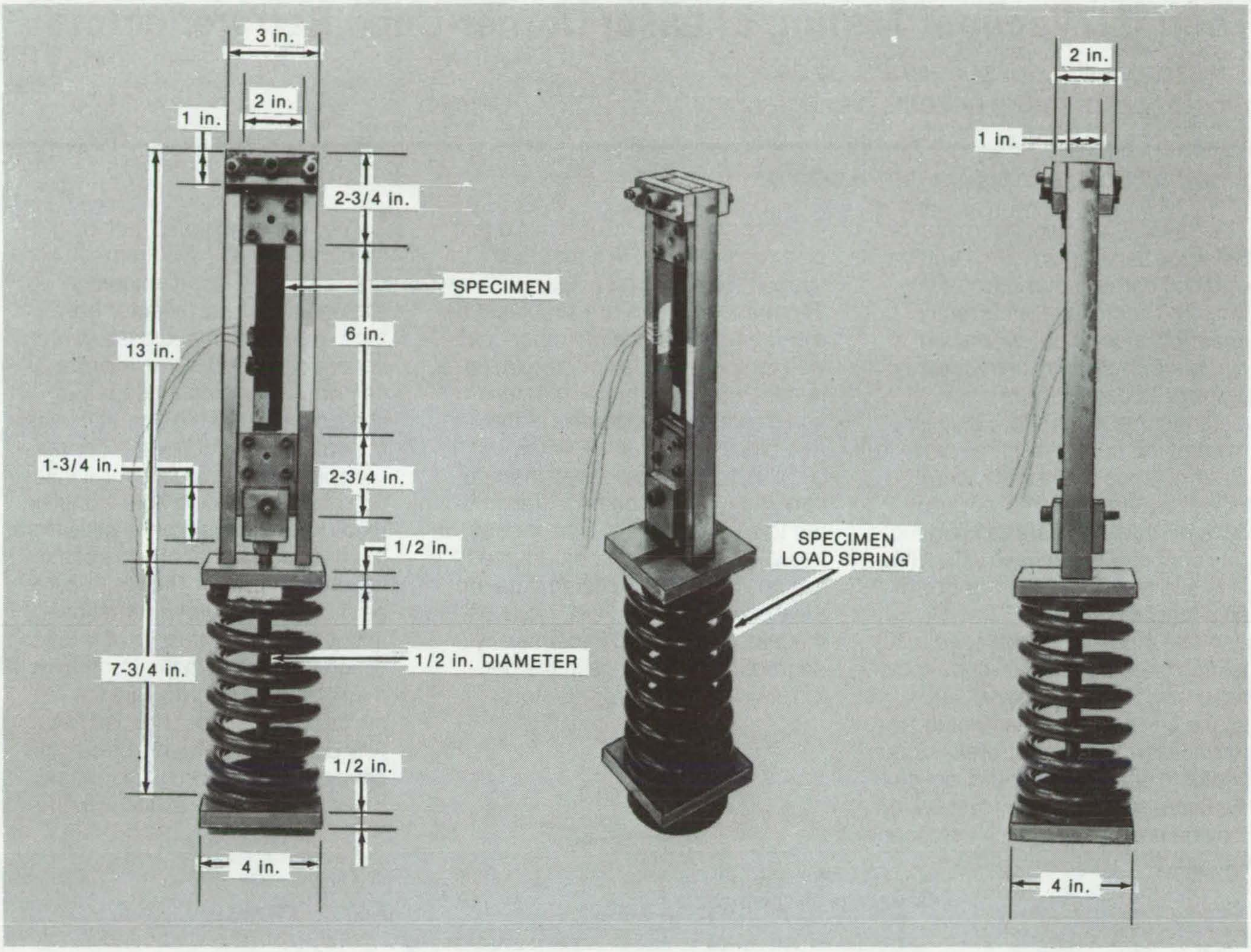

The **Spring-Loading Fixture** was designed to facilitate the application of a controlled-tensile preload during thermal-cycling tests.

screw-clamped gripping jaws, loading coil spring, and a threaded loading rod with a clevis link. Mounting and loading of the specimen require a careful procedure. To insure the alinement of the specimen axis with the central pivot holes of the jaws, the specimen is clamped in the jaws in an alining jig outside the loading fixture. The specimen with the clamped jaws is then mounted in the reaction frame, the clevis and loading rod are attached, and the coil spring is slipped over the rod. The clamping jaws fit closely between the longitudinal bars of the reaction frame to prevent twisting of the specimen during spring loading. The spring is compressed in a testing machine to a predetermined calibrated length, and the nut on the rod is tightened against the spring-loading plate. Release of the test-machine load transfers the spring load to the specimen. The loading spring for each specimen is selected with a sufficiently large deflection to insure that thermal expansion during subsequent thermal cycling does not change the specimen load significantly.

This work was done by Isaac M. Daniel and Theodore Liber of IIT Research Institute for **Lewis Research Center.** *Further information may be found in NASA CR-134826 (N75-30264), "Lamination Residual Stresses in Fiber Composites," a copy of which may be obtained at cost from the New England Research Application Center (see page A7).*

Further information may also be found in "The Effects of Thermal Cycling on Advanced Composite Angle-Ply Laminates" by T. Liber, I.M. Daniel, and C.C. Chamis, Proceedings of the 30th Annual Technical Conference of the SPI Reinforced Plastics/Composites Institute, Washington, D.C., February 4-7, 1975.

Lew-12432

Thermal/Vacuum Testing of Laser Corner-Cube Retroreflectors

A test procedure for optimum cube design records beam-return patterns photographically.

Marshall Space Flight Center, Alabama

A transmitted laser beam can be reflected back to its source station by using corner-cube retroreflectors. This technique is currently under consideration for use with a number of transmission measuring systems to determine precise distances between sites. Measurement of the total travel time permits determination of the distance. However, large thermal perturbations or gradients generated in the retroreflector when used with satellites can result in optical-performance degradations.

A test procedure developed for testing uncoated corner-cube retroreflectors under simulated aerospace environments has yielded information about the retroreflectors useful to designers of other optical systems, suggesting the test system may be useful outside the aerospace industry.

Retroreflectors mounted in a test block are installed in a thermal/vacuum chamber (see figure). Thermal conditions are simulated by a combination of the chamber cold-wall temperature, solar-simulation lamps, infrared-simulation lamps, and direct thermal control of the test-block temperature. After stabilization at the desired thermal condition, a laser beam is transmitted to a retroreflector, and the return beam is viewed and photographed. Various beam photometric data are measured in the far field. None of the tests were found to cause any degradation or change in the performance of the retroreflectors.

Thermal conditions (including predicted worst-case thermal gradients) and laser incidence angles at the retroreflector front face were varied, and data were obtained for six different retroreflectors. Heat is controlled by a shroud on the test fixture. It consists of heat-exchanger coils, a copper baseplate, and a multilayer-insulation blanket. A liquid heat-transfer medium is pumped to the coils from the heat exchanger outside of the vacuum chamber. The test fixture controls the angular orientation about the horizontal axis of rotation, which is in line with the front faces of the retroreflectors (to vary the incident-laser-beam field angle). Any one of the three retroreflector-cavity locations can be placed on the rotational axis, in line with the

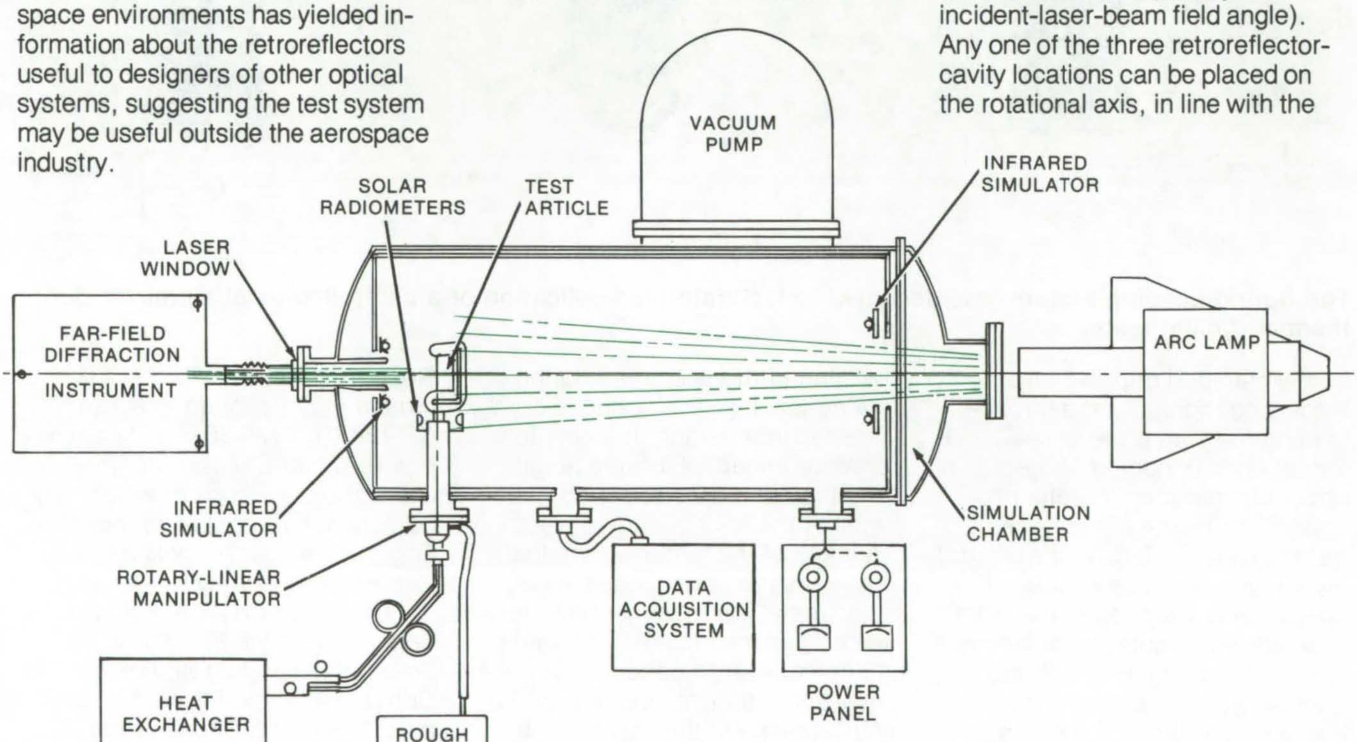

The **Thermal/Optical Test Setup** uses a far-field diffraction instrument. It contains the necessary equipment for generating a linearly-polarized laser beam and projecting the beam at the test article. It accepts the return beam from the test article and provides a visual display and photograph of the far-field diffraction pattern and a means of measuring the relative intensity of the return pattern, in a selected annular region. It also measures the relative intensity of the transmitted beam and the ratio of the return-beam intensity to the transmitted-beam intensity. The orientation of the linearly polarized beam can be controlled, and a circularly polarized beam can be selected for transmission to the test article.

(continued on next page)

laser beam at the chamber centerline. The control of angular orientation and longitudinal location is accomplished manually from outside the chamber.

Each group of three retroreflectors is manually set up on the rotational axes prior to their respective tests. Thermocouples are mounted at the apex, front face center, and tab outer edge on each similar retroreflector, on mounting rings, and on the front face of the test panel. A solar radiometer measures intensity of the solar-simulator beam, and a separate radiometer is used for intensity of the infrared simulator.

This work was done by The Bendix Corp. for **Marshall Space Flight Center.** *For further information, Circle 68 on the TSP Request Card.*
MFS-23565

Acoustic Testing of Materials

Sound-absorption coefficients can be measured with or without an anechoic chamber.

Langley Research Center, Hampton, Virginia

Most measurements of sound-absorption coefficients for oblique angles of incidence are either interference methods or are methods based on the determination of small differences between large signals. Interference methods are not suitable for testing materials with large absorption coefficients, as they rely on measuring wave-interference maximums and minimums that will be quite small if there is little reflection.

Difference techniques are either complex and expensive or are sensitive to small changes in geometry, tracking-amplification factor, and other variables. These drawbacks are overcome by a new method that is simple and accurate.

In this method, sound pressure-level recordings are made in an anechoic chamber with the configurations shown in the illustrations: (a) directly, (b) with a line-of-sight barrier, and (c) with a line-of-sight barrier and the sample in place. Without the barrier and sample, the output signal of the receiver, $p_1(f)$, is a function of distance d_1, the wave number in air, and F(f), a function describing the frequency dependence of the source/receiver system.

With the barrier in place without the sample, the receiver output, $p_2(f)$, is a function of d_2, F(f), the phase change due to the barrier, and $|B(f)|$, which is the absolute value of the barrier attenuation.

The receiver output with both the barrier and sample in place, $p_3(f)$, is a function of F(f), $p_2(f)$, d_3, the phase angle of the reflection factor, and $|R(f)|$, the absolute value of the reflection factor of the sample for the particular angle of incidence.

By properly combining the expressions for $p_1(f)$, $p_2(f)$, and $p_3(f)$, one can obtain expressions for $|R(f_{max})|$ and $|R(f_{min})|$, where the subscripts max and min represent the frequencies when the reflected and scattered signals are in phase (max) and 180° out of phase (min).

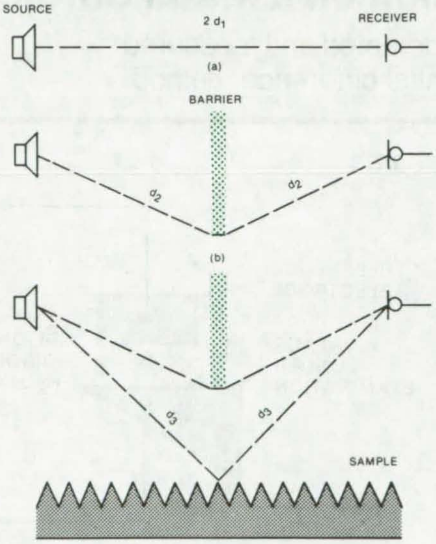

Configurations of the Source, Barrier, Sample, and Receiver are shown for measuring (a) direct response, (b) response with a barrier blocking the line of sight between source and receiver, and (c) response with the barrier and the sample in place. Positioning the lower edge of the barrier at a height equivalent to 1/2 wavelength at the cutoff frequency of the wedges [for the test case about 6 inches (15.2 cm)] prevents interaction effects.

$$|R(f_{max})| = \frac{d_3}{d_1}\frac{|p_2(f_{max})|}{|p_1(f_{max})|}\left[\frac{|p_3(f_{max})|}{|p_2(f_{max})|} - 1\right]$$

$$|R(f_{min})| = \frac{d_3}{d_1}\frac{|p_2(f_{min})|}{|p_1(f_{min})|}\left[1 - \frac{|p_3(f_{min})|}{|p_2(f_{max})|}\right]$$

The sound-absorption coefficient is by definition

$$\alpha(f, \Theta) \equiv 1 - |R(f, \Theta)|^2$$

for angle of incidence Θ.

As can be seen from these expressions, the determination of α requires only the amplitudes of the sound pressure levels (easily recorded on a chart recorder) and d_1 and d_3. No phase information is needed, and the absence of d_2 indicates that the details of how the barrier attenuates sound are inconsequential.

This technique could also be used for in situ measurements of α for concrete, gravel, ground, and other subjects that could not be placed in an anechoic chamber. The direct response of the source/receiver configuration is first recorded in an anechoic chamber at a convenient distance, d_0. From the resulting response curve, the responses for other distances, d_1, can be derived by a distance correction term. For application, one need record only the response curve for configuration (c).

This work was done by Bolt Beranek and Newman Inc. for **Langley Research Center.** *For further information, Circle 69 on the TSP Request Card.*
LAR-11659

Leak Testing Glass Ampoules

Test sensitivity is enhanced greatly by using a mass spectrometer.

Langley Research Center, Hampton, Virginia

Glass ampoules are extensively used in the pharmaceutical and chemical industries for the storage and shipment of solutions of drugs and chemicals, both liquids and gases. Proper sealing of the ampoules is required to maintain the purity, concentration, and often, the sterility of the contents. Common industrial leak-testing procedures consist essentially of determining if a dye can enter the sealed ampoule when it is submerged in a solution of the dye and is exposed to a partial vacuum followed by positive pressure. For many purposes these methods are inadequate. Ampoules passing such tests have been demonstrated to have holes as indicated by the presence of dried material on the outside near the seal. Microscopic examination shows that the holes have external diameters of approximately 40 μm, narrowing to about 3 μm typically.

A more rigorous leak test has been developed to prove the structural integrity and sterility of nutrient-containing ampoules for the Viking Lander Biology Instrument. A helium atmosphere is placed in the ampoule prior to sealing. After sealing and sterilization, the ampoule is tested with a mass-spectrometric leak detector for the passage of helium. Using a mass spectrometer with a sensitivity limit of 1×10^{-10} standard cm^3 of He/s, it is calculated that a hole 0.9 μm in diameter and with a length of 1 mm would be detectable with a leak rate of 3.5×10^{-8} standard cm^3/s. (Bacteria cannot pass through holes this small.) This technique could also be applied with nitrogen, or air atmospheres.

This work was done by Burton J. Kallman of TRW, Inc., for **Langley Research Center.** *No further documentation is available.*
LAR-11988

Detecting Contamination on a Metal Surface

Thin layers of foreign matter are detected and measured by a noncontacting surface-potential difference method.

Marshall Space Flight Center, Alabama

The presence of a thin layer of contaminant on a metal surface can be detected by measuring the surface-potential difference between a reference electrode and the surface of interest. Films only a few atom-planes thick can be detected by this technique, so it is useful in checking the cleanliness of a surface before electrodeposition or other impurity-sensitive processes.

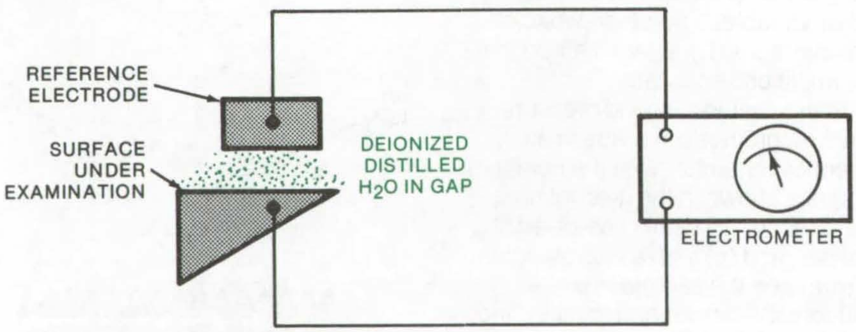

Electrometer Deflection Indicates Impurity Layers on metal surface under inspection by measuring the surface potential relative to the reference electrode. The thickness of the surface layers can be read directly if the meter scale is calibrated against optically determined thicknesses. This surface-potential technique detects contamination that cannot be found by visual methods.

As shown in the figure, the measurement does not require mechanical contact with the surface under examination; the surfaces are wet with deionized distilled water, and the reference electrode serves as an ionization source.

The thickness of the impurity layer can be determined from the surface-potential difference read on an electrometer, along with calibration curves established by methods such as optical interference techniques. The part under inspection is put on a table capable of three-dimensional motion so that the gap can be adjusted; the measurement is performed under controlled temperature and humidity conditions.

This work was done by James M. Harris, Harris L. Marcus, and Tennyson Smith of Rockwell International Corp. for **Marshall Space Flight Center.** *For further information, Circle 70 on the TSP Request Card.*
MFS-19260

Detection of Surface Impurities on Processed Metals

Simple and inexpensive electrolytic conductivity test for cleanliness of metal surfaces

Lyndon B. Johnson Space Center, Houston, Texas

A new method is used to detect impurities on the surfaces of processed metals. The method is based on the measurements of electrical conductivity through a layer of distilled water that has been deposited on the metal surface. Since the impurities are soluble in water, the water conductivity increases, indicating that the metal surface is contaminated.

Metal samples are tested in an apparatus as shown in the illustration. A sample is placed inside a Plexiglas cell resting on a plastic plate. The cell is 5 cm (2 in.) in diameter and has O-rings on top and bottom for a tight seal. Next, an O-ring-shaped Mylar spacer 0.13 mm (5 mils) thick is placed on top of the sample. Approximately 0.5 ml of distilled water is added to the sample surface, and a stainless-steel plate is placed on top. The steel plate and the sample are then connected to a conventional conductivity-bridge circuit. Another plastic plate is placed on top of the entire assembly and is tightened down with bolts.

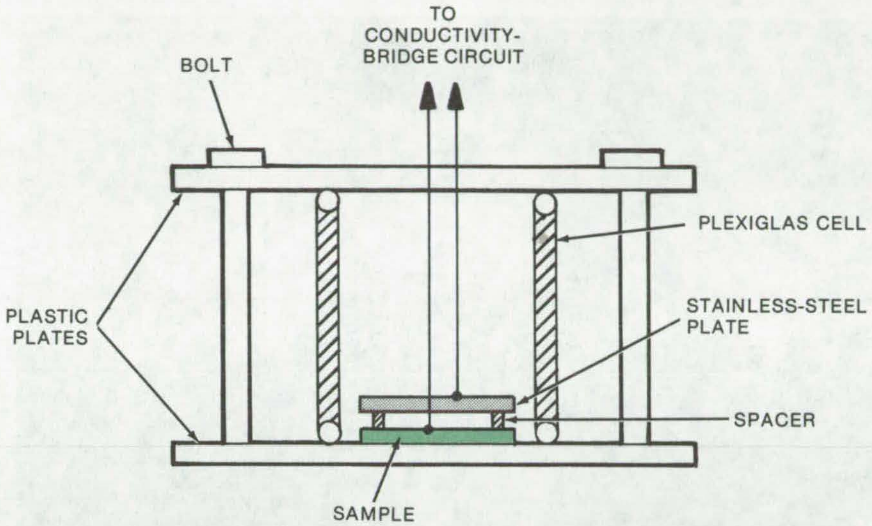

The **Surface-Impurities Test Apparatus** is used to identify the presence of contaminants after chemical processing and improper cleaning, by measuring the conductivity of a thin layer of distilled water applied to the surface of the metal under test.

Conductivity is measured for a period of 15 to 30 minutes, which is sufficient time to allow the surface impurities to dissolve in water. If the conductivity increases, impurities are present. Normally conductivity through clear samples is 5 times less than through those with impurities.

A more sensitive technique is to measure the ac impedance and to calculate the resistance and capacitance of the solution layer at the metal surface. An alternative is the use of a small test piece which is heated in distilled water, the conductivity of which is a measure of contamination. Results are compared with the conductivity of distilled water containing clean samples.

This work was done by John V. Kenkel, Florian B. Mansfeld, Harris L. Marcus, and Neil E. Paton of Rockwell International Corp. for **Johnson Space Center.** *No further documentation is available.*
MSC-19670

Economical Solar Heating for Homes

A do-it-yourself system to supplement existing forced-air heating may be installed by a homeowner. Materials are readily available, no professional skills are required, and costs are low enough to be recovered by savings in fuel. Information on construction and performance is available.
(See page 626.)

Portable, Wind Sensitive, Directional Air Sampler

A programable air sampler, part of a pollution monitoring system, can automatically collect samples from predetermined positions with respect to wind direction. Particles collected on slides for designated time periods are automatically stored for later analysis. Wind speed and direction are also monitored and recorded.
(See page 546.)

NASA Technology Utilization House

NASA's Technology Utilization House incorporates numerous energy-saving features and other aerospace spinoffs. However, it can be constructed from materials and techniques available in today's marketplace. It features solar heating and cooling, improved insulation, a water-recycling system, security and fire-alarm systems, and many other innovations. It is now open to the public.
(See page 625.)

Heat-Transfer Coefficients of Pin-Finned Cylinders

Surface measurements indicate a high heat-transfer rate for variable flow direction.

Lewis Research Center, Cleveland, Ohio

The **Pin-Finned Cylinder** (shown installed in a wind tunnel) can increase the heat-transfer rate to more than 4 times that of a plain cylinder, depending on pin diameter and spacing.

Convective heat-transfer coefficients have been measured on a cylinder 6 in. (15.24 cm) in diameter with pin fins on its surface (see figure). Coefficients were measured on the surface of the cylinder for pin diameters of 0.125 and 0.250 in. (0.3175 and 0.6350 cm), pin spacing of 3 and 4 pin diameters, and pin lengths of 5, 7, and 9 pin diameters. The airflow was normal to the axis of the cylinder with a Reynolds number from 3,600 to 27,750.

Pin-finned cylinders are advantageous when the flow direction is variable because they maintain a high heat-transfer rate compared to annular fins when the flow is not parallel to the fin surface. Although there is much published literature on pin-finned cylinders, heat-transfer data are lacking for pin fins on the surface of a single cylinder. The pins were found to increase the heat-transfer rate from 1.6 to more than 4 times that of a plain cylinder, depending on pin diameter and spacing. The highest local heat-transfer coefficient was obtained at an angle of 45° from the stagnation point, while the lowest local heat-transfer coefficient was obtained at an angle of 135°.

The smallest diameter, closest spacing, and largest pin length-to-diameter ratio gave the highest average effective heat-transfer coefficients. The combinations of pin diameters, spacings, and lengths tested were not sufficient to develop a general correlation.

This work was done by G. James Van Fossen, Jr., of **Lewis Research Center.** *Further information may be found in NASA TM-X-3173 [N75-14990], "Surface Heat-Transfer Coefficients of Pin-Finned Cylinders," a copy of which may be obtained at cost from the Aerospace Research Applications Center, Indiana University [see page A7].*
LEW-12557

Miniature-Angular-Position Transducer

Solar cells are used to monitor rapidly rotating surfaces.

Langley Research Center, Hampton, Virginia

Small precision potentiometers normally used for accurate angular measurements of aircraft-model control surfaces were found to be unsatisfactory because of size and space constraints. Therefore a miniature angular-position transducer, utilizing solar cells, has been designed and built. It has been successfully used to measure rapidly-responding active control surfaces of aeroelastically-scaled wind-tunnel models of aircraft at Langley Research Center. The transducer has a linear response and allows control surfaces to be measured to within 0.10°. Extensive laboratory and wind-tunnel flutter tests have established that the device is both reliable and durable.

The miniature angular-position transducer (see illustration) is simple and inexpensive. It uses two silicon solar cells mounted on a common base and separated by a 0.010-in. (0.025-cm) gap. A housing block 0.9 by 0.6 by 0.4 in. (2.3 by 1.5 by 1.0 cm) with a cylindrical hole isolates the solar cells from external light sources. The cells and their common base are attached to a small shaft, fitted to the inner bore of two, miniature, precision, ball bearings; and the entire assembly is hand pressed into one end of the housing block.

The bearing arrangement allows only rotary motions of the solar cells with respect to a stationary light source mounted in the opposite end of the housing block. A circular piece of ground glass and a half-moon-shaped baffle are located in the center of the housing block in such a way as to illuminate one-half of each solar cell with a uniform light. The arrangement of the illuminated area with respect to the solar cells is shown in the illustration, as is the electrical circuit arrangement. For successful operation, a null position must be

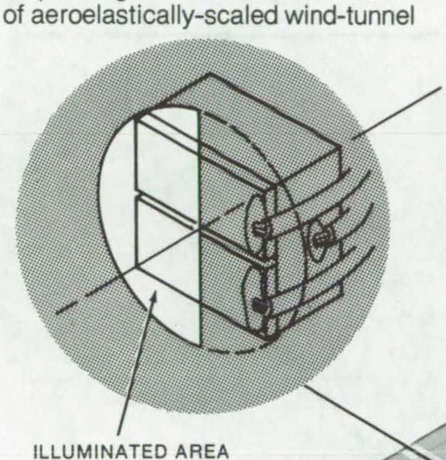

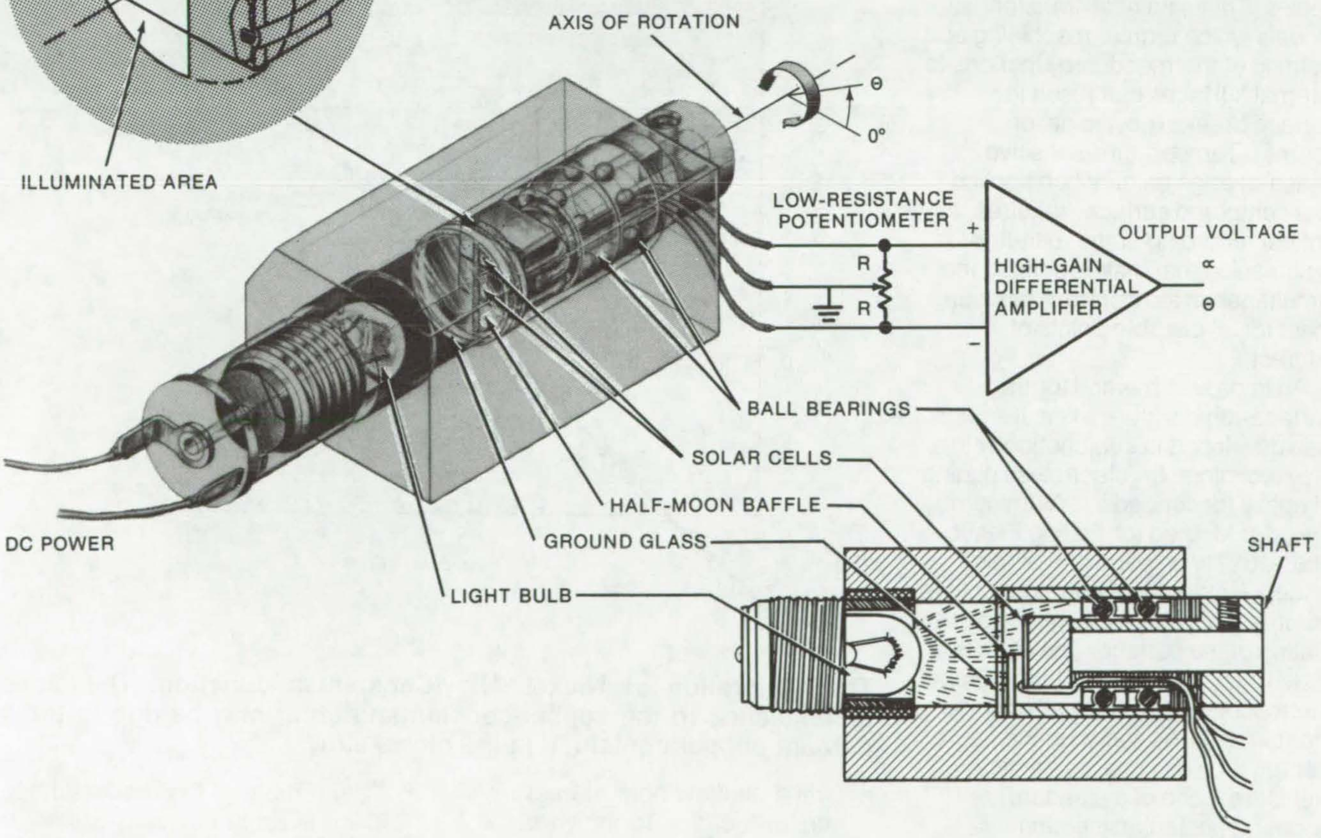

The **Miniature Angular-Position Transfer** was developed to monitor the rapid rotation of the control surface of wind-tunnel models. The shaft is connected to a control surface (not shown) that is being monitored. As the surface rotates, the illuminated portion of the solar cells varies, producing an output voltage proportional to the angular position of the control surface.

(continued on next page)

established by positioning geometrically the straight edge of the illuminated area perpendicular to the gap between the cells. This resultant intersection point must aline precisely with the shaft axis of rotation as shown.

The solar-cell assembly is a three-terminal device that is wired in a bridge circuit with a low-resistance potentiometer to obtain good linearity and to obtain a null output for zero angle. As the control-surface shaft rotates from a zero null position, one solar cell receives more illumination than the other, and thereby a differential voltage between the two cells is produced which is proportional to the shaft rotational angle. This voltage output is amplified by a high-gain differential amplifier, and the output can be related, through a calibration procedure, to the control-surface angular position. Output values as high as 1.0 volt per degree have been obtained and successfully used in critical angular-position feedback circuits.

This work was done by David L. Gray and Maynard C. Sandford of **Langley Research Center.** *For further information, Circle 71 on the TSP Request Card.*

Inquiries concerning rights for the commercial use of this invention should be addressed to the Patent Counsel, Langley Research Center [see page A8]. Refer to LAR-11999.

One-Wire Thermocouple

A nickel alloy/constantan thermocouple can accurately measure surface temperature at precise locations.

Lyndon B. Johnson Space Center, Houston, Texas

The accurate placement of temperature sensors is very critical in many applications; however, for some measurements, especially on complex surfaces, there are difficulties. Thin-skin heat-transfer models which require machining and welding of thermocouple junctions to internal surfaces can result in surface breaks (i.e., joints or seams). Temperature-sensitive, phase-change paint, when applied to a contoured surface, requires optical recording of the melt-line progression that makes difficult the simultaneous temperature measurement for all discrete points of interest.

An improved method for the surface-temperature measurements was developed in conjunction with a new technique for electroless plating of epoxy (described in "Aluminum Transfer Method for Plating Plastic," MSC-16221, on page 000 of this issue). A plate/wire thermocouple is automatically formed by electroless plating of the surface. The plate is a nickel alloy that forms a high-output thermocouple junction with a constantan wire. As shown in the figure, this junction has characteristics similar to those of a standard copper/constantan junction.

The following procedure is used to form the one-wire junctions over a plated epoxy surface:

- Locate the sensor sites on the external surface of a pattern or submaster of the model.

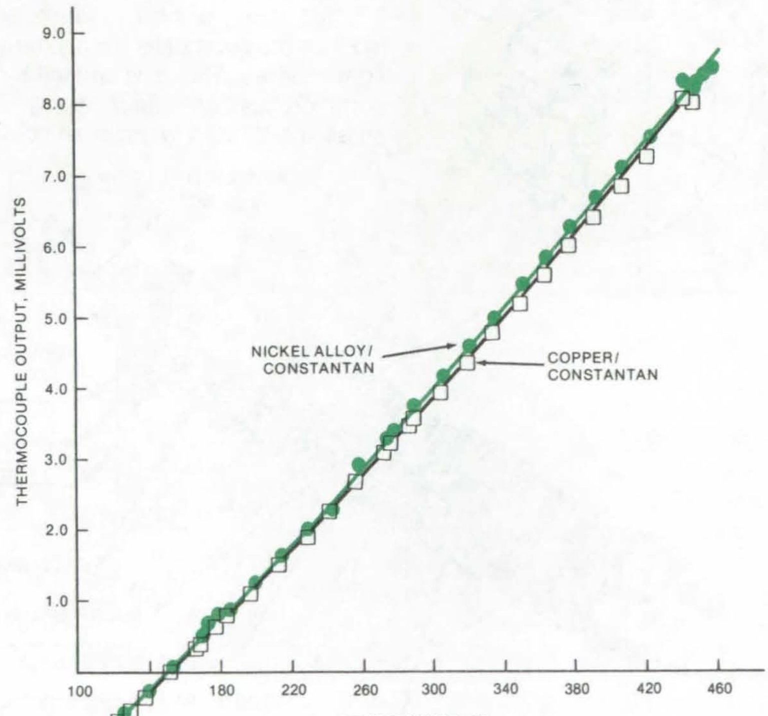

The Calibration of Nickel Alloy/Constantan Junction: The close resemblance to the copper-constantan output may be due to the 1 percent copper contained in the nickel alloy.

- Drill a shallow hole at each sensor location to the wire diameter (e.g., 0.008 cm).
- Insert a short length of wire into each hole with the other ends extending approximately 0.159 cm past the surface.
- Cast a mold of the model with silicone rubber.
- Insert one constantan wire into each hole cast in the mold material.
- Pour the epoxy material into the mold and cure.

(continued on next page)

- Remove the casting, and chemically condition the plastic surface for electroless plating (leaving wires protruding from surface).
- Plate nickel alloy to approximately two-thirds of final plate thickness.
- Clip and polish wires flush to plate surface.
- Reactivate and plate the surface to final skin thickness.

The new one-wire thermocouple improves accuracy, is moderate in cost, and simplifies the fabrication of highly-instrumented seamless-surface heat-transfer models. Features and benefits include:
- automatic formation of surface thermocouple junctions during plating operation,
- continuous outer surface,
- accurate sensor placement,
- close spacing of one-wire sensors, and
- high-output junctions.

The plate/wire thermocouple can also be applied to metal surfaces if the constantan wire has an insulative coat so that it makes electrical contact only with the plate on the model surface.

This work was done by Winston D. Goodrich of **Johnson Space Center** *and Charles J. Stalmach, Jr., of LTV Aerospace Corp. Further information may be found in NASA CR-144364 (N75-29356), "Developments In Corrective Heat Transfer Models Featuring Seamless and Selected-Detail Surfaces Employing Electroless Plating," a copy of which may be obtained at cost from the National Technical Information Service, Springfield, Virginia 22151.*
MSC-16220

Pulse Detector

Simple detector spots opens and shorts during shock and vibration testing.

Lyndon B. Johnson Space Center, Houston, Texas

Mechanical shock, vibration, or acceleration can change the conductive state of electrical and electronic components from a normally open to a closed circuit or vice versa. Although the effect is usually momentary, it may produce a serious system failure. Special laboratory test equipment designed to monitor these changes before the components are put to actual use has been bulky, complex, and not very reliable.

A new pulse detector is a combination of integrated circuits and modular packaging resulting in reduced size and complexity. It has excellent temperature stability and consistent timing accuracy. The range of detected pulse widths, or time intervals is adjustable, and either positive-going or negative-going signals may be monitored.

This test set (see figure), can be used with relay contacts, connectors, cable and wire assemblies, manually activated or motor-driven switches, slip-ring assemblies, batteries, printed circuits, integrated circuits, resistors, capacitors, inductors, transistors, diodes, and other semiconductors. During dynamic environmental tests, such as shock, vibration, or acceleration, momentary opening of normally

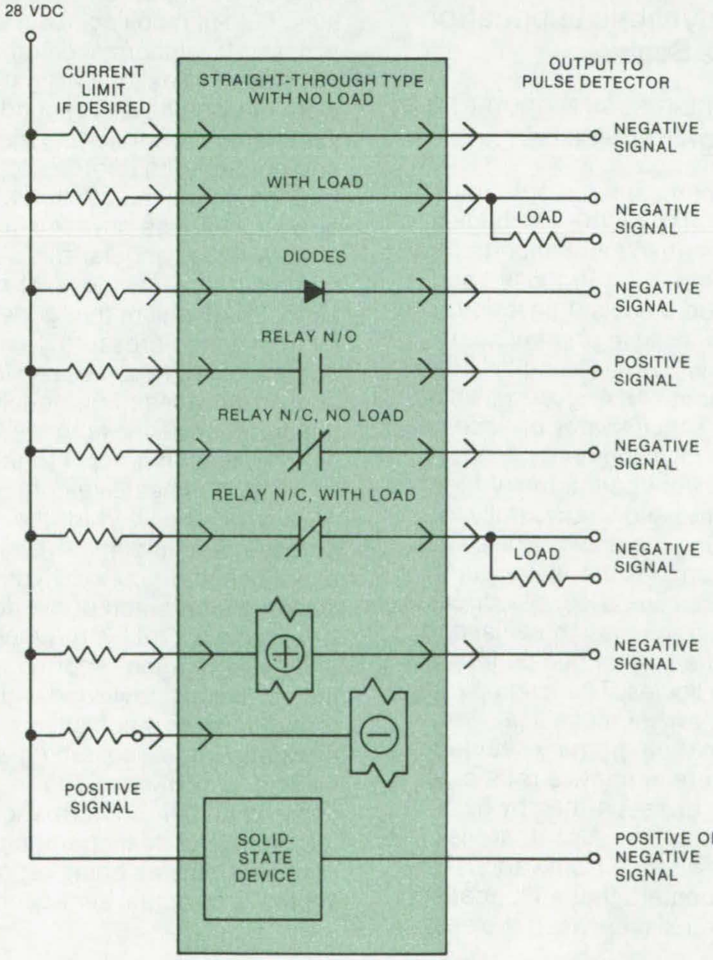

Applications of the Pulse Detector include testing components, such as relays, diodes, and IC's, under shock and vibration. Typical test setups are shown for these applications.

(continued on next page)

closed contacts or momentary closure of normally open contacts is detected when it exceeds a preselected time duration (i.e., pulse width), usually specified in microseconds.

There are two channels of detector circuits. Each channel contains independent elapsed-time range adjustments for preselecting the desired pulse-width response and a pilot lamp (indicator) which lights when the pulse-width response setting is exceeded. A single pushbutton switch simultaneously resets both channel indicators. The detector requires 5 Vdc, 200 mA input power.

Each channel is internally adjustable with component selection from 10 to 500 μs and has a nominal input impedance of 35 kΩ. The signal input polarity is selected by a front panel switch.

This work was done by Norman E. Simmons of Rockwell International Corp. for **Johnson Space Center.** *For further information, Circle 72 on the TSP Request Card.*
MSC-16268

Books and Reports

These reports, studies, and handbooks are available from NASA as Technical Support Packages (TSP's) when a Request Card number is cited; otherwise they are available from one of NASA's Industrial Application Centers or the National Technical Information Service.

Hydrodynamic Lubrication of Face Seals

Mechanisms, seal geometries, and angular misalinement

Two companion reports have been written on the mechanism of hydrodynamic lubrication of face seals. Report I, "Proposed and Published Models," describes the various possible primary-seal geometries, while Report II, "Theory of Response to Angular Misalinement," concentrates on face-seal angular-misalinement geometry.

Liquid-lubricated, radial face seals are used successfully in many long-life applications. Common examples are water pump seals in automobiles, oil-lubricated aircraft transmission seals, and seals in a host of pumps for various liquids. The long operating life of many of these seals suggests that the primary-seal faces (which are in relative rotational motion) are separated by a lubricating film. Also, there is direct evidence from various experimenters that a lubricating film can exist between the seal faces.

Report I describes various possible primary-seal geometries, and it reviews the various hypotheses that have been put forward to explain the mechanisms responsible for the development of the lubricating film pressure that acts to separate the faces of the primary seal. These hypotheses include angular misalinement, surface waviness, surface asperities, fluid-film boiling, axial vibration, and local thermal deformation. Hypothetical seal operating models were devised having secondary-seal friction, primary-ring inertia, and primary-ring degrees of freedom that simulate actual seal operation. These new seal models employ either angular misalinement, surface waviness, or both as the mechanism that generates hydrodynamic pressure. Stable operation was hypothesized for the angular-misalinement models and the surface-waviness models. The assumptions that apply to thin-film lubrication of seal-like configurations were reviewed for the purpose of obtaining governing equations that apply to hydrodynamic lubrication of the devised new models. Finally, the theories of seal lubrication reported in the literature were reviewed with regard to their mechanisms of lubrication, their governing equations (and corresponding restrictions), and their conformance to the models of seal-operating configurations as being representative of actual seal operation.

In Report II a theoretical analysis was made of a hypothetical seal operating mode. The analysis did not impose conditions of constant centerline film thickness or fixed relative face misalinement. Rather, in the hypothetical seal model the primary ring is free to respond to seal-face misalinement, and as a result of secondary-seal friction the primary-seal surfaces take on relative angular misalinement. This misalinement forms, in effect, a converging and diverging film in the circumferential direction. Positive hydrodynamic pressure is generated in the converging portion. An analysis of this seal model (which is only one of a number of possible seal operating models) resulted in a closed-form solution that yields values of film thickness when secondary-seal friction values are known or assumed. A design example of an actual seal was evaluated by using the derived mathematical expressions.

The analysis in Report II was based on dynamic response of the primary ring and was developed from a hydrodynamic viewpoint only; that is, hydrostatic effects due to sealed pressure and seal balance are not included. Thus, the model is most directly applicable to a class of seals that operate with small or no sealed pressure, such as in helicopter and aircraft accessory gearbox transmissions. The hydrodynamic mechanism however, is operable in high-pressure seals also, but hydrostatic effects are also significant.

This work was done by Lawrence P. Ludwig and Gordon P. Allen of **Lewis Research Center.** *Further information may be found in:*

NASA TN-D-8101 (N76-21560) "Face-Seal Lubrication, I - Proposed and Published Models" and NASA TN-D-8102 (N76-20484) "Face-Seal Lubrication, II - Theory of Response to Angular Misalinement."

Copies of these reports may be obtained at cost from the New England Research Application Center (see page A7).
LEW-12710

Computer Programs

These programs may be obtained at very reasonable cost from COSMIC, a facility sponsored by NASA to make new programs available to the public. For information on program price, size, and availability, circle the reference letter on the COSMIC Request Card in this issue.

Impact Response Analyses

IMPRES calculates dynamic responses of two impacting elastic bodies.

IMPRES is a general-purpose computer program that establishes the dynamic response of two impacting elastic bodies, each containing a linear or nonlinear impact attenuation mechanism. The program is formatted to apply to a wide range of configurations. Although intended for orbital-docking response analyses, it is not restricted to this particular problem and may, with minor modifications, be used for analysis of a broad spectrum of impact motion response investigations.

The equations of motion are cast in first-order form, and system state variables include inertial position, attitude and elastic normal coordinates of each vehicle, and attenuation mechanism generalized displacements. Additional state variables include ordinary translational and rotational momenta and modal-generalized momenta.

The program contains equations of motion and constraint to describe translational momenta, rotational momenta, modal momenta, auxiliary velocities, translational velocities, rotational velocities, and modal velocities for target and chase vehicles, as well as the impact attenuation mechanism and constraint equations.

In simulating the geometry of the impact response, the program establishes and enumerates a finite number of elemental points at which forces can be applied and to which motion can be referred. Elemental points are defined for the target vehicle, chase vehicle, mechanism components, and point of inertial reference. The contact problem is approached by calculating position vectors and rotation transformations.

Lagrange multipliers are used in simulating the kinematics of the impact response, the principle of virtual work is used to eliminate the action of the inner forces necessary to maintain prescribed kinematic conditions.

FORTRAN
UNIVAC 1100/EXEC VIII
Stromberg-Carlson 4020 Plotter

This program was written by Carl S. Bodley, David M. Warner, and A. Colton Park of Martin Marietta Corp. for **Marshall Space Flight Center.** *For further information, Circle P on the COSMIC Request Card.*
MFS-23335

Impact of a Solid Body with Water

A digital simulation calculates dynamics and loads.

SWIRL, a rigid body, three-degrees-freedom, digital-simulation program was developed to calculate the dynamics and loads expected on the rocket boosters for the Space Shuttle (SRB's). These reusable boosters will be dropped by parachutes into the ocean to be recovered for later flights. They must withstand the forces and moments caused by re-entry, and those occurring upon water impact are among the most significant.

Loads on the SRB case are calculated from initial contact with the water through maximum penetration. It is assumed that the SRB is rigid and enters the water tail first. Vehicle motion is planar, allowing horizontal and vertical translation and allowing rotation about the pitch axis. The effects of buoyancy, drag, water intake, apparent mass, cavity formation and collapse, and gravity are included. The basic theory for the initial impact forces on a body impacting water has been formulated by Von Karman, Wagner, and Bisplinghoff. To this basic theory have been added the effects of compression of the air under the skirt, water intake through the nozzle, and water cavity formation and collapse.

The basic equations of motion are developed in body coordinates with the origin of the coordinate system being the SRB center of gravity. These equations of motion are derived from Lagrange's equations for a moving coordinate system. The longitudinal drag force is considered to be flat plate drag only.

The impact moments and lateral impact forces arise from terms that involve growth of the external water mass. The apparent mass is assumed to be a half cylinder with a radius equal to the chord of the submerged portion of the vehicle. The longitudinal impact force is calculated from a spring/mass model. This model is used to calculate the longitudinal force on the SRB from impact through peak negative acceleration, peak positive acceler-

(continued on next page)

ation, and back to zero spring force, or through one cycle of the spring.
FORTRAN
UNIVAC 1108

This program was written by Dennis A. Kross of **Marshall Space Flight Center** *and Charles M. Bishop, Bruce E. Clingan, John R. Colson, Charles J. Heffron, and Charlotte Wiser of Boeing Aerospace Co. For further information, Circle Q on the COSMIC Request Card.*
MFS-23512

Design Analysis of Radial-Inflow Turbines

Velocity-diagram analysis for estimating performance

The analysis of a power or propulsion system involves many repetitive calculations of component performance and geometry over a range of conditions. Such calculations are most easily and quickly done by a computer. One component of interest for small gas turbine systems is the radial-inflow turbine. There has been no readily available computer program, such as this newly developed program, for performing the velocity-diagram analysis required for determining geometry and estimating performance for radial-inflow turbines.

Input design requirements are power, mass-flow rate, inlet temperature and pressure, and rotative speed. The design variables include stator-exit angle, rotor-exit-tip to rotor-inlet radius ratio, rotor-exit-hub to tip radius ratio, and the magnitude and radial distribution of rotor-exit tangential velocity. The program output includes diameters, total and static efficiencies, and all absolute and relative temperatures, pressures, velocities, and flow angles at stator inlet, stator exit, rotor inlet, and rotor exit.

An important part of any turbine design problem is the estimation of losses. The losses accounted for by the internal loss model are the three-dimensional (profile plus end wall) viscous losses in the stator and the rotor, the disk-friction loss on the back side of the rotor, the loss due to the clearance between the rotor tip and the outer casing, and the exit-velocity loss.

The flow analysis is one-dimensional at the stator inlet, stator exit, and rotor inlet, each of these calculation stations being at a constant radius. At the rotor exit where there is a variation in flow-field radius, an axisymmetric two-dimensional analysis is made using constant height sectors (maximum of 15 sectors). Simple radial equilibrium is used to establish the static pressure gradient at the rotor exit.
FORTRAN IV
IBM 7094/UNIVAC 1110

This program was written by Arthur J. Glassman of **Lewis Research Center.** *For further information, Circle R on the COSMIC Request Card.*
LEW-12684

Thermal-Radiation Model

Thermal environment around a rocket plume is calculated.

View-factor methods for calculating thermal environments due to solid rocket booster (SRB) plumes cannot account for influences on plume radiant heating of parameters such as chamber pressure, propellant composition, altitude, approach Mach number, afterburning, and spatial variations in plume properties.

The influence of these above parameters on the magnitude and distribution of thermal radiation emanating from SRB plumes are accounted for by a recent SRB thermal-radiation model. The geometry model for the SRB plume structure considers the plume to be constructed of homogeneous regions wherein appropriate values of gaseous and particle properties are defined. These homogeneous regions are stacked along the axis and the radius of the axisymmetric flow field. Regions are bounded along the radial coordinate by concentric conical surfaces that emanate from a common vertex. They are bounded along the axial coordinate by planes at right angles to the conical-surface axes. Properties are defined in a cylindrical coordinate system with its origin at the vertex of the cones. Average properties for each region are calculated based on assigned properties at the four corners of each region. Any valid definition of the spatial distribution of plume properties may be used as input data.

Two SRB plumes are considered in the model. The plume locations are defined in a central Cartesian coordinate system [X(1), X(2), X(3)] centered between the dual SRB nozzles. The X(1) coordinate is parallel to the plume Z axis at zero gimbal. The X(2) coordinate passes through the center of the exit plane of the two SRB nozzles, and the X(3) coordinate is at right angles to X(1) and X(2). Both plumes are considered to be axisymmetric; the distribution of plume properties along the axial and radial coordinates are approximated by defining homogeneous regions along the axis and radius of the plume. The geometry model allows the SRB plumes to be gimbaled parallel to one another in the yaw and pitch planes or to be gimbaled independently with different yaw and pitch gimbal angles.

The radiative heat exchange between surfaces is calculated by the Monte Carlo method, which is especially useful when the geometry of the exchange surfaces is complex. The assumption required with the Monte Carlo method is that the reflector surface is of some reasonable finite size so that the number of bits recorded on the surface will be statistically meaningful. The energy bundles are emitted from a surface uniformly in a cosine distribution. The process involves picking an emission site on the surface and choosing a direction of the trajectory. When a large number of energy bundles are dispensed, the emission sites will be distributed uniformly over the emitter surface, and the trajectory directions will be distributed according to the cosine law.

(continued on next page)

FORTRAN
UNIVAC 1100/ECEC VIII
Memory requirements approximately 96K 36-bit words

This program was written by W. C. Claunch of **Marshall Space Flight Center** *and G. H. Watson and A. L. Lee of Lockheed Missiles & Space Co. For further information, Circle S on the COSMIC Request Card.*
MFS-23538

General Instability Analysis

Analysis of inhomogeneous, anisotropic, stiffened cylinders under combined loads

The HOLBOAT computer program provides an instability analysis of an inhomogeneous, anisotropic, right-circular cylinder (or segment) under combined loading. It is an efficient, closed-form solution based on the Kirchhoff-Love hypothesis, general anisotropic constitutive equations, and Flugge's differential equations of equilibrium. Proper use of this program requires familiarity with composites technology, nomenclature, and theory; shell instability theory; and FORTRAN programing. The analyses for axial loads, pressure, and torsion are based upon the formulation of Cheng and Ho, who developed a solution in terms of classical small deflection theory and Flugge's differential equation of equilibrium. Their analysis has been extended to include bending.

Three operating modes are available:

1. Input of experimentally determined values of stiffness from isolated axial compression, torsion, and internal pressure tests
2. Direct input of stiffness matrices
3. Input of cylinder geometry and wall construction

This program can be used to analyze right-circular cylinders or segments of right-circular cylinders. Vertical and circumferential stiffening members may be included in the modeling. Stringers or rings may be on the inside or outside of the cylinder. Wall construction may consist of a skin alone or a skin reinforced with stiffening members. The skin may be a laminated cylinder constructed of layers of different materials having different elastic properties or orientations. Each individual layer may be isotropic or orthotropic; symmetric or balanced arrangement of layers is not required.

UNIVAC 1108, EXEC 8
Central Memory Requirement Approximately 19K 36-Bit Words

This work was done by C. J. Bianca of **Marshall Space Flight Center** *and A. A. Holston, Jr., John R. Lager, and J. M. Toth, Jr. of Martin Marietta Corp. For further information, Circle T on the COSMIC Request Card.*
MFS-23407

Transpose of Finite-Element Data

Examine a single point of a structural-analysis model under many loads.

The presentation of digital output data for engineers and management requires various selection options in order that the bulk of the data can be analyzed and understood very quickly. If the analysis requires the study of different loading conditions at a particular point, the output presentation must be a function of loading conditions. TRANSPOSE was developed to help in the data reduction and analysis of the structural behavior of a system under various loading conditions.

The number of loading conditions to be investigated may well be in the hundreds. The TRANSPOSE program was developed to reduce data and save the output for subsequent postprocessing. By providing the users with options for selecting only certain points (nodes), finite elements, components, loading conditions, data blocks, and specific substructures, the time required to analyze the structure can be greatly reduced. The TRANSPOSE program essentially transposes the finite-element data from one loading condition for all element and node data to the case of one-node-point data for all loading conditions. Thus, this program changes finite-element data from one format called 'COMBINE' to another format called 'TRANSPOSE'.

IBM FORTRAN IV, G Compiler
IBM 360 Series
Minimum Requirement 280K Bytes of Memory

This program was written by Tetsuo Furuike of Rockwell International Corp. for **Johnson Space Center.** *For further information, Circle U on the COSMIC Request Card.*
MSC-19644

Estimating Subsonic Aerodynamic Characteristics of Complex Planforms

A vortex-lattice FORTRAN program for complex planforms with separated vortex flows

This program uses a vortex-lattice method to estimate subsonic aerodynamic characteristics of complex planforms and interacting lifting surfaces with separated flow around sharp edges. It has been applied to the problem of preliminary analysis and parametric evaluations, as well as to computing side-edge suction forces for both isolated and interacting planforms. The suction analogy is used to estimate the aerodynamic characteristics associated with the separated flow field.

The program represents the lifting planforms with a vortex lattice. These complex planforms include wings with variable-sweep outer panels, wings with several changes in dihedral angle across the span, wings with twist and/or camber, and a wing in conjunction with either tail or a canard.

The aerodynamic characteristics of interest are lift and pitching moment for both the flat and/or twisted wing, drag-due-to-lift parameter, leading-edge thrust, leading-edge suction, distributions

(continued on next page)

of leading-edge thrust and suction coefficients, distributions of several span-loading coefficients, distribution of lifting-pressure coefficient, damping-in-pitch parameter, damping-in-roll parameter, and lift coefficient due to pitch rate.

The attached flow side force is developed in accordance with the Kutta-Joukowski law for forces generated by a vortex filament. The situation treated includes vortex filaments which have a streamwise component interacting with the net downwash at the filament midpoint to produce an elemental side force. In the determination of the total lift coefficient, the additional lift contribution caused by the separated flow around the edges is estimated by the use of the suction analogy. For planforms having sharp edges, the drag coefficient is represented as the experimental value of the drag coefficient when the lift coefficient is zero, plus the total lift coefficient times the tangent of the angle of attack. The pitching-moment contribution about the Y-axis associated with the side edge suction force is determined from each elemental horseshoe vortex, applying the suction analogy locally.

Updates to the program provide for more accurate thrust results and user flexibility in choosing the leading-edge region of the wing over which vortex lift is assumed to exist. For reliable side-edge loading results, the program is restricted to planforms which do not have swept-forward leading edges.
Computations for separated flow aerodynamic characteristics should be only made for wings without twist and/or camber.

FORTRAN
CDC Run Compiler/6000 Series

This program was written by John E. Lamar, Richard J. Margason, and Blair B. Gloss of **Langley Research Center.** *For further information, Circle V on the COSMIC Request Card.*
LAR-11047

Trimmed Noncoplanar Planforms with Minimum Vortex Drag

Vortex-lattice method for the mean camber shapes

A new subsonic method is used to determine the mean camber surface for trimmed noncoplanar planforms with minimum vortex drag. With this program, multiple surfaces can be designed together to yield a trimmed configuration with minimum induced drag at some specified lift coefficient. The method uses a vortex-lattice and overcomes previous difficulties with chord-loading specification. A Trefftz plane analysis is used to determine the optimum span loading for minimum drag. The program then solves for the mean camber surface of the wing which will provide the required loading. Pitching-moment or root-bending-moment constraints can be employed at the design lift coefficient. Sensitivity studies of vortex-lattice arrangements have been made with this program, and comparisons with other theories show generally good agreement. The program is versatile and has been applied to isolated wings, wing-canard configurations, a tandem wing, and a wing-winglet configuration.

The design procedure is essentially an optimization or extremization problem. A Lagrange multiplier technique is used to perform the spanwise factor optimization including lift and moment constraints on bent lifting lines in the Trefftz plane. The problem of determining the necessary circulation matrix is simplified by having the chordwise shape of the bound circulation remain unchanged across each span, though the chordwise shape may vary from one planform to another. The circulation matrix is then obtained by using the optimized spanwise scale factors with the specified chordwise shapes. A chordwise summation of the lift and pitching-moment is utilized in the Trefftz plane solution because of the assumptions that the trailing wake does not roll up and because the general configuration has specifiable chord-loading shapes. The contribution to the vortex drag coefficient at one chordwise row due to another chordwise row is performed in the Trefftz plane for simplicity.

CDC 6000 Series
Central Memory Requirement 51K to 112K
Octal Words [depending on overlay]

This program was written by John E. Lamar of **Langley Research Center.** *For further information, Circle W on the COSMIC Request Card.*
LAR-12121

Estimating Aircraft States

A quasi-linearization technique using flight data

A recently developed computer program provides weighted least-squares estimates of aircraft states (attitude angles, positions, and velocities) from measurements recorded during routine flight tests. The program contains the standard six-degree-of-freedom kinematic equations; inputs to the equations are the measured time histories of linear accelerations and rotational rates. The estimated time histories of output states from the kinematic equations include three linear velocities, three Euler angles, and three linear positions. Unknown parameters such as the initial conditions and bias terms are determined by an iterative parameter-identification method (quasi-linearization) that seeks to minimize the weighted least-squares difference between the estimated set and the measured set (or partial set) of output states.

(continued on next page)

The program has been used successfully, in particular, for trajectory smoothing during the transition and hover of V/STOL aircraft and for measurement of turbulence during the flight of a probe aircraft through the vortex wake of a large jet-transport. Other uses include estimation of instrument calibration terms and states not originally measured, as well as determination of winds and aerodynamic derivatives.

This program was written by Rodney C. Wingrove of **Ames Research Center.** *For further information about the estimation technique, see: Wingrove, R.C., "Quasi-Linearization Technique for Estimating Aircraft States from Flight Data,"* Journal of Aircraft, *vol. 10, No. 5, p. 303 (1973). For further information on this computer program, Circle X on the COSMIC Request Card.*
ARC-10969

Stability of an Elastic Airplane

FLEXSTAB — predicting static and dynamic stability of a flexible body

A new program, FLEXSTAB, is used to evaluate trim state, static, and dynamic stability characteristics, inertial and aerodynamic loading, and elastic deformations of aircraft configurations at subsonic and supersonic speeds. It is based on unified, linear aerodynamic, structural, and dynamic analytical methods valid for a wide variety of aircraft configurations.

Low-frequency dynamics of a flexible body are merged with low-frequency unsteady aerodynamics to perform aircraft dynamic stability analysis. Empirical or wind tunnel data can be incorporated to modify or replace program computed aerodynamic quantities used in the stability analysis. Empirical and theoretical corrections can be incorporated in the aerodynamic and stability analyses.

Aircraft stability and control analysis is performed at prescribed flight conditions defined by Mach number, altitude, angle of bank, pitch, yaw, and roll rates, and either flightpath angle or thrust. Using linear equations of motion, the dynamic modes of motion are computed together with the associated frequencies and damping coefficients. If the perturbation equations of motion are nonlinear (as a consequence of the user supplying nonlinear aerodynamic data or wanting to investigate large perturbations), or if discrete gust disturbances are input, dynamic stability characteristics are evaluated from time-history plots. Lifting-pressure distributions on the aircraft can be calculated in the course of the solution of the trim problem. Also, structural loads, deflections, and rotations are calculated at aerodynamic panel centroids.

The FLEXSTAB system can be used to calculate either the jig shape or design point shape of an elastic aircraft. The effects of configuration changes, such as planform, camber shape, structural elasticity, etc., can be evaluated by performing any of the above analyses for each configuration change. Present FLEXSTAB capabilities can be extended through interfacing or linking with computer programs outside the FLEXSTAB system. An example is taking the loads or elastic deflections at the structural grid points calculated by FLEXSTAB and inputting them into the NASTRAN Structural Analysis Computer Program to calculate internal structural stresses at specified flight conditions.

The FLEXSTAB system is written in FORTRAN for CDC 6000 and 7000 and IBM 360.

This program was written by Larry L. Erickson and Perry P. Polentz of **Ames Research Center** *and Arthur Dusto, Garry Hink, and Stanley Hansen of the Boeing Company. For further information, Circle Y on the COSMIC Request Card.*
ARC-11086

Independent Trajectory Determination System

A stand-alone subsystem calculates flight data analytically or numerically.

A stand-alone subsystem of the Goddard Trajectory Determination System (GTDS) was developed to support research and development efforts in trajectory determination preflight and postflight analysis, simulation of tracking data, and ephemeris generation. The GTDS stand-alone version is an orbit ephemeris generation program and is a subsystem of the comprehensive GTDS (a flight dynamics system). The program uses numerical, analytical, or semianalytical techniques to generate spacecraft trajectories, advance the initial elements to a new epoch, rotate the ascending node, or propagate the covariance matrix (matrix mapping) to a new epoch.

The ephemeris generation program either uses an analytical theory, or it numerically integrates the equations of motion and the associated variational equations to produce the spacecraft trajectory and partial derivatives of the state. The analytical theory used is that of Brouwer. The integration method is the Cowell type, utilizing such options as time regularization, multistep starting, variable stepsize, "corrector only", variable force model, and others to optimize computational efficiency. The reference coordinate system for the equations of motion can be either the mean equator and equinox of 1950.0 or a true equator and equinox system reference to a specific epoch (called a true-of-reference-date system). Coordinate transformations account for precession, mutation, and polar motion of the Earth's spin axis. Planetary positions are determined from an ephemeris file containing Chebychev polynomial coefficients derived from JPL ephemeris data.

(continued on next page)

The force model option includes the following acceleration sources:

- N-body point mass gravitational accelerations: These include all planets in the solar system, the Sun, and the Moon;
- Nonspherical gravitational accelerations: The nonspherical gravitational model allows the inclusion of up to a 15 by 15 potential field for the Earth and/or Moon;
- Atmospheric drag accelerations: The drag acceleration for Earth includes (optionally) a Harris-Priester model or a Jacchia (1971) model;
- Solar-radiation accelerations: The solar-radiation model includes shadowing and variations with distance from the Sun;
- Attitude-control systems accelerations: A generalized model is included to provide for the propagation of residual accelerations from an attitude-control system; and
- Thrust-maneuver accelerations; A generalized model is included for accommodating propulsive maneuvers in both simulation and estimation.

The program is written in FORTRAN for the IBM 360. The software package contains the source code, overlays, executable load module, the 1950.0 SLP ephemeris data file, a True-of-Date SLP ephemeris data file, timing coefficients, and necessary control language.

This work was done by Michael G. Armstrong and Isabel B. Tomaszewski of **Goddard Space Flight Center.** *For further information, Circle Z on the COSMIC Request Card.*
GSC-11923

Machinery

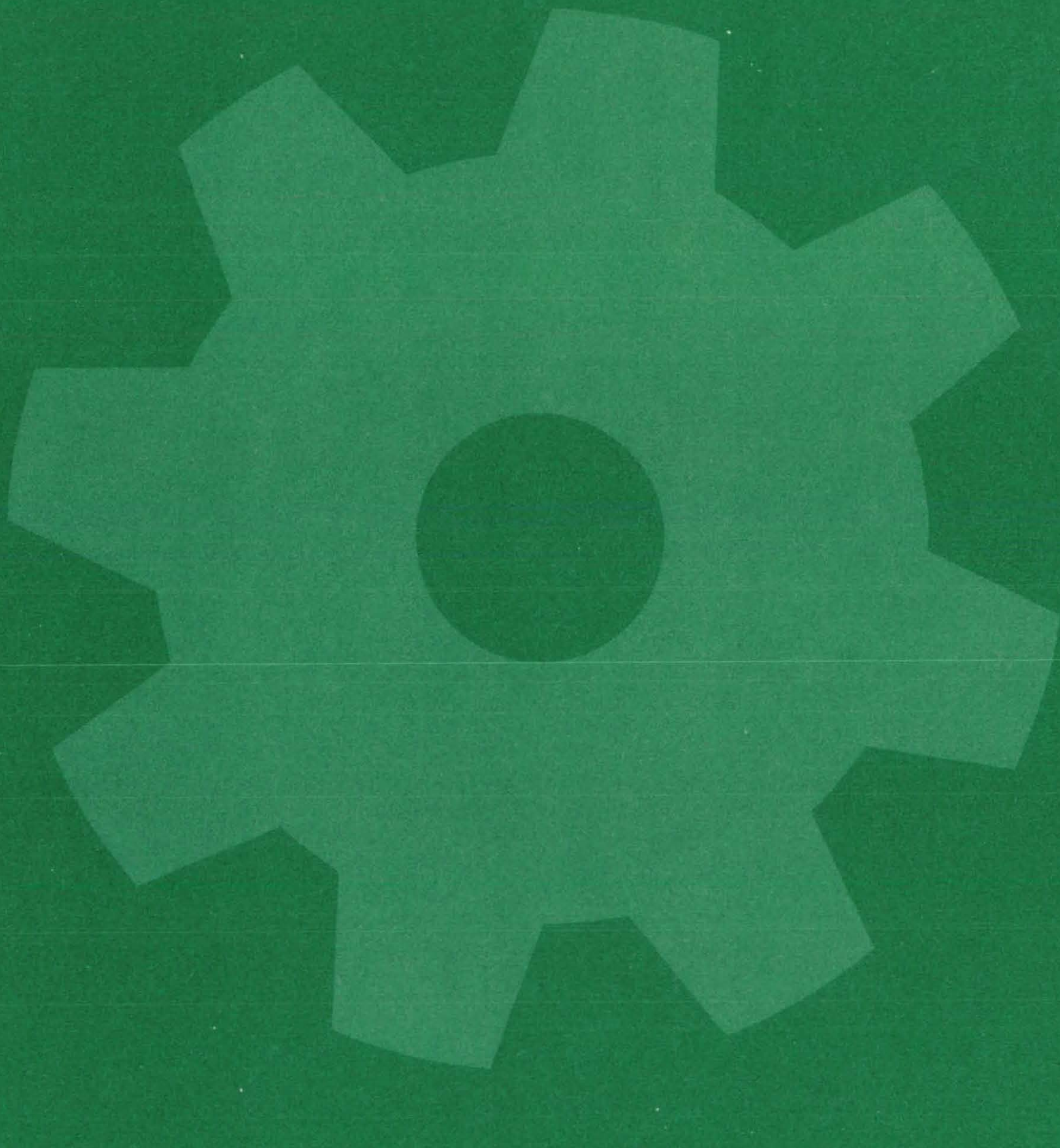

Hardware, Techniques, and Processes

NASA Technology Utilization House

A "house of the future"
is ready today.

Langley Research Center, Hampton, Virginia

The NASA Technology Utilization House (Tech House), constructed at Langley Research Center, was designed and built to demonstrate how the application of aerospace technology could advance the building industry in residential construction. Tech House is a single level structure of contemporary design which is comprised of two square modules connected by a hallway and contains approximately 140 m^2 (1,500 ft^2) of living space. One module consists of a living room, dining area, and kitchen; the other, three bedrooms and two baths. The connecting hallway has an entry vestibule and a laundry room. In developing Tech House, NASA incorporated the latest technology and used special features when either the initial cost could be recovered in energy savings over the useful life of the feature or if it provided a specific benefit such as personal or structural safety. The one other criterion for application of advanced technology was that the feature was projected to be commercially available within five years.

It is forecast that within five years the house with all its special features can be built commercially for approximately $45,000 (based on 1976 costs). With the incorporation of solar energy, energy efficient appliances, and the water reuse system, it is predicted the homeowner would save approximately $20,000 in utility costs over a period of twenty years, after recovering the additional cost of these special features. (This forecast is based on a ten-percent annual increase in utility costs.)

The following special systems and features, most of which are an outgrowth of NASA's aerospace technology, have been incorporated into Tech House:

Heating and Cooling System

- Solar collectors on the roof are used, together with nighttime radiators, two wells, and a heat pump, to supply major heating and cooling requirements.
- Additionally, the fireplace is outfitted with a duct system to bring in combustion air from the outside, and fire grate water coil, enabling the accumulation and storage of heat for later distribution.
- Exterior retractable shutters provide energy savings when closed by preventing heat loss during the winter and heat gain during the summer and, at the same time, function as a security measure.
- A nonflammable, nonpetroleum based foam provides highly efficient insulation, supplemented by metal exterior doors which have a thermal break, polystyrene core and magnetic weather stripping.

Water Recycling System

- A 50-percent reduction in water consumption is attained through use of low-profile water fixtures and a water reuse system which collects waste water from the shower, bathtub, bathroom sinks, and laundry in a holding tank where it is chlorinated, filtered, and recycled for toilet flushing.

Hot Water System

- Solar energy heats the water used in the domestic hot water system.

Security System

- Interior security is provided by detectors at doors, windows, and under carpets which set off an alarm when an intrusion occurs.
- An exterior security system uses a seismic device to sound an alarm when an intruder approaches within 80 m of the house.
- A smoke detector is used to sense the presence of combustion products and sound an alarm.
- A battery charged by a solar cell provides power for a driveway spotlight and emergency lighting. The smoke detector and security system may also be powered by the solar-charged battery.
- A tornado detector is attached to the television screen and sounds an alarm upon the appearance of a

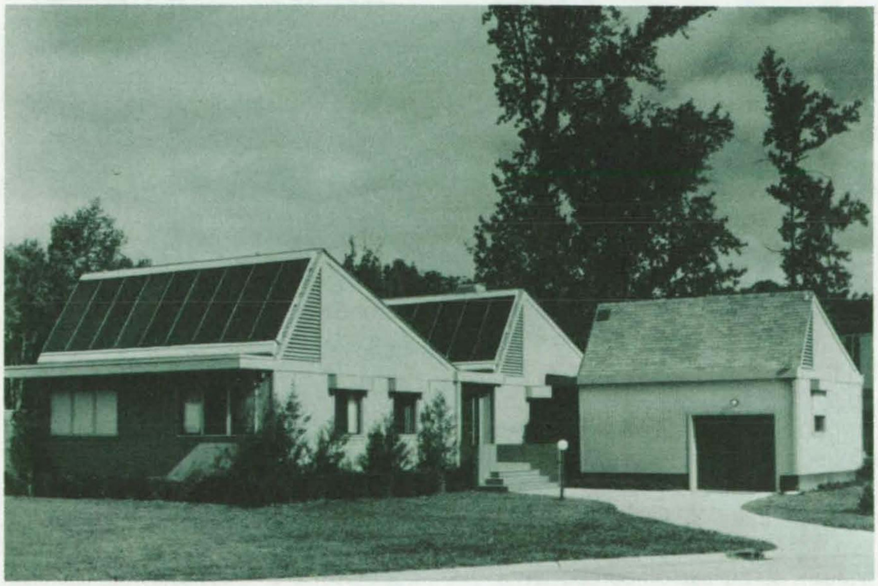

NASA's **Tech House** at Langley Research Center incorporates solar heating, cooling, and hot water. A security system includes intruder and fire alarms, a tornado detector, and emergency lighting. A water recycling system and energy-saving lighting fixtures help reduce the homeowner's costs.

(continued on next page)

tornado within a radius of 18 mi.

Additional

- Thermistors installed in lamp sockets significantly increase the life of the light bulbs by a minimum of 300 percent.
- Seat custions are made of an advanced foam rubber that contours to a body shape, thereby distributing weight evenly over the contact surface.
- Flat conductor electrical wiring, covered with plastic baseboard, which has greater current capacity was installed after the building was completed and the carpet installed.

These features are all examples of the innovations utilized in the construction of the Tech House to demonstrate the application of advanced technology to minimize energy and water consumption and provide for the comfort and safety of the homeowner and his family.

This work was done by the Technology Utilization Office of **Langley Research Center.** *For further information, Circle 73 on the TSP Request Card.*

While no patent action is contemplated by NASA on the Technology Utilization Home as such, many of the components and systems included in the house are covered by patents. Some components were developed by private industry and industry owns those patents. Inquiries regarding which items are patented and concerning rights for the commercial use of these inventions may be directed to the Patent Counsel, Langley Research Center [see page A8]. Refer to LAR-12134.

Economical Solar-Heating for Homes

A do-it-yourself supplementary solar-heating system for about $2,000

Langley Research Center, Hampton, Virginia

A low-cost solar home heating system has been built and tested at the Langley Research Center (LRC). It can be installed by a homeowner who is only moderately skilled in the use of hand tools and has the time available to order and install the components. This system can be used to supplement a warm-air heating system at a saving to the homeowner of approximately 40 percent of his annual heating bill. All of the required materials, from collector panels and heat exchanger to paint and screws, can be purchased for approximately $2,000. This investment should more than be recovered within the lifetime of the system.

A report on this system has been published which not only presents the specifics needed by the homeowner for installation but also gives a general description of a solar heating system and how it works. It describes how this information was applied at LRC and gives an analysis of the system performance. This report contains 39 illustrations which give a graphic representation of the system, as well as all components and how they are used. A total of 26 of these illustrations give installation particulars.

A bill of materials with costs (March 1975) is shown in table form with all items being readily available, with the exception of the modification to the existing forced-air duct. A complete description of each item is given, and several manufacturers are listed in most cases. Five appendixes contain the actual assembly and installation instructions. These include the assembly of the solar collector and its installation on the roof, and instructions for assembling an alternative do-it-yourself collector panel. The installation of the water storage tank and construction of the tank foundation are fully explained for indoor or outside installation. Air-duct modification and heat-exchanger installation are described, along with information needed to size the heat exchanger. One appendix has a system schematic and covers the method of installation of the hot-water distribution system. This appendix also lists safety requirements for handling the solvents and cements used in the assembly of plastic pipes and fittings. The instructions to install the required electrical power components and the differential temperature flow controller are completely explained, and alternative components are listed.

This report describes the design, construction, testing, and economic analysis of a low-cost solar heating system. The minimum-cost approach requires the homeowner to supply all labor necessary to install the readily available off-the-shelf components which make up the system. Background information is given in the report to help a specially skilled homeowner understand how a solar collector works and what it can be used for.

The results of the tested demonstration system indicate that the homeowner can supplement his existing forced-warm-air heating system and reduce his heating bill by approximately 40 percent for a 140-m^2 (1,500-ft^2) house insulated to 1974 FHA minimum standards. The completely automatic system does not require antifreeze protection and is fail-safe. Loss of electrical power causes the system to automatically drain itself back to the storage tank.

This work was done by Johnny W. Allred, Joseph M. Shinn, Jr., Cecil E. Kirby, and Sheridan R. Barringer of **Langley Research Center.** *Further information may be found in NASA TM X-3294 [N76-27671], "An Inexpensive Economical Solar Heating System for Homes," a copy of which may be obtained at cost from the North Carolina Science & Technology Research Center [see page A7].*
LAR-12135

Leveling Apparatus for Precision Instruments

An inexpensively-constructed leveling platform is easy to use and accurate.

Ames Research Center, Moffett Field, California

The leveling platform shown in the illustration can be easily locked into position to provide a shock- and vibration-resistant support for precision instruments. Its chief advantage over existing leveling platforms is its relatively simple construction, which reduces the costs of parts and machining.

The device consists of an instrument platform secured to a shaft that fits within a hollow steel pipe. Three segments of the shaft have different diameters: The upper section (the upper table) is larger than the steel pipe; the middle section fits tightly within the pipe; and the lower section is smaller than the inside diameter of the pipe.

A nylon tension ring secures the instrument platform to the upper section of the shaft tightly enough to prevent relative vertical motion of the two parts. A rotary-adjustment screw allows the instrument platform to be rotated about the shaft and then locked into place. The level of the platform may be set with two level-adjustment screws. These are set in threads bored through the pipe at an angle, and the screws fit into a circumferential groove in the shaft.

Because of the tolerance between the lower portion of the shaft and the pipe, the screws may be used to force horizontal motion on the lower shaft. Even though the middle section of the shaft fits tightly within the pipe, the upper end of the pipe will be slightly deformed and acts as a fulcrum for minor adjustments in the platform level. Also, as both screws are tightened, the shaft is pulled downward, securing the set position.

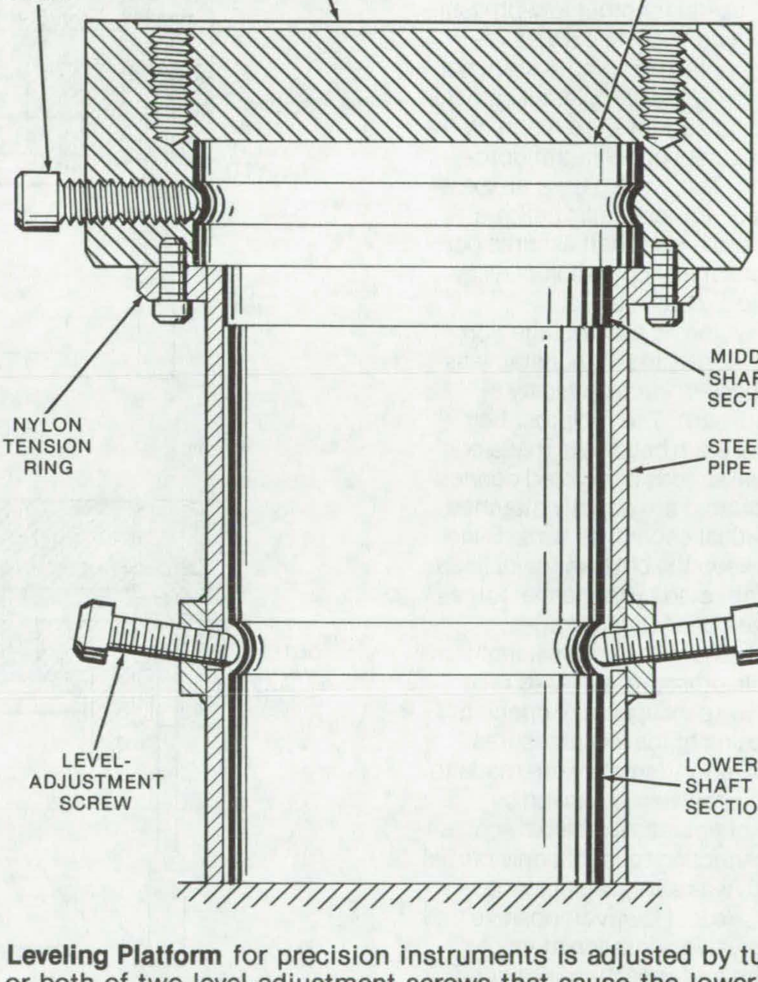

The Leveling Platform for precision instruments is adjusted by turning one or both of two level-adjustment screws that cause the lower shaft section to move horizontally. This motion causes some deformation of the steel pipe and a resultant slight adjustment of the instrument platform.

This work was done by Robert W. Delaplaine and Daniel L. Mossolani of ***Ames Research Center.*** *For further information, Circle 74 on the TSP Request Card.*

This invention is owned by NASA, and a patent application has been filed. Inquiries concerning nonexclusive or exclusive license for its commercial development should be addressed to the Patent Counsel, Ames Research Center [see page A8]. Refer to ARC-10981.

Low-Pressure-Gas Sampling Pump

A bellows pump raises the sampled-gas pressure to a level compatible with available compressors.

Ames Research Center, Moffett Field, California

A multistage bellows pump developed for sampling the stratosphere may be useful for other low-pressure applications. Because it was required that the pumping system not contaminate the sample, all sample-contacting surfaces are made of stainless steel or polytetrafluoroethylene. The system uses an existing design for a metallic bellows pump, and a camshaft assures positive mechanical operation of all intake and exhaust valves.

The system is a four-stage compressor consisting of four stainless-steel bellows, each driven by a separate cam. The reciprocating action of each bellows is made positive at all speeds by pivoted connecting links that are directly attached to individual eccentric cams. Slide guides keep the bellows travel linear and unaffected by tangential forces from the connecting linkages.

It was shown by analysis that the available pressure-actuated reed valves were incapable of opening and closing at the low pressures anticipated. Attempts were made to provide positive reed action by means of actuators driven by cams and connecting rods, but only partial success was achieved at low operating speeds. However, positive and smooth valve operation at any pressure and speed was obtained with cam-driven sliding valves which opened and closed ports in synchronization with the intake and compression strokes of a bellows system. Figure 1 depicts the general arrangement of the sliding valves and bellows for the prototype compressor.

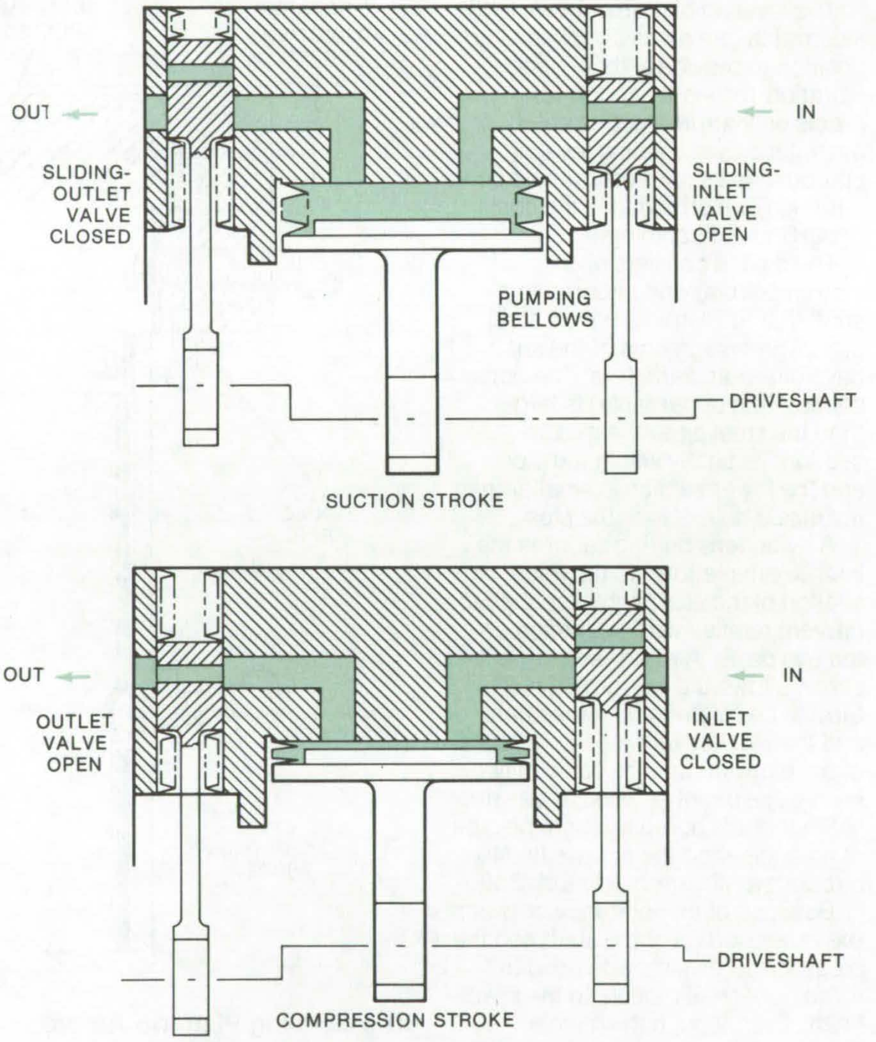

Figure 1. The **Bellows and Valves** act as a first-stage pressure booster for the low-pressure pumping system. During the suction stroke, the bellows reaches its lowest and most expanded position; the inlet valve is open, and the outlet valve is closed. As the compression stroke begins, the inlet valve closes. With both valves closed, the bellows compresses the trapped gas; at the top of the compression stroke, the outlet valve opens, and the gas sample is vented into the next stage of the compressor.

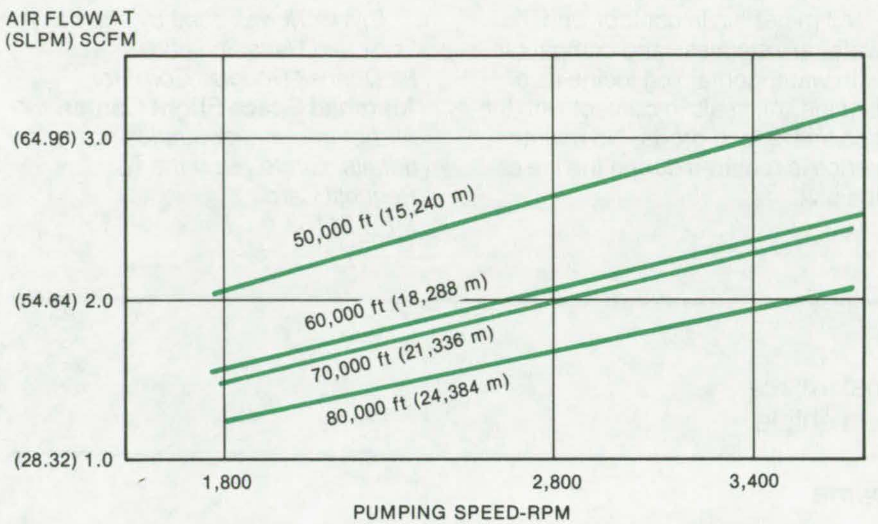

Figure 2. **Characteristics of the Final Design** of the pumping system are shown. Airflow is given in standard liters per minute (SLPM) and in standard cubic feet per minute (SCFM).

The sliding valves are stainless-steel cylinders, appropriately bored and positively coupled by links and wristpins to valve-lifting cams. The valve-body cylinders are equipped with polytetrafluoroethylene elastomer rings to abate blowby. Bellows seals installed at each end of the sliding valve act as secondary seals, preventing any leakage to or from ambient.

A single-stage prototype pump working at a 1-to-1 compression ratio and an actual displacement of 0.072 liter per stroke at pressure equivalent to an altitude of 24,384 meters was found to have valve-related efficiency losses of the order of 1 percent at 1,800 rpm. At an operating speed of 3,600 rpm, the valve efficiency losses were found to be of the order of 9 percent. Figure 2 is a performance curve that illustrates efficiency vs. altitude.

This work was done by Peter L. Fontecchio of Metal Bellows Corp. for **Ames Research Center.** *For further information, Circle 75 on the TSP Request Card.*
ARC-10941

Dispensing a Measured Quantity of a Liquid

Pushbutton-controlled unit ejects a fixed volume of fluid and monitors consumption.

Marshall Space Flight Center, Alabama

A hand-held dispenser connected by hose to a supply of liquid squirts out a predetermined amount of the liquid when its trigger is squeezed and released. Each such cycle is recorded on a counter that is an integral part of the dispenser.

The device was designed to shoot half an ounce of drinking water into an astronaut's mouth each time he operated the pushbutton; however, it is equally useful in soda fountains, cocktail bars, medical dispensaries, chemical laboratories, manufacturing plants, and the like.

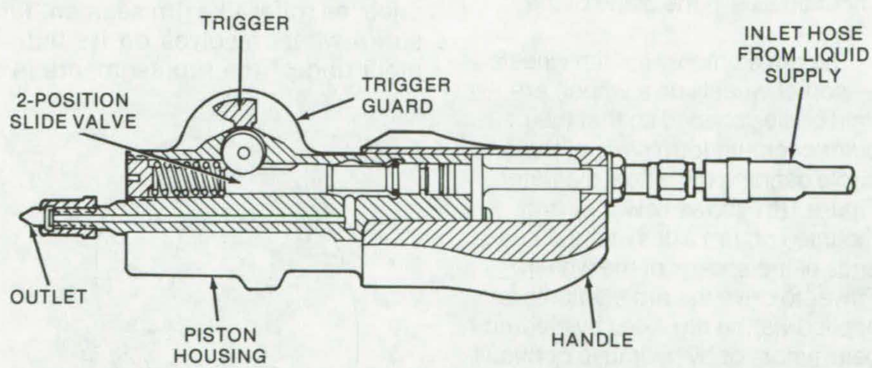

This **Handy Dispenser for Liquids** takes in a cylinderful of liquid when the pushbutton is squeezed and squirts it out when the button is released. A counter tallies the number of squirts. Neither the liquid pressure nor the ambient pressure affect the volume dispensed.

The water (or whatever liquid) from the supply is blocked at the inlet port of the dispenser by a slide valve (see figure). To operate the unit the trigger must be depressed so that the slide valve moves to the open position. Water then enters the dispenser and forces the spring-loaded piston back until the cylinder is full. When the trigger is released, the slide valve moves into a position that blocks the inlet port, and the spring-loaded piston ejects the water through the outlet.

Once the trigger has been depressed, the dispenser meters out the liquid automatically. The repeatable accuracy of the dispenser is obtained by using a piston that must complete its full stroke cycle for the unit to become ready for the next cycle. An accidental double triggering during the cycling is not possible; the dispenser is ready for the

(continued on next page)

next cycle only after it has completed the previous cycle. The water-supply pressure and the air pressure have no influence on the mechanical operation, but the time of one complete cycle is a function of the water pressure.

All materials in contact with the water are stainless and compatible with water containing iodine as a biocide. All seals in contact with the cooler are food grade. No maintenance is required during the life of the unit.

This work was done by Thomas A. Cook and Hans Scheibe of McDonnell Douglas Corp. for **Marshall Space Flight Center.** *For further information, including design details, Circle 76 on the TSP Request Card.*
MFS-21163

Omnidirectional Wheel

Wheel with rotating rim elements maximizes the directional driving capability of a vehicle.

Marshall Space Flight Center, Alabama

A specially built wheel provides mobility in any direction for a ground vehicle, without requiring any change of orientation relative to the vehicle. Such wheels will enable a car to get in and out of tight parking spaces, a crane to maneuver directly sideward, or a Moon rover to travel easily over difficult terrain.

Figure 1(a) illustrates the principle of the omnidirectional wheel: It travels forward or backward by turning on its axle, just like any other wheel, and it travels sideward (i.e., in the direction of its axle) by the rotation of a roller-like rim element about an axis in the plane of the wheel.

The rim elements (or rim wheels — sort of wheels on a wheel) are rigid bodies shaped so that their outer contours form parts of the circle defining the wheel diameter. Figure 1(b) shows how they are mounted on rim axles at the outer ends of the spokes of the wheel. Power to drive the rim elements is applied via the rim axles by electric gearmotors or by hydraulic or pneumatic devices.

Simultaneous rotations of the wheel and of the rim segments allow a ground vehicle to move in any direction from a given spot, as depicted in Figure 2. Varying one of the two rotational speeds steers the vehicle along a curved path.

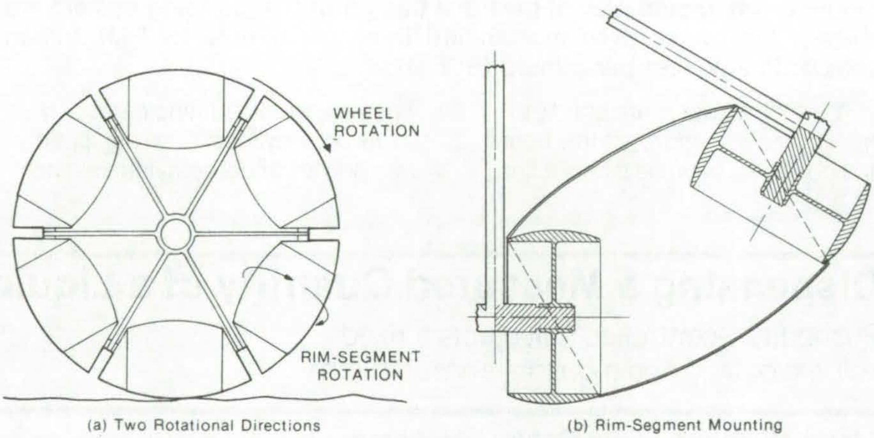

Figure 1. Omnidirectional wheel **Rolls in Two Orthogonal Directions** at once, as roller-like rim segment turns about axle in plane of wheel while entire wheel revolves on its hub. The two rotations are shown in (a); mounting of the rim segments is shown in (b).

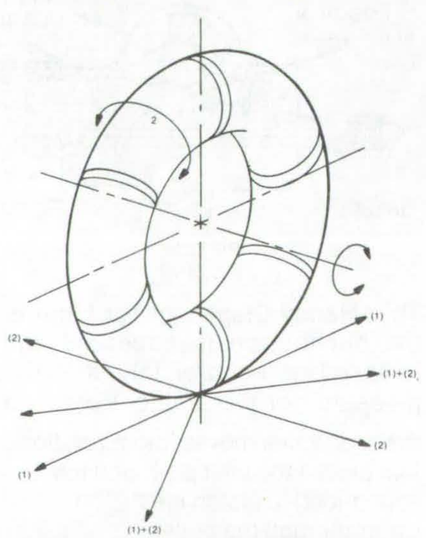

Figure 2. The wheel is **Steered Without Orientation Change** by varying one of the two rotation rates. A vehicle equipped with such wheels can move in any direction from a fixed spot.

This work was done by J. F. Blumrich of **Marshall Space Flight Center.** *For further information including the details of construction and powering of the rim segments, Circle 77 on the TSP Request Card.*

This invention has been patented by NASA [U.S. Patent No. 3,789,947]. Inquiries concerning nonexclusive or exclusive license for its commercial development should be addressed to the Patent Counsel, Marshall Space Flight Center [see page A8]. Refer to MFS-21309.

Long-Life Ball-Valve Design

Eccentric mounting of ball on stem reduces wear on valve seal.

Marshall Space Flight Center, Alabama

The operating life of a ball valve is prolonged by minimizing wear on the seal that contacts the ball. The seal gets worn down when the ball rubs against it and particularly when the edges of the hole through the ball scrape against it. By mounting the ball so that it turns eccentrically on the valve stem, much of the rubbing and all of the scraping can be eliminated. Thus a ball valve with an eccentric ball has long life.

The figure, which is a section through the ball perpendicular to the axis of rotation (valve stem), illustrates the eccentric-ball-valve operation. As the stem is turned clockwise to open the valve, the ball rotates, and the portion of the ball that contacts the seal moves to the right. The seal cannot follow the ball very far to the right because of the stop, so the ball moves free of the seal before the edge of the hole can scrape across the seal. Likewise, when the valve closes, the ball does not make contact with the seal until after the edge of the hole has passed beyond the seal circle.

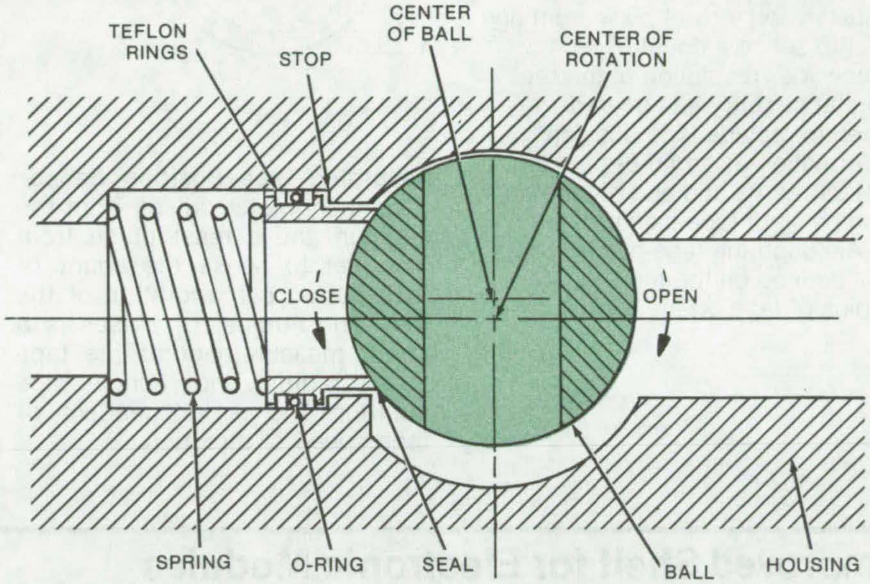

The **Ball Moves Away From the Seal** as it is rotated clockwise to open the valve because the axis of rotation does not go through the center of the ball. Therefore the ball does not wear down the seal. The spring presses the seal firmly against the ball when the valve is closed, but the stop prevents the seal from continuing to contact the ball when the valve is open.

As the ball continues to rotate to the closed position, friction forces act on the two parts of the seal shown in the plane of the section. The vertical components of these forces try to twist the seal clockwise about its point of support at the O-ring, and the horizontal components try to twist it counterclockwise. If these forces are unbalanced, the seal does twist, causing increased wear at the point of higher force and decreased seal pressure and possible leakage at the point of the weaker force. However, the support point can be located so that the forces balance to give uniform pressure around the seal. This ideal support location is determined by an analysis of the valve design.

This work was done by D. F. Ferris and W. A. Gillon, Jr., of Rockwell International Corp. for **Marshall Space Flight Center.** *For further information, including an analysis of the ideal support location, Circle 78 on the TSP Request Card.*
MFS-19282

Recording-Tape Position Sensor

Tape position is determined without marking the tape or adding hardware that contacts the tape.

Goddard Space Flight Center, Greenbelt, Maryland

A digital end-of-tape sensor and tape-position sensor can be used to command motor reversal or stop upon reaching the end of the tape and to locate data on the tape. This method also makes it easy to adjust for different lengths of tape by programing the proper count at the main and minor counters.

The amount of tape on a reel is determined from two pieces of data: a pulse representing one revolution of the tape reel and a simultaneous measurement of capstan rotation. The capstan rotation depends only on the length of tape passing; thus the length

(continued on next page)

of tape corresponding to one rotation of the reel may be calculated. This is directly related to the radius of the tape wound on the reel and thus the length of tape wound on the reel.

The technique, as applied, uses the tachometer pulses from the capstan and a reset pulse from one reel to sense a count of tach pulses per revolution of the reel. Digital circuitry has been developed to provide tape-position information as serial or parallel data streams and end-of-tape and beginning-of-tape signals.

Although the tape-position data will depend on the tension (the radius of tape on the reel depends on how tightly the tape is wound), this same system can be used to maintain a constant tape tension across the tape head. This could be done by converting the tape-position parallel data to an analog voltage and feeding it to an electrical network and power amplifier for the takeup reel motor.

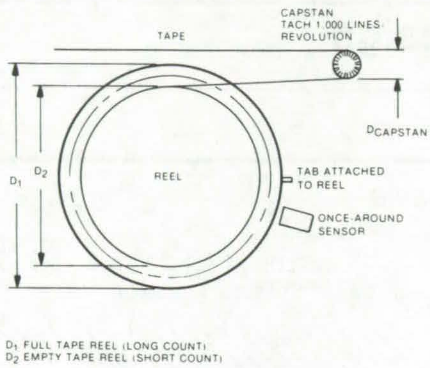

Recording-Tape Position Sensor uses tachometer pulses from the capstan and a reset pulse from one reel to sense the count of tach pulses per revolution of the reel. The number of pulses is a direct measurement of the tape stack radius and hence tape position and is independent of tape speed or direction.

This work was done by George C. Schoppet of **Goddard Space Flight Center.** *For further information, Circle 79 on the TSP Request Card.*

This invention is owned by NASA, and a patent application has been filed. Inquiries concerning nonexclusive or exclusive license for its commercial development should be addressed to the Patent Counsel, Goddard Space Flight Center [see page A8]. Refer to GSC-12056.

Improved Shelf for Electronic Modules

A self-alining slide assembly features better air circulation

Caltech/JPL, Pasadena, California

Cabinet-mounted electronic equipment often includes a slide-out shelf to simplify repair and maintenance. The shelf moves along two independent slides. Normally, the mounting holes for the slides must be placed very carefully to avoid binding when sliding out the shelf. In addition, the crossmember and the relatively-wide chassis support shelf used with this system impede the free flow of cooling air to the chassis.

A redesigned bottom slide assembly is shown (see figure) in comparison with the old slide assembly. The improvement in the bottom slide assembly reduces the amount of airflow blockage caused by the previously-used wide mounting plate, yielding a threefold airflow increase. Since the required alinement accuracy is now built into the slide assembly during fabrication, the previous requirement for mounting-hole location accuracy has also been significantly reduced.

The new slide assembly design eliminates the previously-necessary load-bearing crossmember, as sufficient load-bearing capability is now built into the mounting platform. The new assembly can be mounted either on the old crossmembers, if previously installed, or on a single Z-bracket attached to the side rails of the cabinet. Consequently, the amount of labor needed for installation, the necessary machining, the hardware, and the number of mounting points have all been greatly reduced.

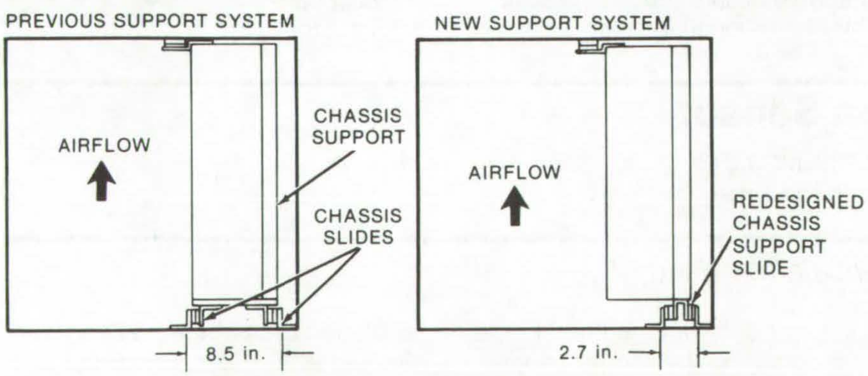

A **Comparison of the Slide Assemblies** shows the previous system that had two independent slides that required careful alinement. In the improved version both slides are combined into a single assembly with a narrow mounting platform.

This work was done by Ronald A. Marzek of **Caltech/JPL.** *For further information, Circle 80 on the TSP Request Card.*
NPO-13158

Fabrication Technology

Hardware, Techniques, and Processes

Forming Hard Aluminum in Complex Shapes

Intricate parts can be shaped in a soft temper condition and subsequently converted to a hard temper.

Lyndon B. Johnson Space Center, Houston, Texas

Aluminum alloys can be heat treated to vary their properties over a range of tempers from a soft, TO, condition to the hardest, T8, temper. There is a complex interrelationship between the temper of the metal and its formability. Not only can softer aluminum be formed into more intricate shapes but the strains resulting from severe forming place limitations on the degree of hardness to which a complexly shaped part can be tempered.

These restrictions have generally prevented the use of aluminum for complex parts requiring the hardest, T8, temper. Yet the weight savings possible through the use of the lightweight metal have become even more desirable with today's emphasis on reducing energy requirements. A cost-effective solution to this problem, recently developed for the fabrication of aircraft panels, could allow the lightweight metal to be used for other intricate components requiring the hardness and stress-corrosion resistance of the T8 temper.

Three basic procedures are combined: (1) mill stock (temper T3) is softened by annealing and is formed to the desired shape; (2) the part is cold worked to bring it back to the T3 condition; and (3) it is artificially aged (precipitation heat treatment) to the T8 condition. If the seemingly more straightforward procedure of heat treating the part from the annealed (TO) condition directly is used, the highest temper achievable is T6. This three-step process allows a controlled amount of cold stretching to bring the part to the same condition as the original mill stock, from which it may be hardened to T8.

In the first step, as-delivered sheet is annealed by the customary heating, soaking, and cooling to reach the TO temper. It is then stretch formed to the shape of a prefabricated die. Except for minor changes, the part is in its essentially final shape at this stage.

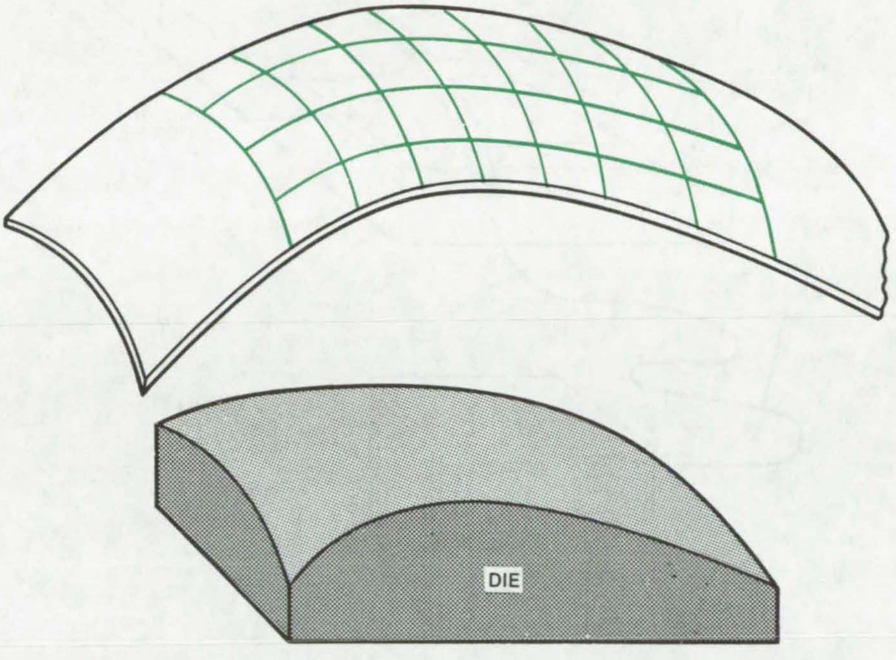

Controlled Cold Forming, after annealing and before precipitation heat treatment, is used to bring a complexly shaped part to the T3 temper. The amount of cold forming is monitored by gridlines added after the initial forming step. The lines greatly facilitate measurement of the amount of elongation induced.

For the second step, the part is solution heat treated and cooled, putting it in the W temper condition. Using the same die, the part is next stretched formed a second time to cold work it to a minor extent, to put it in the T3 condition. The cold work comprises elongation of 1-1/2 to 2 percent. The amount of elongation is monitored by a set of gridlines on the surface of the part (see figure).

The final hardening is accomplished by heating the part to an elevated temperature (less than the annealing temperature) and holding it there long enough for intermetallic compounds to precipitate at the grain boundaries. This leaves the part in the T8 condition.

This work was done by Irvin J. Wilson of Rockwell International Corp. for **Johnson Space Center.** *For further information, Circle 81 on the TSP Request Card.*

This invention is owned by NASA, and a patent application has been filed. Inquiries concerning nonexclusive or exclusive license for its commercial development should be addressed to the Patent Counsel, Johnson Space Center [see page A8]. Refer to MSC-19693.

Electric Heating for Metal Surface Hardening

Electrical element heats only the desired area
and permits precise control of temperature and cooling rate.

Marshall Space Flight Center, Alabama

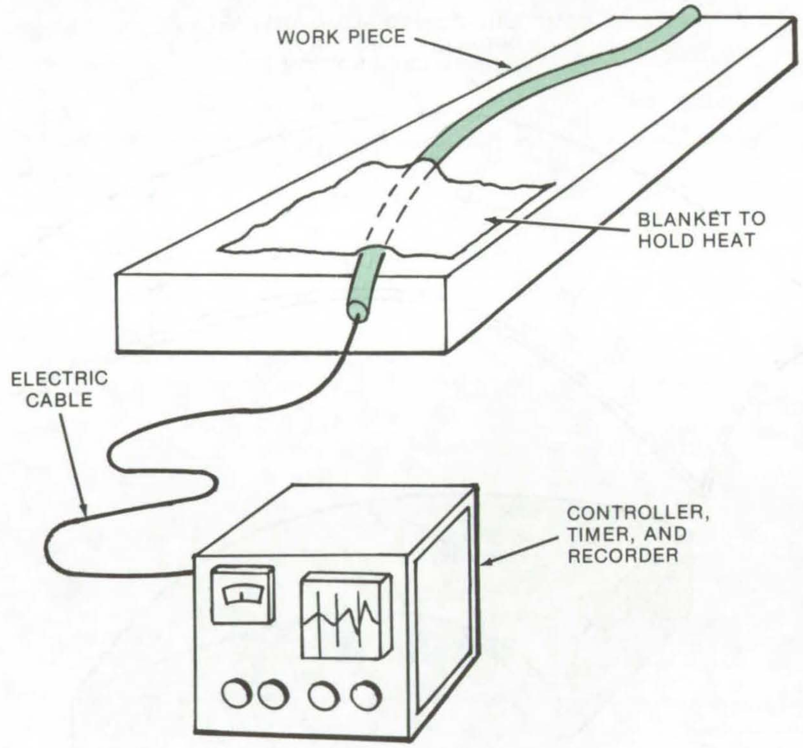

For **Heat Treating** localized surface areas and surfaces that are difficult to reach, the use of an electrical heating element is a practical alternative to flame hardening.

Electrical heating elements provide precise control of temperature and of cooling rate in hardening a localized or irregularly shaped area on a metal surface. This technique thus keeps the metal piece from being warped, which can occur in the usual flame-hardening process.

As illustrated in the figure, the heating element is placed on the area of the surface to be heat treated and is covered with insulation to prevent heat loss. The settings of an automatic controller determine the temperature, duration of treatment, and rate of cooling.

This process may serve as a useful alternative to flame hardening for treating localized areas, particularly if the areas are difficult to reach without affecting more of the workpiece than is desired. Metal-treating firms, and the manufacturers and users of items that are normally flame hardened, can use this concept.

This work was done by Ned L. Lockman of Rockwell International Corp. for **Marshall Space Flight Center.** *For further information, Circle 82 on the TSP Request Card. MFS-19268*

Yield-Pressure Determination

The stress/strain relationship of a complex-shape
vessel is recorded under hydrostatic pressure

Lyndon B. Johnson Space Center, Houston, Texas

A simple and effective technique has been developed to test the yield pressure of sealed containers. It is particularly suitable for testing vessels which are difficult to represent mathematically, e.g., those of complex shape or made of dissimilar materials. In essence, the technique consists of recording the stress/strain relationship of the vessel during pressurization to determine the yield pressure.

The test system is shown in the illustration. The vessel under test is placed inside a container that is entirely filled with water. The pressure inside the test vessel is increased gradually, and its expansion is measured by observing the amount of water leaving the outer container. The pressure at which a plot of pressure versus expansion becomes nonlinear is the yield point (zero-percent strain offset) for some part of the test vessel.

Pressure is applied with a positive-displacement hydrostatic pump. The water-filled outer container is connected to a burette or a manometer, and a bleed valve allows the entire

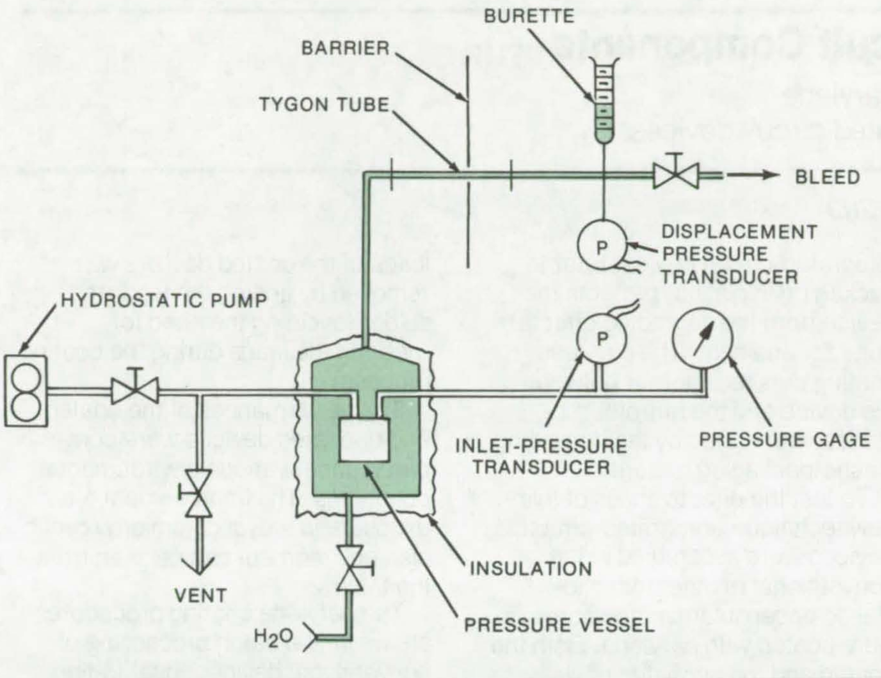

In the **Yield-Pressure Determination Scheme,** the vessel is pressurized via a positive-displacement hydrostatic pump while contained within an outer vessel. The outer vessel allows total water bleed-in through a calibrated burette or manometer. The rising burette level is a direct visual indication of pressure-vessel strain during pressurization. By choosing a suitable burette diameter and displacement transducer range, a continuous recording of pressure-vessel volumetric growth vs. inlet pressure may be made.

system (outer container, connecting tubing, and burette) to be freed of air spaces and bubbles. The diameter of the burette may be chosen small enough to allow slight water-volume changes to cause sizeable changes in the water level of the burette.

The test data are recorded with a pressure transducer on the pump line and a displacement pressure transducer attached to the burette. Using this arrangement, the technique has been used to test pressurized gas cylinders and tubular transition joints made of dissimilar metals. It may also be used to determine burst or system-failure pressures.

This work was done by Michael E. Wakefield of Martin Marietta Corp. for **Johnson Space Center.** *No further documentation is available. MSC-14655*

Crystal Orientation for Solid-State Photolithography

Method determines the desirable direction to apply photoresist mask when fabricating semiconductor lasers.

Langley Research Center, Hampton, Virginia

One step in the fabrication of continuous-wave "mesa" semiconductor laser diodes requires that a pattern of parallel grooves be made in the (100) surface of the grown wafer. A photoresist is used to mask the wafer except where the grooves are to be etched. The cross sections of these grooves generally show one of the two possible profiles shown in the illustrations.

While experimenting with different methods for applying the photoresist mask, a method to obtain the preferred [0$\bar{1}$1] orientation was discovered. The back surface of a substrate wafer is lapped with #305 Carborundum and is then etched with A-B etch for 30 seconds at a temperature of 80° C. This provides a pattern of oriented and elongated etch pits that serve as a reference for indicating the desired orientation. The long dimension of the pits indicates the preferred [0$\bar{1}$1] direction. Since only the bottom of the wafer is etched, the method can be applied to the finished wafer without affecting the device yield.

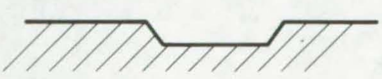

Figure 1. **Sloping-Sides** are needed in subsequent processing steps; the sides of the groove are positioned in the [0$\bar{1}$1] direction.

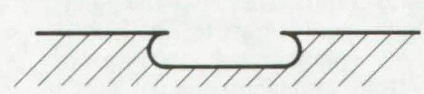

Figure 2. **Curved and Partially Obstructed** or concealed sides make it very difficult to obtain uniform SiO_2 deposit on its surface. This occurs when the groove is positioned in the [011] direction.

This work was done by Donald Paul Marinelli of RCA Corp. for **Langley Research Center.** *No further documentation is available.*

Title to this invention has been waived under the provisions of the National Aeronautics and Space Act [42 U.S.C. 2457(f)], to the RCA Corp., Princeton, N. J. 08540. LAR-11940

Parylene Coating for Circuit Components

An inexpensive internal coating of parylene improves the reliability of encapsulated circuit devices.

Marshall Space Flight Center, Alabama

In high-reliability programs the use of plastic-packaged integrated circuits is avoided since they are inferior to hermetically packaged devices when exposed to severe environmental conditions. Hermetically packaged devices, however, are often 5 to 10 times as expensive as their less-reliable plastic-packaged counterparts.

The reliability of plastic-packaged parts can be increased through the use of parylene (a thermoplastic-film polymer) for internal protection of plastic-encapsulated devices; this method compares favorably with hermetically packaged devices. The application of parylene to an integrated-circuit device, prior to packaging in plastic, protects the device from the degrading effects of humidity and heat. The parylene coating acts as a barrier between the device and the harmful substances generated by the degrading plastic-packaging material.

To test the effectiveness of this new technique, integrated-circuit devices were assembled in the conventional manner for solid-plastic encapsulation, and some were coated with parylene. Both the coated and the uncoated devices were subjected to the conventional plastic-encapsulation process. After encapsulation, the coating on the leads of the coated devices was removed by tinning the leads in solder (avoiding the need for masking the leads during the coating process).

Part Description	Failure Rate (Percent)
Hermetically packaged	0
Plastic packaged, internally parylene coated	3
Plastic packaged, no internal protection	90

The performances of the coated and uncoated devices were compared under various environmental conditions. The improvement after exposure to a cyclic humidity/cyclic bias environment can be seen from the table.

The parylene coating procedures allows in-line batch processing of conventional devices, dual-in-line packages and flat-pack plastic packages, in large quantities.

This work was done by M. J. Berkebile of **Marshall Space Flight Center,** *and R. J. Holbrook and F. W. Oberin of Hughes Aircraft Co. For further information, Circle 83 on the TSP Request Card.*

Inquiries concerning rights for the commercial use of this invention should be addressed to the Patent Counsel, Marshall Space Flight Center [see page A8]. Refer to MFS-23450.

Inexpensive Tags for Tubes or Cables

A split brass paper fastener can be used where adhesive tags won't work.

Lewis Research Center, Cleveland, Ohio

Inexpensive split brass paper fasteners are being used to identify tubes and cables in environments in which standard adhesive-backed identification tags do not adhere.

Standard adhesive-backed identification tags, which are wrapped around tubes or cables, lose their ability to adhere when the tags are exposed to environments such as heat, oil, hydraulic fluids, fuels, or Freon. These cause the identification tag to fall or be blown off, and the tube or cable must then be re-identified.

Tubes and cables can be identified easily and inexpensively by using common, expendable, split brass paper fasteners. The identification number is etched into the 7/16-in. (1.11-cm) head of the paper fastener. The fastener is then preformed to the approximate diameter of the tube or cable to which it is to be applied. The tabs of the fastener are cut, one longer than the other, and the fastener is slipped onto the tube or cable. The longer tab is bent over the shorter tab and is crimped, thus locking the fastener onto the tube or cable.

The process for installing the paper fastener can be accomplished in less than two minutes, thus saving many man-hours in tracing out tubes and cables that have lost their identification tags.

This work was done by Anthony J. Fakolt of **Lewis Research Center.** *No further documentation is available.*
LEW-12676

Rigid Cable Support for Blind Installations

A mechanical clamp eliminates the need for line clamps and raceways.

Lyndon B. Johnson Space Center, Houston, Texas

Coaxial cables installed in inaccessible areas, such as in ship and aircraft bulkheads and in buildings undergoing renovation, must remain serviceable or replaceable in the future. The cable is installed in a raceway housing, which is preshaped before installation to accommodate the cable, where it is routed and fastened to the side of the support structure. Then the cable is snaked through and fastened with line clamps, which are unavoidably made inaccessible by the raceway protection.

A mechanical support structure for electrical conductors eliminates the need for line clamps and raceways. Although originally designed for use with electrical cables, this structure can support hydraulic, pneumatic, and cryogenic lines where bends are required, assemblies are inaccessible, and conduits are impractical.

The structure consists of a support fitting (Figure 1) and a metallic hollow sphere (Figure 2). Prior to installation the conductor cable is threaded through a tubular conduit or cylindrical confinement structure. The sphere is brazed onto the cable which comes to rest within the round fittings (seen in Figure 1) that provide it with lightweight automatic support.

The support fitting has an internal diameter which nearly matches its associated sphere. The nonmetallic supports are lightweight and also offer a means of damping vibration. The fittings are located on frame or bulkhead webs for cable penetration and on brackets for additional support. Cable access is permitted via the ends, although in some instances a tool may be needed to extricate the cable. The tool is threaded around the old cable and is used to pull it out of the bulkhead. It is then rethreaded around the new cable for reassembly, and the assembly process is reversed.

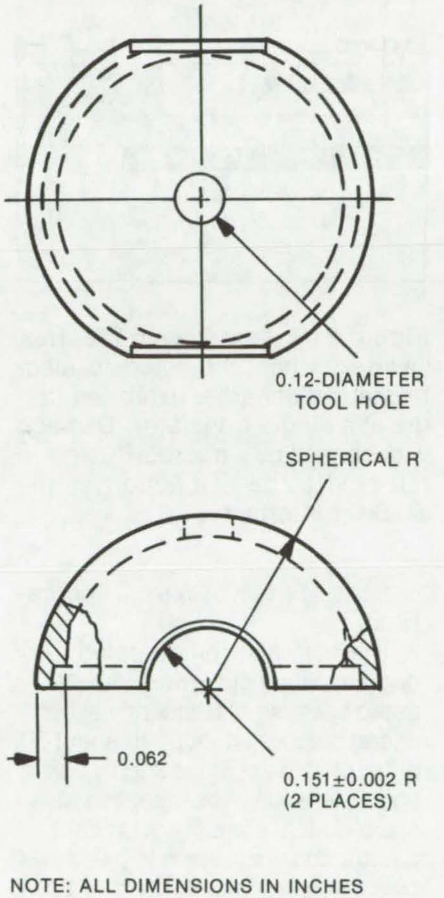

Figure 1. The **Sphere Support** eliminates the need for line clamps and raceways. It can be used with electrical cables, as well as hydraulic, pneumatic, or cryogenic lines.

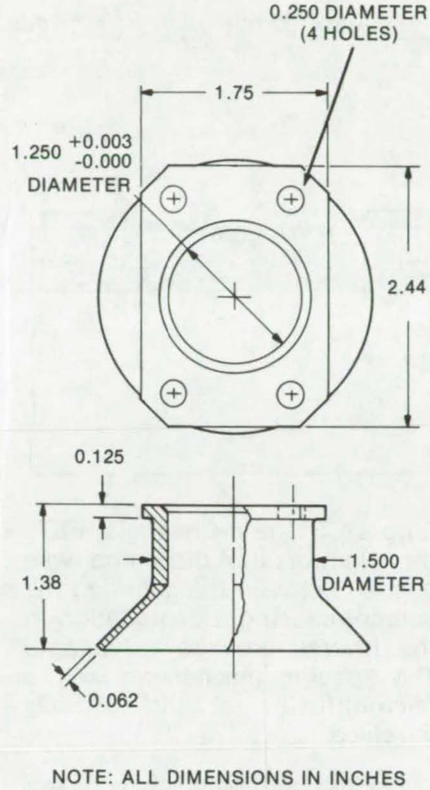

Figure 2. The **Split Coaxial-Cable Spacer** is a hollow metallic sphere. The cable is threaded through the spacer prior to being welded in place.

This work was done by James R. Abbott of Rockwell International Corp. for **Johnson Space Center.** *For further information, Circle 84 on the TSP Request Card.*
MSC-19473

Electrostatic-Discharge Damage to Semiconductors

Failure mechanisms, test techniques, and quality control procedures for a difficult-to-detect class of failures.

Langley Research Center, Hampton, Virginia

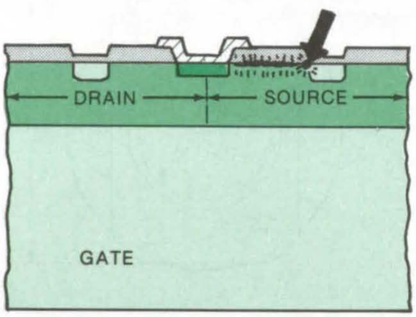

Figure 1. In the **n-Channel J-FET,** the electrostatic discharge was applied between the gate and the source, causing a degradation in the reverse breakdown voltage. The specific mechanism was a microdiffusion at the Si/SiO_2 interface.

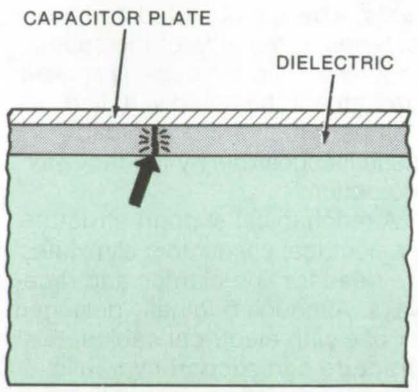

Figure 2. An **MOS Capacitor** in the internally-compensated op amp shorted out when subjected to a discharge. Such damage sites are extremely small, but may sometimes be seen under a 500x magnification.

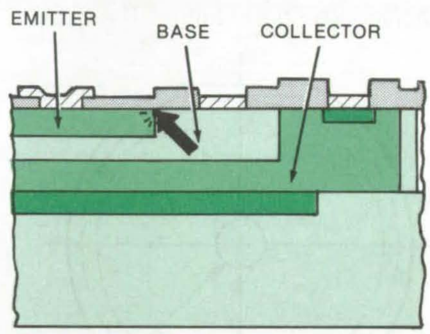

Figure 3. A **Low-Power TTL Hex Inverter,** when subjected to electrostatic discharge, exhibited failure at a single transistor. Damage was caused by a microdiffusion in the emitter/base junction at the Si/SiO_2 interface.

Electrostatic-discharge damage is responsible for a large number of failures in semiconductor devices. Because of the difficulty in detecting this class of microscopic failures, they often become evident only upon failure of the completely assembled device.

Electrostatic discharges can be caused by the kind of static discharge experienced after touching a ground on a cold dry day. Surprisingly, however, it has been found that even in warm humid environments sufficient potential exists to damage many types of semiconductor devices. Damage can occur during shipping, handling, assembly, or testing.

A study of this type of damage has provided some information about failure mechanisms, susceptibility criteria, and preventive measures that will be of interest throughout the electronics industry. In addition, a new test circuit, developed for providing an electrostatic discharge similar to those encountered in a production situation, will assist in the evaluation of the susceptibility of specific circuits and devices.

Three devices examined — a J-FET, an internally-compensated operational amplifier, and a TTL hex inverter — exhibit similar, but distinct, failure modes that are typical of the types caused by electrostatic discharges. An n-channel J-FET (Figure 1), when subjected to a single discharge of 2,000 to 6,000 V (typical discharge from a human body on a cold day is about 6,000 V), exhibited a degradation in the reverse breakdown voltage from 83 to 28 V. This is below the leak-test voltage and is sufficient degradation to cause catastrophic failure in most applications.

The internally-compensated operational amplifier was investigated because of frequently experienced output "latchup" to about 80 percent of the positive supply voltage. The failure was identified as a shorted MOS compensation capacitor and was shown to be caused by a discharge at potentials of 1,500 to 2,000 V. The third example, a TTL hex inverter (Figure 3), occurred in a hybrid circuit that failed to respond to a digital command. The failure was identified as reduction in the beta of one transistor from over 15 to approximately 2. This type of failure is reproduced with charges of 2,500 to 3,000 V.

"Generators" of electrostatic charges capable of causing the types of damage discussed above include benches, floors, chairs,

clothing, plastics, gas flows, and many others found on every assembly line. It is nearly impossible to eliminate such damage, but it can be reduced by identifying the most susceptive components and exercising the proper controls when handling them. Conductive mats can be placed over benches, chairs, and floors (to the extent allowed by safety considerations): paper gowns and boots can be worn on assembly lines, and conductive packaging materials can be used.

This work was done by Eugene R. Freeman, Jr., and James R. Beall of Martin Marietta Corp. for **Langley Research Center.** *For further information, Circle 85 on the TSP Request Card.*
LAR-11739

Transducer Bonding Kit

An inexpensive kit improves bond quality, saves time, and can be used in hard-to-reach areas.

Lyndon B. Johnson Space Center, Houston, Texas

A new transducer bonding kit saves setup time and can be used in areas where C-clamps and weights are not practical. A vacuum clamp holds the kit in place, and a spring-loaded plunger applies the proper bonding pressure to the transducer. The kit was developed to bond small-surface (on the order of 0.25- to 4-cm^2) rectangular strain gages to aluminum and titanium surfaces. The bonding agents used are high-performance epoxy resins that must be cured at 350° F (177° C) and 15 to 40 psi (103×10^3 to 276×10^3 N/m^2) applied pressure for 1 hour. The kit can, however, be used to bond other types of small parts to various surfaces.

The kit has several advantages over conventional methods:

- Precise pressure loading, even with different bond areas
- The bond area is visible and accessible to heat lamps
- Easily and quickly set up
- Pressure is easily monitored during curing
- Can be clamped in most any area

The kit, with a universal three-legged vacuum adapter, is shown in the illustration. Two other adapters are available: a mechanical toggle clamp and a "teeter-totter" clamp for attaching in limited-access areas. A set of standardized plungers, for different bond areas, is calibrated so that bonding pressure may be set precisely (in psi rather than force). Each plunger is clearly marked to allow quick pressure checks throughout the curing cycle. Currently, the curing temperature is achieved by infrared heat lamps. A small (10- by 10-cm) electric heating blanket with thermostatic control is under development.

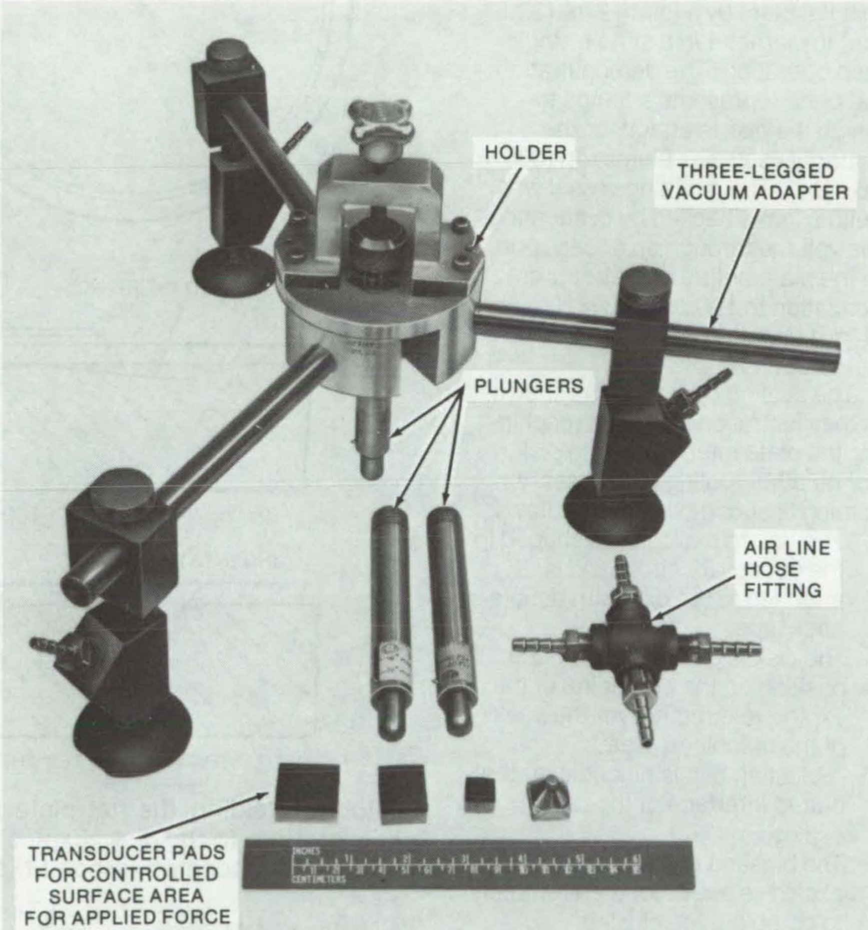

The **Transducer Bonding Kit** is shown with one of three available adapters. A spring-loaded plunger is chosen, depending on the transducer size, and then the desired pressure is set by using the adjusting knob. The plungers have spherical ends that fit into conical depressions in the surface (not visible in the photograph) of the pads. This allows the plunger-pad angle to be adjusted.

This work was done by Roscoe M. Roush, Jr., Donald A. Lott, and Andrew R. Keir of Rockwell International Corp. for **Johnson Space Center.** *For further information, Circle 86 on the TSP Request Card.*
MSC-19690

Explosive-Seam Welding Seals Large Pressure Vessels

A simple single-step operation hermetically seals aluminum, brass, steel, copper, and titanium vessels.

Langley Research Center, Hampton, Virginia

A technique recently developed and demonstrated at Langley Research Center closes and hermetically seals large-diameter metal pressure vessels. It is a further extension of the NASA explosive-seam welding process (NASA Tech Briefs B72-10002 and B73-10180) and has been used to join a flat disk to a flat plate by a joint 12 in. (30.5 cm) in diameter in a simple single-step operation. The demonstration flat plate represents a flange to which the disk is attached; the material used was aluminum (6061-T6 alloy). The resulting vessel was helium leak checked by evacuating the volume through an access port in the plate before and after pressurization to 100 psi (6.89×10^5 N/m^2) dry nitrogen, with no leaks detected.

The sealing operation, as shown in the illustration, requires machining the plate interface to the disk, but no other tooling is necessary. Joining is accomplished as follows:

1. The ribbon explosive is shaped in the necessary circle and is attached to the disk with double-back tape.
2. The disk is placed on the plate, positioning the centerline of the explosive directly over the peak of the machined area.
3. A blasting cap is placed over the butted interface of the ribbon explosive.
4. The blasting cap and ribbon explosive are detonated remotely to complete the closing operation.

The explosive welding process effaces the mating surfaces and, in pressing the disk and plate together, effects interatomic bonding at the interface. This joining technique can be extrapolated to very large diameters with the only limitation being the manufactured length of the explosive: 500 ft (152.4 m). Proper splicing of the explosive ribbon could eliminate even this limitation.

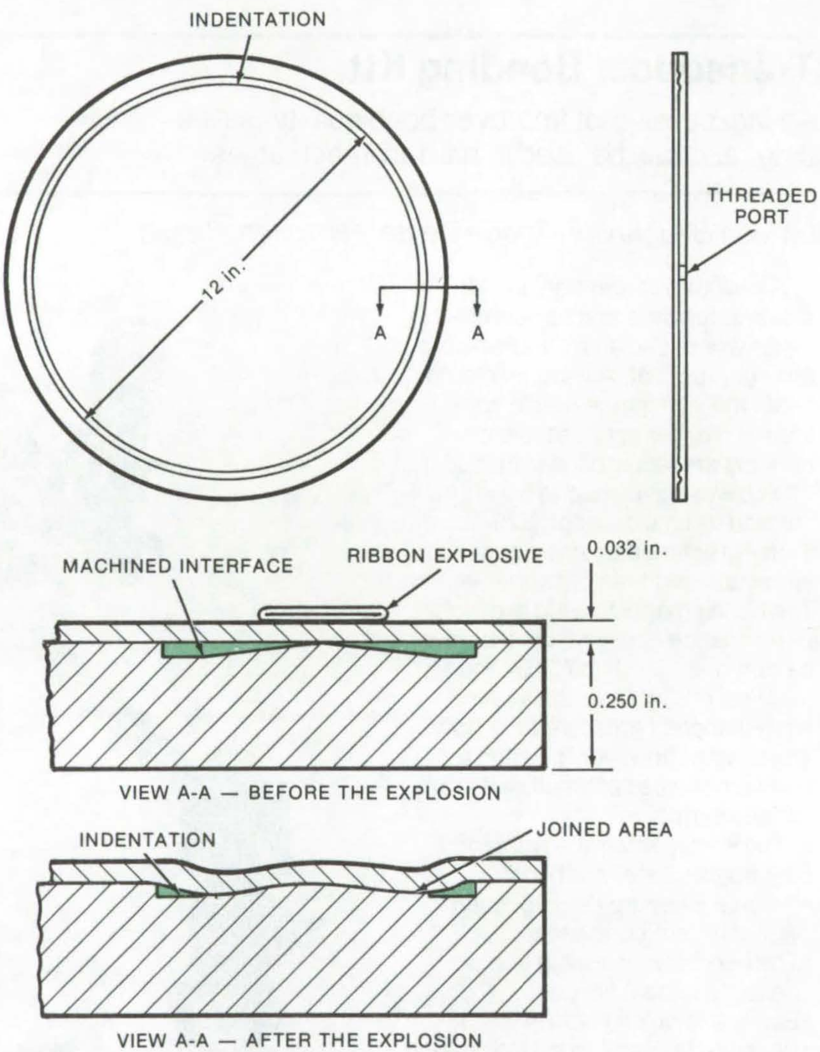

Explosive Welding the flat plate to a flat disk requires machining the plate interface to the disk. Explosive ribbon centered over the machined interface is detonated to bond the two pieces.

This explosive-seam welding technique has been demonstrated in aluminum, brass, and copper to thicknesses of 0.125 in. (3.17 mm) and in stainless steel (300 series) and titanium (6A1-4V) to thicknesses of 0.063 in. (1.59 mm). It has been applied to circumferential joints in small diameters (2.54 cm) with hermetic sealing equivalent to that described previously, but it can be extended to larger diameters.

This work was done by Laurence J. Bement of **Langley Research Center.** *No further documentation is available.*
LAR-12132

Vacuum Holddown Fixture

Variable-contour jig supports concave or convex objects.

Lyndon B. Johnson Space Center, Houston, Texas

A manually-adjustable plate-deflecting mechanism holds down cylindrically contoured parts. It uses a linkage mechanism that rotates a pair of parallel shafts upon which are mounted four gear sectors, two sectors per shaft. As the shafts rotate the sectors, the edges of a centrally-fixed flexible plate are moved upward or downward, thus matching the contour of the part. The plate, originally designed to support brittle prefired ceramic insulation tiles, can hold down any object with a varying cylindrical (concave or convex) contour.

This work was done by Paul P. Zebus and Poley N. Packer of Rockwell International Corp. for **Johnson Space Center.** *For further information, Circle 87 on the TSP Request Card.*

This invention is owned by NASA, and a patent application has been filed. Inquiries concerning nonexclusive or exclusive license for its commercial development should be addressed to the Patent Counsel, Johnson Space Center [see page A8]. Refer to MSC-19666.

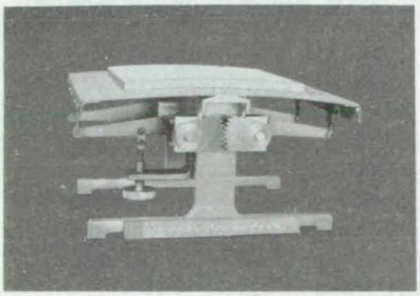

Figure 1. The **Holddown Fixture** knurled knob is used to shift the linkage that rotates the two shafts. The mating gear sectors are linked to the centrally-fixed vacuum plate which is moved upward or downward to match part contour.

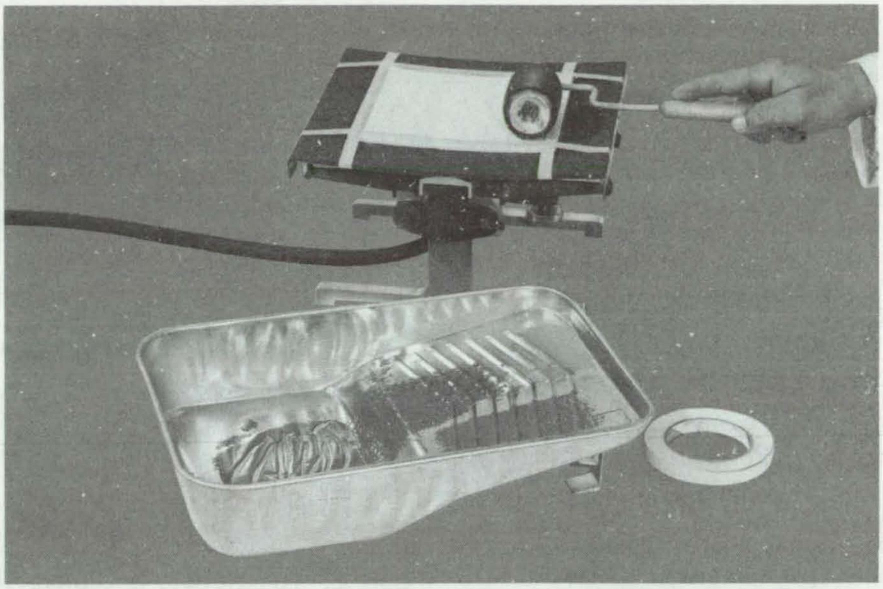

Figure 2. A **Cork/Rubber Backing** covers the plate surface. A tile, its edges taped down, is being roller coated with RTV adhesive prior to mounting.

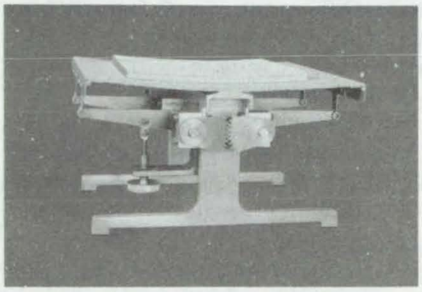

Figure 3. A **Concave Tile** is supported by the fixture.

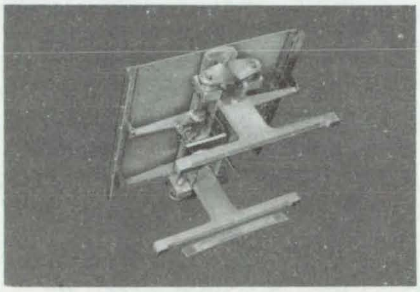

Figure 4. **Shafts and Gears,** and the inlet tube which connects the plate to a vacuum hose, are seen from below.

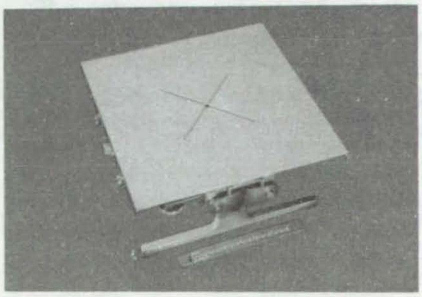

Figure 5. A **Bonded-On Plastic Sheet** is shown slotted around the central vacuum inlet. The inlet connects through the rigid central plate support and the flexible plate to provide vacuum holddown.

Visual Projection Reticle

Designers can use this lightweight reticle to superimpose visual-sensitivity and response contours on displays.

Ames Research Center, Moffett Field, California

A small, lightweight sighting device will visually superimpose visual-sensitivity and response contours on displays and instrument panels. Designers can then place indicators at locations that will elicit the fastest and most-accurate visual detection. The instrument is a hand-held reticle with visual-sensitivity, polar-coordinate contours at the appropriate positions.

Called the designer's projection reticle (DPR), the device comprises a coated objective lens (2.85-cm diameter, 8.9-cm focal length) located approximately 1.5 cm in front of a flat glass plate upon which has been deposited an aluminized reticle pattern (see Figure 1). The reticle plane lies at the focal point of the objective lens which acts as a concave mirror. Other elements of the assembly include a spacer and a field stop, as well as the usual sealing, compression, and threaded retaining rings. All components are fitted within a main enclosure tube that is 2.5 cm long and 3.5 cm in diameter; the total weight of the assembly is 30 grams.

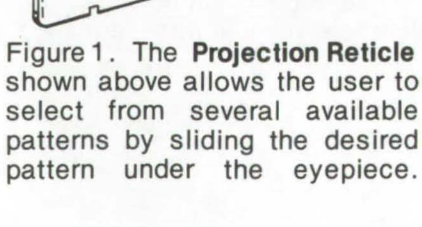

Figure 1. The **Projection Reticle** shown above allows the user to select from several available patterns by sliding the desired pattern under the eyepiece.

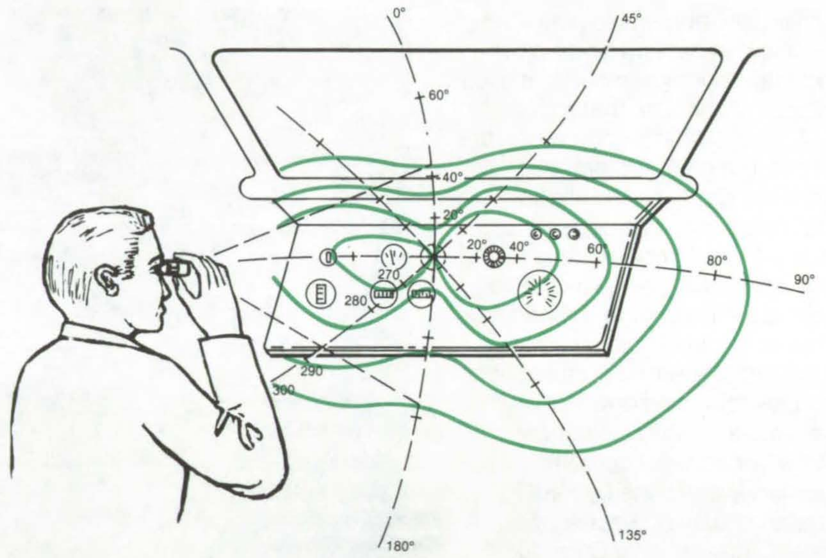

Figure 2. The **Reticle Is Simple To Use** as seen above. An observer merely holds it up to his eye and the desired pattern will appear superimposed on the panel.

Figure 2 depicts the use of the DPR to position indicator warning lights on an instrument panel. The visual field is seen clearly through the clear regions of the reticle plate, and the reticle pattern is seen superimposed upon the viewed surface. Some ambient illumination is required in order to see the reticle pattern.

This optical system provides a 45° arc/diameter field of view; however, special wide-angle optics could be substituted without a significant size or weight penalty. A source of internal (artificial) illumination could be added if necessary. Additional modification could permit the use of a standard slide projector, where the reticle pattern would appear as white or colored lines.

This work was done by Richard F. Haines of **Ames Research Center.** *For further information, Circle 88 on the TSP Request Card.*

This invention is owned by NASA, and a patent application has been filed. Inquiries concerning nonexclusive or exclusive license for its commercial development should be addressed to the Patent Counsel, Ames Research Center [see page A8]. Refer to ARC-10976.

Antireflection Coating for Plastic Lenses

Low-temperature plasma polymerized coating improves light transmission through plastic lenses.

Ames Research Center, Moffett Field, California

Injection-molded plastic lenses have attracted considerable interest lately because of the reduced material and labor costs required for their production. For many applications, however, they remain inferior to glass lenses because of problems in applying antireflection coatings to the low-melting-point plastic. These coatings improve light transmission through the lenses by reducing the amount of reflection at the lens surface.

The difficulty in applying a conventional antireflection coating of magnesium fluoride lies in the elevated temperature required to make the coating adhere properly to the surface of the lens. Although these temperatures (e.g., 300° to 500° C) are compatible with glass lenses, they severely distort plastic lenses.

Now a very satisfactory antireflection coating can be applied to plastic by the low-temperature plasma polymerization of perfluorobutene-2. Using the apparatus shown in the figure, the polymer can be formed directly on the lens at temperatures around 100° C. The lens is first cleaned with solvents and is further cleaned and activated in an oxygen plasma. It is then placed between the electrodes in the reactor chamber, and a vapor of monomer is introduced. Under the conditions of the reaction, a plasma of the monomer is formed; this plasma then polymerizes on the surface of the activated plastic.

Perfluorobutene-2 (PFB-2) has been used as the monomer for polymethyl methacrylate (PMMA) lenses, but other monomers may be more suitable for different plastics. When the deposition time is about 400 seconds and the power is 30 watts, a PFB-2 coating on a single side of a lens increases transmittance from about 92 percent to 94 percent in the 500-nm to 600-nm wavelength region.

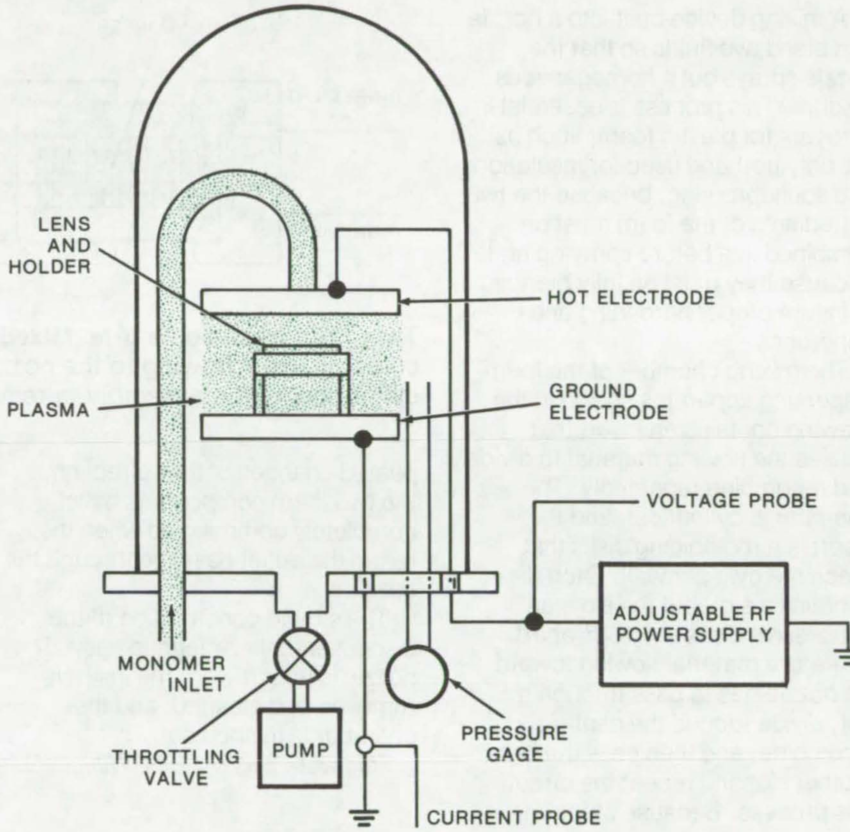

The **Plasma Polymerization Reactor** for coating plastic lenses is an evacuated chamber containing a grounded electrode and an electrode connected to an adjustable RF power supply. The object to be coated (e.g., a lens) is placed midway between the electrodes, which are about 5 cm apart. Monomer pressure before plasma initiation is around 7×10^{-2} mm Hg (9.3 N/m^2), and the RF voltage is at 13.56 MHz ranging from 93 to 122 V, peak to peak.

This work was done by Theodore J. Wydeven of **Ames Research Center** *and Ronald M. Kubacki of Bell & Howell Co. For further information, Circle 89 on the TSP Request Card.*

This invention is owned by NASA, and a patent application has been filed. Inquiries concerning nonexclusive or exclusive license for its commercial development should be addressed to the Patent Counsel, Ames Research Center [see page A8]. Refer to ARC-10983.

Mixing Ingredients in Foam Dispenser

An insert in combining chamber mixes two fluid components of plastic foam before spraying from nozzle.

Marshall Space Flight Center, Alabama

A mixing device built into a nozzle can blend two fluids so that the nozzle sprays out a homogeneous mixture. This process is essential in sprayers for plastic foam, such as the polyurethane used for insulation and soundproofing, because the two ingredients of the foam must be combined just before spraying and because they must be fully blended to insure proper hardening and adherence.

The mixing chamber of the foam-dispersing apparatus shown in the drawing contains an insert that causes the flowing material to divide and recombine repeatedly. The chamber is cylindrical, and the insert is a rod holding disks that reach the cylinder wall. Each disk contains a slot, but the slots on successive disks are 180° apart. Therefore material flowing toward the nozzle has to pass through a slot, divide around the center rod, recombine, and then pass through another slot and repeat the circuitous process. Because of the repeated changes of flow direction, the two foam components have completely commingled when they reach the outlet passage through the nozzle.

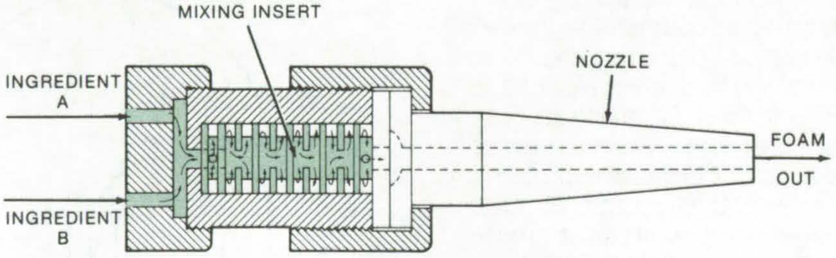

Two fluid Ingredients Are Mixed as they repeatedly divide and recombine while flowing to the nozzle of this plastic-foam dispenser. The cylindrical baffle assembly is removable for quick cleaning after use.

The simple construction of the dispenser makes cleanup easy. The nozzle is unscrewed, the insert is removed and cleaned, and the chamber is flushed out.

This work was done by William G. Simpson of **Marshall Space Flight Center.** *For further information, Circle 90 on the TSP Request Card.*

This invention has been patented by NASA [U.S. Patent No. 3,941,355]. Inquiries concerning nonexclusive or exclusive license for its commercial development should be addressed to the Patent Counsel, Marshall Space Flight Center [see page A8]. Refer to MFS-20607.

Aluminum Transfer Method for Plating Plastics

Electroless plating of a metallic film on plastic products yields improved surface replication.

Lyndon B. Johnson Space Center, Houston, Texas

A hard, very-smooth metallic film can be strongly bonded to the surface of a plastic such as epoxy by using a new electroless plating technique. The film thickness will be uniform, even over sharp corners and in holes.

Electroless plating is a means of depositing metal through controlled-autocatalytic chemical reduction. Since electrical current is not involved in the deposition, the surfaces of nonconductors such as plastics may be plated by seeding the surface with a catalyst. The growth of the deposit originates from multitudinous point sources (catalytic centers) on the surface. On a properly prepared surface, the number of nuclei is so large that the growth proceeds as a plane front parallel to the original surface.

Thus electroless plating produces a plate of uniform thickness wherever the solution may reach, including blind holes and sharp corners that give problems in conventional electroplating. Most of the electroless nickel alloys contain phosphorus, which results in a very hard plate that is comparable to chrome. Hardness and abrasion resistance can be increased further by heat treatment at 750 °F (399 °C). The nickel-phosphorus alloy has a very low thermal conductivity that can be used to great advantage in models experiencing high surface-temperature gradients.

The procedure involves casting epoxy into a mold containing a film of aluminum powder. When the epoxy hardens in the mold, the

aluminum powder remains on the surface of the epoxy. The aluminum layer permits good adherence of electroless-deposition hard alloy, yet excellent fidelity of surface detail is maintained.

This method results in a plating having several useful characteristics:

- uniform plate thickness regardless of the surface contour;
- seamless coating over many materials, including plastics or combinations of surface materials;
- abrasion resistance;
- low thermal conductivity; and
- moderate cost and less time for fabrication as compared to conventional machining methods.

This work was done by Winston D. Goodrich of **Johnson Space Center** *and Charles J. Stalmach, Jr., of LTV Aerospace Corp. Further information may be found in NASA CR-144364 [N75-29356], "Developments in Convective Heat Transfer Models Featuring Seamless and Selected-Detail Surfaces, Employing Electroless Plating," a copy of which may be obtained at cost from the National Technical Information Service, Springfield, Virginia 22151.*
MSC-16221

Elimination of Thermally Generated EMF's on PC Boards

Dissimilar-metal contacts are placed on a "temperature-controlled" substrate.

Lyndon B. Johnson Space Center, Houston, Texas

When a PC board includes contacts of dissimilar metals, they can act as thermocouples and produce unwanted EMF's in the circuit. The problem becomes significant when the dissimilar metals are sufficiently far apart to be at different temperatures.

This situation arose on a computer interface board where lead junctions between the copper PC board and a Kovar hybrid amplifier (for the signal-input pin and the signal ground pins) were physically separated and at different temperatures. The difference in the thermally generated EMF's acted as a signal input and caused the amplifier to have a high offset. On the same board a similar problem occurred with reference-diode leads.

In this and similar cases, the unwanted signal can be eliminated by keeping the dissimilar metals at the same temperature. One successful way of doing this is shown in the illustration. The copper-to-Kovar junctions are removed from the PC board and are mounted on a beryllia substrate. The substrate is mounted on a metal surface in such a way as to insure good thermal contact. (In this case, the metal surface is a metal-encased module on the PC board.) Thus "thermally connected," both metal contacts are kept at the same temperature, and the temperature-induced EMF's cancel.

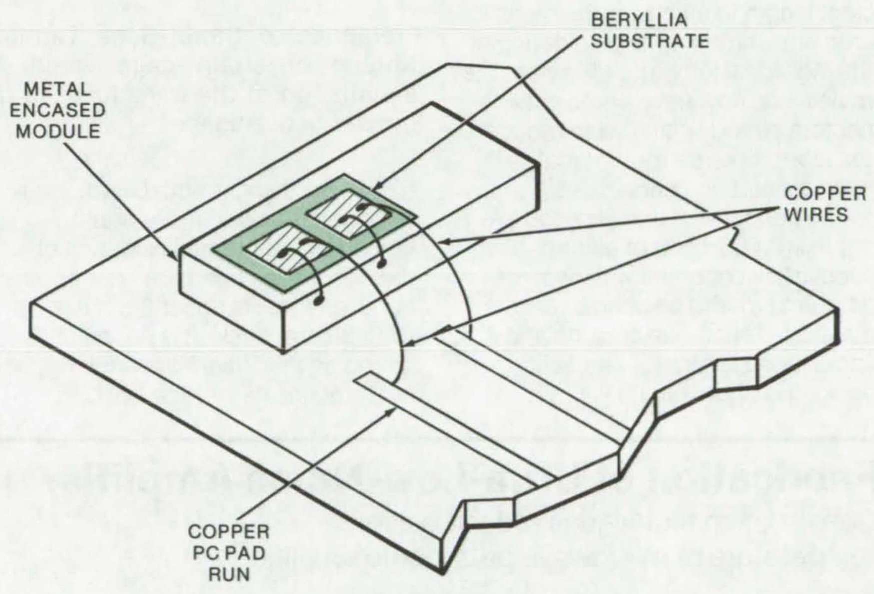

A **Common Thermally Conductive Substrate** keeps dissimilar-metal junctions on a PC board at the same temperature. Thus any thermally generated EMF's will cancel.

This work was done by Richard G. Holden and Martin T. Smid, of The Singer Co. for **Johnson Space Center.** *No further documentation is available.*
MSC-16125

Prefabricated Strain-Gage Connectors

Terminals incorporating copper loops reduce on-site installation time for instrumentation.

Lyndon B. Johnson Space Center, Houston, Texas

For many applications, purchased strain-gage terminals are bonded to a structure, and the jumper and main lead wires are individually cut, tinned, and soldered to connect the terminals from each gage to instrumentation. Under certain conditions, prefabricating the wire jumpers and main wire leads at the manufacturing site prior to shipment can reduce strain-gage installation time in the field.

The prefabricated terminals incorporate copper loops of sufficient length to eliminate the measurement, trimming, and soldering of the individual jumpers. Likewise, the main leads now have crimp connectors already installed to reduce the labor required for terminal-to-instrumentation connections.

The bondable terminals used are 1.4 mil (0.0035 cm) of electrodeposited copper foil with two different types of backing or carrier material: Teflon-film backing and epoxy-bond laminate. The Teflon backing is approximately 4 mils (0.01 cm) thick, is suitable for long-term general use, and is primarily limited by the gradual oxidation of the copper-foil interface. The epoxy-bond laminate is about 3.5 mil (0.0089 cm) thick. It is not quite as strong as the Teflon-film backing, but it retains its surface-bond characteristics better at very low temperatures including cryogenic.

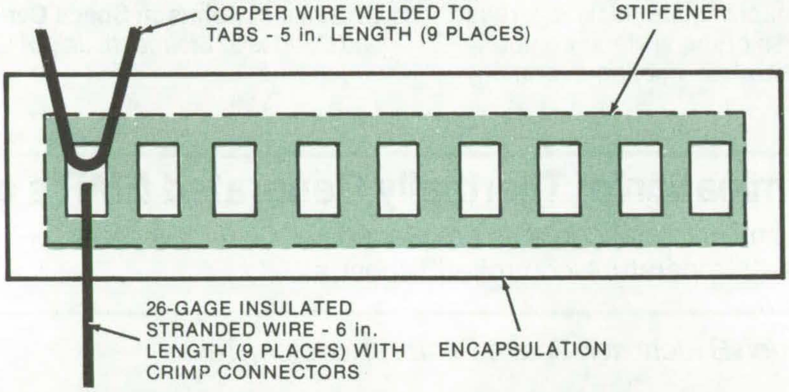

Prefabricated Strain-Gage Terminals eliminate on-site trimming and tinning of strain gage wires. Time is thereby saved during the installation of the transducer to the test instrument, besides affording greater convenience.

This work was done by Albert W. Baker of Rockwell International Corp. for **Johnson Space Center.** *No further documentation is available.*
MSC-19522

Fabrication of Ultra-Low-Noise Amplifier

Construction techniques reduce noise temperature of microwave parametric amplifier.

Goddard Space Flight Center, Greenbelt, Maryland

Three novel construction techniques minimize the noise figure of a K_u-band parametric amplifier that was developed for operation in a spacecraft environment. These are:

Electroformed Idler Cavity. The inner walls of the idler cavity have an extremely fine finish (10^{-5} cm) and are free of seams. These smooth surfaces were produced by electroforming the cavity on a polished aluminum mandrel and then dissolving the aluminum.

Screw-Tuned Idler. The electroformed idler cavity has no movable short circuit that can be used for tuning, so a hole is drilled in the fixed end wall. The hole forms a waveguide beyond cutoff, which provides a reactance that depends on its length. Therefore the resonant frequency of the idler cavity can be raised or lowered by turning a quartz or metal screw in the hole.

Low-Loss Matching Section. The signal circuit, which houses a transformer for matching to the varactor diode in the parametric amplifier, is specially designed for low losses. To reduce contact resistance, the outer conductor is screwed tightly to the varactor mount, and the transformer is screwed into a stud connected to the varactor ribbon.

The completed parametric amplifier represents a substantial advance in low-noise K_u-band amplifiers. It has a noise temperature of only 140 K and successfully meets the severe environmental requirements of spacecraft applications.

This work was done by Erich Kraemer and John Leeper of Cutler-Hammer Inc. for **Goddard Space Flight Center.** *For further information, Circle 91 on the TSP Request Card.*
GSC-12186

Mathematics and Information Sciences

Document Restoration by Computer Techniques

Digital processing of image data recovers information from barely legible writing, printing, or drawings.

NASA Headquarters, Washington, D.C.

Instead of painstakingly puzzling out the content of a stained, faded, barely legible document, an archivist may be able to produce a legible copy with an automated electronic data-processing machine. The technology for this process has been developed; the before-and-after example in Figure 1 shows how successfully information can be recovered from deteriorated records.

As the first step in generating a cleaned-up copy, an electro-optic scanner automatically measures the darkness of the original document (or of a photograph of the document) every 0.00001 inch (2.5×10^{-5} cm). The darkness of each tiny area is given a numerical value from zero (pure black) to 255 (pure white), and these numbers are recorded on magnetic tape. Additional information on the tape indicates where the edge of the document is reached and where the next line of black, white, and gray squares starts. This tape can be used to control the brightness of the dots on a TV screen; however, the picture just reproduces the original illegible document with all of its flaws.

To remove the flaws from the image, and thus improve the legibility of the copy, the numerical values recorded on the tape are changed. One simple procedure is to change all of the lighter gray levels to white and all of the darker gray levels to black. Then the image on the TV screen shows clearly-defined black markings against a white background; all of the weak stains and bleedthrough are eliminated, but unfortunately the faded symbols that carried information are eliminated too. Of course the darker dirt, dust, and stains are retained, producing images just as black as the writing or printing does.

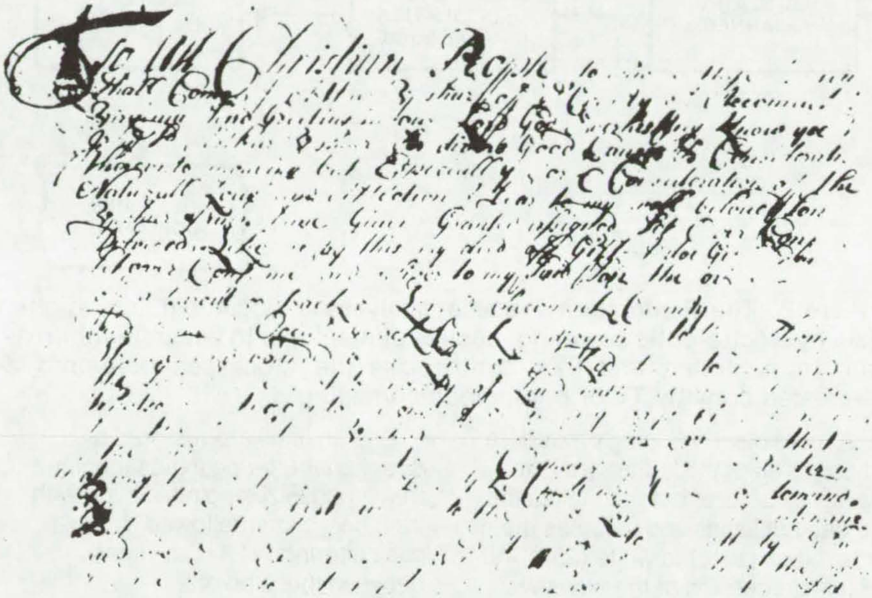
To all Christian People

(a) Original Document

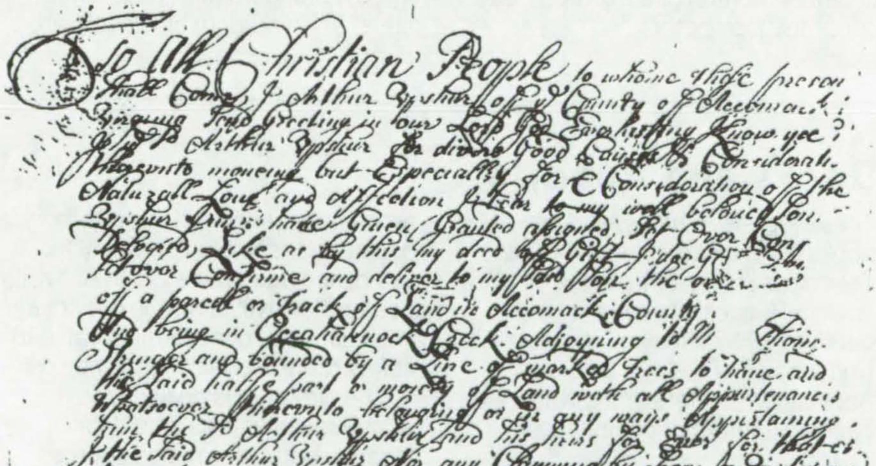
To all Christian People to whome these presen

(b) Restored Document

Figure 1. The **Successful Recovery of Information** in this 196-year-old deed from the Mississippi state archives demonstrates the value of computer-aided document restoration. Material that is almost undecipherable in the original (a) is legible to a casual reader in the re-creation (b).

(continued on next page)

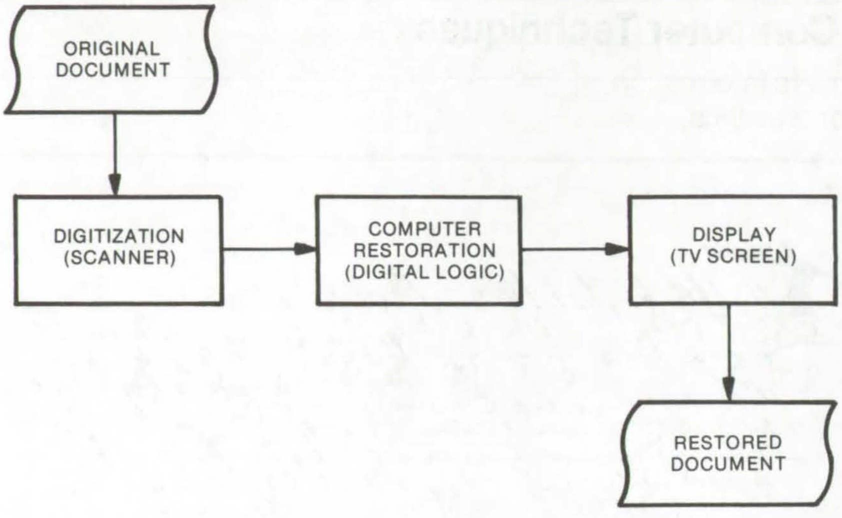

Figure 2. The **Restoration Process** analyzes a document into digital data by electro-optic scanning, applies digital logic to separate information from clutter, and then synthesizes the processed data into a re-created copy by TV or photographic imaging.

A more discriminating procedure changes all of the lighter grays to white, as before, but then takes the 60 darkest levels and rescales them from black (zero) to white (255). All of this processing of the gray levels is done by digital logic circuitry under the control of a microprocessor or minicomputer.

Broken lines are restored by a directional-filtering logic technique that emphasizes points alining with their neighbors, followed by low-pass filtering to fill in the lines between these points.

The edges of letters are sharpened by standard high-pass digital filters. Then random black dots are removed from the image by processing steps that measure the perimeters of all black objects and eliminate any with a perimeter below a specified threshold.

These logic techniques and many others, including optical character recognition, are all available for information recovery and document restoration (Figure 2). The re-created document can be displayed on the screen of a cathode-ray tube, or hard copy can be produced in any desired size down to microfilm.

Potential users of an automated restoration/information-recovery system include public and private archives, libraries, museums, and law-enforcement agencies. The total market in the United States for such a system is estimated at about 50 million pages.

This work was done by Louis Mogavero of **NASA Headquarters,** *William Spuck of* **Caltech/JPL,** *and I. M. Levitt of the Office of the Mayor of Philadelphia. For further information, Circle 92 on the TSP Request Card.*
HQN-10910

Books and Reports

These reports, studies, and handbooks are available from NASA as Technical Support Packages (TSP's) when a Request Card number is cited; otherwise they are available from one of NASA's Industrial Application Centers or the National Technical Information Service.

Safety Organizations and Experts

"Directory of Aerospace Safety Specialized Information Sources — Volume Two"

Volume Two of the "Directory of Aerospace Safety Specialized Information Sources" has now been published, completing NASA's present effort to compile a handbook of organizations and experts in specific, well-defined areas of safety technology. Although this directory has been assembled primarily for use by the aerospace community, its comprehensive coverage provides information of considerable value to safety professionals in many fields.

The directory is designed for safety specialists as an aid for locating both information sources and individual experts in engineering-related fields. Volume One, published in 1974 and announced in NASA Tech Brief B74-10019, lists over 170 organizations and approximately 300 individuals who can provide safety-related technical information in the form of documentation, data, and consulting expertise. Volume Two lists over 150 additional organizations and approximately 580 additional individuals. The two volumes are complementary but are not collated.

The information sources listed maintain specialized collections or files of material relevant to aerospace safety and regularly provide qualified users with information on a particular subject or with referrals to outside experts. The directory covers sources of data on aerospace design, tests, and operations, as well as information on hazard and failure cause identification, accident analysis, and materials characteristics. Special emphasis is given to relevant safety information sources on aircraft fire hazards and aircraft interior flammability. Related areas covered include the handling and transportation of hazardous chemicals, radioactive isotopes, and liquefied natural gases.

Information sources and experts are indexed both alphabetically and by subject areas of expertise.

This work was done by George Mandel of **Lewis Research Center** *and Richard I. Rubinstein, James J. Pinto, and Sanford Z. Meschkow of Franklin Institute Research Laboratories. Copies of the "Directory of Aerospace Safety Specialized Information Sources" — Volume Two, NASA CR-134929 [N76-25153], and Volume One, NASA CR-121206 [N74-10887] — can be obtained at cost from the New England Research Application Center [see page A7].*
LEW-12742

Computer Programs

These programs may be obtained at very reasonable cost from COSMIC, a facility sponsored by NASA to make new programs available to the public. For information on program price, size, and availability, circle the reference letter on the COSMIC Request Card in this issue.

Library Information Retrieval System

Indexing and retrieval system for books and documents

The Library Information Retrieval System (LIRS) provides for information retrieval by one or more of the following data elements: a) subject, b) title, c) authors/editors, d) source, e) contract number, or f) report number. It consists of the four programs EDIT, UPDATE, EXTRACT, and REPORTS.

The input is read by the EDIT program, reformatted, and sorted internally. The sorted records are then validated in the main body of the program. The accepted and rejected records will appear on the Acception and Exception Register in the REPORTS program. UPDATE updates the Master File and History File. This is done by adding records to the Master and/or History File, correcting or deleting existing records, and retiring records to the History File during the Yearly History Merge. EXTRACT is designed to format the requested report records and establish a key on each record for sequencing. It extracts data from the New History File (if required) and the Source Code File. The data will be used to create a report tape which will be sorted and then formatted in the REPORTS program. REPORTS writes the requested reports on a tape after the report records have been sorted. All reports are stocked on one tape.

ANS COBOL, Batch Mode
IBM 370 Model 158 OS/VS2
Maximum Core Storage Requirement 256K

This work was done by Irene Y. Chan of **Caltech/JPL.** *For further information, Circle α on the COSMIC Request Card.*
NPO-14017

CAMSP

Classification and mensuration software package

A system of computer programs has been developed to analyze many types of remotely sensed earth resources data in both batch and interactive mode. The LACIE system can handle data from various imaging sensors, including the ERTS/LANDSAT satellite (both MSS and RBV data), the MSC 24-channel multispectral scanner, the EREP S-192 experiment, and the Michigan 12-channel scanner, and can be easily modified to support additional sensors.

The primary analysis software packages in the LACIE system are the "Pattern Recognition" application, which performs multispectral analysis, and the "Image Registration" application. The Pattern Recognition application applies stochastic processes to digitized multispectral image data to classify unknown data into distinct materials. This application is based on the LARSYS Program developed by the Laboratory for Applications of Remote Sensing (LARS) at Purdue University. The Pattern Recognition application allows the user to classify each picture element (pixel) or group of picture elements (field) of an image into user-defined classes or categories. This is the only executable application in the Batch Production mode.

The Image Registration application provides the user with two basic capabilities: first, it allows the user to register two images together, and second, it allows the user to register an image to a latitude/longitude (UTM) grid. In either type of registration, the final output from the registration application is an image. This image can then be combined with other images in LACIE by using an Image Composition application, and/or it can then be processed by any other application in LACIE.

This batch/interactive system can be used to analyze any remotely-sensed Earth resources data. The configuration requirements are: 300K bytes of main storage, 230K bytes of storage for IMS, 600K bytes for LCS, five 2314 disk drives, seven 9-track tape drives, and one cluster of digital television equipment.

Assembler H, PL/I
FORTRAN Compilers
IMS DB/DC
IBM 360 Series EOS

This program was written by the Federal Systems Division of IBM Corp. for **Johnson Space Center.** *For further information, Circle β on the COSMIC Request Card.*
MSC-14979

Oblique Orthographic Projections and Contour Plots

Graphical display reduces cost of analysis

Studies based on mathematical models of structural configurations yield large amounts of output data which must be comprehensively analyzed. Manual reduction of the data is time consuming and sometimes necessitates reducing only those data associated with particular regions of the model. Furthermore, errors in the analyst's judgment in selectively examining the data can cause critical regions to be completely overlooked.

Now two computer programs have been developed to operate together and graphically display analytical information by oblique orthographic projections and contour plots over large portions of the model. They allow the analyst to assimilate accurately and evaluate the data with a consequent reduction in time and manpower cost.

Generally, a three-dimensional analytical model consists of a user-prepared set of grid points with given spatial coordinates (X, Y, Z) and a set of elements (e.g., rod, beam, triangular, or quadrilateral elements) connected at the grid points. Oblique orthographic projections allow a model to be viewed in any selected orientation. Euler-angle transformations are used to specify orientation of the model to be projected. This transformation resolves the coordinate system of the model to a principal plane (i.e., viewing plane) on which the display is to be plotted. In addition to plots of the undeformed structure, oblique orthographic plots can be used to display the deformed structure by adding given displacements to the coordinates of the grid points before transformation and subsequent plotting of elements. Exploded plots may be used to check the topology of an analytical model when the absence or presence of elements in the model cànnot be determined from a conventional oblique orthographic projection. Another option specifies sectioning or cutting planes to isolate a portion of the model for detailed examination.

The contour plotting program is used to display the distribution of data over an arbitrary planar surface. The contour surface can have an irregular boundary and cutouts. This generality is provided by representing the contour surface as a series of triangular planes with their vertexes connected at either the grid points of the model or at its element centroids where the data to be plotted are located. A computationally efficient algorithm which uses linear interpolation is used to determine the location of contour lines on each of the triangular planes.

FORTRAN IV
CDC 6000 Series

This program was written by Gary L. Giles of **Langley Research Center.** *For further information, Circle γ on the COSMIC Request Card.*
LAR-11877

Data-Management and Information System

System changes can be made by the user without programer assistance.

The task of organizing, storing, updating, and locating particular pieces of information easily in large data files has always been a problem. Computer technology has aided in the solution of this problem, but at the same time has added the need for specialized computer personnel.

JPLDIS — JPL Data-Management and Information System — has been developed to provide all the capabilities of data storage and retrieval without the need of constant programer interface between the computer and the user.

The development of JPLDIS has been from a user's viewpoint. To communicate with JPLDIS the user needs only some basic concepts of computer data storage and of the user command language. The user command language consists of unabbreviated English words so that the user can immediately identify and easily associate the word to the computer operation. JPLDIS allows the user to create files, delete files, transfer all or a portion of a file to another file, save files on tape or as elements on an EXEC 8 program file, punch data files, transfer JPLDIS structured files to data file records suitable for entry to external systems, sort, merge, or update data file records, append and insert records from other files, and display and modify the structure of a file.

There are four types of files incorporated into JPLDIS. They are Data files, Command files, Form files, and Memory files. The Data file accommodates structured data records. A record can be composed of character fields (254 characters maximum in each field) and numeric fields (12 digits maximum per field). The numeric fields can be in the form of integers, decimals, or scientific notation. The Command file consists of modules containing a sequence of command statements. They provide the user with a place to save a set of frequently used command sequences and to execute them at will by entering a single command. The Form file is used to retain the format information required to produce a report. The Memory file is used to save certain constants of data values which can be used in subsequent calculations.

The JPLDIS can be used to solve the present day business problem of requiring up-to-date information at "one's fingertips" and, at the same time, reduce operational costs. This system reduces the time required to

access large data files, reduces the cost required to store large amounts of data, and solves the problem of organizing and updating the files.

The system was developed for use on a UNIVAC 1108 with the EXEC 8 operating system. Approximately 20K words of core are required for the system. The source code contains FORTRAN (76%) and Assembler (24%).

This program was written by Jeb J. Long, Jack N. Hatfield, Michael R. Diethelm, and George Masters of **Caltech/JPL.** *For further information, Circle δ on the COSMIC Request Card.*
NPO-13716

Code-Usage Analysis System

Software package for analyzing software performance

The Code-Usage Analysis System (CUAS) is a set of computer programs that help interpret the execution characteristics of application programs. The objective of CUAS is to apply software technology to questions concerning software performance and quality, which historically have been answered by detailed and laborious manual methods requiring considerable time and expense.

The typical method proposed and implemented for automating program analysis through software technology involves source code modification, which may become burdensome for the user to apply and may impose a considerable primary storage overhead. The technique used by CUAS does not involve source code modification; instead the analysis is performed directly on the executable code generated by machine collection of the source code. Thus, CUAS has a small constant primary storage, which for most application programs should be negligible, and affords the user more information than is possible with a typical source code modification technique. The objective of CUAS is realized by providing the user with reports of subroutine usage, program errors, and segment loading which occurred during the execution of the application program.

The CUAS consists of a preprocessor, a contingency subroutine, and a postprocessor. The first step in the application of the system is for the user to collect his program, including the CUAS contingency subroutine. The CUAS preprocessor is used to prepare the absolute element such that the jump history stack file will be created during execution. Once the execution of the user's program is complete, the CUAS postprocessor is executed to prepare the reports from the jump history stack file.

The external usage report consists of three alphabetically ordered lists: (1) every external definition included in the application program; (2) every external definition name referenced by an LMJ instruction during program execution and the number of references to each; and (3) all external definitions not referenced by an LMJ instruction during program execution. The error location report locates the element name, the relative location within the element, and the overlay segment name within which a program error occurred. A walk back, which traces the calling sequence from the main program to the element of the error, is also provided. The segment loading report informs the user how many times each segment of an overlaid program was transferred from secondary storage into primary storage during execution of a segmented and overlaid program. An itemized report details those subroutines that were called to result in the segment being loaded.

This program has been implemented on a UNIVAC 1110 operating under EXEC VIII. CUAS cannot be expected to execute properly under any other machine configuration. CUAS has a central memory requirement of from 15K to 20K 36-bit words.

This work was done by M. A. Goodwin and Pat H. Horsley of Lockheed Electronics Co., Inc., for **Johnson Space Center.** *For further information, Circle ε on the COSMIC Request Card.*
MSC-16214

FORTRAN CODE-EVALUATION SYSTEM

Automatically detects coding errors before execution-time malfunctions occur.

FACES, an automated code evaluation system, can be used to detect coding errors and unsound coding practices in any ANSI FORTRAN IV source code before they can cause execution-time malfunctions. This evaluation system does not duplicate compiler functions, but rather it enhances error-detection capabilities.

FACES is organized into a driver section with three subsystem components. The main driver is responsible for file manipulations and interpreting user commands. The three subsystem components are: (1) the FORTRAN Front End Subsystem (FFE), (2) the Automatic Interrogation Routine (AIR), and (3) the Report Generator. The FFE analyzes the submitted source code and constructs tables which characterize module operation. New modules and references to other modules are inserted in a module Directory for system use. The source code of a submitted module is captured in a Source Code Catalog file for use in generating reports. Situations which limit processing effectiveness are recorded on a Flag file.

(continued on next page)

The second subsystem component the AIR, examines the tables generated by the FFE for the constructions selected by the user. If the specified constructions are found, diagnostic messages are recorded on the Flag file. The third subsystem component, the Report Generator, combines the contents of the Flag file with the module source code to produce user reports.

FACES is designed to operate in conjunction with a compiler to extend its error-detection capability. The compiler is responsible for policing acceptable constructions which can be executed; FACES is responsible for analyzing syntax which is compiler acceptable. The FACES system provides analysis services for FORTRAN-based software systems not normally available from system software. For maximum adaptation to FORTRAN dialects, the code presented to FACES is assumed to be compiler acceptable and ANSI FORTRAN IV.

The FACES system concentrates on acceptable FORTRAN code features which are likely to produce undesirable results. Emphasis is placed on the following areas:

- Interface integrity among modules
- Misleading code subject to maintenance problems
- Keypunch errors likely to escape the compilation process
- Potentially-malformed execution sequences
- Use of compiler-sensitive code

The purpose of FACES analysis is to identify potential trouble areas before they become execution-time malfunctions.

To implement the system, three disk files are required; two are of a fixed length of 9.6 and 8.0 million bytes. The third is of variable length (the Flag file) and is controlled by JCL statements; 50K bytes maximum should be sufficient. A maximum of 260K bytes of core memory is required for execution of the largest module (the Automatic Interrogation Routine) on the IBM 360/65. The system operates in batch mode, has been implemented on the IBM 360/65 Release 21.8 with H compiler, and requires the IBM SORT/MERGE package (Release 21.6).

This program was written by John D. Capps and Richard Kleir of **Marshall Space Flight Center.** *For further information, Circle ζ on the COSMIC Request Card.*
MFS-23539

Transfer-Function Parameters

Estimations using frequency-response data

A computer program has been written which fits a linear-factored form transfer function to given frequency-response data. The program is based on a conjugate-gradient search procedure that minimizes the error between the given frequency-response data and the frequency response of a transfer function that is supplied by the user. The user-supplied transfer function consists of a product of terms that can include a gain, an integrator (or differential), a dead time, multiple first-order leads and lags, and multiple second-order leads and lags.

The program consists of a main program called MODEL and two subroutines, CGFM and CFG. The MODEL program organizes the data, subroutine CGFM conducts the conjugate-gradient search, and subroutine CFG does the actual work of computing the index of performance and gradient.

The procedure for use of the program consists of entering a table of amplitude and phase-shift frequency-response data and a trial, factored form transfer function; the user also supplies roughly estimated parameter values such as time constants, gains, etc. The computer program then iterates on the supplied parameter values until it has optimized the fit to the experimental data; the excellence of this fit is constrained by the form of the user-supplied transfer function. The computer output consists of the optimized parameter values and a number indicative of the fit error. The program does not change the signs of the user-supplied parameter values or the given transfer-function structures. The user can "build" a transfer function by trying a series of increasingly complex transfer-function structures using the fit errors as a guide.

To reduce the complexity of a high-order transfer function that might result from a dynamic analysis, an option is provided in the program for entering the complex transfer functions in factored form to take the place of the normal table of frequency-response data. The simpler model can then be "built" by the usual procedure until it is a reasonable fit to the more complex model.

Efficient computer algorithms are used for the calculation of the index of performance and gradient and the execution of the search. This results in rapid calculations and a small program size suitable for running on a minicomputer.
FORTRAN IV
IBM 360-67-TSS

This program was written by Robert C. Seidel of **Lewis Research Center.** *For further information, Circle η on the COSMIC Request Card.*
LEW-12612

Information Retrieval and Display System

A flexible data-management system requires no programing experience.

The Marshall Information Retrieval and Display System (MIRADS) is a versatile command-driven data management system. MIRADS offers the user, through a simplified command language, a means of storing and searching data files, sorting the data files into specified orders, performing simple or complex computations, effecting file updates, and printing or displaying output data. MIRADS was designed to be used by people other than computer or programing professionals. The commands are simple to use and flexible enough to meet most data-management requirements. They can be learned and understood in only a few hours. To date, MIRADS has been used for personnel management, manpower analysis, task management, and shuttle payload planning and has a myriad of other potential data-management applications.

The most important aspects of MIRADS are its simplified command language and flexibility. Flexibility is provided through various options such as:

- Data files structured to 8 levels of file subordination, with each level containing from 1 to 10 different record types,
- Data security provided at the data base file, record, and field levels,
- User-formatted output displays and reports,
- Computing capabilities including counting, summing, exponentiation, multiplication, division, addition, and subtraction,
- Saved-query sets with text editing,
- Ascending/descending sort sequences,
- Free format user inquiry language with multiple users of multiple files,
- Response time of 3 to 5 seconds for files of 5,000 records through the use of an inverted list indexing scheme.

UNIVAC 1108, EXEC VIII
Central Memory Requirement Approximately 32K 36-Bit Words
Batch Mode or On-Line

This program was written by J. L. Groover and W. L. King of Computer Sciences Corp. for **Marshall Space Flight Center.** *For further information, Circle ϑ on the COSMIC Request Card.*
MFS-23510

Linear Stochastic Optimal Control and Estimation

The LSOCE problem is solved by using a time-domain formulation.

The linear stochastic optimal control and estimation (LSOCE) problem is defined as that of designing controls for a linear time-invariant system, which is disturbed by white noise, in such a way as to minimize a quadratic performance index. The major subroutine solves the algebraic matrix Riccati equation by using an eigenvector method. Other major subroutines provided are a Lyapunov equation subroutine, an eigenvalue subroutine, an eigenvector subroutine, and a subroutine for solving the matrix Riccati differential equation. Program LSOCE is designed so that the user has options to solve all or part of the LSOCE problem.

Program LSOCE was written so as to handle systems of any order and is restricted only by computer storage size and accuracy.

UNIVAC 1100 Series/EXEC 8
FORTRAN V
IBM 7094-FORTRAN IV

This program was written by Lucille C. Geyser and F. K. Bruce Lehtinen of **Lewis Research Center.** *For further information, Circle λ [UNIVAC 1100] or μ [IBM 7094] on the COSMIC Request Card.*
LEW-12540/LEW-12505

Integral-Matrix Procedure for Boundary-Layer Problems

Accurate and economical solutions for energy, momentum, and composition

A new program, BLIMP, provides a fast, highly accurate solution to the general class of gas-phase boundary-layer flow problems encompassing a broad range of boundary conditions. The solution procedure applies to the laminar or turbulent, nonsimilar, multicomponent, equilibrium boundary layer for axisymmetric or planar flow and for general chemical systems. This program should be applicable in many industries which use processes involving boundary-layer reactions.

The prorgam BLIMP (Version J of the Boundary-Layer Integral-Matrix Procedure) computes the nonsimilar, chemically reacting laminar or turbulent boundary layer for ablating, transpiration cooled, or nonablating internal flow configurations in rocket engine thrust chambers. The flow can be considered to be planar or axisymmetric. The program considers either local thermodynamic equilibrium or frozen composition for a general propellant gas (no restriction on elemental composition). Mass addition, either by surface ablation or injection, for as many as three different materials is permitted. A wide variety of surface boundary conditions are available ranging from assigned wall temperatures and mass injection rates to surface equilibrium while satisfying a steady-state wall energy balance.

In this program the mathematical model of the boundary layer is derived from the usual turbulent-flow technique of breaking the species. velocity, and enthalpy fields into mean and fluctuating components; time averaging; and making the appropriate order of magnitude approximations. The results of these

(continued on next page)

manipulations are taken as the departure point for the development of all the conservation equations. The solution of the boundary-layer equation is obtained by a novel numerical technique termed an integral-matrix approach that was developed specifically for the solution of chemically reacting, nonsimilar, coupled boundary layers. This numerical technique is roughly equivalent to a high-order finite difference approach using spline fit. The program is capable of obtaining accurate and economical solutions to the governing differential equations of momentum, energy, and species.

UNIVAC FORTRAN/Assembler
UNIVAC 1108, EXEC VIII
Memory Requirement Approximately 60K 36-Bit Words

This program was written by K. W. Gross of **Marshall Space Flight Center** *and R. M. Evans of Acurex Corp. For further information, Circle ξ on the COSMIC Request Card.*
MFS-23348

Systems Improved Numerical Differencing Analyzer

An updated version of a program to solve problems involving diffusion-type equations

SINDA, the "Systems Improved Numerical Differencing Analyzer", is a software system which possesses capabilities which make it well suited for solving lumped-parameter representations of physical problems governed by diffusion-type equations, such as Fourier, Poisson, or LaPlace equations. (See NASA Tech Briefs B72-10736 and B72-10721 for descriptions of an earlier version of this and a similar program.) The system was originally designed as a general thermal analyzer accepting resistor-capacitor (RC) network representations of thermal systems, although, with due attention to units and thermally oriented peculiarities, SINDA will accept RC networks representing other types of systems (e.g., electrical networks).

The SINDA system consists of two main pieces: the preprocessor and the library. The preprocessor is a program that accepts problems written in the SINDA language and converts them to the FORTRAN language. The preprocessor also accepts programlike logic statements and subroutine calls (requesting some particular routine from the library) as data. This permits the user to tailor the program to suit his particular problem. The SINDA library consists of many prewritten FORTRAN subroutines that perform a large variety of commonly needed actions and reduce the programing effort required to solve a given problem. These routines are fully compatible with the FORTRAN routines produced by the preprocessor. It should be recognized that the use of a preprocessor provides a system with a large capability and considerable flexibility, but because of the numerous options that are generally offered, user instructions are more difficult than other thermal analyzer-type programs which have less flexibility.

As a thermal analyzer, SINDA can handle such interrelated complex phenomena as sublimation, diffuse radiation within enclosures, transport delay effects, sensitivity analysis, and thermal network error correction methods. The thermal analysis is performed on thermal analog modes presented in network format. The network represents a one-to-one correspondence with both the physical and mathematical models. SINDA has been used in the analysis of networks containing about 2,000 nodes without requiring unreasonable amounts of computer time. The thermal network can be coupled to an iterative solution of a lumped-parameter fluid network. Nonlinear material properties and boundary conditions may be calculated simultaneously as a function of one or more independent variables.

The general fluid-flow capabilities include extensive valve characterization and the ability to match pump curves and system pressure-flow characteristics. The valves have been formulated so that either cooling or heating situations may be controlled with any of the valve types. Pump options included are pressure rise as a tabulated function of system flow rate and pressure rise as a polynomial function of flow rate. Special subroutines in SINDA facilitate the thermal analysis of systems containing counterflow heat exchangers, parallel-flow heat exchangers, crossflow heat exchangers, condensing heat exchangers, and any heat exchanger with an input effectiveness. The flow-hybrid method is incorporated for calculating fluid temperatures, with improved calculation accuracy obtained by using fluid enthalpy rather than specific heat for the convective term of the fluid temperature equation. To facilitate the speedy analysis of a general flow problem, provisions have been made for the user to divide the flow system network into subnetwork elements.

The use of SINDA is based on a lumped-parameter representation of a physical system. Thus, SINDA solves numerically a set of ordinary (in general nonlinear) differential equations that represent the transient behavior of a lumped-parameter system or a set of nonlinear algebraic equations representing steady-state conditions. The numerical techniques used by

SINDA are based on finite-difference algorithms as opposed to finite-element methods. In problems involving radiation heat transfer and complex geometric configurations, the finite-element methods have been found inappropriate due to nonlinearities. For user flexibility, SINDA provides a number of numerical solution methods. These include finite-difference formulations of the explicit methods such as:

- Forward-difference explicit approximation,
- Dufort-Frankel approximation,
- Exponential approximation, and
- Alternating-direction approximation;

and formulations of the implicit methods, such as:

- Backward-difference implicit approximation and
- Crank-Nicolson approximation.

UNIVAC 1100 Series, EXEC VIII
Stromberg-Carlson SC 4020 Plotter
Control Memory Never Exceeds 65K 36-Bit Words

This work was done by Lawrence C. Fink of TRW, Inc., for **Johnson Space Center.** *For further information, Circle π on the COSMIC Request Card.*
MSC-13805

Input/Output Error Analyzer

Analyzer for UNIVAC 1108 aids in system assessment.

The I/O Error Analyzer for the UNIVAC 1108 is a configuration-independent assembly-language utility program designed to operate under level 27 or level 31 of the EXEC 8 Operating System (modifications are now underway to allow the program to operate under level 33). It scans user-selected portions of the system log file whether located on tape or mass storage and searches for and processes I/O error (Type 6) entries. The several different types of output returned by the analyzer are arranged so as to assist the installation manager and systems programers in assessing the system performance, gaging overall peripheral activity, and distinguishing marginal media from faulty equipment.

Outputs

- Type I output consists of individual summaries of the contents of each I/O error packet encountered during processing. The entry information is output sorted by subcode/equipment type/subsystem/unit; multiple errors that are similar in all respects (except for time stamp) are indicated by fields delineating the times of the first and last of such errors that occurred. The information printed out for each entry is as follows: device type mnemonic, subsystem, unit, IOC/MSA number, IOC/MSA channel number, CPU channel number, EI-status-word(s), external function word(s), time of first/last errors of this type, date, reel number (pack ID), total number of errors of this type, and total number of references since last error.
- Type II output consists of synoptic matrices (SM's), one for each subcode/equipment-type (SC/EQ) pair. Each SM tabulates a number of fault/status (F/S) conditions which occurred for each subsystem/unit (SS/U) pair during the analysis of the user-specified portion of the log file. Each F/S type can be masked out by the user at assembly time. The software is designed in such a way that each matrix has a self-compacting feature, i.e., any SS/U for which none of the preselected F/S conditions occurred will not appear as a row, and any F/S condition which did not occur for at least one of the SS/U pairs will not appear as a column. In addition, row totals (number of F/S occurrences for each SS/U) and column totals (number of occurrences of each F/S type) are output for each SM. This compactness is particularly useful in keeping the SM's of reasonable size when they are to be output on scopes.
- Type III output consists of a set of equipment-independent statistics, e.g., mean-time-to-error, average errors per unit time, average references per unit time, and variance of error. For convenience in comparing the performance of similar devices, this information is arranged in separate tables, one for each SC/EQ pair.

Each page of Type II and Type III output has a header detailing the time range of the data processed and a mnemonic indicating the SC/EQ of the device, e.g., U16 for 7-track UNISERVO 16's and F40 for FASTRAND-formatted 8440 disk.

At the present time, the mechanism exists to provide Type II and Type III outputs for the following types of equipment: UNISERVOS VIIIC, VIC, VIIICB, VICB, VIIIC9, and VIC9; UNISERVOS 12, 16, and 20 (both 7 and 9 track); FH-432 and FH-1782 Magnetic Drums; UNIVAC 8440 Disk; FASTRAND II and III; UNIVAC 8460 Disk; UNIVAC 8414/8424/8425 Disk; Type 0716 Card Reader/Type 0604 Card Punch and Type 0768 and Type 0770 Printers. The header will also indicate whether the user has elected, by the use of options, to process only unrecoverable (hard) errors or only recoverable (soft) errors.

Inputs

- Option Letters - By using option letters, the user can elect to not use the run-I.D. or reel number when creating Type I packets ('I' and/or 'J' options), to restrict processing to unrecoverable or recoverable errors only ('U' or 'R' options), to print only Type II and Type III output ('S' option), to process the log file from tape

(continued on next page)

rather than from mass storage ('T' option), and to print out detailed information about the assignment and deassignment of F-Cycles or log tapes during processing ('Z' option).

- Key-ins (Data Cards) - Three key-ins are currently implemented: (1) The "time range" key-in allows the user to specify a "start time" and a "stop time" within which the search for Type 6 entries is to take place; (2) the "subsystem/unit" key-in enables the user to restrict investigations to a particular set of subsystems or subsystem/unit pairs; and (3) the "equipment type" key-in allows the user to confine processing to a particular group of peripherals.

The "subsystem/unit" and "equipment type" key-ins, when used together, operate in an inclusive-or mode. These key-ins are particularly useful in conjunction with the "T" key-in when all types of output (Types I, II, and III) are to be scrutinized for a suspected faulty peripheral. Output of Type I for the entire configuration in such an instance would be relatively voluminous and wasteful.

This program was written by Edwin T. Vaughan of **Goddard Space Flight Center.** *For further information, Circle ϱ on the COSMIC Request Card.*
GSC-12132

SUBJECT INDEX

National Aeronautics and
Space Administration

Washington, D.C
20546

Official Business
Penalty for Private Use $300

SPECIAL FOURTH CLASS MAIL
BOOK

Postage and Fees Paid
National Aeronautics and
Space Administration
NASA 451

U.S.MAIL

NASA

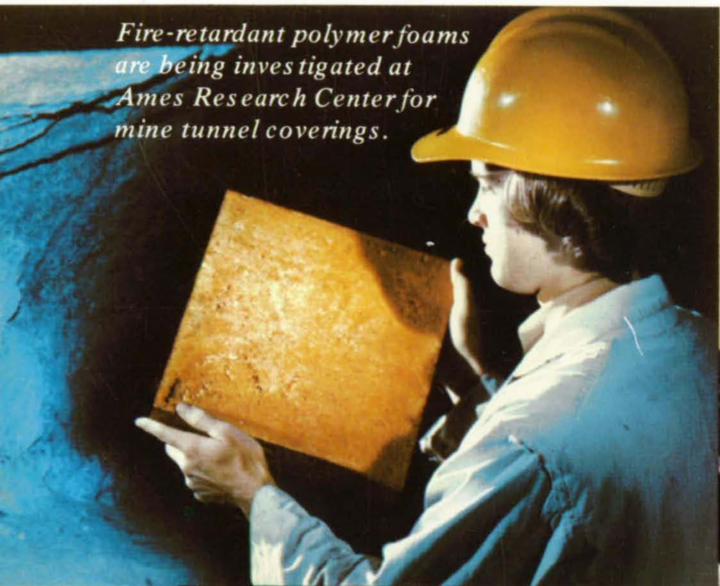

Fire-retardant polymer foams are being investigated at Ames Research Center for mine tunnel coverings.

A junction-diode temperature sensor and circuit, developed at Langley Research Center, has been incorporated into a hand-held thermometer/digital multimeter.

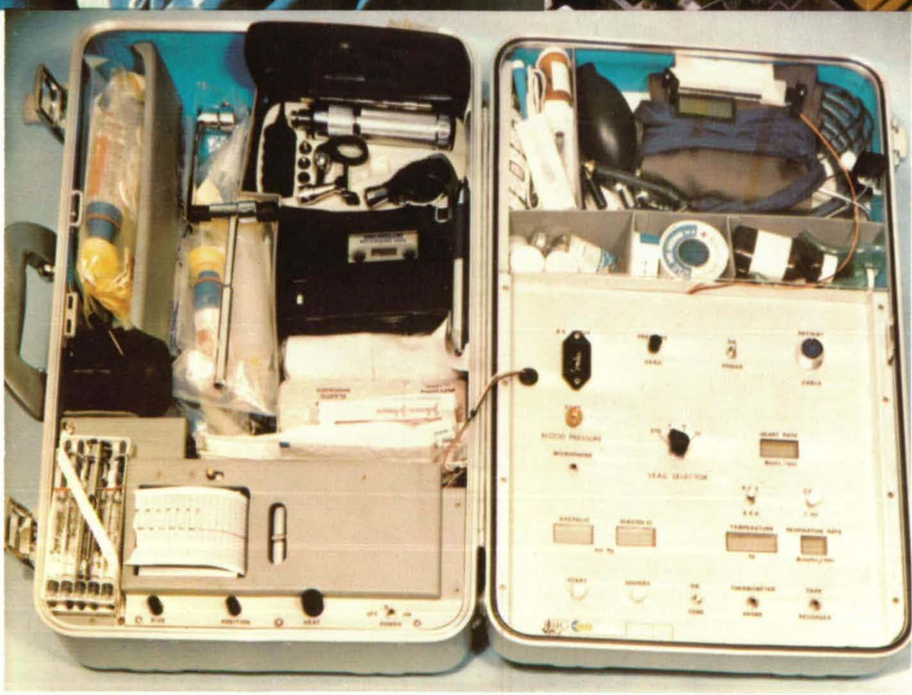

Technology developed to monitor astronauts has been used at Johns Space Center to design a portable medical status system. This physician's "black bag" contains equipment for monitoring vital sign electrocardiograms, and electroencephalograms.